2020

CHARACTERIZATION OF THE DYRK1A PROTEIN-PROTEIN INTERACTION NETWORK

Varsha Ananthapadmanabhan
Virginia Commonwealth University

CHARACTERIZATION OF THE DYRK1A PROTEIN-PROTEIN INTERACTION NETWORK

A dissertation submitted in partial fulfillment of the requirements for the degree Doctor of Philosophy at Virginia Commonwealth University

By

Varsha Ananthapadmanabhan
MS, Human Genetics, Virginia Commonwealth University, 2015
B.Tech, Biotechnology, D.Y. Patil University, 2013

Advisor: Larisa Litovchick, MD, PhD.
Associate Professor
Division of Hematology/Oncology and Palliative Care
Department of Internal Medicine

Virginia Commonwealth University
Richmond, Virginia
April 2020

ACKNOWLEDGMENTS

I express my sincere gratitude to my advisor Dr. Larisa Litovchick for her constant support and guidance during the course of my graduate training. I have been fortunate to be provided with opportunities to explore and broaden my scientific interests and acquire several skills for which I would always be grateful. I really appreciate all the advice I have received from her over the years which has boosted my professional life. I couldn't have asked for a more caring and understanding mentor.

I thank my committee members Dr. Andrei Ivanov, Dr. Steven Grossman, Dr. Amanda Dickinson and Dr. Zheng Fu for their insights and advice during the course of my PhD. I would also like to thank my graduate program director Dr. Rita Shiang for her encouragement and support.

I also thank members of the department of Human and Molecular Genetics, members of Massey Cancer Center, the School of Medicine, the VCU graduate school and the Global Education Office for all their support over the years.

The Litovchick lab members, both past, and present will always be close to my heart. I have enjoyed working with each one of them. A special thank you to Dr. Vijay Menon with whom I worked extensively for Chapter 2 of this dissertation. Vijay was there to help me for work related to this chapter even after he moved away from VCU. Dr. Siddharth Saini was always there to help me with anything I needed during his tenure in the lab and I have learnt a lot from him. Polina Bukina has been an awesome person to work with. I am very happy to have had the opportunity to see her grow her research skills in the lab. I am grateful to Jessica Rusbasan for all her help and friendship during her tenure in the lab. I would also like to thank Sophia Gruszecki for technical support and for all the love she has given me over the years. I thank Supriya Joshi

for having my back, always. I am very happy that we went through the different phases of our PhD training together, supporting each other, through each phase. I am thankful to Fatmata Sesay for standardizing the *in-vitro* kinase assay that I have used in Chapter 3 of this dissertation. I also thank her for all the laughs and all the good times in the laboratory. During the last year, it has been a lot of fun to work with Hayley Walston and I thank her for all her support.

My sincere thanks to the members of the Flow core and Microscopy core at VCU for all their patience, help and training.

I would also like to thank all our collaborators including Dr. Mikhail Dosmorov, the proteomics core at Stowers institute and the Sequencing core at UT Health, San Antonio for their help. Their work has largely contributed to the work in my dissertation.

I also thank all the Grossman lab members for their kindness and support during my training and for their inputs during 'group meetings'.

I have been extremely lucky to have best friend, my husband Ajinkya by my side, be it a good day or bad. Ajinkya, my parents, my brother, in laws and my entire loving extended family back in India have all supported and believed in me even on days that I didn't myself and contributed to me being able to move forward with a smile. I cannot thank my parents enough for their hard work and struggle which is a major reason why I was able to pursue my studies here in the US. I also thank all my friends but especially Amrita, Mary Ann and Jacob who have helped me sail through this wonderful journey.

Lastly, I am extremely grateful to my teacher Robbie Norris and everyone at 'Richmond City Yoga' for the unconditional support that I have received. My practice here over the last couple of years has helped me put my best foot forward and complete this journey.

TABLE OF CONTENTS

LIST OF FIGURES

LIST OF TABLES

LIST OF ABBREVIATIONS AND SYMBOLS

53BP1	p53-binding protein 1
AA/DD	alanine-alanine/ asparate-asparatate
AD	Alzheimer's disease
ATM	Ataxia telangiectasia mutated
ATP	Adenosine Tri-phosphate
AUTS2	Autism susceptibility candidate 2
Aβ	Amyloid-β
ChIP	Chromatin immunoprecipitation
CMGC	Cyclin Dependent kinases, mitogen activated protein kinase, glycogen synthase kinase, CDC-like kinase
CRISPR	Clustered regularly interspaced short palindromic repeats
CtIP	C-terminal binding protein-interacting protein
DAPI	4',6-diamidino-2-phenylindole
DCAF7	DBB1 and cullin associated factor 7
DIAPH1	Diaphanous-related formin 1
DNA	Deoxyribonucleic Acid
DREAM	dimerization partner, RB-like, E2F and multi-vulval class B
DS	Down syndrome
DSCR	Down syndrome critical region
DYRK	Dual Specificity Tyrosine Regulated kinase
EDN1	Endothelin-1
EDTA	Ethylenediaminetetraacetic acid

EGCG	Epigallocatechin-gallate
FAM117B	Family with sequence similarity 117-member B
FBS	Fetal bovine serum
FH	Flag-HA
GFP	Green fluorescence protein
GLI1	Glioma-associated oncogene 1
Gy	Gray
H2A-K119-Ub1	Monoubiquitination of histone H2A at Lysine 119
H2AX	Histone H2AX
HIPK	Homeodomain-interacting protein kinase
IP	Immunoprecipitation
IRIF	γ-irradiation induced foci
KD	Kinase dead
kDa, kd	Kilo Dalton
KO	Knockout
LZTS	Leucine zipper tumor suppressor
MDC1	Mediator of DNA Damage Checkpoint protein 1
MEKK1	Mitogen-activated protein kinase kinase kinase 1
Mnb	Minibrain
MRN	MRE-11-RAD 50-NBS1
MudPIT	Multidimensional Protein Identification Technology
N/ C terminal	Amino/ carboxy terminal
NFT	Neurofibrillary tangles
NLS	Nuclear localization sequence

PCR	Polymerase chain reaction
PD	Parkinson's disease
pMSCV	Murine stem cell virus expression system plasmid
PRC	Polycomb repressibe complex
PRP4	Pre-mRNA processing protein 4
RT-qPCR	Reverse transcriptase-quantitave-PCR
RB	Retinoblastoma
RNF168	Ring finger protein 168
RNF169	Ring Finger protein 169
S/T	Serine/Threonine
S phase	Synthesis phase
TROAP	Trophonin associated protein
USP7	Ubiquitin specific protease 7
WB	Western blot
WDR	Tryptophan- Aspartic acid repeat
WT	Wildtype
Y	Tyrosine
β	Beta
β-ME	β-Mercaptoethanol
γ	Gamma
Δ	Deletion
μ	Micro
λ	lambda
DEGs	Differentially regulated genes

ABSTRACT

CHARACTERIZATION OF
THE DYRK1A PROTEIN-PROTEIN INTERACTION NETWORK

By

Varsha Ananthapadmanabhan
MS, Human Genetics, Virginia Commonwealth University, 2015
B. Tech., Biotechnology, D.Y Patil University, 2013

A dissertation submitted in partial fulfillment of the requirements for the degree of
Doctor of Philosophy at Virginia Commonwealth University.

Virginia Commonwealth University, 2020

Thesis Director: Larisa Litovchick, M.D., Ph.D.
Associate Professor
Division of Hematology/Oncology and Palliative Care
Department of Internal Medicine

Human Dual specificity tyrosine (Y)-Regulated Kinase 1A (DYRK1A) is a protein kinase encoded by a dosage-dependent gene. An extra copy of *DYRK1A* contributes to Down syndrome (DS) pathogenesis while loss of one allele causes severe mental retardation and autism. DYRK1A is involved in phosphorylation of several proteins that regulate cell cycle control and tumor suppression. However, the function and regulation of this kinase is not well understood and current knowledge does not fully explain dosage-dependent function of this important kinase. Our previous proteomic studies identified several novel DYRK1A interacting proteins including RNF169, FAM117B, TROAP, LZTS1, LZTS2 and DCAF7. In this dissertation, we report the proteomic, biochemical and functional characterization of this DYRK1A protein-

protein interaction network. Firstly, we show that DYRK1A regulates that recruitment of 53BP1 to DNA double strand breaks (DSBs) in part through its interaction with RNF169. This revealed a novel role of DYRK1A in DSB repair pathway choice. Secondly, we identify LZTS1 and LZTS2 as novel regulators of DYRK1A activity towards LIN52. Thirdly, we observed that DCAF7 interacts with several other DYRK1A-binding proteins including RNF169, TROAP, FAM117B, LZTS1 and LZTS2 giving rise to various multi-subunit protein complexes, but it does not act as a scaffold for these interactions. We also observed an unexpected role of DYRK1A in mediating the interaction between these DYRK1A-binding proteins and DCAF7, which could explain some aspects of the dosage-dependent function of DYRK1A.

As DCAF7 was the most highly enriched DYRK1A-interacting protein, we generated and analyzed the DCAF7 interactome in order to understand the functional significance of the DYRK1A-DCAF7 interaction. We show that DCAF7 interacts with the components of a multi-subunit Polycomb Repressive Complex 1.3/5 (PRC1.3/5) independent of DYRK1A, but DYRK1A could influence the molecular size of the PRC1.3/5 complex. Furthermore, our data suggest that DYRK1A and DCAF7 regulate the monoubiquitination of H2A at K119 by PRC1.3/5. Using RNA-seq analysis, we identified a common set of genes regulated by DYRK1A and DCAF7. Our data shows that DCAF7 requires DYRK1A for its transcriptional effect. Future studies will be focused to determine the molecular mechanism by which DYRK1A and DCAF7 regulate the transcription of the PRC1.5 target genes.

In conclusion, DYRK1A interacting proteins could regulate the activity and function of DYRK1A and play a role in its biological functions including tumor suppression, the DNA damage response and transcription.

CHAPTER 1: GENERAL INTRODUCTION

1.1. The DYRK family

DYRK, or Dual specificity Tyrosine Regulated Kinases, belong to the CMGC group of eukaryotic protein kinases that includes cyclin-dependent kinase [CDK], mitogen-activated protein kinase [MAPK], glycogen synthase kinase [GSK3], and CDC-like kinase [CLK] (Aranda et al., 2011; Hanks & Hunter, 1995). Based on the degree of conservation in their kinase domain, the DYRK family can be further divided into three sub-families: 1) DYRK kinases 2) PRP4s (pre-mRNA processing protein 4- kinases) and 3) HIPKs (Homeodomain-interacting protein kinases) (Figure 1). Out of these, the DYRK sub-family can be further divided into three branches including 1) yeast kinase Yak1p which has no members in animals; 2) DYRK1 and 3) DYRK 2. DYRK1 and DYRK2 have members ranging from yeast to humans and are highly conserved across evolution (Aranda et al., 2011) (Figure 1). Minibrain in Drosophila is the closest homolog of mammalian DYRK1A (Aranda et al., 2011).

Based on ectopic expression of the DYRK family members in cell lines, they were also classified as cytosolic kinases (DYRK2, DYRK3, DYRK4) and nuclear kinases (DYRK1A and DYRK1B) (Becker et al., 1998). However, it has been observed that the endogenous expression of these proteins varies from this classification. For example, under overexpressed conditions DYRK1A localizes to the nuclear speckles while endogenous DYRK1A is observed both in the nucleus and cytoplasm (Álvarez et al., 2003; Hämmerle et al., 2003; Martí et al., 2003; Wegiel et al., 2004). DYRK1B has been found to be predominantly nuclear in some cell lines while it is mostly cytoplasmic in muscle fibers as well as in rhabdomyosarcoma and pancreatic ductal carcinoma cells (Friedman, 2007).

DYRK1A is the most ubiquitously expressed member in tissues of adult and fetal origin (Guimera et al., 1999; Okui et al., 1999) while DYRK2, DYRK3 and DYRK4 have limited tissue distribution (Becker et al., 1998; Sacher et al., 2007).

Structurally, DYRK family members share a conserved kinase domain and an adjacent DYRK homology domain (DH) but differ more towards the N and C terminal regions (Aranda et al., 2011). In addition to the conserved catalytic kinase domain, DYRK1A has two nuclear localization signal sequences (NLSs): a classical bipartite NLS at the N-terminal region of the protein and a complex NLS within the catalytic domain (Aranda et al., 2011). The kinase domain is followed by a PEST domain and then by a histidine-rich domain that targets DYRK1A to the nuclear speckles compartment where it may co-localize with splicing machinery (Figure 2) (Álvarez et al., 2003; Aranda et al., 2011).

DYRKs phosphorylate themselves on tyrosine (Y) and serine/threonine (S/T) residues but phosphorylate their substrates only on serine and threonine residues. This is why they are referred to as dual specificity tyrosine regulated kinases. The Y autophosphorylation in the activation loop on all DYRKs occurs in cis with translation. Specifically, the phosphorylation on the second tyrosine (Y) in the YxY motif is required for the activity of all DYRK members (Himpel et al., 2001; Li et al., 2002; Lochhead et al., 2003). This phosphorylation on DYRK seems to be constitutive unlike the regulatory phosphorylation on the mitogen-activated protein kinases (MAPK) (Glenewinkel et al., 2016). Interestingly, in contrast to former observations, it has been observed that DYRK1A retains its Y phosphorylation ability even after translation (Walte et al., 2013).

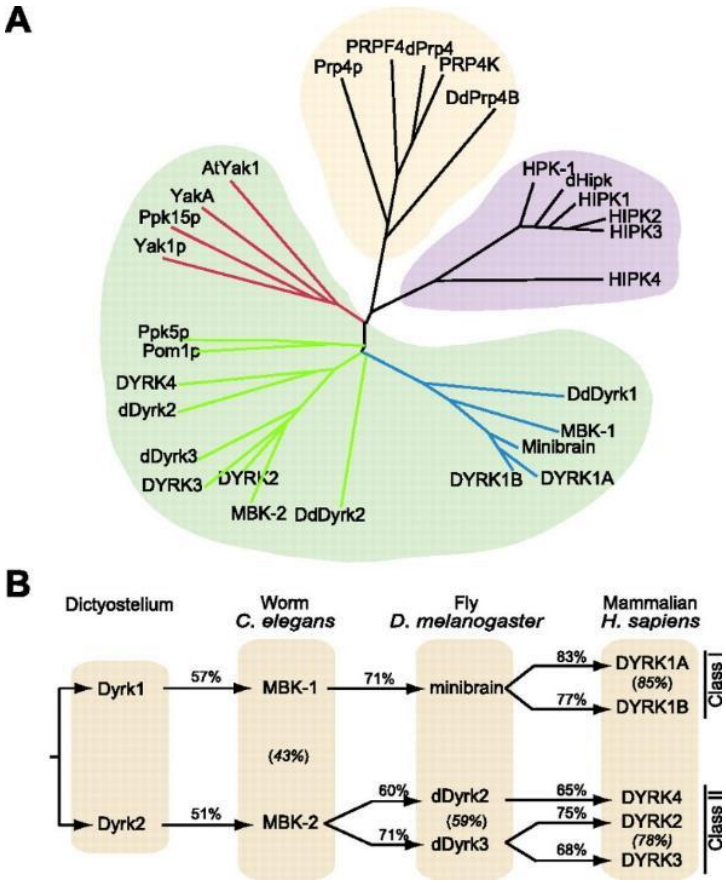

Figure 1: The DYRK kinase family.
A) An unrooted phylogenetic tree depicting the evolutionary divergence of the kinase domain in the DYRK family members. The DYRK sub family has members ranging from yeast to humans. B) The DYRK sub family members can be classified as Class I and Class II DYRKs. The percentage of conservation at the protein level between orthologues is indicated above the arrows and between 2 paralogues is indicated in parentheses within the boxes [Adopted from (Aranda et al., 2011)].

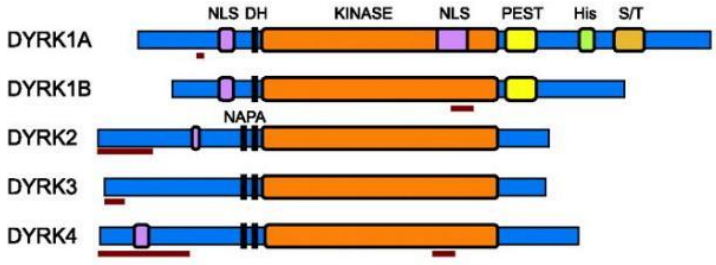

Figure 2: Schematic representation of the domain structure of the 5 mammalian DYRKs.
Different functional motifs are indicated. Red lines indicate regions of the protein affected by alternate splicing events [Adopted from (Aranda et al., 2011)].

1.2. *DYRK1A* is a dosage sensitive gene

In humans, DYRK1A protein is encoded by the *DYRK1A* gene which is located in the 'Down syndrome Critical Region' on chromosome 21 (Korbel et al., 2009; Ohira et al., 1997). Trisomy of this critical region results in Down syndrome (Korbel et al., 2009; Ohira et al., 1997). It was suggested that DYRK1A overexpression could contribute to the depletion of neurons in the developing brain of the DS fetuses either due to the precocious onset of neurogenesis in progenitors leading to the concomitant depletion of the proliferating progenitor pool or by inducing a premature cell cycle arrest of the neurogenic progenitors leading to a decrease in the number of neurons generated by each progenitor (F. J. Tejedor & Hämmerle, 2011). On the other hand, intragenic deletion or loss of one copy of DYRK1A gene has also been recognized as a syndrome with characteristic features such as microcephaly, severe mental retardation and speech impairment (Bronicki et al., 2015; Ji et al., 2015). As both gain and loss of one allele of *DYRK1A* results in developmental abnormalities, this gene is highly dosage sensitive. This dependence on optimum dosage of *DYRK1A* is conserved across evolution. Mini brain (*Mnb*) in Drosophila is the closest homolog of mammalian *DYRK1A* (Figure 1b) and is involved in neural proliferation and differentiation in Drosophila. It was observed that flies with a *Mnb* loss of function developed a smaller adult brain (Tejedor et al., 1995). Furthermore, in mice, homozygous deletion of *Dyrk1a* is embryonically lethal, whereas mice having only one copy of *Dyrk1a* have reduced brain size and display specific neurological and behavioral defects and febrile seizures (Fotaki et al., 2002; Raveau et al., 2018). Moreover, mouse models of *Dyrk1a* trisomy recapitulate some of the DS phenotypes (Ahn et al., 2006; Altafaj et al., 2001; F. J. Tejedor & Hämmerle, 2011). DYRK1A also plays a role in neural stem development and is

necessary for neurogenesis, neural differentiation, cell death and synaptic plasticity across different species (Dierssen & de Lagrán, 2006; F. J. Tejedor & Hämmerle, 2011).

1.3. DYRK1A in other neurological diseases

DYRK1A is also implicated in several other neurological diseases like dementia, Alzheimer's disease, Parkinson's disease and Pick's disease. DYRK1A is one of the kinases responsible for phosphorylation of α-synuclein which is a candidate biomarker of Parkinson's disease (PD) (E. J. Kim et al., 2006; Spillantini et al., 1997). An increase of α-synuclein in the brain, leading to aggregation and subsequently sequestration in Lewy Bodies, is a hallmark of PD.

Alzheimer's disease pathology includes amyloid-β (Aβ) accumulation and hyperphosphorylation of the microtubule binding protein -Tau (Querfurth & LaFerla, 2010). Hyperphosphorylated Tau is pathologic and has lesser affinity to microtubules. Pathological Tau forms neurofibrillary tangles (NFTs) and insoluble inclusions which is a feature of Alzheimer's disease and other Tauopathies (Medina et al., 2016). DYRK1A is about 1.5 fold overexpressed in DS (Becker et al., 2014). Early onset AD is common in DS patients and one possible reason is the hyperphosphorylation of Tau by DYRK1A (F. Liu et al., 2008; Wegiel et al., 2011). Indeed, DYRK1A phosphorylates Tau at multiple serine and threonine residues (Azorsa et al., 2010; Ryoo et al., 2008). Interestingly, mice overexpressing DYRK1A have increased phosphorylated Tau in the brain and crossing the DYRK1A heterozygous mice with DS mice regulates phosphorylated Tau and amyloid load (García-Cerro et al., 2017). Furthermore, overexpression of DYRK1A was observed in postmortem brains of AD patients, supporting the contribution of DYRK1A to tau hyperphosphorylation and accumulation of NFTs (Ferrer et al., 2005). Thus, inhibition of DYRK1A is being considered to alleviate problems caused by Tau phosphorylation in AD. Furthermore, studies in AD mice models or transgenic mice with Tau pathology have

further supported that DYRK1A can be a potential target for AD and other Tauopathies (Branca et al., 2017; Melchior et al., 2019).

1.4. Some of the known DYRK1A substrates

Several reported substrates of DYRK1A harbor a consensus sequence that includes the R-X(XX)-S/T-P motif. Analysis of *in-vitro* phosphorylated synthetic peptide substrates established DYRK1A's preference for arginine residue in the -2 or -3 position and for a proline at the +1 position (Himpel et al., 2001; Himpel et al., 2000).

Depending on its cellular localization, DYRK1A is responsible for the phosphorylation of several proteins involved in important signaling pathways, such as the cell cycle and transcription (Duchon & Herault, 2016; Kaczmarski et al., 2014; Martí et al., 2003; Park et al., 2012). Apart from the substrates already mentioned above, DYRK1A phosphorylates Nuclear Factor of Activated T cells (NFAT), cAMP Response Element Binding protein (CREB), Signal Transducer and Activator of Transcription 3 (STAT3), Glioblastoma associated oncogene protein (GLI1), splicing factors (cyclin L2, SF2, SF3), a translation factor (eIF2Be), miscellaneous proteins (glycogen synthase, caspase-9, Notch) and synaptic proteins (dynamin I, amphiphysin I, synaptojanin) (Duchon & Herault, 2016). Additional DYRK1A substrates include cyclin D1, p53, p27, RNA polymerase II and the LIN52 subunit of the DREAM repressor complex, as well as Caspase 9 ((J.-Y. Chen et al., 2013; Di Vona et al., 2015; Litovchick et al., 2011; Najas et al., 2015; Park et al., 2009, 2010; Soppa et al., 2014). In addition to these substrates, DYRK1A interacts with several proteins that may regulate its function or subcellular localization including DCAF7 and 14-3-3 (Alvarez et al., 2007; Glenewinkel et al., 2016; D. Kim et al., 2004; Miyata & Nishida, 2011; Ritterhoff et al., 2010).

1.5. DYRK1A's role in DREAM complex assembly and cancer

The activity of E2F transcription factors is regulated by the retinoblastoma (RB) family of proteins which includes pRB, p107 and p130 (Cobrinik, 2005). The RB family proteins act as tumor suppressors in a hypo-phosphorylated form when they bind E2F transcription factors and inhibit E2F mediated transcription. Phosphorylation of RB family members by cyclin-dependent kinases (CDKs) in the G-1 phase of the cell cycle relieves the binding and inhibition of E2Fs (Cobrinik, 2005; Malumbres & Barbacid, 2009). In cells entering quiescence, p130 accumulates in response to serum starvation, confluency or pINK4a expression (Cam et al., 2004; E. J. Smith et al., 1996). Furthermore, p130 was found to be the predominant RB family member that interacts with MuvB core protein complex consisting of RBBP4, LIN9, LIN37, LIN52 and LIN54. Mass spectroscopy proteomic analysis and biochemical validation in human cell lines revealed that p130 interacts with E2F4, DP1 and the MuvB core, forming the DREAM complex in G0/G1 but not in the S-phase, and subsequently causes repression of DREAM target genes (Litovchick et al., 2007; Schmit et al., 2007). In S phase, the MuvB core dissociates from the p130-DREAM complex and binds BMYB in order to promote transcription of the MMB (MYB-MuvB) target genes (Litovchick et al., 2007; Schmit et al., 2007). DYRK1A specifically phosphorylates the serine 28 (S28) residue on LIN52 (Figure 3) (Litovchick et al., 2011). This phosphorylation of LIN52 at S28 was found to be required for DREAM assembly. Furthermore, DYRK1A overexpression was found to inhibit proliferation of several human cancer cell lines including T98G, U-2 OS, but not HEK 293T (Figure 3) (Litovchick et al., 2011).

Further, point mutation of LIN52 at S28 or inhibition of DYRK1A activity disrupts DREAM assembly and reduces the ability of cells to enter quiescence or undergo Ras-induced senescence

(Litovchick et al., 2011). Thus, DYRK1A has been found to play an important role in the regulation of DREAM activity and entry into quiescence.

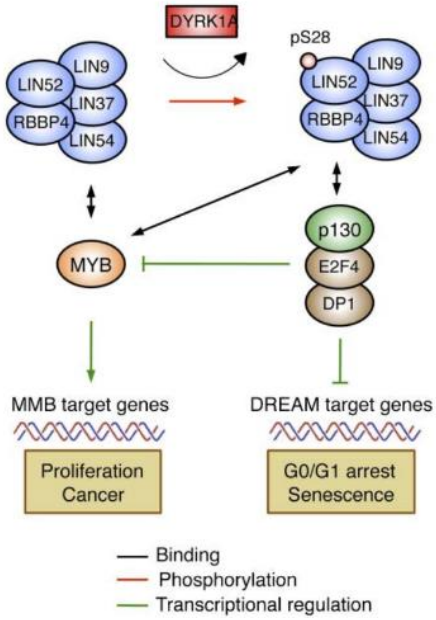

Figure 3: Schematic representation depicting how DYRK1A promotes DREAM complex assembly, G0/G1 arrest and senescence. [Adopted from (Litovchick et al., 2007)].

Interestingly, DS patients have a lower risk of solid tumors but DS children specifically carry a higher risk for developing leukemias (Hasle et al., 2000). DYRK1A is known to influence both tumor suppressive and tumorigenic activities by regulating its substrates and hence it has been termed as a double edged kinase (Fernández-Martínez et al., 2015). DYRK1A substrates can function as pro- or anti-oncogenic factors (Figure 4).

1.6. DYRK1A inhibitors

Due to DYRK1As role in human disease, its pharmacological inhibition has been a focus of research for several years. Potent plant derived inhibitors of DYRK1A include Harmine and Epigallocatechin-gallate (EGCG), the poly phenolic compound in green tea. Synthetic DYRK1A

inhibitors include INDY, proINDY, roscovitine, purvalanol A, pyrazolidine-diones, amino-quinazolines, meridianins, pyridine and pyrazines, and chromenoidole with varying potencies towards DYRK1A (H. Kim et al., 2016; B. Smith et al., 2012). DYRK1A inhibitors can further be divided into three major classes. The type I inhibitors bind the ATP binding site in the kinase domain of DYRKs and type II and type III inhibitors are non-ATP mimetics. Harmine, an ATP competitive inhibitor of DYRK1A, is a plant alkaloid derivative, whereas EGCG is a non-competitive ATP inhibitor of DYRK1A (Adayev et al., 2006; Bain et al., 2003; Duchon & Herault, 2016; Göckler et al., 2009). The use of EGCG has been limited due to poor pharmacokinetic properties and limited bioavailability (Duchon & Herault, 2016). Along with effectively inhibiting DYRK1A mediated substrate phosphorylation, Harmine has been found to inhibit the autophosphorylation of DYRK1A (Walte et al., 2013). Although very potent, clinical use of Harmine is limited because it is also a monoamine oxidase inhibitor (Duchon & Herault, 2016). Other potent inhibitors of DYRK1A include INDY or proINDY but their use has also been limited (Duchon & Herault, 2016). Recently, the well-known ATP competitive casein kinase II and CLK inhibitor CX4945 was also found to be a potent inhibitor of DYRK1A (H. Kim et al., 2016). This drug has already been successful in clinical trials for cancer treatment (Siddiqui-Jain et al., 2010). It has also proven efficient in Drosophila and mouse models of DYRK1A overexpression and hence holds promise (H. Kim et al., 2016). Additional novel DYRK1A inhibitors have been identified that can induce DYRK1A degradation and are supposed to be more potent than the current inhibitors, but further research is required to evaluate their potential for therapeutic use (Branca et al., 2017; Melchior et al., 2019; Velazquez et al., 2019).

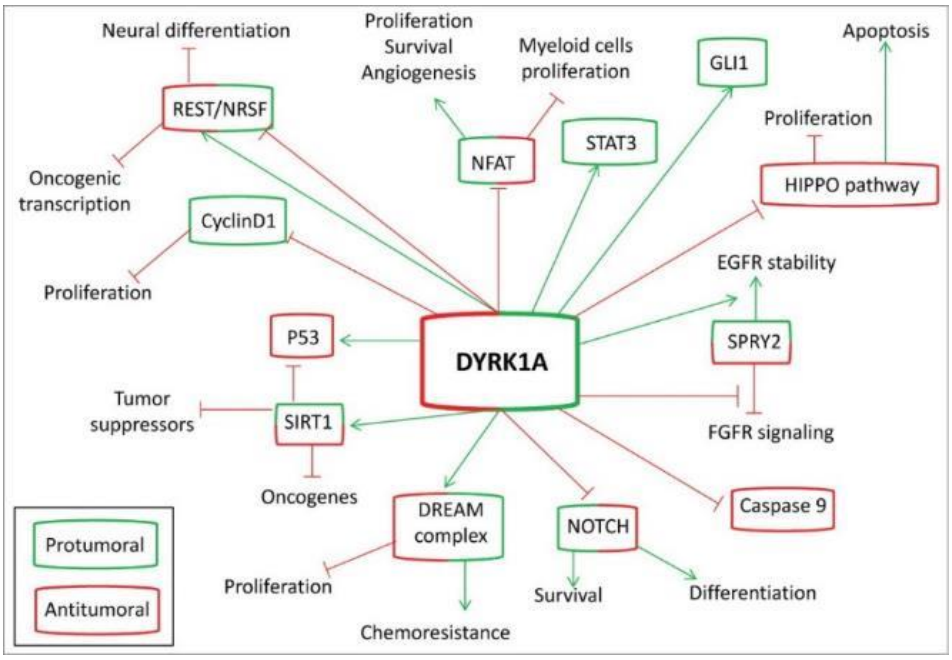

Figure 4: Pro and anticancer functions of DYRK1A.
DYRK1A has been associated with pro-tumoral activity (green boxes) by activating (green arrows) known oncogenes or by inhibiting (red lines) tumor suppressors (red boxes) [Adopted from (Fernández-Martínez et al., 2015)].

1.7. Understanding the function and regulation of DYRK1A through its interacting proteins

Even though DYRK1A is such an important kinase, its function and regulation is poorly understood. Hence, multiple groups have recently studied the proteomic landscape of DYRK1A. The BioGrid protein interaction network database lists 90 unique proteins that interact with human DYRK1A (thebiogrid.org). Most of these interactors have been identified by high-throughput affinity-capture mass spectrometric analyzes performed in HEK293T cells. The glioblastoma cell line T98G, but not HEK293T, was one of the cell lines whose proliferation was suppressed with ectopic expression of DYRK1A (Litovchick et al., 2011). Therefore, we used the sensitive MudPIT proteomic approach (Florens & Washburn, 2006; Swanson et al., 2009) to

detect DYRK1A interacting proteins in T98G cells. We identified 120 proteins specifically detected in at least two out of four biological replicate analyses of DYRK1A immunoprecipitates, including 98 novel interactors not reported to bind DYRK1A in the BioGrid protein interaction database (Figure 5) (Menon et al., 2019).

Furthermore, our analysis detected 51 proteins in 3 out of 4 DYRK1A pull-down repeats and 7 proteins including DYRK1A, DCAF7, FAM117A, FAM117B, LZTS2, RNF169 and TROAP, were identified in all 4 biological replicates (Menon et al., 2019). These interacting proteins were also the most enriched in the samples and their interaction with DYRK1A was confirmed using reciprocal pull-down assays (Menon et al., 2019). Of note, average enrichment of DCAF7 in the immunoprecipitated samples (as shown by Normalized Spectrum Abundance Factor, or dNSAF (Sardiu et al., 2008), was comparable to that of DYRK1A itself, indicating a potentially stoichiometric interaction. Further, bioinformatic analysis of the 51 DYRK1A-binding proteins revealed a complex network of interactions of factors involved in different cellular processes, with notable enrichment of the mRNA processing, transcription and DNA damage response functional categories (Menon et al., 2019). Previous proteomic analysis of DYRK1A in HEK293T cells identified 24 interacting proteins, 14 of which were also detected in our study (Menon et al., 2019; Varjosalo et al., 2013). Two other groups also subsequently reported the DYRK1A interactome in HeLa cells. Interestingly, even with different cell types, there is a considerable overlap of DYRK1A interacting proteins found in our study with the proteins reported in these studies (Guard et al., 2019; Menon et al., 2019; Roewenstrunk et al., 2019; Varjosalo et al., 2013), including DCAF7, RNF169, FAM117B, LZTS2 and TROAP.

In this thesis, we have focused on characterizing some of the novel DYRK1A protein-protein interactions, and an introduction to each of these is included in subsequent chapters 2 and 3.

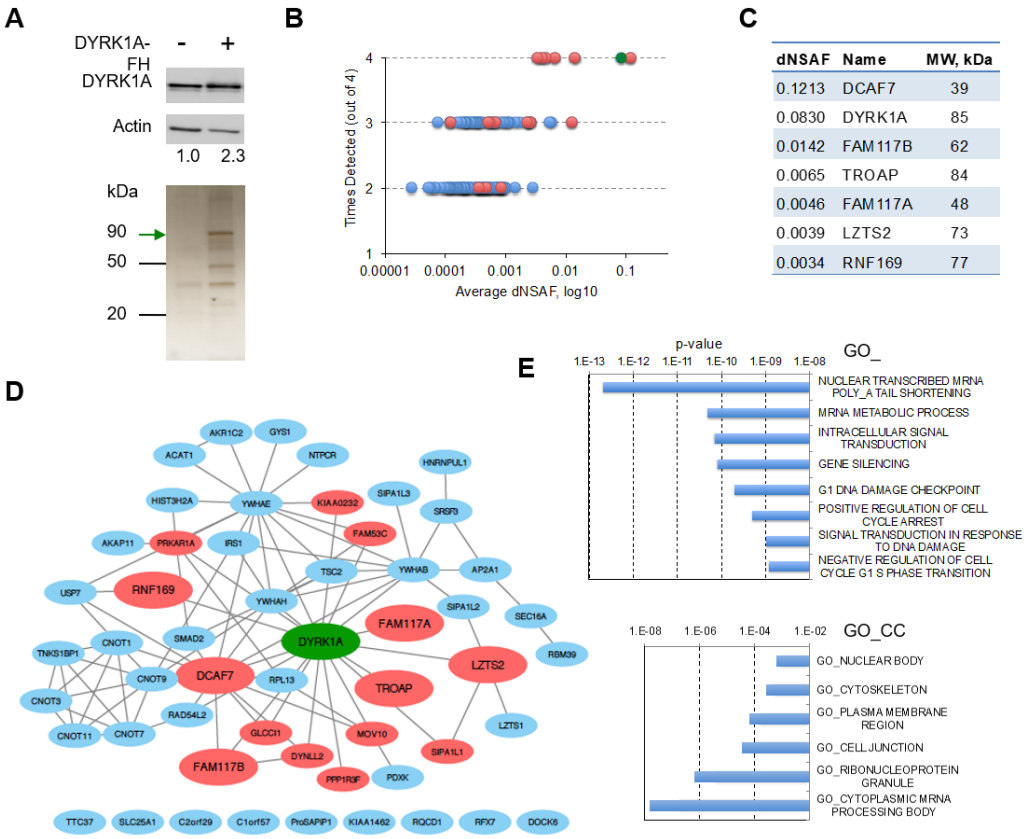

Figure 5: Analysis of the DYRK1A-interacting protein network.
(A). Purification of DYRK1A for MudPIT proteomic analysis. Top: representative western blot showing levels of DYRK1A in T98G cells expressing HA-Flag-tagged DYRK1A (DYRK1A-FH) and DYRK1A band density relative to Actin (control). Bottom: representative silver stained gel containing 10% of HA-peptide eluted control or DYRK1A-FH IP samples analyzed by MudPIT. Green arrow indicates DYRK1A. (B) Graph shows relative enrichment (dNSAF) of proteins detected in two, three or all four DYRK1A MudPIT experiments. DYRK1A is shown as a green circle whereas red and blue circles correspond to interacting proteins either listed in the BioGrid database, or new DYRK1A-binding proteins, respectively. (C) dNSAF (corresponds to relative enrichment) and molecular weight (MW) of seven proteins specifically detected in four DYRK1A-FH MudPIT replicate experiments. (D) Hierarchical network of interactions (CytoScape) involving DYRK1A-binding proteins identified in this study, constructed using MetaScape analysis tool. Larger nodes correspond to proteins detected in all four replicates, smaller nodes correspond to proteins detected in three replicates. Unconnected nodes are not known to interact with other factors. Colors, as in panel B (E) Molecular Signature Database (MSigDB) annotation of the genes encoding DYRK1A-interacting proteins reveals significantly enriched functional gene ontology (GO) categories. Proteins detected in at least 3 DYRK1A MudPIT repeats were analyzed using Molecular Signature Database annotation tool to compute overlaps with GO Biological Process (GO_BP) and GO Cellular Component (GO_CC) gene sets [Adopted from (Menon et al., 2019)].

CHAPTER 2: CHARACTERIZATION OF THE DYRK1A-RNF169 INTERACTION AND ITS FUNCTION IN THE DNA DAMAGE RESPONSE PATHWAY

(Adapted from Menon V, Ananthapadmanabhan V et al., 2019)

2.1. INTRODUCTION TO THE CHAPTER

MudPIT analysis carried out to identify DYRK1A interacting proteins detected RNF169 (Ring Finger protein 169) in all four biological replicates (Figure 5) (Menon et al., 2019). RNF169 plays a role in the DNA damage response (An et al., 2018; Poulsen et al., 2012) while DYRK1A had no known role in this process. We therefore carried out a functional characterization of the DYRK1A-RNF169 interaction in this chapter.

2.1.1. The DNA damage response

Cellular exposure to various DNA damaging agents, be it environmental or endogenous, is harmful and leads to impaired DNA integrity and genomic instability leading to disease. Of the many types of DNA lesions, DNA double strand breaks (DSBs) are considered the most harmful. This is because a single DSB is sufficient to cause growth arrest and cell death (Bennett et al., 1993; Panier & Boulton, 2014; Sandell & Zakian, 1993). Whenever there is a DNA DSB, the MRE-11-RAD 50-NBS1 (MRN) complex senses the break. This leads to recruitment of the serine/threonine kinase Ataxia Telangiectasia Mutated (ATM) which phosphorylates itself and becomes activated (Panier & Boulton, 2014; Paull, 2015). At the break site, ATM in turn phosphorylates H2A.X at ser 139 (γH2AX) (Panier & Boulton, 2014; Rogakou et al., 1998). γH2AX is used as an early marker of the DNA DSB response. γH2AX is recognized by Mediator of DNA Damage Checkpoint protein 1 (MDC1), leading to the sequential recruitment of E3

ubiquitin ligases RNF8 and RNF168. RNF8, RNF168 and an E2 conjugating enzyme UBC13 together regulate the ubiquitination of histones surrounding the DSB sites. One of the outcomes of RNF8 and RNF168-mediated chromatin ubiquitylation is a stable recruitment of oligomerized p53-binding protein 1 (53BP1), which directly binds to RNF168-ubiquitylated H2AK15 and to mono- and di-methylated H4K20 (Panier & Boulton, 2014). 53BP1 is a key factor that can influence pathway choice during the repair process. Specifically, 53BP1 phosphorylation by ATM leads to recruitment of RIF1, and the 53BP1-RIF1 complex promotes the DNA repair via the Non-Homologous End Joining pathway or NHEJ (Escribano-Díaz et al., 2013). This pathway can introduce errors in the genome as it involves minor processing of the DNA ends prior to the direct ligation of the DSB. In the S-G2 phase of the cell cycle, BRCA1 antagonizes the 53BP1-RIF1 complex and promotes the more accurate HRR (Homologous Recombination Repair) facilitated by end resection via Mre11 and C-terminal binding protein-interacting protein (CtIP) (Escribano-Díaz et al., 2013).

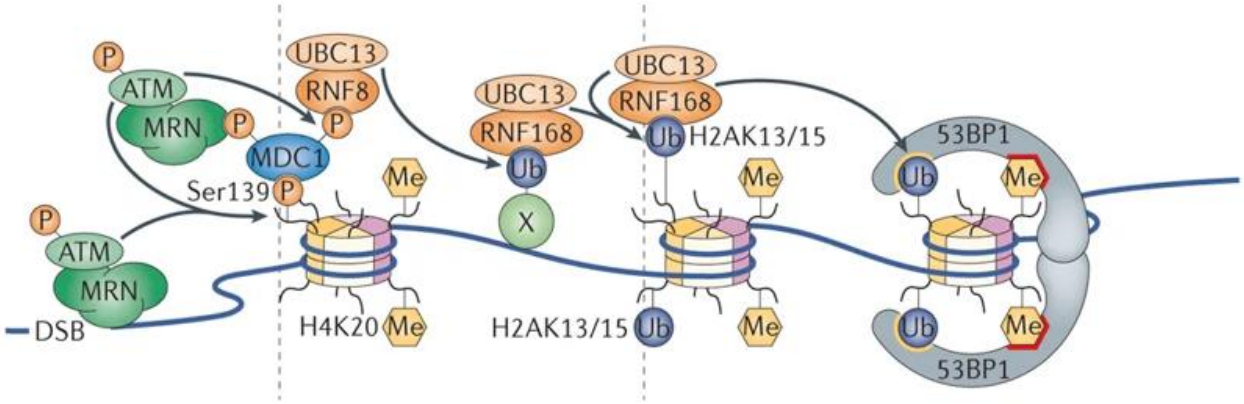

Figure 6: The complexity of signal transduction pathway following a DNA DSB break. DNA damage response elicits a sequential cascade leading to accumulation of 53BP1 at the damage sites [Adopted from (Panier & Boulton, 2014)].

RNF169 has been reported to be a negative regulator of 53BP1 accumulation at the sites of DNA DSBs (Poulsen et al., 2012). RNF169 binding thereby promotes cells to favor HR repair instead

of NHEJ (An et al., 2018). The role of DYRK1A in the DNA damage response was poorly studied and this chapter will highlight our findings on the role of the DYRK1A-RNF169 interaction in the DNA DSB response pathways. Notably, post the publication of our study, two other groups also reported the DYRK1A-RNF169 interaction and its role in the DNA damage response (Guard et al., 2019; Roewenstrunk et al., 2019).

2.2. RESULTS

2.2.1. DYRK1A and RNF169 interact at the endogenous level and co-fractionate together

First, we confirmed the interaction between exogenously expressed HA-tagged RNF169 and endogenous DYRK1A in T98G cells using immunoprecipitation and Western blot analysis (IP/WB) (Figure 7A). Using reciprocal IP/WB analysis, interaction between DYRK1A and RNF169 was also confirmed at the endogenous level in both T98G and U-2 OS cell lines (Figure 7B, C). We also observed that the kinase activity of DYRK1A was not required for the DYRK1A-RNF169 interaction (Figure 7D). Furthermore, we found that DYRK1A and RNF169 co-fractionated together in T98G cell lysates subjected to glycerol gradient ultracentrifugation, and the estimated approximate size of the DYRK1A-RNF169 complex was 280 kDa (Figure 7E).

2.2.2. DYRK1A and RNF169 regulate the recruitment of 53BP1 at sites of DNA DSBs

U-2 OS cells retain wild type p53 making this cell line a common model for DNA damage-focused studies. Moreover, these cells have also been used to characterize the regulatory role of RNF169 towards 53BP1 recruitment into γ-irradiation induced foci (IRIF). In preliminary experiments, we observed that U-2 OS cells displayed the maximum number of distinct 53BP1 IRIF at 3h post γ-irradiation (5Gy, data not shown). We therefore decided to induce DNA damage using γ-irradiation followed by analysis of foci accumulation 3 hours post irradiation in our subsequent experiments. We used U-2 OS cell lines stably expressing either wild type or

kinase inactive DYRK1A-K188R mutant under control of a doxycycline (dox)-inducible promoter to analyze the role of DYRK1A in the regulation of 53BP1 upon DNA damage (Himpel et al., 2001; Litovchick et al., 2011). Interestingly, induced expression of WT but not kinase-inactive DYRK1A resulted in significantly decreased number of cells displaying more than 10 53BP1 IRIF compared to the un-induced control (Figure 8A, B and 9A). In order to analyze if RNF169 was required for this effect, we transiently knocked down RNF169 and observed that recruitment of 53BP1 into IRIFs in the WT DYRK1A overexpressing cells was rescued to the control cell levels (Figure 8C, D and 9B).

We further investigated the role of DYRK1A kinase activity by using the DYRK1A inhibitor Harmine. U-2 OS cells were treated with 10μM of Harmine for 16 hours prior to γ-irradiation and the accumulation of 53BP1 IRIFs was quantified. Interestingly, recruitment of 53BP1 to foci was increased with Harmine pre-treatment as compared to vehicle treated controls (Figure 10A, B). For most accurate quantification of our observations, we calculated both the percentage of cells containing more than ten IRIF, as well as an average number of IRIF per nucleus, using ImageJ software (Schneider et al., 2012). Consistent with previous reports, with stable HA-RNF169 overexpression, we also observed a 50% reduction in the number of cells with more than 10 53BP1 IRIFs as well as fewer IRIFs per nucleus (compare grey bars, figure 10C).

Harmine treatment of HA-RNF169- expressing cells resulted in increase in 53BP1 foci formation although it was not fully rescued to the control levels (red bars and graph on the right Y-axis). Interestingly, in the cells treated with Harmine, HA-RNF169 foci formation was reduced by approximately 30% as compared to controls (compare green bars, figure 10C). This could explain the increase in 53BP1 IRIFs with Harmine treatment. We also analyzed the binding between DYRK1A and RNF169 after the cells were treated with Harmine. Similar to kinase-

dead DYRK1A, RNF169 from Harmine treated cells also bound endogenous DYRK1A efficiently (Figure 10D). These results demonstrate that RNF169 and DYRK1A interact at the endogenous level in human cells and that DYRK1A facilitates RNF169's limiting function towards 53BP1 IRIF recruitment.

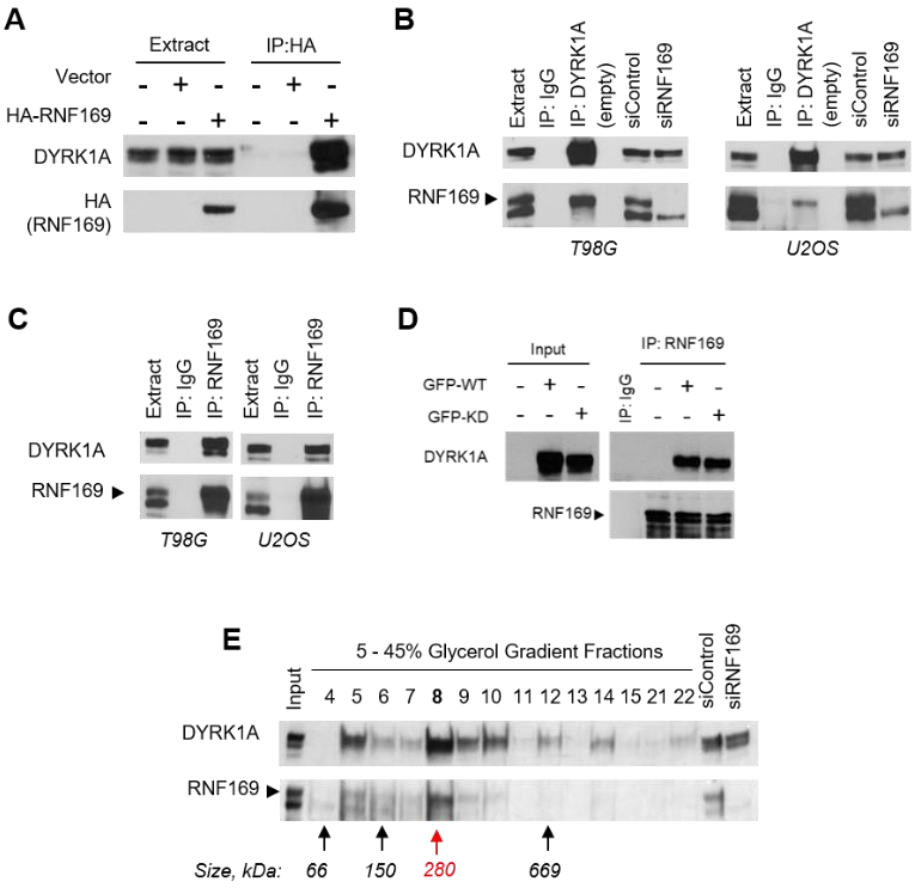

Figure 7: DYRK1A and RNF169 interact at the endogenous level and co-fractionate together.

(A) IP/WB assay shows binding between transiently expressed HA-tagged RNF169 and endogenous DYRK1A in T98G cells. (B, C) IP/WB analyzes of the interaction between the endogenous RNF169 and DYRK1A in T98G and U-2 OS cells. RNF169-depleted cell extract (siRNF169) is included to identify the RNF169-specific protein band. IgG, negative control. (D) IP/WB assay shows interaction between the wildtype and the kinase-inactive DYRK1A (Y321F) and the endogenous RNF169 in U-2 OS cells. (E) WB of the U-2 OS cell extract separated by 5–45% glycerol gradient ultracentrifugation shows co-fractionation of RNF169 and DYRK1A. Black arrows indicate the positions of the molecular weight markers. Red arrow indicates estimated size of the DYRK1A-RNF169 complex.

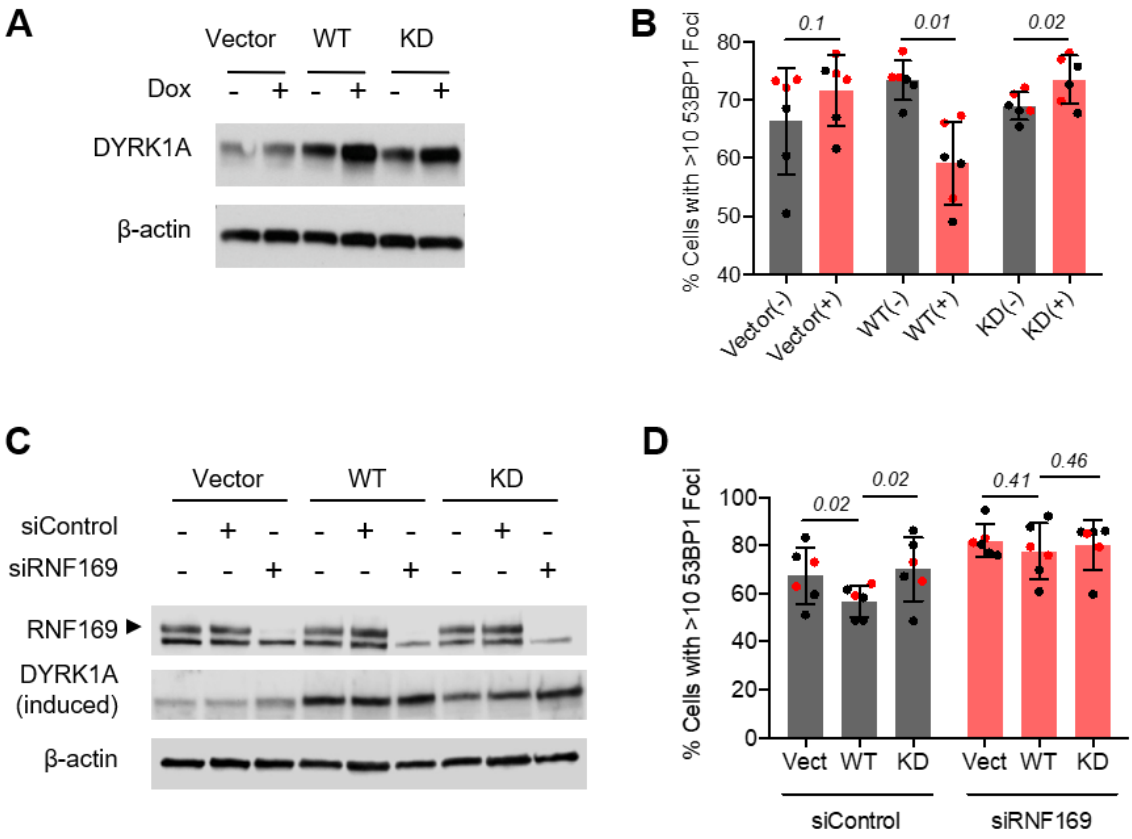

Figure 8: DYRK1A and RNF169 regulate 53BP1 recruitment at DNA DSB.
(A) WB shows the DYRK1A levels in the inducible U-2 OS cell lines under un-irradiated conditions before and after doxycycline (Dox) treatment for 12h. Actin is shown as loading control. (B) The inducible U-2 OS cell lines were pre-incubated with or without Dox for 12h, treated with radiation (5 Gy) and processed for 53BP1 staining after 3h. Induced expression of active but not kinase-inactive (KD) DYRK1A (K188R) inhibits 53BP1 IRIF formation. Graph shows quantification of cells with 53BP1 foci in cell lines with (+) or without (-) Dox induction of 3 biological replicate experiments. Error bars show standard deviation. Red and black dots indicate quantifications by two independent observers. p-values were calculated using Student's two-tailed t-test and are indicated on the graphs. (C, D) Knockdown of RNF169 rescues DYRK1A-mediated inhibition of 53BP1 foci formation. Inducible U-2 OS cell lines were transfected with non-targeting (siControl) or RNF169-specific siRNA and treated with doxycycline as in panels A, B to induce expression of DYRK1A. WB in panel C shows expression of proteins of interest. Panel D shows quantification of the 53BP1 foci in cells. Samples were processed in the same way as in B. Graph shows average of 3 biological replicates. Error bars show standard deviation. Red and black dots same as in B and p-values calculated using Student's two-tailed t-test are indicated on the graphs.

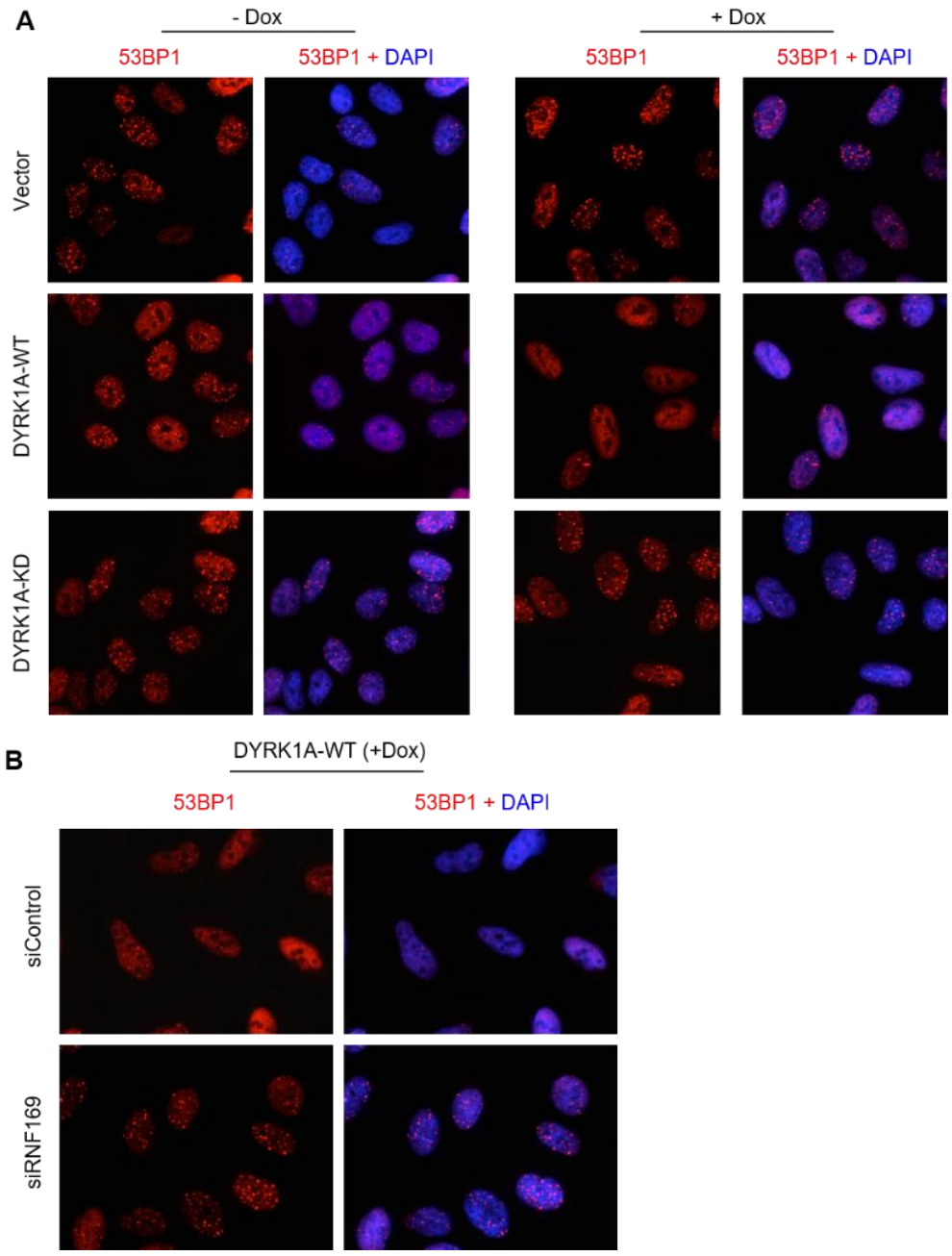

Figure 9: Induced expression of DYRK1A inhibits 53BP1 accumulation at the DSB sites. (A) Representative images of inducible U-2 OS cell lines expressing wild-type DYRK1A (WT) or kinase inactive mutant (KD), with or without treatment with doxycycline for 16h. Cells were γ-irradiated (5Gy) and incubated for 3h before staining with anti-53BP1antibody and DAPI. (B) Representative images of U-2 OS cells with induced expression of the wild-type DYRK1A, transfected with either non-targeting (siControl) or RNF169-specific siRNA, γ-irradiated (5Gy) and incubated for 3h before staining with anti-53BP1antibody and DAPI. See Figure 8 for representative WB showing expression of proteins of interest in the cell lines used.

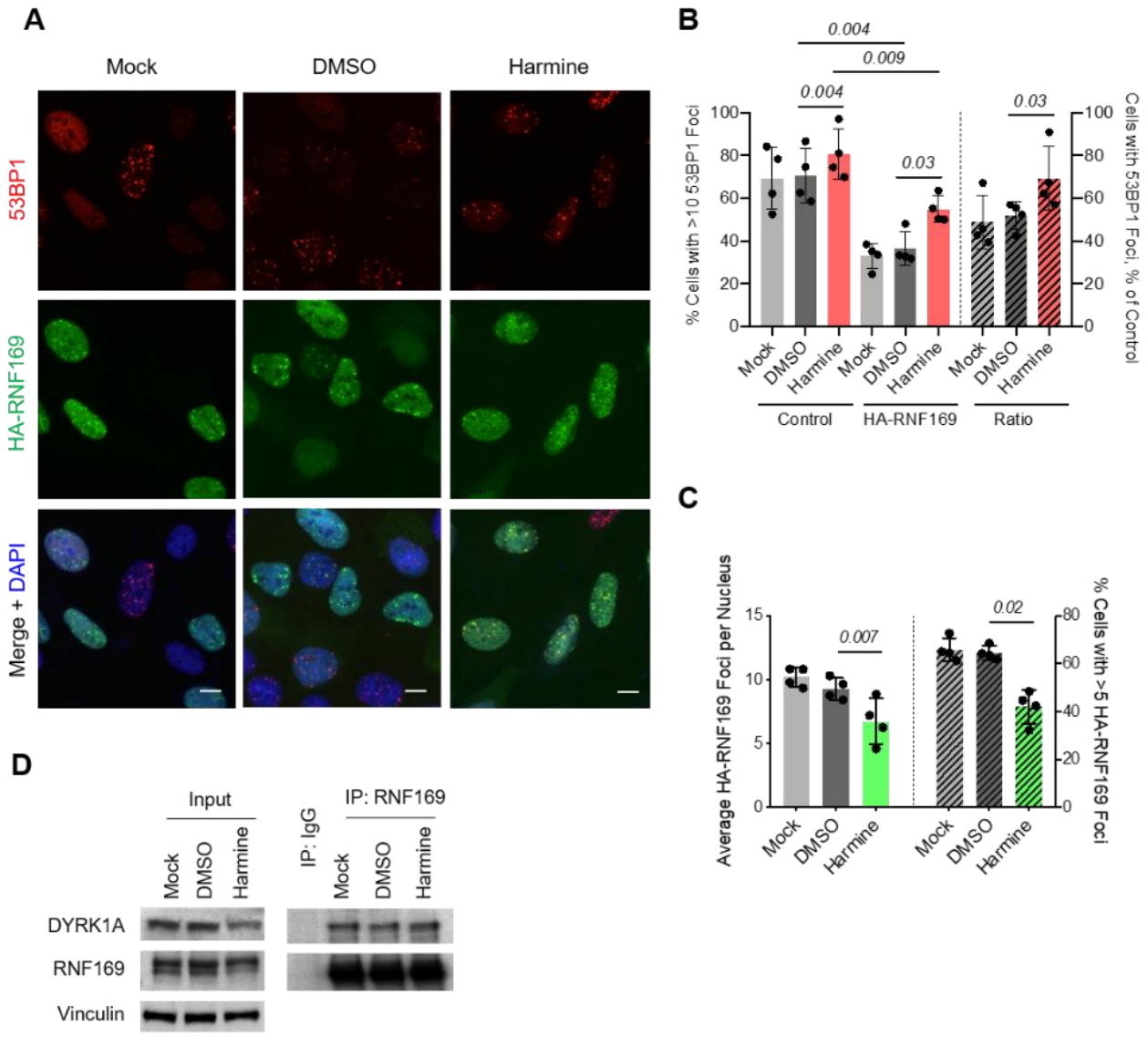

Figure 10: Inhibition of DYRK1A increases 53BP1 recruitment to IRIF.
(A) Representative images of HA-RNF169 and 53BP1 irradiation induced foci in U-2 OS cells stably expressing HA-RNF169 that were either untreated (Mock), or pre-treated with 10 μM Harmine or DMSO (vehicle) for 16h before irradiation (5 Gy) and processed for staining after 3h. (B, C) Graphs show quantification of the 53BP1 or HA-RNF169 IRIF from 4 biological replicate experiments. Error bars show standard deviation. p-values were calculated using Student's two-tailed t-test and are indicated on the graphs in panels B and C. (D) IP/WB shows that DYRK1A-RNF169 interaction is unaffected by Harmine treatment.

2.2.3. DYRK1A phosphorylates RNF169 at functionally important Ser368 and Ser403 residues

By scanning through the RNF169 protein sequence, we found that RNF169 contains two predicted DYRK1A consensus phosphorylation sites (Menon et al., 2019). These sites were identified at positions S386 and S403 in the human RNF169 protein sequence. The region in RNF169 encompassing these sites was found to be highly conserved but had no known function. Both of these sites were reported in Phosphosite plus database as detected in several high throughput phosphoproteomic studies (Hornbeck et al., 2012). Using stable cell lines expressing mutants of RNF169, and *in-vitro* kinase assays with recombinant DYRK1A, we found that DYRK1A indeed phosphorylates RNF169 at both the predicted sites - S386 and S403 (Menon et al., 2019).

To characterize the functional significance of DYRK1A phosphorylation sites in RNF169, we analyzed accumulation of 53BP1 and RNF169 after induction of DNA damage by γ-irradiation in U-2 OS cell lines stably expressing either wild type HA-RNF 169, non-phosphorylatable S368A/S340A (RNF169-AA) mutant, or phospho-mimetic S368D/S340D (RNF169-DD) mutant (Figure 11). Interestingly, there was approximately two-fold higher number of cells with more than ten 53BP1 foci in either RNF169-AA or RNF169-DD-expressing cells compared to the wild type HA-RNF169 cell line (Figure 11A, B). As compared to the wild-type expressing cells, there was a modest but significant increase in the number of 53BP1 foci per nucleus in the cells expressing mutant RNF169 alleles, indicating that phospho-site mutant RNF169 proteins inhibit accumulation of 53BP1 at DSB sites to a significantly lesser extent than the wild type RNF169 (Figure 11A, B). This result is consistent with the effect of Harmine, supporting the contribution of DYRK1A to the RNF169-mediated inhibition of 53BP1 accumulation at the DSB sites.

Next, we analyzed the recruitment of the HA RNF169-AA and DD mutants to DSB sites in γ irradiated U-2 OS cell lines. Interestingly, there was a slight but significant decrease in the number of HA positive foci in the cells expressing the mutant proteins as compared to the wild type RNF169 (Figure 11A, C). Despite the differences observed with accumulation of 53BP1 and HA-RNF169 at IRIF between the wild type and RNF169 mutant expressing cell lines, the expression levels of the respective HA-RNF169 or 53BP1 proteins were similar across the cell lines (Figure 11E). We also observed that IRIF formed by the mutant HA-RNF169 proteins appeared to be larger in size than in case of the wild type protein (Figure 11D). Indeed, analysis of the foci size using ImageJ software revealed a significant increase of the mean size of the RNF169- AA and DD foci compared to the wild type control. Of note that the phenotype we observed with the phosphomimetic mutant of RNF169 (RNF169-DD) was very similar to that of the phospho deficient (RNF169-AA) mutant. This could mean that the phosphomimetic mutant of RNF169 does not accurately represent a constitutively phosphorylated state of the protein. It appears that it instead disrupts the same function. Therefore, it was important to test the impact of the mutation of DYRK1A phosphorylation sites on some other known function of RNF169.

The ubiquitin-binding MIU domain of RNF169 recognizes RNF168-polyubiquitylated histones. This recognition has been found to be required for the recruitment of RNF169 at the DSB sites and for the displacement of 53BP1 (J. Chen et al., 2012; Panier & Boulton, 2014; Poulsen et al., 2012). Interestingly, we observed that RNF169-AA and RNF169-DD mutants were able to bind polyubiquitin chains similar to the wild type RNF169, further supporting our conclusion that S368 and S403 sites do not play a significant role in RNF169's accumulation at the DSB sites (Menon et al., 2019). USP7 (Ubiquitin Specific protease 7) has been reported to be important for RNF169 function in DNA repair (An et al., 2018). We found that mutations of DYRK1A

phosphorylation sites on RNF169 did not affect the interaction between RNF169 and USP7 (Menon et al., 2019). However, we found that both mutants showed a dramatically reduced binding to DYRK1A, both in the un-irradiated controls or post treatment with γ-irradiation (Menon et al., 2019). Therefore, these RNF169 mutants not only lack DYRK1A mediated phosphorylation but also bind less to DYRK1A. We were therefore able to support the conclusion that DYRK1A binding and phosphorylation of RNF169 increases its ability to limit the recruitment of 53BP1 at the DSB sites after γ-irradiation.

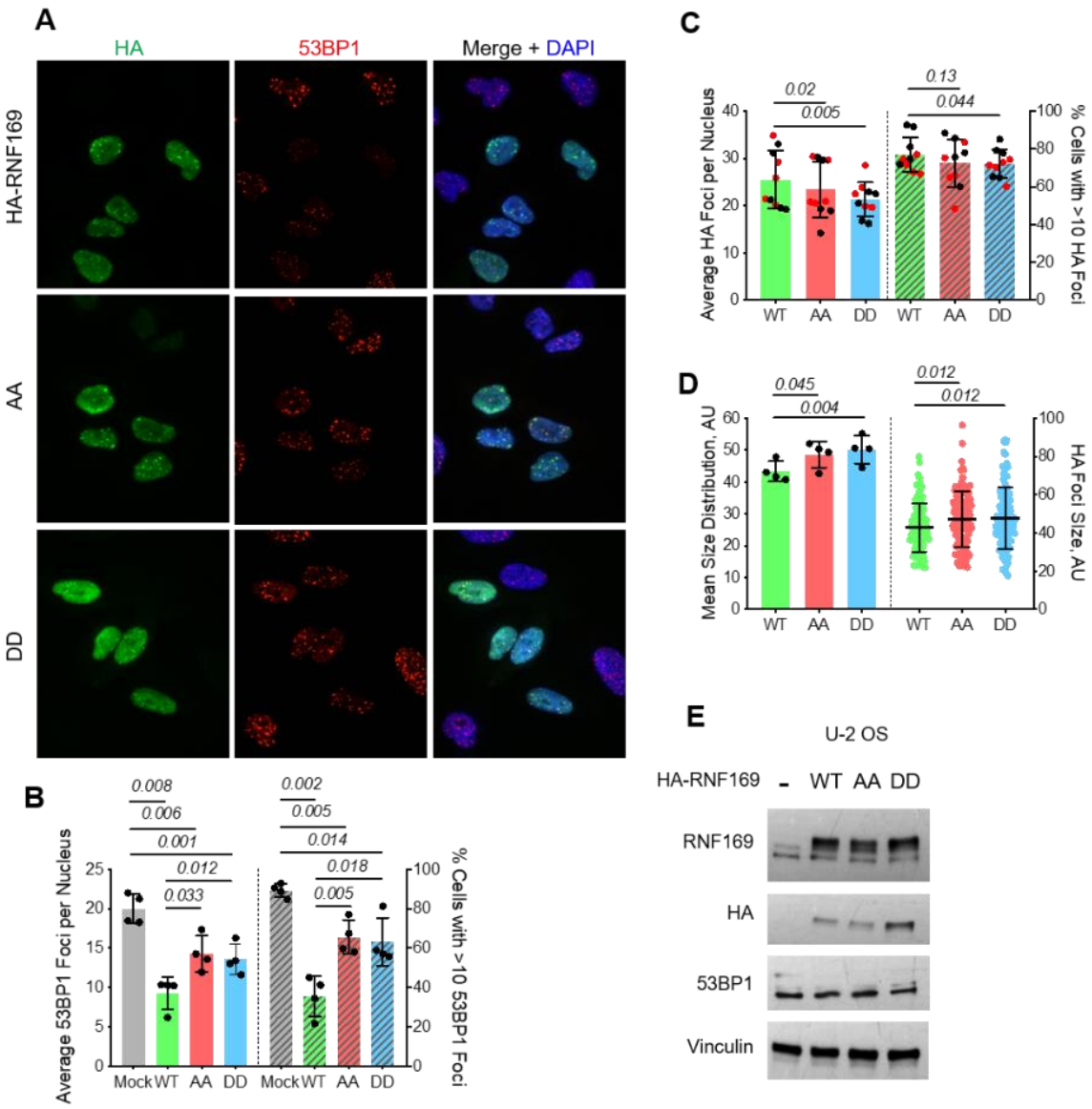

Figure 11: The functional significance of S368 and S403 residues in RNF169.
(A) Representative images of the HA-RNF169 (green) and 53BP1 (red) foci 3h after γ-radiation (5 Gy). U-2 OS stable cell lines expressing HA-RNF169 (WT), or the S368A/S403A (AA), or S368D/S403D (DD) mutants were stained using anti-HA and 53BP1 antibodies, and DAPI. (B) Graph shows quantification of the 53BP1 IRIF from 4 biological replicate experiments shown in panel A. All cells were scored in the control U-2 OS cells (Mock, shown as reference) whereas only HA-positive cells were scored in the HA-RNF169, RNF169-AA or RNF169-DD expressing cell lines. Here and below, error bars show standard deviation and p-values calculated using Student's two-tailed t-test are shown on the graphs. (C) Graph shows quantification of HA-RNF169 IRIF from 4 experiments in A. Red and black dots indicate values scored by two independent observers. (D) Quantification (average foci sizes, left Y-axis and size distribution, right Y-axis) of HA-RNF169 foci sizes measured in 4 biological replicate experiments. (E) WB shows expression of proteins of interest in the cell lines used in panels A-D.

2.2.4. Loss of DYRK1A causes a decreased DSB recruitment of RNF169 and 53BP1

In order to investigate the effects of loss of DYRK1A on 53BP1 and RNF169 IRIF, we generated U-2 OS cell lines with CRISPR Cas-9 mediated KO of DYRK1A in the lab [(Menon et al., 2019)., and the Methods section]. The KO clones were analyzed for DYRK1A protein expression using WB with DYRK1A antibodies targeting different regions of the protein [Figure 12A (Menon et al., 2019)]. Two independent U-2 OS DYRK1A-KO clones were expanded and further validated by WB and genomic DNA sequencing (Menon et al., 2019). We have developed an *in-vitro* kinase assay in the lab to analyze DYRK1A activity in cell extracts. Purified LIN52 is used as a substrate and incubated with cell lysates with or without DYRK1A (Menon et al., 2019). Using this assay, we confirmed that there was a significant loss of DYRK1A kinase activity in the U-2 OS DYRK1A- KO cell lines (Menon et al., 2019). Therefore, we chose to use these DYRK1A KO cell lines in our subsequent assays because transient siRNA knockdown or stable shRNA knockdown of DYRK1A resulted in significantly higher residual LIN52 kinase activity (data not shown).

Using transiently transfected HA-RNF169 or GFP-RNF169, we compared the recruitment of RNF169 into the IRIF in the control and the DYRK1A-KO U-2 OS cells. Similar to the phenotype observed with Harmine treatment, both HA-RNF169 and GFP-RNF169 displayed a modest but significant decrease in DSB recruitment in γ-irradiated U-2 OS DYRK1A-KO cell lines compared to controls (Figure 12B, C). However, unlike Harmine-treated cells, DYRK1A-KO cell lines showed significantly reduced 53BP1 IRIF formation at 3h post γ-irradiation when compared to control cell lines, nor did accumulation of 53BP1 at the DSB sites in the DYRK1A-KO cell lines increase at 6h post γ-irradiation, as both DYRK1A-KO cell lines continued to

display a significantly decreased 53BP1 IRIF recruitment compared to controls (Figure 12D, E, F).

U-2 OS cell lines have only one copy of *DYRK1A* (Menon et al., 2019). It is possible that these cell lines have intrinsically reduced DYRK1A expression resulting from loss of one copy of the *DYRK1A* gene. Therefore, we further validated our findings described above using mouse NIH-3T3 fibroblasts in which Dyrk1a was similarly knocked out using a CRISPR-Cas9 approach. In the case of NIH-3T3 cells, accumulation of 53BP1 foci reaches its peak at 1h post γ-irradiation (3Gy), and then starts to decrease at 3h (data not shown). Using these experimental conditions, we again observed a decreased 53BP1 IRIF formation in two independent, clonal NIH-3T3 Dyrk1a-KO cell lines compared to control cells. Indeed, while a majority of the control and Dyrk1a-KO NIH-3T3 cells contained more than ten 53BP1 foci at 1h post γ-irradiation, the average number of 53BP1 IRIF per nucleus was significantly lower in the Dyrk1a-KO cells compared to control (Menon et al., 2019). Moreover, at 3h post γ-irradiation, the number of 53BP1 foci per nucleus decreased by approximately 50% in both the control and Dyrk1a-KO cell lines, indicative of a similar rate of resolving the lesions and removal of 53BP1 foci in these cells lines (Menon et al., 2019).

To further confirm that the phenotype of the DYRK1A-KO U-2 OS cells was specific to a loss of DYRK1A protein and kinase activity, we re-introduced either active DYRK1A or kinase-inactive K188R-DYRK1A (KD) mutant into one of our knockout clones and created stable cell lines. Indeed, we observed that expression of wild-type DYRK1A, but not the kinase inactive mutant, resulted in a complete rescue of the 53BP1 IRIF defect in these cells (Figure 13A, B). These results strongly support the role of DYRK1A in regulation of 53BP1 recruitment to the DNA double strand breaks caused by γ-irradiation.

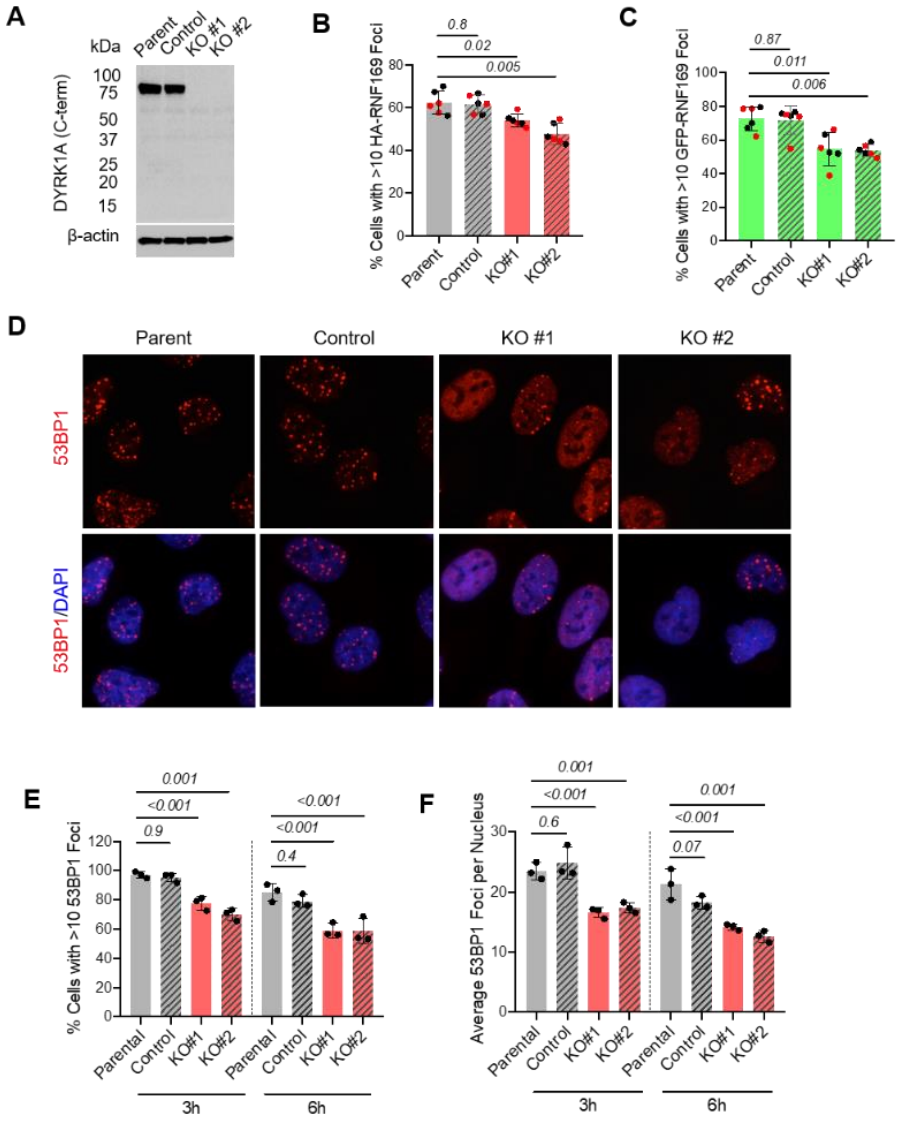

Figure 12: DYRK1A-deficient cells have impaired recruitment of RNF169 and 53BP1 to the DSBs.

(A) WB confirms absence of the full length DYRK1A protein expression in two different U-2 OS DYRK1A-KO clones. (B, C) Quantification of HA-RNF169 IRIF in U-2OS cells transiently expressing HA-RNF169 or GFP-RNF169 after 3h post-irradiation (5Gy) of the parental, control (non-targeting sgRNA clone) or DYRK1A-KO U-2 OS cell lines from three biological replicates. Red and black dots indicate counts by two independent observers. Here and below, the error bars show standard deviation. For statistical analysis, cell lines were compared to the parental U-2 OS cells using a Student's two tailed t-test; p-values are shown on the graphs. (D, E, F) Representative images 3h post γ-irradiation and graphs show quantification of 53BP1 IRIF from the cell lines processed for staining 3h or 6h post γ-irradiation (5Gy). Graph show values obtained from three biological replicates. For statistical analysis, each cell line was compared to parental U-2 OS line (gray bars) as above.

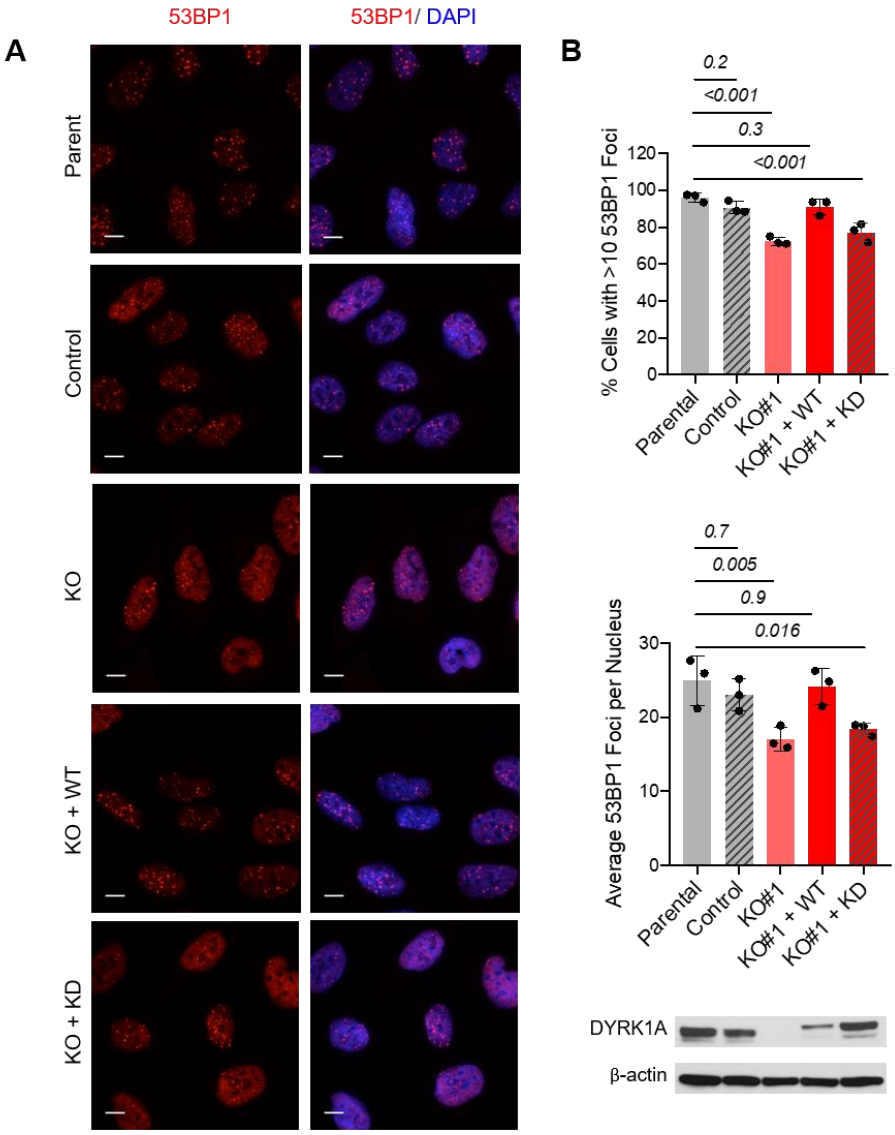

Figure 13: Rescue of the 53BP1 foci formation in DYRK1A-KO cells by re-expression of active DYRK1A.

(A) Representative images of the 53BP1 staining in parental U-2 OS cells, control sgRNA clone, the DYRK1A-KO clone #1 (KO), and the KO clone #1 before or after stable re-expression of the wild type (KO + WT) or kinase-inactive mutant (K188R) DYRK1A (KO + KD). Scale bar, 10 μm. (B) Quantification of the 53BP1 IRIF from three independent experiments using cell lines described in A. For statistical analysis, each cell line was compared to the parental U-2 OS line (gray bars) using a Student's t-test and p-values are shown on the graphs. Error bars indicate standard deviation. Lower Panel: WB shows levels of DYRK1A in the cell lines used in this experiment. Slower gel migration of the recombinant DYRK1A alleles is due to the presence of dual Flag-HA tag. Actin serves as loading control.

Further, we investigated if DYRK1A was required for overexpressed RNF169 to displace 53BP1 from IRIF. Overexpression of GFP-RNF169 in the DYRK1A-KO U-2 OS cells also resulted in inhibition of the 53BP1 recruitment to DSBs. The differences between the GFP and GFP-RNF169-expressing cells were highly significant in all cell lines, p- value < 0.001 (Figure 14A-C). This result was consistent with our findings that RNF169 was able to inhibit 53BP1 IRIF formation in cells treated with DYRK1A inhibitor Harmine. Furthermore, recruitment of 53BP1 foci was significantly lower in both the GFP- and GFP-RNF169-transfected DYRK1A-KO cells compared to the corresponding control cell lines (Figure 14A-C). This suggested that knockout of DYRK1A in U-2 OS cells could impair 53BP1 IRIF formation independent of RNF169.

2.2.5. Depletion of RNF169 does not fully rescue the 53BP1 recruitment defect in DYRK1A-KO cells

To determine whether the effect of DYRK1A loss on 53BP1 is mediated by RNF169 or not, we depleted RNF169 in U-2 OS cell lines using siRNA transfection. Interestingly, RNF169 depleted DYRK1A KO cells still had a reduced recruitment of 53BP1 as compared to their respective controls. The 53BP1 was not completely rescued with RNF169 depletion (Figure 14D, E). This phenotype was unlike what we observed with DYRK1A overexpressing cells. This result suggests that the 53BP1 recruitment defect in the absence of DYRK1A is not likely due to a more efficient displacement by RNF169. Together, our data support the conclusion that DYRK1A regulates the recruitment of 53BP1 to damaged chromatin in an RNF169-dependent as well as independent manner.

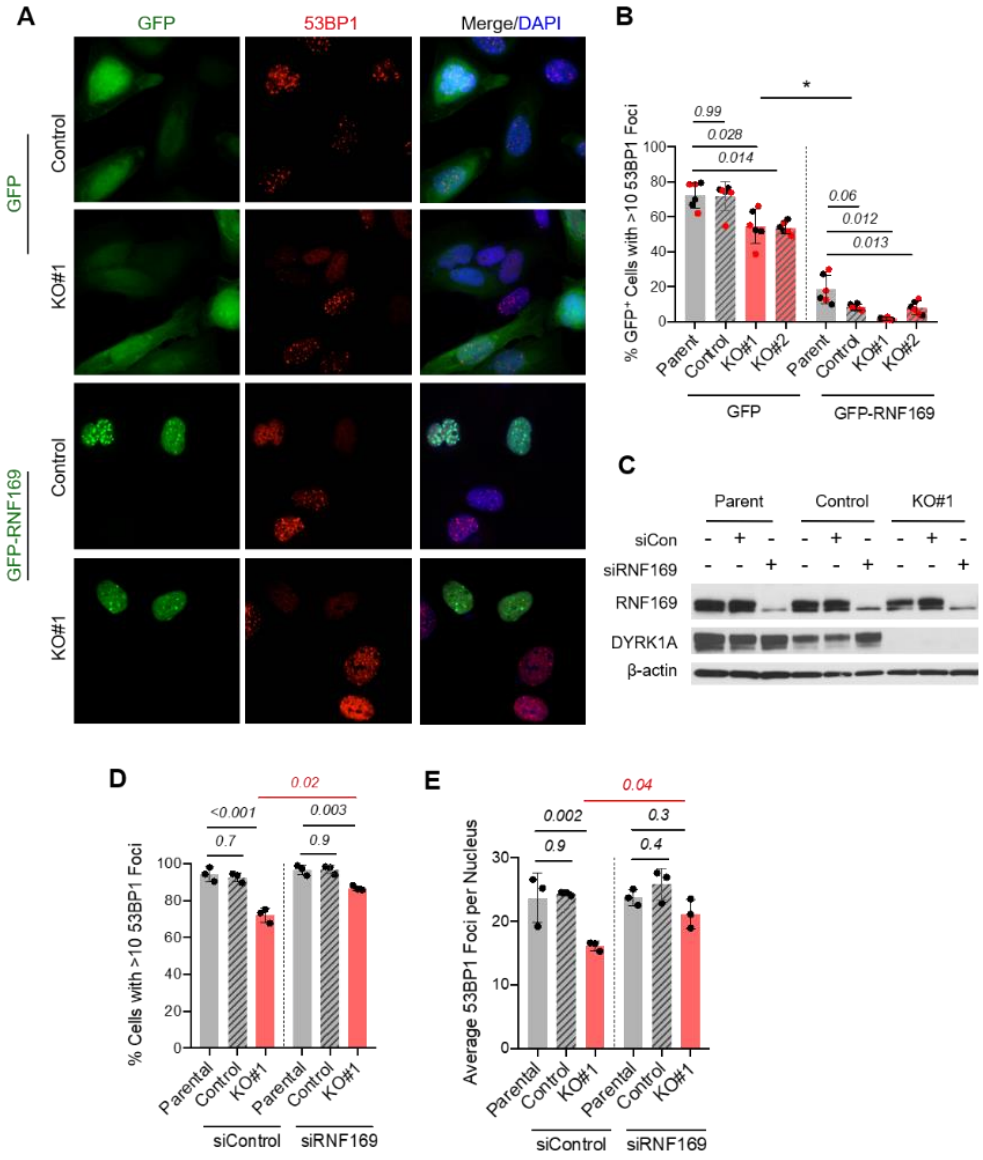

Figure 14: Impaired 53BP1 IRIF formation in DYRK1A-KO cells is RNF169 independent. (A, B) Representative images and quantification of GFP-RNF169 (green) and 53BP1 (red) foci 3h after γ-radiation (5 Gy). Indicated U-2 OS cell lines were transiently transfected with GFP or GFP-RNF169 and stained using 53BP1 antibody and DAPI. Graphs show values from 3 biological replicates. Red and black dots indicate counts by two independent observers. Here and below, the error bars indicate standard deviation. Data were analyzed using ANOVA with Dunnett's multiple comparisons test (p-values shown). All comparisons between the corresponding GFP-transfected and GFP-RNF169-transfected samples were significant ($p < 0.01$, indicated by an asterisk). (C) WB showing the expression levels of RNF169 and DYRK1A in the representative experiment analyzed in panels (D) and (E). (D, E) Quantification of the 53BP1 IRIF in control or DYRK1A-KO U-2 OS cell lines after siRNA knockdown of RNF169 from three biological replicates. Statistical significance was calculated using Student's two tailed t-test and p-values are indicated on the graphs.

To address the mechanism of the 53BP1 recruitment defect in DYRK1A-KO cells, we analyzed the expression of several DNA damage response markers during DNA repair. First, we looked at the early markers of the DNA damage response by WB analysis. There was no change in the induction of p53 or γH2AX in the DYRK1A-KO cells compared to control (Menon et al., 2019). Analysis of the ubiquitylation of histones and accumulation of γH2AX and at the DNA damage sites also appeared to be unchanged in the DYRK1A-KO cells compared to controls (Menon et al., 2019). This suggests that the initial DNA damage response was similar in control and DYRK1A KO cells. Furthermore, we analyzed if loss of DYRK1A in U-2 OS affected the DNA damage checkpoint. Cell cycle analysis revealed accumulation of cells in G1 and G2 phases after γ-irradiation indicating that loss of DYRK1A in U-2 OS cells did not affect the DNA damage checkpoint (Menon et al., 2019). An increase in 53BP1 and BRCA1 protein levels was observed in the DYRK1A KO cells with or without induction of DNA damage (Menon et al., 2019). Since accumulation of both 53BP1 and BRCA1 at the DSB sites requires the activity of RNF168 and RNF8 E3 ubiquitin ligases, we also analyzed the recruitment of BRCA1 in these cells and found it was unchanged in the DYRK1A-KO cells (Menon et al., 2019). Therefore, we were able to conclude that decreased recruitment of 53BP1 to the damage sites was likely not because of abnormal DNA damage signaling or histone ubiquitylation in the DYRK1A-KO cells.

2.2.6. Loss of DYRK1A promotes HRR and DNA repair

There is evidence that 53BP1 suppresses HR-mediated DNA repair by blocking end resection (Canny et al., 2018; Durocher & Pelletier, 2016). Since loss of DYRK1A decreased accumulation of 53BP1 at DSB sites, we investigated the effect of DYRK1A loss on DNA repair pathway choice, using control and DYRK1A-KO U-2 OS cell lines stably expressing the direct

repeat (DR) GFP reporter for the HR repair pathway (Pierce et al., 1999). In this model system, I-SceI restriction nuclease is used to generate a DSB by cleavage of the non-functional GFP gene fragment. If the generated DSB is repaired by NHEJ, there would be no GFP protein expression. However, if the DSB is repaired by HRR, using the downstream GFP sequence, a GFP protein is expressed (Menon et al., 2019). Consistent with reduced recruitment of 53BP1 to DSBs in the DYRK1A-KO cells, we observed an approximately two-fold increase in the percentage of GFP-positive cells after I-SceI expression (Menon et al., 2019). The same trend was observed with both DYRK1A-KO clones. As compared to the control U-2 OS cells, this result was statistically significant with one of the DYRK1A-KO clones but not with the second U-2 OS DYRK1A-KO clone because of high variability between biological replicates.

2.3. DISCUSSION AND FUTURE DIRECTIONS

Through the results discussed in this chapter, we provide functional characterization of the DYRK1A-RNF169 interaction. Our study revealed the role of DYRK1A in the DNA damage pathway by regulating one of the key response factors to DNA DSB lesions - 53BP1 (Panier & Boulton, 2014). Overexpression of RNF169 prevents the accumulation of 53BP1 at DSBs, resulting in increased HR-mediated DNA repair efficiency due to a more efficient resection of the DNA ends (J. Chen et al., 2012; Poulsen et al., 2012). However, the mechanism by which RNF169 regulates 53BP1 accumulation, as well as the factors that regulate RNF169 recruitment and dissociation from the DSB sites are still not known. Our study not only validated the role of RNF169 as a negative regulator of 53BP1 accumulation but also supported the role of DYRK1A as an RNF169 effector that positively regulates its activity through both direct and indirect mechanisms. Since the publication of our study, two other groups also reported the DYRK1A-

RNF169 interaction and its role in the DNA damage response (Guard et al., 2019; Roewenstrunk et al., 2019).

Previous studies found that a high-affinity ubiquitin-binding MIU domain in RNF169 is required for its ability to inhibit 53BP1 accumulation at the damage sites (J. Chen et al., 2012; Q. Hu et al., 2017; Poulsen et al., 2012). Our study shows that the binding of RNF169 to ubiquitin may be necessary, but not sufficient, to fully prevent the accumulation of 53BP1 at DSB sites. Indeed, the phosphorylation-deficient RNF169 mutants show reduced ability to displace 53BP1 from the DSBs despite almost normal recruitment to these sites. Interestingly, several ATM-regulated phosphorylation sites in 53BP1 are required for interaction with its key effector RIF1 but dispensable for its recruitment to the damage sites (Escribano-Díaz et al., 2013; Isono et al., 2017). It is possible that DYRK1A phosphorylation of RNF169 serves to recruit an additional factor that is essential for displacing 53BP1, or for stabilizing the binding of RNF169 to ubiquitylated chromatin. The phosphomimetic DD mutant of RNF169 also showed a reduced ability to displace 53BP1 from DSBs. One possibility is that this mutant does not accurately represent the constitutively active form of RNF169. Another possibility is that the RNF169 DD mutant causes a dominant negative effect. An RNF169 dimer could be responsible for inhibiting 53BP1 foci formation, wherein one molecule of RNF169 is in the phosphorylated form and the other is not phosphorylated. Thus, when the AA mutant is expressed, there is an excess of un-phosphorylated RNF169, which may dimerize and cause inhibition of 53BP1 recruitment. When the phosphomimetic mutant is present in excess, a possibility is that there is not enough unphosphorylated RNF169 to form the active dimer and therefore, there is reduced 53BP1 recruitment. Moreover, the constitutive presence of the DYRK1A-RNF169 complex both in the intact cells and after damage, as well as the estimated size of the DYRK1A-RNF169 complex

also indicate that other factor(s) is/are likely present in this complex that could be regulated by DNA damage signaling. Further proteomic studies of the RNF169-DYRK1A complex in the cells before and after DNA damage will help to identify such a factor. Of note, our analysis of the DYRK1A interactome detected an interaction with USP7, a ubiquitin-specific protease that has been recently shown to bind directly to RNF169 and increase the stability of 53BP1, RNF169 and RNF168 (An et al., 2018; X. Liu et al., 2016; Zhu et al., 2015). Although disruption of the DYRK1A phosphorylation sites in RNF169 did not influence its interaction with USP7, the role of USP7 in the DYRK1A-RNF 169 mediated regulation of 53BP1 should be further investigated.

In our study, DYRK1A overexpression or depletion both caused a decrease in 53BP1 IRIF. Interestingly, while increased expression of DYRK1A appears to attenuate the displacement of 53BP1 from the DSBs by RNF169, the 53BP1 DSB recruitment defect in DYRK1A-depleted cells appears to be, at least in part, RNF169-independent. This is because 53BP1 IRIF accumulation was not completely rescued with RNF169 depletion in DYRK1A-KO cells. Indeed, DYRK1A-KO cell lines displayed decreased RNF169 IRIF formation. Recent studies have revealed that in addition to the histone H2A-K15ub mark, 53BP1 recognizes and binds to the H4K20Me2 mark via its conserved Tudor domain, and this process is regulated by several factors including histone methyltransferases SETD8 and MMSET, as well as Polycomb proteins L3MBTL1 and JMJD2A that occupy these marks in the absence of DNA damage [reviewed in (Panier & Boulton, 2014)]. Furthermore, in S/G2 phases of the cell cycle, BRCA1 plays an active role in removing 53BP1 from chromatin around damage sites by a mechanism that is not fully understood, requiring CDK activity and CtIP (Chapman et al., 2012; Escribano-Díaz et al., 2013; Isono et al., 2017). It will be interesting to investigate in the future whether changes in

these 53BP1-regulating factors are responsible for the phenotypes observed in the DYRK1A-KO cells.

There is also a possibility that there is another kinase capable of phosphorylating RNF169 at the same sites as DYRK1A, and this kinase is inhibited when DYRK1A is present in optimum amounts. When DYRK1A is present in excess, there could be an increased phosphorylation of RNF169 leading to decreased 53BP1 recruitment. On the other hand, when DYRK1A is depleted, the alternate kinase may phosphorylate RNF169 leading to decreased 53BP1 recruitment. Although further studies will be needed to determine if this is true, it is important to note that there are several examples of redundant kinases phosphorylating a single substrate in the DNA damage response, such as ATM and DNA-PK kinases that are both capable of phosphorylating H2AX (Stiff et al., 2004).

Since BRCA1 gene expression could be regulated by DYRK1A through recruitment of the DREAM repressor complex (Litovchick et al., 2011; Yakovlev, 2013), the relationship between DYRK1A expression levels and the outcomes of the DNA damaging therapy in cancer should be further investigated. Importantly, loss of 53BP1 can rescue the HR defects associated with inactivation of BRCA1, and is one of the factors responsible for the acquired resistance of the BRCA1-mutant tumors to PARP inhibitor therapy (Jaspers et al., 2013). Therefore, future studies will be needed to establish the exact role of DYRK1A in the context of cellular processes that regulate the recruitment of 53BP1 to the DSBs, and to validate the significance of DYRK1A as a factor that can influence the outcomes of cancer therapy.

CHAPTER 3: CHARACTERIZATION OF NOVEL DYRK1A INTERACTING PROTEINS

3.1 INTRODUCTION TO THE CHAPTER

Of the DYRK1A interacting proteins we reported earlier, we validated its interaction with DCAF7, LZTS1, LZTS2, FAM117B, RNF169 and TROAP (Menon et al., 2019) in human cells. Although we did not validate the interaction of LZTS3 with DYRK1A, its close relationship with LZTS1 and 2 lead us to review the literature on LZTS3 as well. In this chapter we will focus on the biochemical and functional characterization of all of these DYRK1A interactors.

Below is a review of current literature on each of these DYRK1A interacting proteins except RNF169 (described in detail in Chapter 2).

3.1.1. DCAF7

Similar to *DYRK1A*, the *DCAF7* gene is conserved in evolution. DYRK family of protein kinases includes members from yeast to humans. Interestingly, out of all the top human DYRK1A interacting proteins in our study only DCAF7 has an orthologue in yeast- Saccharomyces cerevisiae (genecards.org) and according to the BioGrid database, an interacting partner of the founding member of the DYRK sub-family member Yak1 includes the yeast DCAF7 orthologue YPL-247. The *DCAF7* orthologue in plants, *AN11* was originally identified as a gene in petunia located in a locus that controls the pigmentation of flowers by stimulating the transcription of anthocyanin biosynthetic genes (de Vetten et al., 1997) The orthologues of this gene have been identified in many species, including humans (Jin et al., 2006). In vertebrates this gene is also

known as *WDR68* (WD-repeat protein 68) or *DCAF7* (DDB1 and Cullin Associated Factor 7) (Lee & Zhou, 2007).

The *DCAF7* ortholog in Drosophila, *CG14614* (official gene symbol *wap*, wings apart, also called *riq*, riquiqui), is essential for normal wing-vein patterning and development of the adult jump muscle (Morriss et al., 2013).. Interestingly, *CG14614* associates with *MNB* in Drosophila, and both genes were shown to control normal wing and leg growth by modulating the Salvador-Wart-Hippo (SWH) pathway (Degoutin et al., 2013). Thus, there is evidence of the importance of the DYRK1A-DCAF7 interaction for development in different organisms. DCAF7 is also involved in craniofacial development in zebrafish where it plays a role upstream of the EDN1 (Endothelin-1) pathway (Nissen et al., 2006). This is of particular interest as DYRK1A itself is involved in development and DS patients have certain craniofacial abnormalities. Interestingly, nuclear access of DCAF7 is required for normal craniofacial development in zebrafish (B. Wang et al., 2013). This is important as DCAF7 is mainly a cytosolic protein. However, DCAF7 binds DYRK1A and this binding induces the nuclear translocation of DCAF7 (Miyata & Nishida, 2011). On the other hand, the localization of DYRK1A has not been found to be dependent on DCAF7 binding (Glenewinkel et al., 2016; Miyata & Nishida, 2011).

Structurally, DCAF7 and its orthologues all encode a protein with several WD40 domains. These domains are characterized by tryptophan-aspartate (WD) dipeptide repeats that are 44-60 amino acids in length (Stirnimann et al., 2010; Wu et al., 2012). These WD40 repeats fold and organize into circularized β- propeller structures and can facilitate protein-protein interactions (Stirnimann et al., 2010; Wu et al., 2012). DCAF7 is predicted to act as a substrate receptor for the DDB1-Cullin complexes although this function has not been experimentally demonstrated till date (Jin et al., 2006; Lee & Zhou, 2007). Interestingly, DCAF7 acts as a scaffold receptor to control

HIPK2 and MEKK1 kinase functions (Ritterhoff et al., 2010). DCAF7 is also required for efficient binding of E1A to DYRK1A, DYRK1B and HIPK2 (Glenewinkel et al., 2016; Skurat & Dietrich, 2004).

There is evidence that DCAF7 could be required for cellular proliferation (Miyata & Nishida, 2011; Ritterhoff et al., 2010). Both DYRK1A and DCAF7 bind to the C-terminal region of oncoprotein E1A (Komorek et al., 2010; Zemke & Berk, 2017). This region of E1A is responsible for restraining its oncogenic and transforming abilities. It was found that an E1A mutant defective in binding DYRK1A and DCAF7 showed a robust increase in proliferation, transformation and tumor formation as compared to wildtype E1A (Komorek et al., 2010). This suggests that E1A interaction with DYRK1A and DCAF7 could inhibit cell proliferation. DCAF7 is also required to maintain normal levels of DYRK1A and DYRK1B in C2C12 and HeLa cell lines (Yousefelahiyeh et al., 2018).

We and others have detected DCAF7 as a binding partner of DYRK1A (Glenewinkel et al., 2016; Guard et al., 2019; Komorek et al., 2010; Menon et al., 2019; Miyata & Nishida, 2011; Morita et al., 2006; Roewenstrunk et al., 2019; Skurat & Dietrich, 2004; Varjosalo et al., 2013). Furthermore, it was found that the interaction between DYRK1A and DCAF7 is evolutionarily conserved (Glenewinkel et al., 2016), as shown in Figure 15. Interestingly, WD40 repeats of DCAF7 alone are not sufficient for the binding of DCAF7 to DYRK1A but the N- and C-termini of DCAF7 are also required (Miyata & Nishida, 2011). It was determined that the minimal region in DYRK1A required for DCAF7 binding is located in the N-terminus and spans amino acids 93-104 of human DYRK1A (Glenewinkel et al., 2016; Miyata & Nishida, 2011).

Additional functions of DCAF7 include a role in the osmotic stress response (Ritterhoff et al., 2010) and control of GLI1 transcriptional activity through interaction with mDia1 (DIAPH1) (Morita et al., 2006). Additionally, it has been reported that DCAF7 is required for nucleotide excision repair by maintaining the cellular levels of ERCC1-XPF (Kawara et al., 2019). This is the first report suggesting a direct role of DCAF7 in regulation of a DNA repair pathway and is interesting given the role of DYRK1A in DNA repair (Guard et al., 2019; Menon et al., 2019; Roewenstrunk et al., 2019). DCAF7 was also recently shown to regulate stability of DNA ligase I (LIG1), one of the key enzymes in the DNA replication and repair of DNA DSBs (Z. Peng et al., 2016). Another DCAF7 interacting protein detected in multiple studies is the molecular chaperone TRiC/CCT. It was shown that molecular chaperone TRiC/CCT binds to DCAF7 and promotes its folding, binding to DYRK1A and nuclear accumulation (Miyata et al., 2014).

Finally, DCAF7 has also been reported to have functions in transcription that will be discussed in detail in Chapter 4.

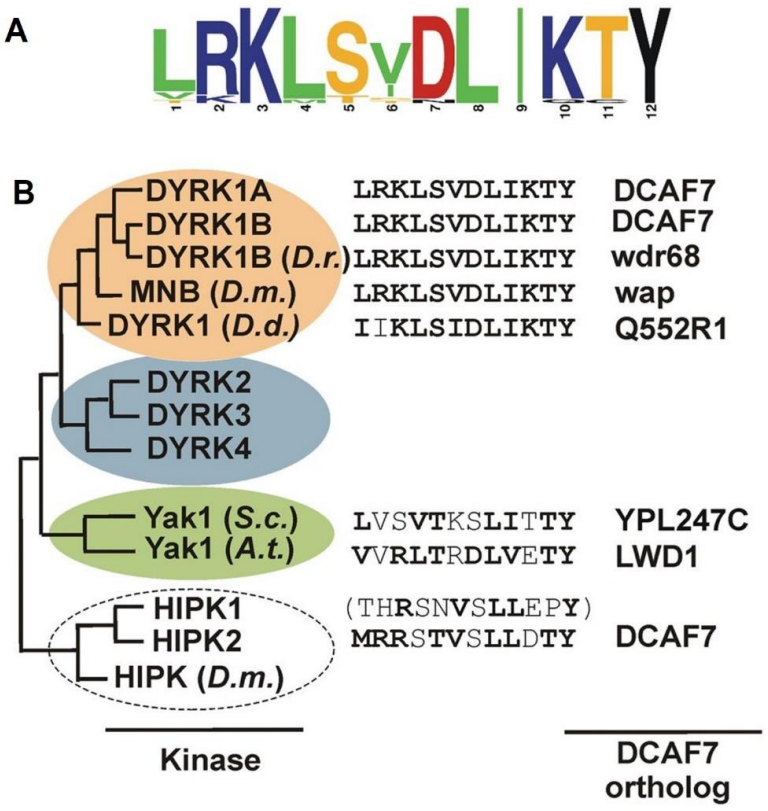

Figure 15: The DYRK1A-DCAF7 interaction is conserved across evolution.
(A) Consensus sequence of the DCAF7 binding motif in class 1 DYRKs created by analyzing 19 representative sequences from Class I DYRKs from the animal kingdom. (B) Phylogenetic relationship of the DYRKs and HIPKs that interact with DCAF7 [Adopted from (Glenewinkel et al., 2016)].

3.1.2. LZTS proteins

In our MudPIT analysis of DYRK1A, we identified PSD-Zip70 (or LZTS1), LAPSER1 (or LZTS2) and ProSAPiP1 (LZTS3), which all belong to a 'Fezzin' family of proteins (Wendholt et al., 2006). Along with the characteristic Fez1 domain/s, LZTS1 and LZTS2 also have a coiled-coil region with an internal leucine zipper motif in the center part of the protein and a PDZ domain at their C-terminus (Wendholt et al., 2006). These proteins can form homo or hetero-oligomers (Schmeisser et al., 2009; Wendholt et al., 2006). Note that LZTS1 is also referred to as FEZ1 in some studies. The function of this family of proteins is not fully understood.

Interestingly, LZTS1, LZTS2 and LZTS3 were identified as Post Synaptic Density (PSD) proteins (Dolnik et al., 2016; Schmeisser et al., 2009; Wendholt et al., 2006), and they all bind directly to the signal-induced proliferation associated (SIPA) family of proteins that includes SIPA1, 2, and 3, also known as SPARs or spine-associated RapGAPs. SPARs are GTPase activating proteins (GAPs) in the brain (Dolnik et al., 2016; Reim et al., 2016; Wendholt et al., 2006). The expression profile of LZTS1 detected in mouse and chick embryos revealed that it is localized to regions involved in neuronal development (Kropp & Wilson, 2012). LZTS1 knock out mice show cognitive and behavioral defects due to abnormal Rap2 activity (Mayanagi et al., 2015), suggesting that the LZTS proteins may be associated with behavioral disorders. A recent publication suggests a previously unknown role of LZTS1 during mammalian cerebral development. This study showed that LZTS1 controls neuronal delamination and outer radial glial-like cell generation (Kawaue et al., 2019). Furthermore, LZTS2 could serve as a negative regulator in regulation of β-catenin localization from the synapse to nucleus, leading to decreased transcription of β-catenin target genes (Schmeisser et al., 2009).

It is not known if there is a functional connection between DYRK1A and the LZTS family in neurological disorders. Interestingly, DYRK1A also phosphorylates proteins that bind to clathrin coated vesicles and inhibits clathrin-mediated endocytosis in neurons (Murakami et al., 2009, 2012). Moreover, DYRK1A may also be regulated by Wnt signaling (Granno et al., 2019). Hence DYRK1A-LZTS interactions in this regard will be an interesting avenue of study.

3.1.3. Role of LZTS proteins in cancer

As suggested by the name (LZTS stands for Leucine Zipper Tumor Suppressor), LZTS1, LZTS2 and LZTS3 have tumor suppressive functions. Indeed, *Lzts1*$^{-/-}$ mice develop tumors with diverse histogenetic backgrounds and LZTS1 expression is frequently lost in various types of cancers

(Ishii et al., 1999; Vecchione et al., 2007) suggesting that it acts as a major tumor suppressor gene in multiple cell types. Reintroduction of LZTS1 into cancer cells that lack its expression suppresses cell proliferation by cell cycle arrest at the G2/M phase of the cell cycle, and this effect is thought to be mediated by its interaction with mitotic kinase CDK1 (Ishii et al., 1999; Vecchione et al., 2007). LZTS1 expression is reduced in hepatocellular carcinoma (Y. He & Liu, 2015; Zhang et al., 2015), and there is evidence of LZTS mediated suppression of proliferation by impairing the PI3K/Akt pathway in hepatocellular carcinoma (Y. He & Liu, 2015). Down regulation of LZTS1 is associated with poor prognosis and causes increased metastasis in breast cancer (L. Chen et al., 2009; W. Chen et al., 2007; Lovat et al., 2014; X.-X. Wang et al., 2011, 2015). LZTS1 is lost or silenced in various other cancers including uveal melanoma (Onken et al., 2008), prostate cancer (Cabeza-Arvelaiz et al., 2001; Ishii et al., 1999), squamous cell carcinoma (Olasz et al., 2015), lung cancer (Lin et al., 2013; Nonaka et al., 2005; Toyooka et al., 2002) and ovarian cancer (Arnold et al., 2006; Califano et al., 2010; Ishii et al., 1999).

Similar to LZTS1, LZTS2 is also frequently deleted in cancer. LZTS2 has been mapped to a sub-region of human chromosome 10q24.3, near the *PTEN* locus (Cabeza-Arvelaiz et al., 2001; Wendholt et al., 2006). In laryngeal squamous cell carcinoma, LZTS2 promoter methylation has been reported (Z. Shen et al., 2018). Loss of LZTS2 in mice leads to renal abnormalities and an increased incidence of cancer (Johnson et al., 2013; Y. Peng et al., 2011). Overexpression of LZTS2 cDNA strongly inhibits cell proliferation and the colony forming efficiencies of some cancer cell lines (Cabeza-Arvelaiz et al., 2001). Increased nuclear localization of β-catenin due to aberrant activation of the Wnt pathway contributes to cancer, and LZTS2 binds to β-catenin and promotes its nuclear exclusion, thus increasing the cytosolic pool of β-catenin (Thyssen et al., 2006). It was recently demonstrated that PTEN and LZTS2 both control β-catenin mediated

transcription (E.-J. Yu et al., 2017). Interestingly, a connection between DYRK1A and β-catenin was recently reported where activation of Wnt signaling altered the sub-cellular localization of DYRK1A by an unknown mechanism (Granno et al., 2019). Furthermore, LZTS2 was seen to inhibit cell proliferation and regulate Lef/Tcf-dependent transcription through the Akt/GSK3β signaling pathway in lung cancer (Cui et al., 2013). LZTS2 inhibits PI3K/AKT activation in nasopharyngeal carcinoma as well (Xu et al., 2018). Finally, the protein interaction network of the mammalian Hippo pathway revealed interaction of LZTS2 with LATS2 (Couzens et al., 2013). Thus, this particular DYRK1A-interacting protein found through the proteomic analysis could provide a connection between cancer-related cellular signaling pathways and DYRK1A.

The role of LZTS3 in cancer has been studied to a lesser extent. Like LZTS1 and LZTS2, it is thought to have a tumor suppressive function (J. He et al., 2018; Teufel et al., 2005).

3.1.4. FAM117B

FAM117B (Family with sequence similarity 117, member B) is a poorly studied but potentially important DYRK1A interacting protein. A study conducted in 215 individuals with either Autism spectrum disorder (ASD) or intellectual disability reported the presence of several gene copy number changes. In this study, *FAM117B* was one of the 46 genes located in a region of 7.8 Mb chromosomal deletion at 2q33.1 to q34. This suggests that FAM117B could also be involved in ASD or intellectual disability and it will be interesting to see if it has a link with the involvement of DYRK1A in neurological conditions (Roberts et al., 2014). Interestingly, a GWAS study recently found that *FAM117B* was one of the genes associated with cerebral small vessel disease. Further, using two independent single cell RNA sequencing datasets from the anterior temporal lobe of adult human brains and cerebrovascular cells of adult mouse brains, researchers found that FAM117B was expressed in various cell types that included astrocytes,

neurons and oligodendrocytes (Chung et al., 2019). This further suggests that FAM117B could play an important role in neurological processes and since it is a DYRK1A-interacting protein, FAM117B could be dependent on or influence DYRK1A's function in neurological conditions.

3.1.5. TROAP

Tastin was initially described as a protein that forms a complex with trophinin and bystin, hence it was renamed as TROphinin Associated Protein or TROAP. The TROAP-trophonin-bystin complex is required for the initial adhesion of the blastocyst to uterine epithelial cells at the time of embryo implantation (Fukuda & Nozawa, 1999). Although TROAP expression is absent in most adult tissues (Nadano et. al., 2002), higher levels of expression are observed in testis, bone marrow and thymus, as well as human cancer cell lines such as HeLa and Jurkat cells (Genomics Institute of the Novartis Research Foundation [GNF] database). In mammalian cells, TROAP is thought to associate with microtubules (Nadano et al., 2002). Levels of TROAP increase in the G2/M phase of the cell cycle and it has been found to be required for maintaining bipolar spindles and the integrity of the centrosome during mitosis (Yang et al., 2008). Ectopically expressed TROAP in COS7 cells forms fibers that localize to the microtubular cytoskeleton and binds to cytoplasmic dynein in HEK293T cells (Nadano et al., 2002). The role of TROAP in cancer has been studied by several groups. TROAP was found to be pro-tumorigenic in lung adenocarcinoma (Z. Chen et al., 2019), non-small cell lung cancer (Huang et al., 2019), breast cancer (Kai Li et al., 2019), ovarian cancer (Godoy et al., 2013), colorectal cancer (X. Ye & Lv, 2018), gastric cancers (Jing et al., 2018) and prostate cancer (J. Ye et al., 2019). In breast cancer, lung adenocarcinoma and gastric cancers, higher expression of TROAP was found to correlate with lower survival (Z. Chen et al., 2019; Jing et al., 2018; Kai Li et al., 2019). However, TROAP may play a dual role and both promote and suppress tumorigenesis in hepatocellular

carcinoma (H. Hu et al., 2019; Jiao et al., 2019; Lian et al., 2018). In breast cancer cells, TROAP depletion was found to cause cell cycle arrest in the G1/S phase of the cell cycle (Kai Li et al., 2019). Depletion of TROAP in gastric and colorectal cancer cells also leads to an arrest in the G0/G1 phase of the cell cycle (Jing et al., 2018; X. Ye & Lv, 2018). In NSCLC, expression of TROAP along with certain other genes was found to be deregulated in pre-cancerous lesions and was gradually altered with disease progression suggesting that TROAP may be involved during tumorigenesis (Huang et al., 2019). These findings suggest that TROAP could be a therapeutic target in several cancer types, and provide the rationale for further research.

3.2. RESULTS

3.2.1. MudPIT proteomic analysis of DYRK1A interacting proteins

In our earlier study, we reported the interaction of DYRK1A with RNF169, FAM117B, LZTS1, LZTS2 and TROAP. MudPIT proteomic analysis of DYRK1A revealed that DCAF7 interacts stoichiometrically with DYRK1A, suggesting that it is a major DYRK1A interacting protein. Since DCAF7 is a known scaffolding protein, we hypothesized that some of these proteins could form multi-protein complexes, which could be important for understanding the function of DYRK1A. We also hypothesized that DCAF7 acts as a scaffold to bring all these proteins together. In order to identify multi-protein complexes, we decided to first analyze the interactome of DCAF7 in T98G cells in a similar way as we did for analyzing the DYRK1A interactome. We detected 55 proteins that reproducibly bound DCAF7 in at least 2 out of 3 replicate experiments. Unexpectedly, we found only a small overlap with DYRK1A interacting proteins (indicated by a black outline, Figure 16). Several known interactors of DCAF7 were also detected, including components of PRC1.3/5 (will be discussed in Chapter 4) and the

chaperone TRiC/CCT complex that binds to DCAF7 and promotes its folding (Miyata et al., 2014).

Next, we similarly analyzed the interactomes of other novel DYRK1A interacting proteins to see if there is any overlap with DYRK1A and DCAF7 interactomes. RNF169, FAM117B, LZTS2, LZTS1 and TROAP reproducibly pulled down 28, 113, 183, 678 and 17 proteins respectively in at least 2 out of 3 biological replicates (Appendix tables and Figure 17A-E), including known, as well as novel, interactors for each of these proteins. As LZTS2, LZTS1 and FAM117B bound a large number of proteins, we sorted these reproducible interactors by their dNSAF score (relative abundance compared to all proteins detected), to identify the top enriched 50 interacting proteins detected in at least 2 biological replicates. We observed that, except for of RNF169, the interactomes of FAM117B, LZTS1, LZTS2 and TROAP did not show major overlap with DYRK1A (Appendix tables and Figure 17). Interestingly, all these proteins did pull down DCAF7 (Figures 17 and 18). Only a few proteins detected in these analyses also bound DCAF7 (shown by yellow labels in Figures 17 A-E and indicated in bold in Appendix tables). In summary, our MudPIT proteomic analysis revealed that while there were no apparent multi-subunit complexes with our novel DYRK1A interacting proteins, all of these proteins bound both DYRK1A and DCAF7 (Figures 17 and 18). This could support a model that DCAF7 plays a scaffolding role to promote these interactions.

3.2.2. DYRK1A interacting proteins bind DCAF7

Next, we wanted to validate if the DYRK1A binding proteins bound DCAF7. Using T98G cell lysates we carried out IP/WB analysis with antibodies against RNF169, FAM117B, LZTS2, LZTS1 and TROAP. Consistent with our previously observed result, all of these proteins bound DYRK1A. Furthermore, consistent with our new mass spec data, all of these DYRK1A

interacting proteins also bound DCAF7 (Figure 19, A-E). Next, we wanted to confirm our finding that these proteins apparently do not form a multi-subunit complex. Therefore, using T98G cells we carried out IP analysis of RNF169, FAM117B, LZTS1, LZTS2, TROAP and DYRK1A followed by WB analysis with DCAF7, DYRK1A and each bait protein. Indeed, we detected both DYRK1A and DCAF7 in all immunoprecipitates, but did not find interaction between most of the pulled-down proteins, thus confirming our results obtained by MudPIT proteomic analysis, suggesting that these proteins were not all present in a single complex (Figure 19F). One exception to this was previously reported binding between LZTS1 and LZTS2 (Figure 19F). Although our LZTS1 MudPIT analysis detected TROAP, we were unable to confirm this interaction by IP/WB (Figure 18, 19F).

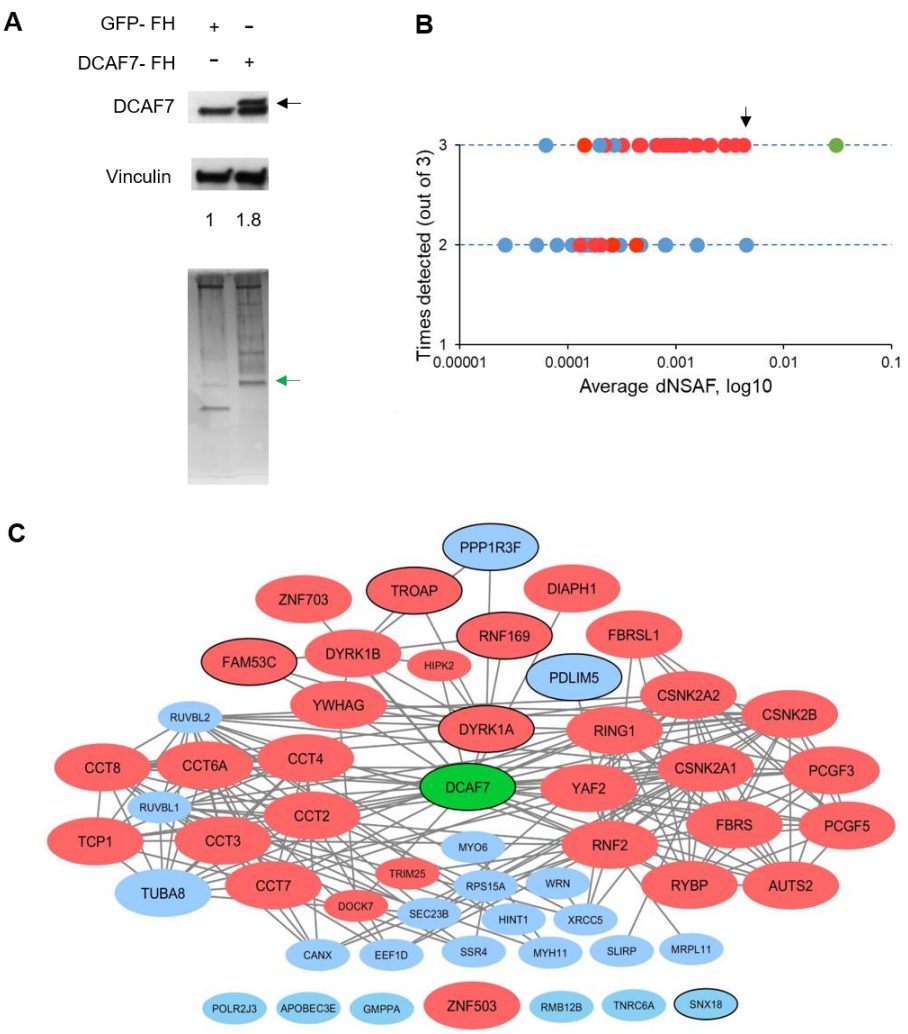

Figure 16: Analysis of the DCAF7-interacting protein network.
(A) Purification of DCAF7 for MudPIT proteomic analysis. Top: Representative western blot showing levels of DCAF7 in T98G cells expressing HA- Flag tagged GFP (GFP-FH) or HA-Flag-tagged DCAF7 (DCAF7-FH). Arrow indicates epitope tagged DCAF7. Values show band density relative to Vinculin (control). Bottom: representative silver stained gel containing 10% of HA-peptide eluted control (GFP) or DCAF7-FH IP samples analyzed by MudPIT. Green arrow indicates DCAF7 (B) Graph shows relative enrichment (dNSAF) of proteins detected in two or all three DCAF7 MudPIT experiments. DCAF7 is shown as a green circle whereas red and blue circles correspond to interacting proteins either listed in the BioGrid database, or new DCAF7-binding proteins, respectively. Black arrow points to DYRK1A. (C) Hierarchical network of interactions (CytoScape) involving DCAF7-binding proteins identified in this study was constructed using MetaScape analysis tool. Colors, same as in (B). Larger nodes correspond to proteins detected in all three replicates and smaller nodes correspond to proteins detected in two biological replicates. Unconnected nodes are not known to interact with other factors. Black outline indicates an overlap with our previous DYRK1A dataset (detected in at least 2 out of 4 biological DYRK1A pull down experiments).

A

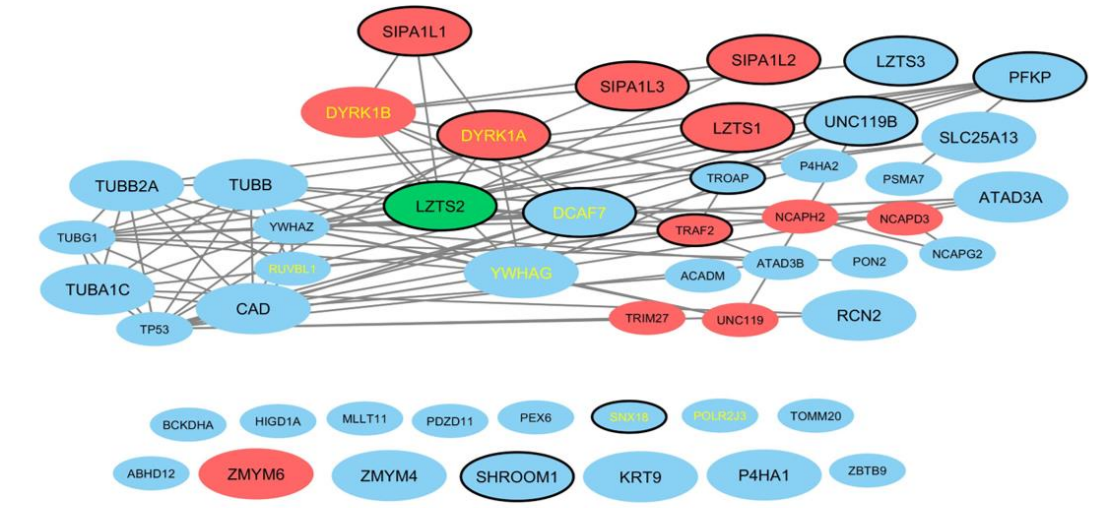

B

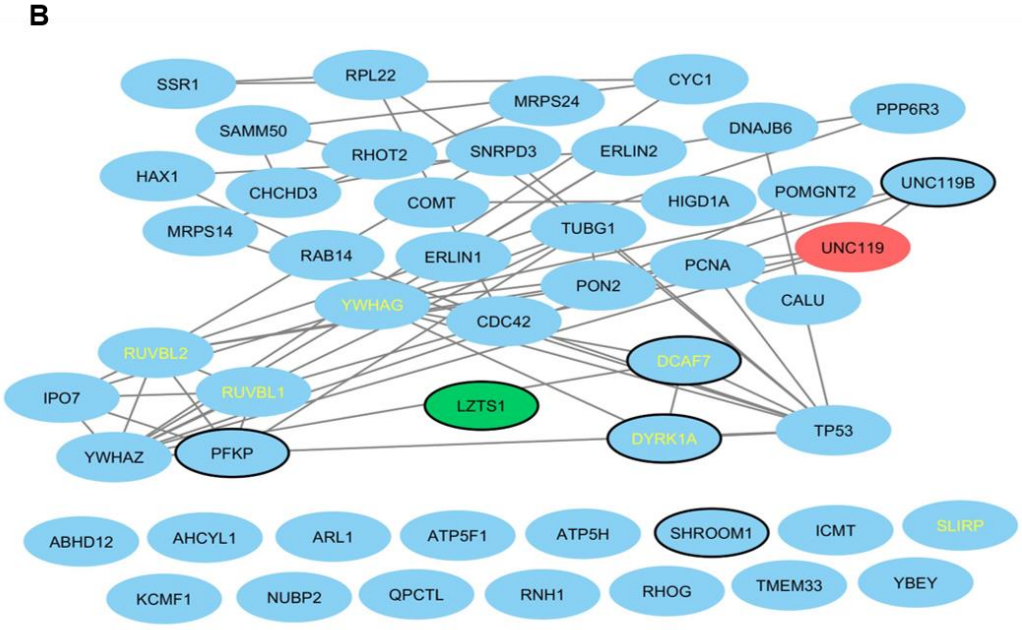

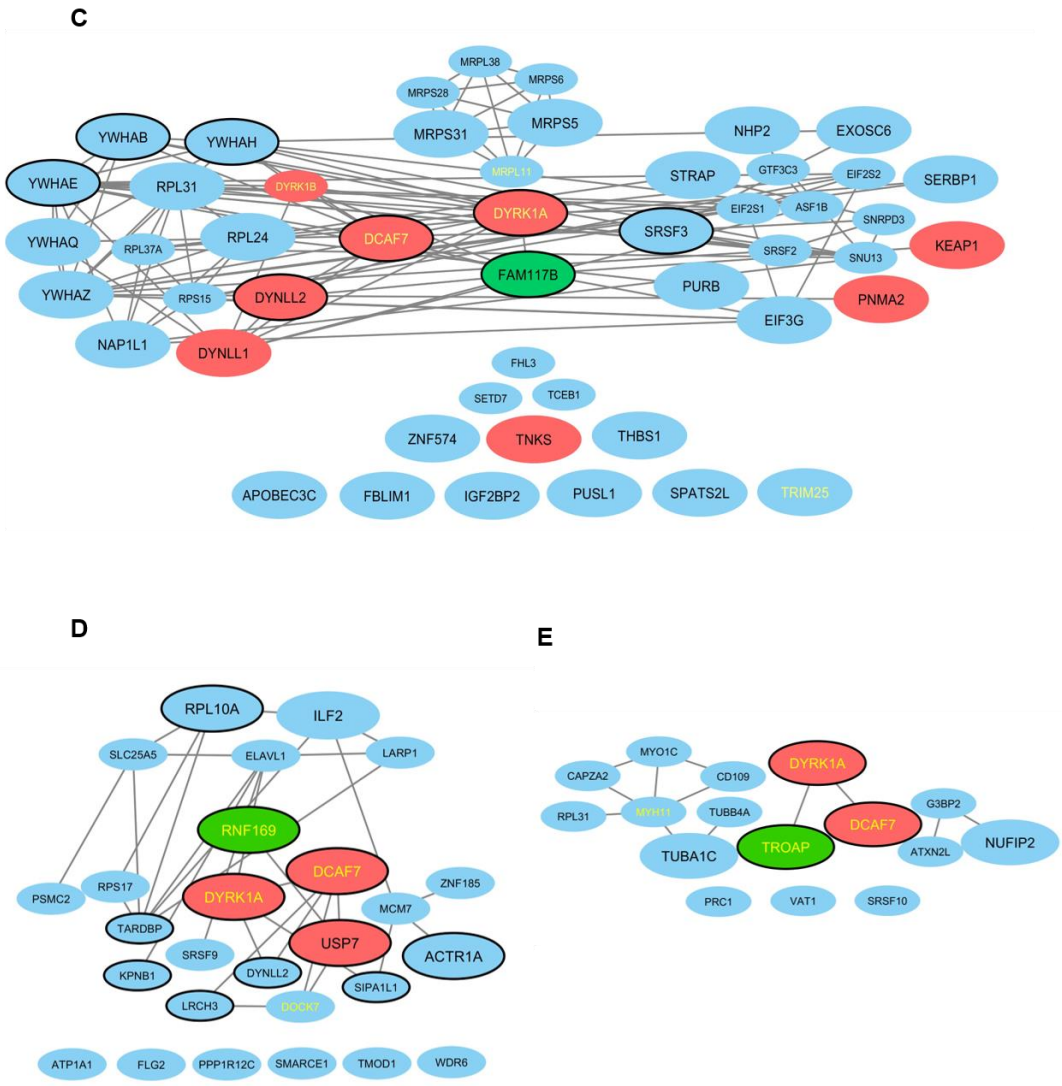

Figure 17: Analysis of protein networks of DYRK1A interacting proteins.
Hierarchical networks of interactions (CytoScape) for (A) LZTS2, (B) LZTS1, (C) FAM117B, (D) RNF169 and (E) TROAP were constructed using MetaScape analysis tool. Larger nodes correspond to proteins detected in all three replicates while smaller nodes correspond to proteins detected in two biological replicates. Unconnected nodes are not known to interact with other factors. Bait protein is shown in green whereas red and blue circles correspond to interacting proteins either listed in the BioGrid database, or new-RNF169 binding proteins, respectively. Black outline indicates an overlap with our previous DYRK1A dataset (detected in at least 2 out of 4 biological DYRK1A pull down experiments). Yellow label indicates an overlap with our DCAF7 dataset (Detected in at least 2 out of 4 biological DCAF7 pull down experiments). Note: Overlap with BioGrid database was analyzed in May 2019, which was before the inclusion of our DYRK1A dataset into the BioGrid.

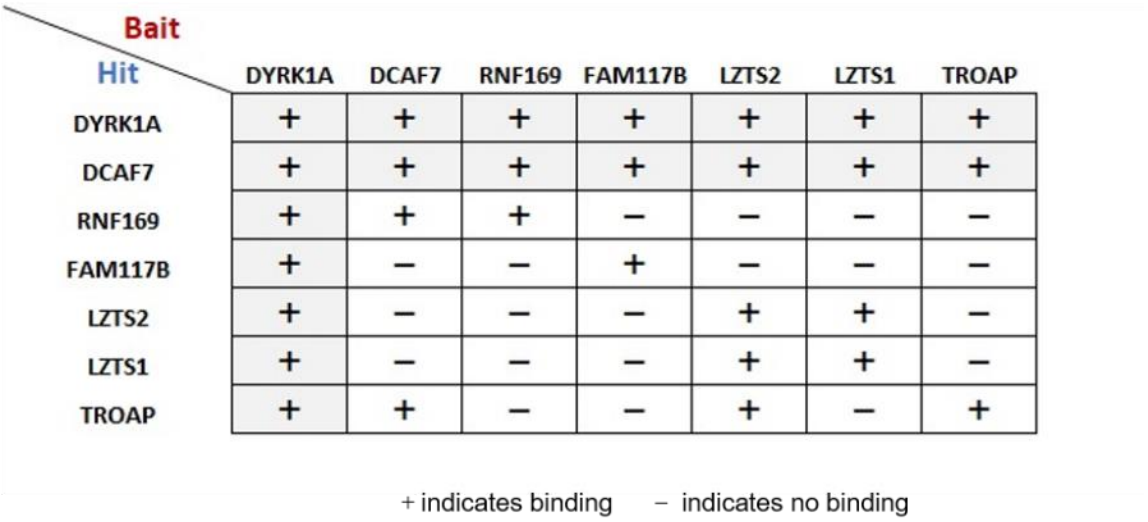

Figure 18: Summary of MudPIT proteomic analysis for our novel DYRK1A interacting proteins.

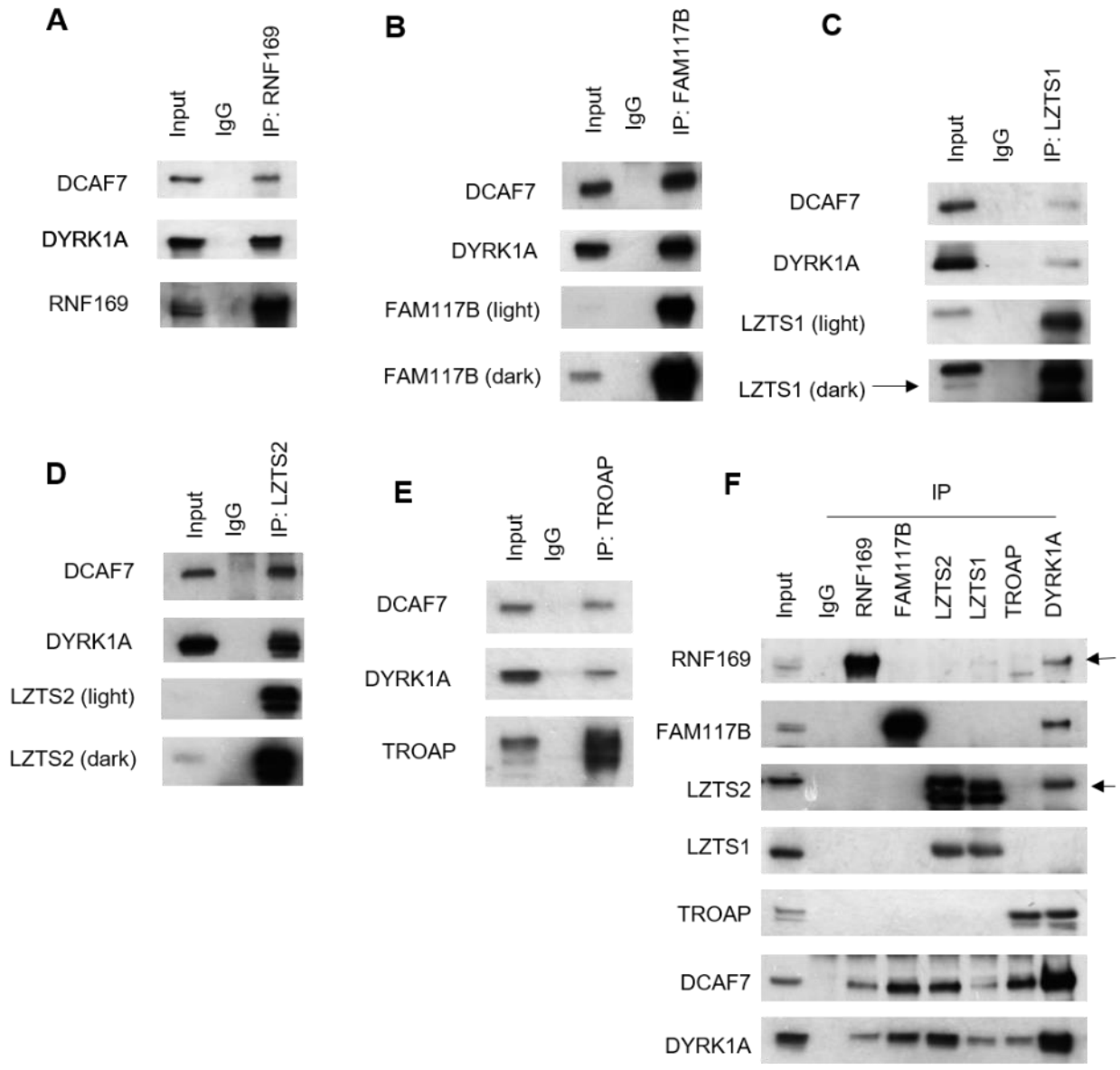

Figure 19: DYRK1A interacting proteins bind DCAF7 but do not form a single complex. (A-F) T98G lysates were used to perform immunoprecipitation analysis with the indicated antibodies or with non-reactive IgG control antibody followed by WB analysis for detection of the indicated proteins. As RNF169, FAM117B, TROAP and LZTS2 have similar molecular weights, Figure 21F is a composite figure made from 4 independent IP/WB experiments in order to avoid any residual overlapping signal from different antibodies during the WB analysis. DCAF7 and DYRK1A were detected in each IP/WB experiment as controls, and looked identical for all four independent experiments, therefore representative panels are shown.

In order to identify if these complexes were mainly present in the nucleus or in the cytoplasm, we carried out cyto-nuclear fractionation of T98G cells and subjected the cytoplasmic and nuclear extracts to IP/WB analysis (Figure 20). Consistent with its role in DNA damage repair, we found that RNF169 is mainly a nuclear protein and that the RNF169-DYRK1A-DCAF7 complex is also mainly nuclear in the cell [Figure 20A, (An et al., 2018; J. Chen et al., 2012; Guard et al., 2019; Menon et al., 2019; Poulsen et al., 2012; Roewenstrunk et al., 2019)]. Interestingly we also observed that the cytoplasmic RNF169 also binds both DYRK1A and DCAF7 (Figure 20A). We also observed that nuclear RNF169 migrates slower as compared to the cytoplasmic form, which could indicate the presence of a post translational modification in the nuclear compartment. Unlike the RNF169-DYRK1A-DCAF7 complex, FAM117B, LZTS2 and LZTS1 complexes were mainly cytoplasmic (Figure 20A-D). Interestingly, we observed that two isoforms of TROAP are present in the cytoplasm whereas only the longer isoform is present in the nucleus, and that the TROAP-DYRK1A-DCAF7 complex was detected mainly in the cytoplasm, but is also present in the nucleus (Figure 20E).

3.2.3. DCAF7 is not a scaffolding protein for DYRK1A tertiary complexes

Next, we investigated if DCAF7 is required for the interaction of DYRK1A with RNF169, FAM117B, LZTS2, LZTS1 and TROAP (Figure 21 A-E). We carried out IP/WB analysis in U-2 OS control or shDCAF7 cell lines in which DCAF7 was depleted by two different shRNA hairpins. Interestingly, we observed that depletion of DCAF7 reduced the levels of DYRK1A. This is consistent with a previous report suggesting that DCAF7 is required to maintain levels of DYRK1A (Yousefelahiyeh et al., 2018). Furthermore, it was found that DCAF7 is not required for RNF169, FAM117B or TROAP to bind DYRK1A but it might be needed for LZTS1/2-DYRK1A binding.

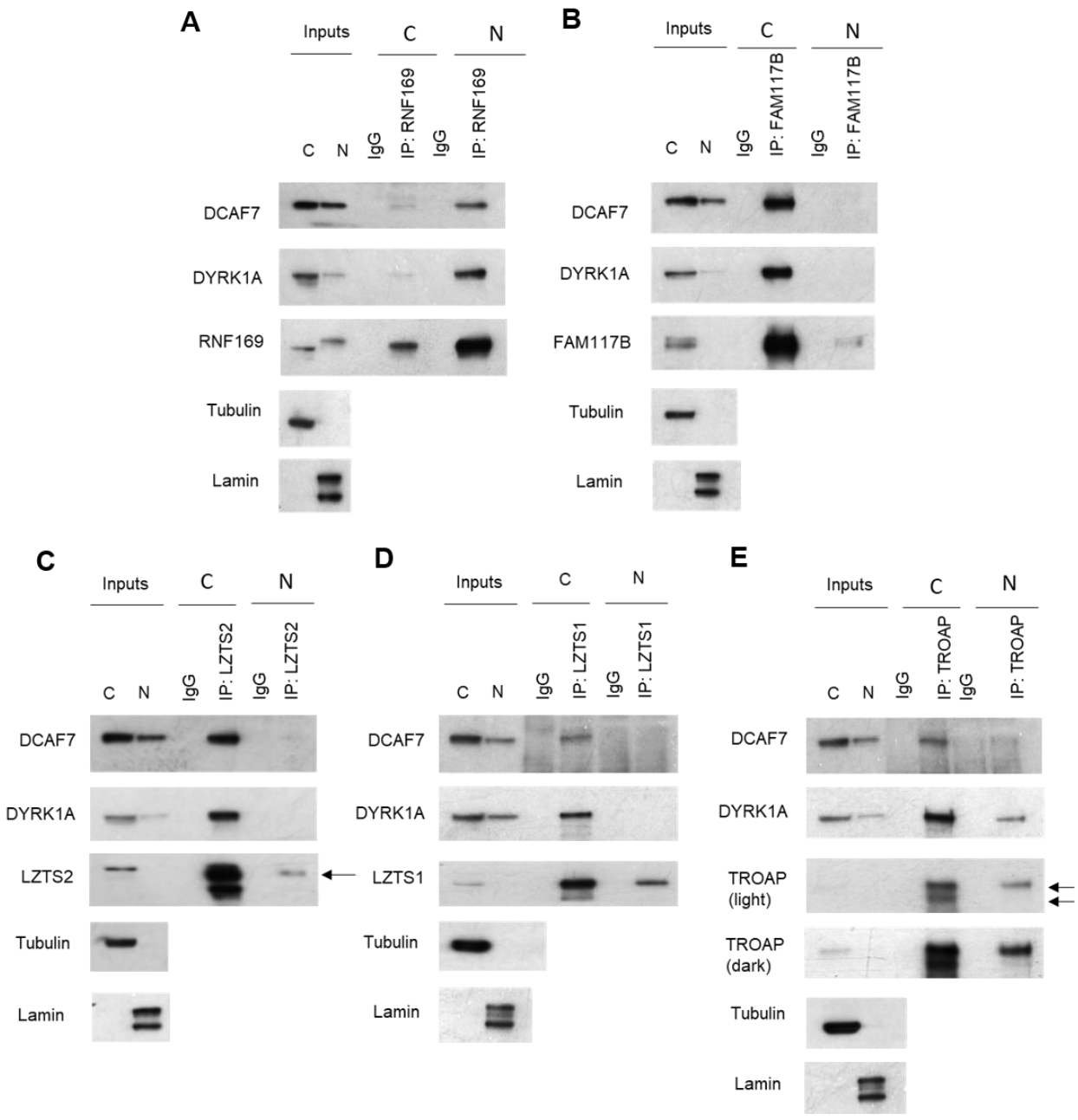

Figure 20: Nucleo-cytoplasmic distribution of the tertiary complexes including DYRK1A and DCAF7.

(A-E): T98G cells were fractionated into nuclear and cytoplasmic compartments followed by IP/ WB analysis with the indicated antibodies. Tubulin and Lamin were used to confirm the cytoplasmic and nuclear fractions, respectively.

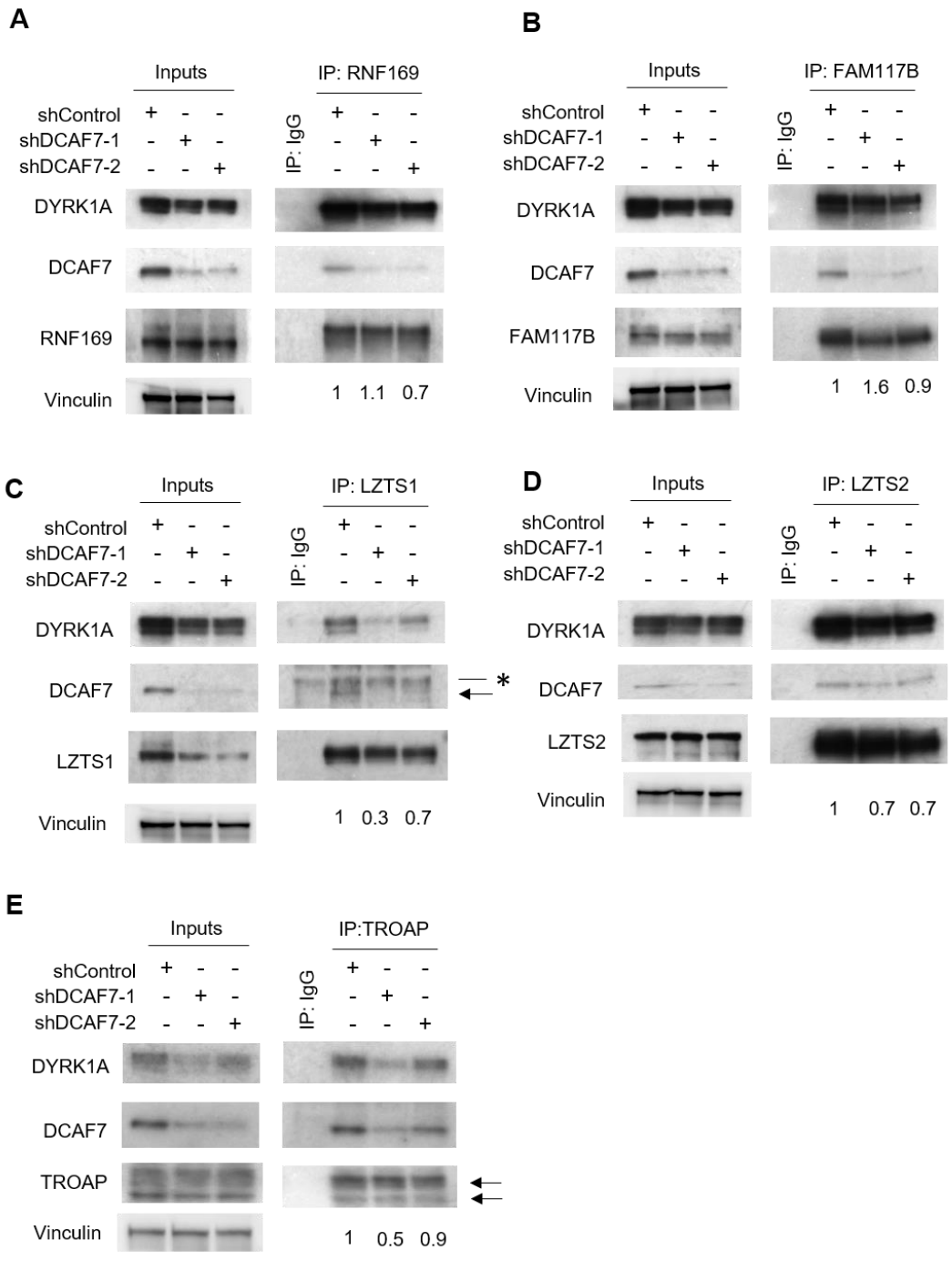

Figure 21: DCAF7 is not required for RNF169, FAM117B, TROAP to bind DYRK1A but it might be needed for LZTS1/2-DYRK1A binding.

(A-E) Lysates from U-2 OS control or shDCAF7 cells were subjected to IP/WB analysis with indicated antibodies. IgG represents non-specific, control antibody. Arrows point to bands of interest and asterisk indicates non-specific band. DYRK1A band density in the IP lanes was quantified relative to bait protein using ImageJ analysis. Numbers indicate DYRK1A band density values relative to input.

Next, we sought to analyze if DYRK1A is required for mediating the interaction of RNF169, FAM117B, LZTS1, LZTS2 or TROAP with DCAF7 (Figure 22). We used U-2 OS control or U-2 OS cell line in which DYRK1A has been knocked out using the CRISPR-Cas9 approach (KO #1 used in Chapter 2). As an additional control, we used a rescue DYRK1A KO cell line in which recombinant DYRK1A was stably re-expressed (same cell line used in Chapter 2). Interestingly, we found that the interaction of RNF169, FAM117B, LZTS1, LZTS2 and TROAP with DCAF7 was reduced in the absence of DYRK1A, but restored in the rescue cell line (Figure 22A-E). Therefore, we can conclude that DYRK1A is required for the interaction of RNF169, FAM117B, LZTS1, LZTS2 and TROAP with DCAF7. Of note, we have consistently observed that FAM117B migrates higher in the presence of DYRK1A than in DYRK1A-KO cells indicating the presence of a post-translational modification. This difference was recapitulated using siRNA knockdown of DYRK1A in T98G cells. Using λ-phosphatase treatment in cell lysates from U-2 OS cells, we were able to confirm that this modification was indeed due to phosphorylation (Figure 23A, B).

It has been reported that the amino acids 93-104 of DYRK1A are required for its interaction with DCAF7 (Glenewinkel et al., 2016). We wanted to determine if the DCAF7 binding site in DYRK1A was also required for its interaction with RNF169, FAM117B, LZTS2 and TROAP (Figure 24). We transiently transfected either GFP (negative control) or GFP-DYRK1A N-terminal deletion constructs or rescue constructs expressing only certain N-terminal regions of DYRK1A (Figure 24A), followed by a GFP-pull down and WB analysis of DYRK1A interacting proteins (Figure 24B). We confirmed that DCAF7 bound to DYRK1A through the 93-104 amino acids (Figure 24A-B; indicated with red boxes), and found that RNF169, LZTS2 or FAM117B were not able to bind DYRK1A when the DCAF7 binding domain was deleted. This suggests

that the DCAF7 binding domain in DYRK1A is required for its interaction with RNF169, LZTS2 and FAM117B. Further, as previously shown, a GFP-DYRK1A fragment comprised of the first 103 amino acids was sufficient for DCAF7 binding (Figure 24A-B; indicated with red boxes). However, this construct did not bind RNF169, FAM117B, or LZTS2. This suggested that the DCAF7 binding region in DYRK1A was necessary but not sufficient for its interaction with RNF169, FAM117B or LZTS2. Interestingly, the minimal region of DYRK1A that binds RNF169, FAM117B and LZTS2 was found to encompass amino acids 77-136 of DYRK1A. Of note, RNF169, FAM117B and LZTS2 bound DYRK1A 77-136 more strongly than DYRK1A 1-176, which also harbors the minimal binding region within it (Figure 24 A-B; indicated with red boxes). Interestingly, a different pattern of binding was observed for TROAP, which bound DYRK1A Δ93-104 even in the absence of DCAF7 binding. However, the deletion of the first 134 amino acids at the N-terminus of DYRK1A was also able to abolish its binding with TROAP while none of the DYRK1A N-terminal rescue fragments were able to bind to TROAP. We therefore used DYRK1A C-terminal constructs and carried out a similar experiment in order to further map the TROAP binding region (Figure 25A-B). Deletion of most of the kinase domain of DYRK1A (DYRK1A Δ174-487) reduced the binding of TROAP to DYRK1A, while a kinase inactive mutant DYRK1A Y321F was able to bind TROAP indicating that the kinase domain but not activity of DYRK1A is required for this interaction (Figure 25A-B).

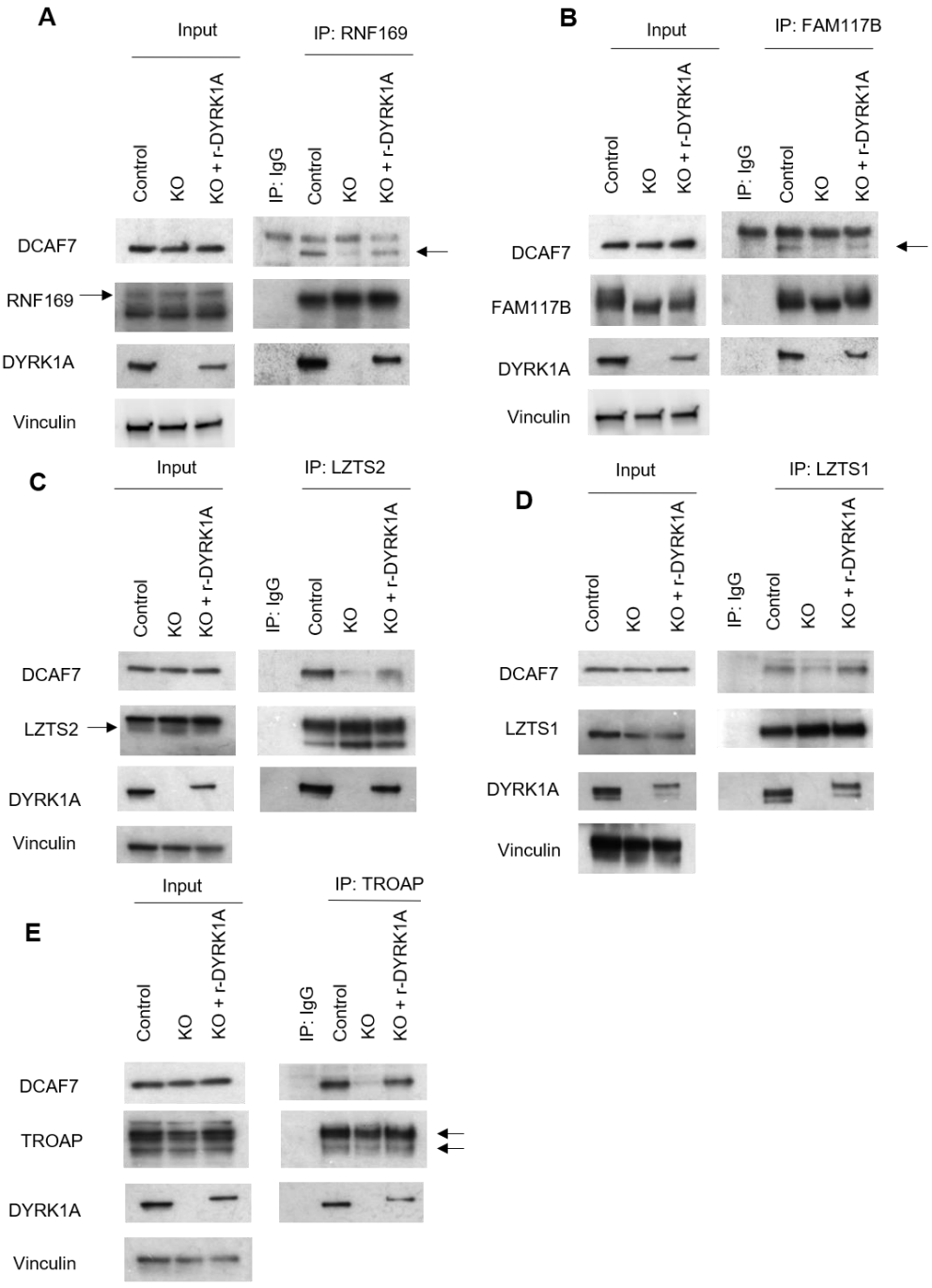

Figure 22: DYRK1A is required for DCAF7 interaction with RNF169, FAM117B, LZTS2, LZTS1 and TROAP.

(A-E) Lysates from U-2 OS control, DYRK1A KO or DYRK1A KO rescue cell line with expression of recombinant DYRK1A were used for IP/WB analysis for indicated proteins. IgG represents a control antibody. Arrows point to bands of interest.

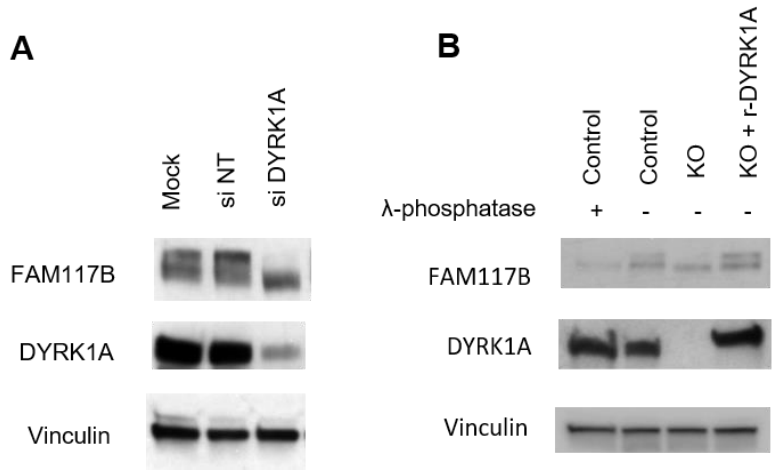

Figure 23: DYRK1A phosphorylates FAM117B.
(A) T98G cell lysates were treated with non-targeting siRNA or siRNA against DYRK1A followed by WB analysis for indicated proteins. (B) Indicated T98G cell lysates were incubated with or without λ-phosphatase followed by WB analysis.

3.2.4. Effect of DYRK1A on localization of its interacting proteins

Since binding to DYRK1A was required for novel DYRK1A interacting proteins to bind DCAF7, we wanted to investigate whether loss of binding was due to a change in sub-cellular localization in DYRK1A-KO cells. We used U-2 OS cells stably expressing epitope-tagged RNF169, FAM117B, LZTS2, LZTS1 or TROAP, followed by immunofluorescence staining using anti-HA antibody and confocal microscopy. Consistent with our cyto-nuclear fractionation, we observed RNF169 to be nuclear, however, its localization did not change in the absence of DYRK1A. All the other DYRK1A interacting proteins were cytoplasmic both in the presence and in the absence of DYRK1A. However, we observed increased FAM117B accumulation in the peri-nuclear space in the absence of DYRK1A. Further studies will be required to confirm this and to analyze the mechanisms that regulate these proteins in the cell (Figure 26, A-F).

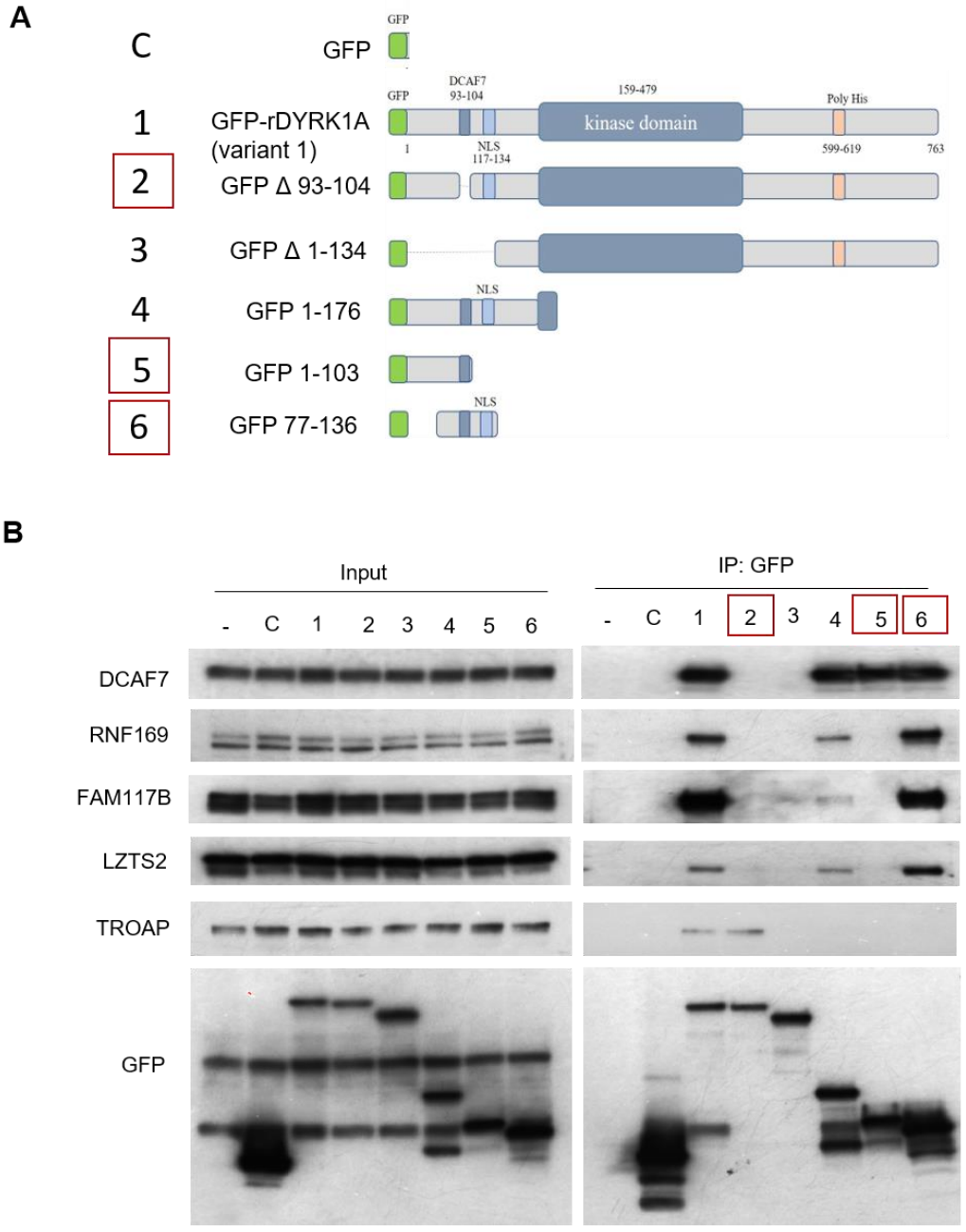

Figure 24: DCAF7 binding domain in DYRK1A is necessary but not sufficient for interaction with RNF169, FAM117B, LZTS2 and is not involved in binding TROAP.
(A) Schema of GFP-DYRK1A constructs used in B. (B) T98G cells were transfected with indicated DYRK1A constructs and used for IP with GFP-trap beads followed by a WB for proteins of interest. A composite figure was created from four different IP/WB experiments in order to avoid any overlapping signals from residual antibodies. The GFP and DCAF7 pull downs were identical in each experiment, and representative panels are shown.

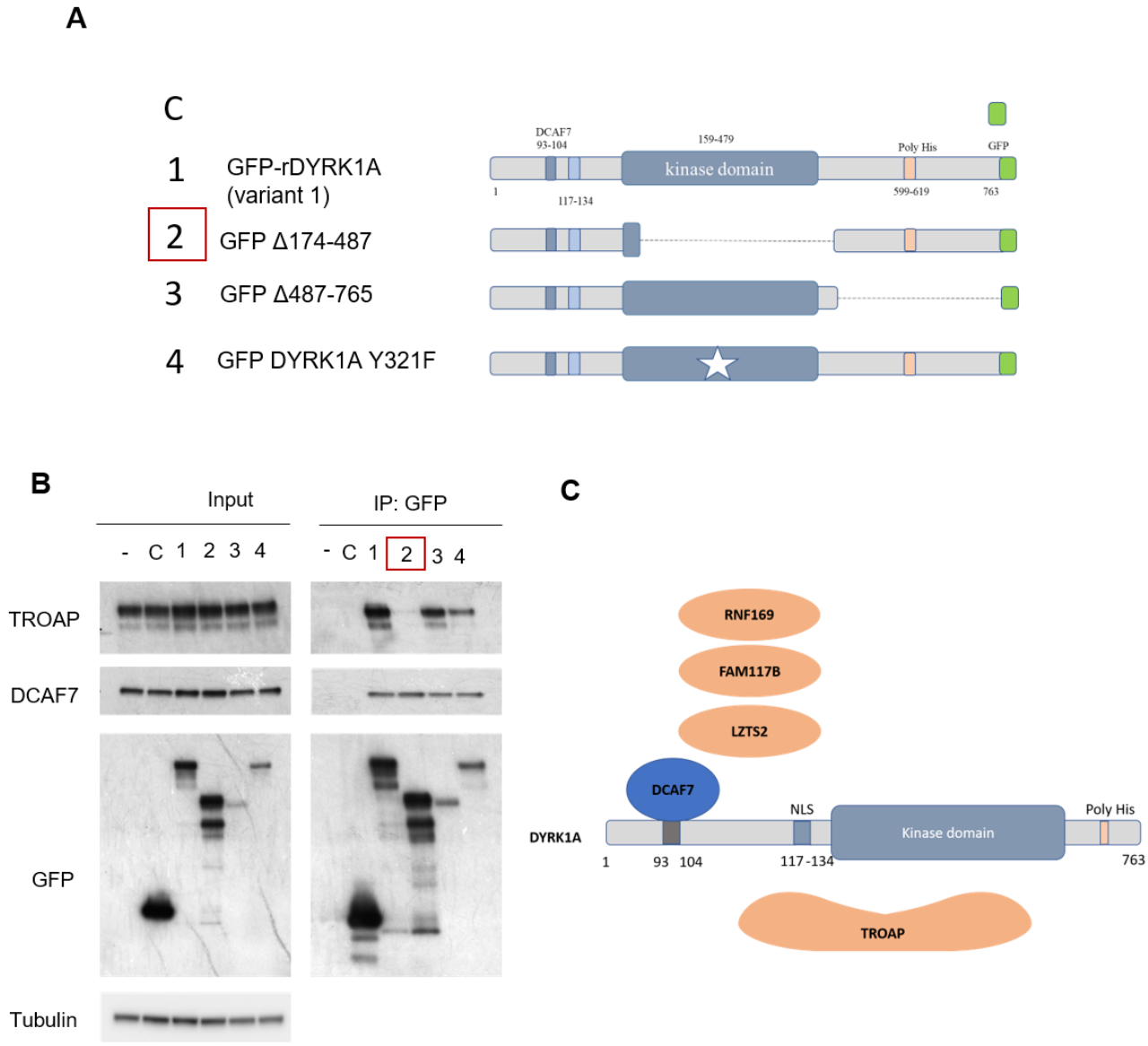

Figure 25: TROAP binding requires the kinase domain of DYRK1A.
(A) Schema of GFP-DYRK1A constructs used in B. (B) T98G cells were transfected with indicated DYRK1A constructs and used for IP with GFP-TRAP beads followed by a WB analysis for proteins of interest. (C) Schema depicting the regions of DYRK1A required for binding DCAF7, RNF169, FAM117B, LZTS2 and TROAP.

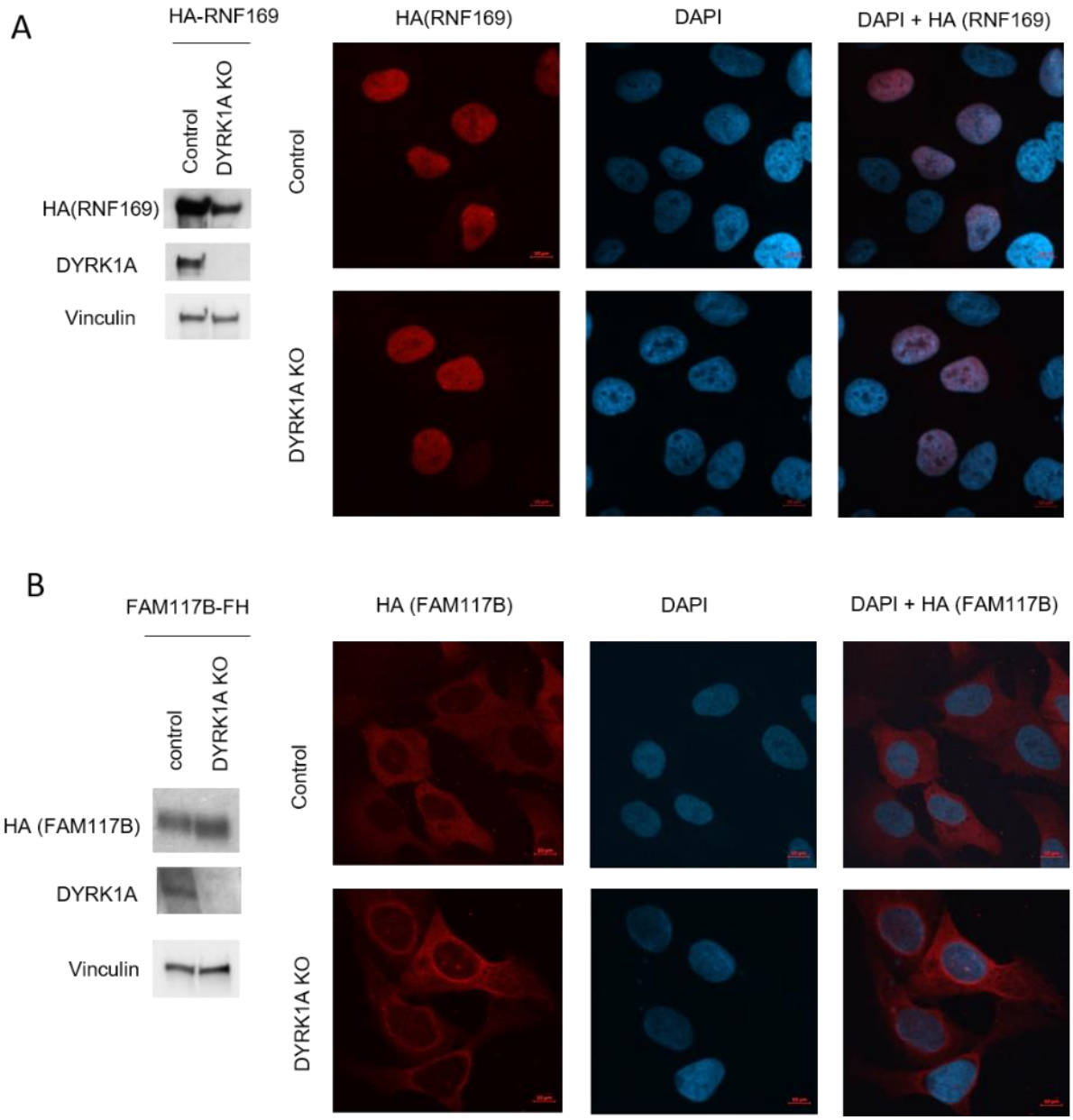

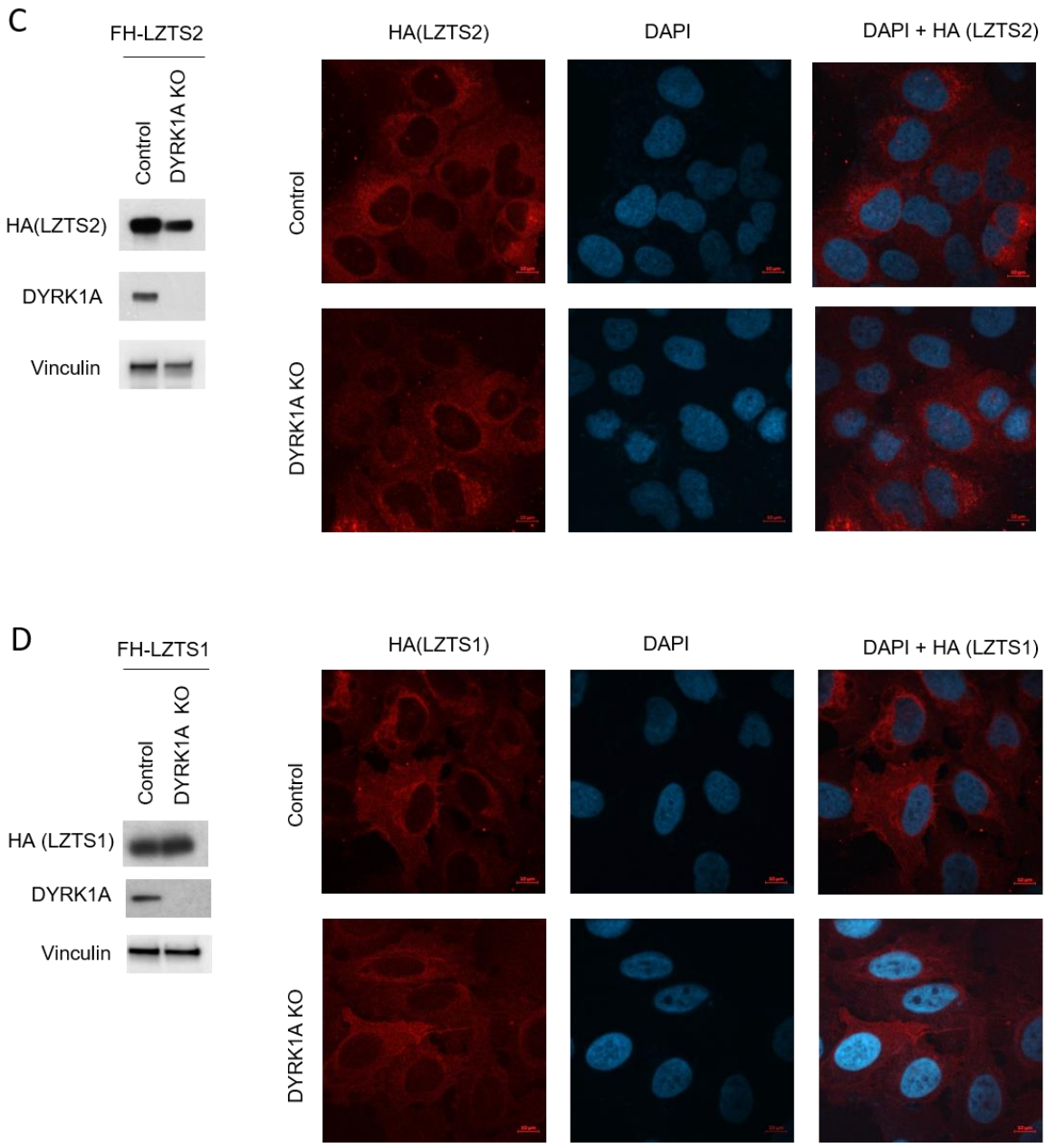

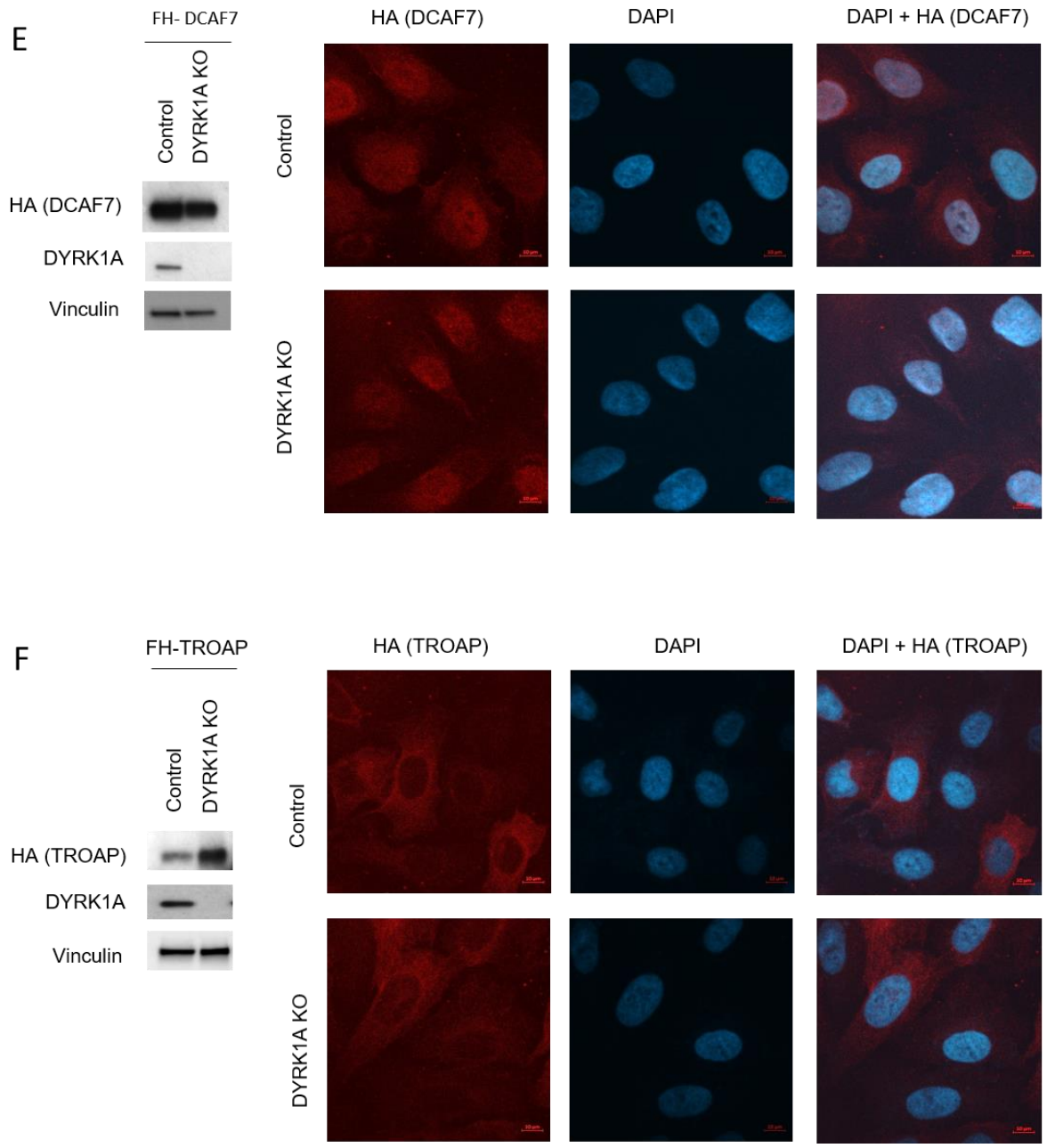

Figure 26: Localization of DYRK1A interacting proteins in the presence or absence of DYRK1A

U-2 OS control or DYRK1A KO cells stably expressing (A) HA-RNF169, (B) FAM117B-FH, (C) FH-LZTS2, (D) FH-LZTS1, (E) FH-DCAF7 and (F) FH- TROAP were plated on coverslips, fixed and stained with an anti-HA antibody followed by immunofluorescence analysis. Left WB panel indicates cell lines used and immunofluorescence images are on the right. Scale bar is 10μm.

3.2.5. Effect of DCAF7 on DYRK1A mediated growth suppression

Overexpression of DYRK1A causes inhibition of cell proliferation and G0/G1 cell cycle arrest in several cell lines, including U-2 OS (Litovchick et al., 2011). Since DCAF7 is a major DYRK1A interacting protein that also binds other DYRK1A interactors, we first analyzed if DCAF7 is involved into DYRK1A mediated growth suppression. We transiently transfected U-2 OS cells with either full length or DYRK1A deletion mutant deficient in binding DCAF7 (GFP-DYRK1A Δ93-104), or GFP alone as a control. This was followed by fixing and staining the cells with anti- Ki67 antibody. Ki67 is a protein that is present in all active phases of the cell cycle but absent in the resting G0 phase. Therefore, it is an excellent marker for measuring the percentage of actively cycling cells (Scholzen & Gerdes, 2000). U-2 OS cells transfected with GFP-DYRK1A had a significantly reduced fraction of Ki67-positive cells as compared to cells transfected with GFP alone (Figure 27B). Cells transfected with GFP- DYRK1A Δ93-104 also had significantly reduced Ki67 positive cells as compared to the GFP alone (Figure 27). This suggests that DYRK1A is able to inhibit proliferation of cells even when unable to bind DCAF7. Moreover, GFP-DYRK1A or GFP-DYRK1A Δ93-104 similarly suppressed proliferation of U-2 OS cell lines stably overexpressing DCAF7 (Figure 27B). This suggests that even when DCAF7 is present in excess, it does not overcome the growth suppressive function of DYRK1A (Figure 27A-B). Overexpression of DYRK1A leads to cell cycle arrest in the G0/G1 phase of the cell cycle (Litovchick et al., 2011). Therefore, we wanted to characterize the cell cycle profile of the cells arrested upon expression of the DYRK1A mutant deficient in binding DCAF7. For additional confirmation, we also used another mutant that lacked the N- terminus of DYRK1A (DYRK1A Δ1-134). We used the GFP-negative cells within each sample as our control. As compared to GFP negative cells in the same samples, cells transfected with GFP-DYRK1A or

GFP-DYRK1A deletion mutants were able to cause a G0/G1 cell cycle arrest (compare orange bars in Figure 28A). Further, DYRK1A overexpression in shDCAF7 cell lines also led to a G0/G1 cell cycle arrest (Figure 28B). These data collectively suggest that DYRK1A does not require DCAF7 for its ability to induce G0/G1 arrest (Figures 27,28). Since RNF169, LZTS2, FAM117B also bind through the N-terminus of DYRK1A, it is likely that they do not play a role in the growth suppressive function of DYRK1A.

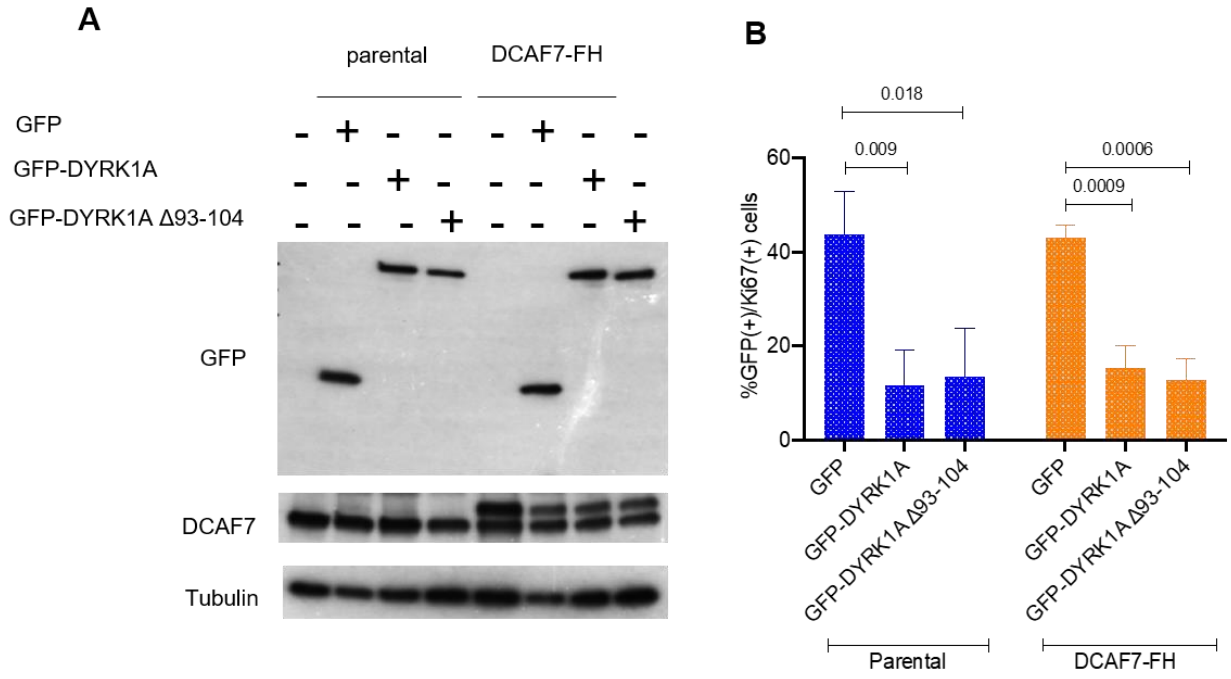

Figure 27: Role of DCAF7 in DYRK1A-mediated inhibition of proliferation.
(A) WB indicating U-2 OS parental and DCAF7-FH cell lines transfected with GFP or GFP-DYRK1A constructs. (B) Graph shows a fraction of GFP (+)/Ki67 (+) cells in the indicated cell lines measured by FACS analysis. Graph indicates average of 3 biological replicates and error bars indicate standard deviation. p-values were obtained using two tailed Student's t-test and are shown on the graphs.

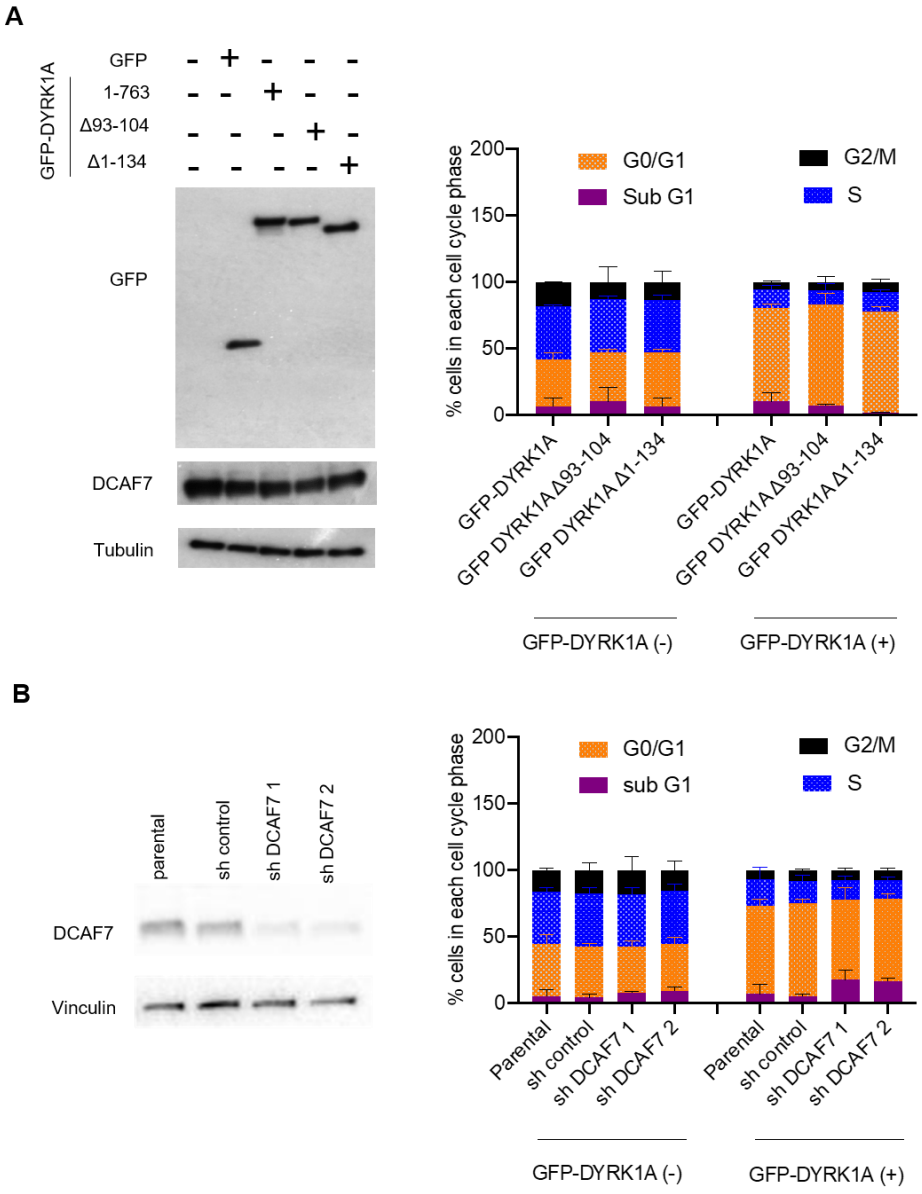

Figure 28: Role of DCAF7 in DYRK1A-mediated growth arrest.
U-2 OS cells or derivatives expressing sh control or sh DCAF7 were transfected with indicated GFP-DYRK1A constructs followed by cell cycle analysis using PI staining of DNA. (A) Left panel shows representative WB indicating expression of GFP or GFP-DYRK1A in U-2 OS parental cells. Graph shows average distribution of GFP DYRK1A (-) or GFP-DYRK1A (+) cells in each cell cycle phase from 2 biological repeats. Here and below, the error bars indicate standard deviation. (B) Left panel shows representative WB indicating expression of DCAF7 in sh control or DCAF7 knockdown (two independent clones) cell lines used for cell cycle analysis. Right panel indicates average counts of cells in each cell cycle phase from GFP DYRK1A (-) or GFP-DYRK1A (+) cells from 3 biological repeats.

The experiments described above analyzed the growth suppressive function of DYRK1A after a transient transfection. We wanted to determine whether DCAF7 could influence the growth suppressive effect of DYRK1A overexpression for an extended time period. We used U-2 OS cells capable of inducible expression of wild type or kinase dead DYRK1A (DYRK1A K188R) under the control of a doxycycline responsive promoter (Himpel et al., 2001; Litovchick et al., 2011), with and without overexpression of DCAF7 in the same background (Figure 29C). We induced DYRK1A expression using doxycycline in U-2 OS control or DCAF7-overexpressing cells for a period of 8 days, and analyzed cell proliferation using crystal violet assay (Figure 29A-B). Consistent with published results, a significant reduction in cellular proliferation was observed with extended overexpression of wildtype DYRK1A but not the kinase dead mutant, as compared to their uninduced controls (Litovchick et al., 2011). However, this effect was observed to a lesser extent in cells over expressing DCAF7 (Figure 29A-B). This suggests that DCAF7 and DYRK1A can have opposing effects on maintenance of cell cycle arrested state.

3.2.6. Effect of DYRK1A interacting proteins on DYRK1A activity towards LIN52

DYRK1A is required for phosphorylation of the LIN52 subunit of the MuvB core leading to the assembly of the DREAM complex (Litovchick et al., 2011). We therefore wanted to analyze if DCAF7 and other DYRK1A-interacting proteins affected DYRK1A activity towards LIN52 phosphorylation. Briefly, lysates from U-2 OS control, or DCAF7 depleted cells or overexpressing cells were incubated with GST-LIN52 and ATP for 0, 30 or 60 minutes. Consistent with lack of effect on G0/G1 arrest function, knockdown or overexpression of DCAF7 did not influence DYRK1A activity towards LIN52 (Figure 30 A, B, C).

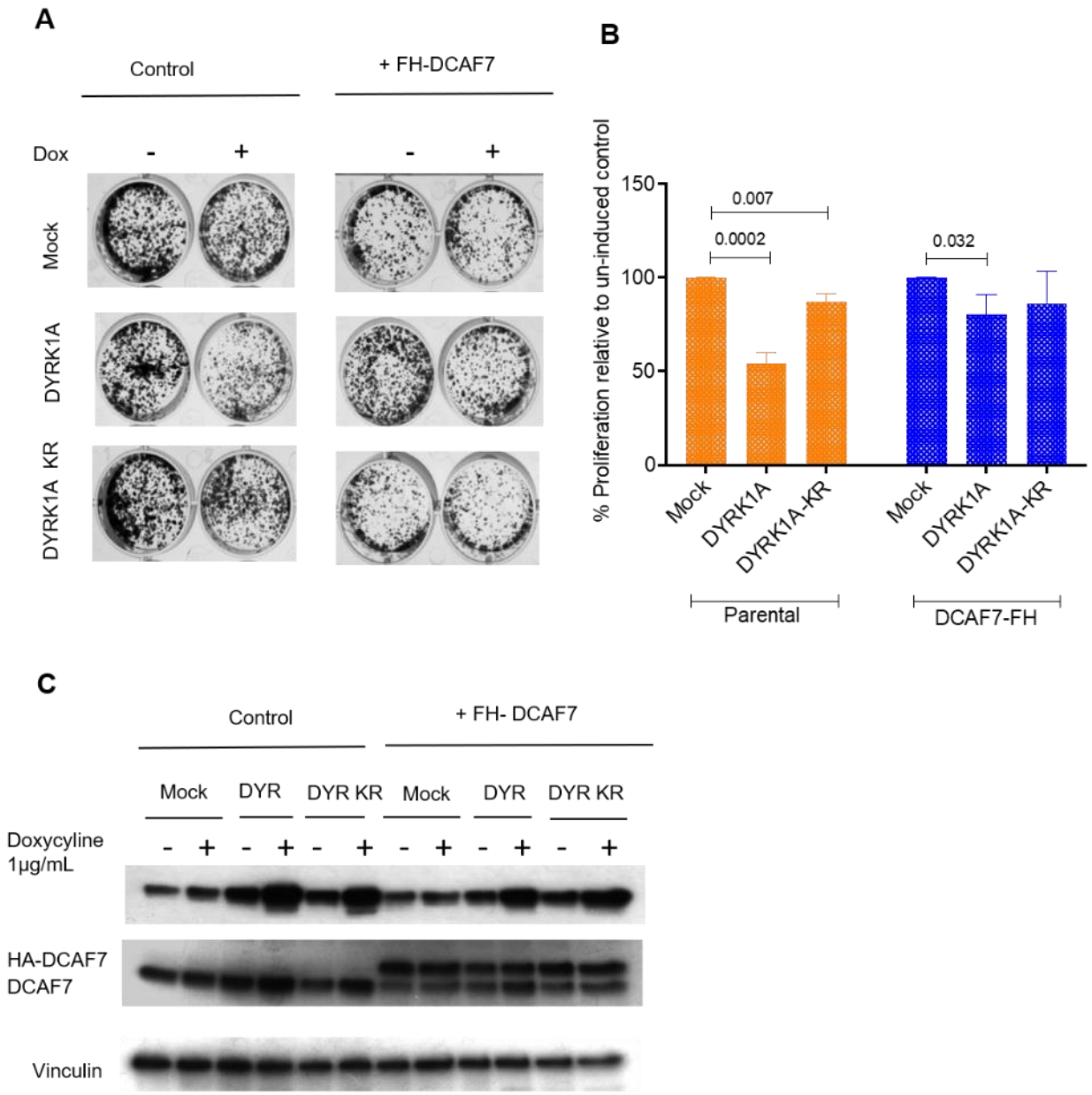

Figure 29: Role of DCAF7 in DYRK1A-mediated growth arrest
U-2 OS control or DCAF7 overexpressing cells were induced with Doxycycline to express DYRK1A WT or DYRK1A KR followed by crystal violet staining, dissolving the dye and colorimetric quantification. (A) Representative images of crystal violet stained plates (B) Graph indicating proliferation of Doxycycline-treated cells relative to untreated control from three biological replicates. Statistical significance was calculated using two-tailed Student's t-test and significant p-values are shown on the graph. (C) Representative WB with cell lines used in this experiment.

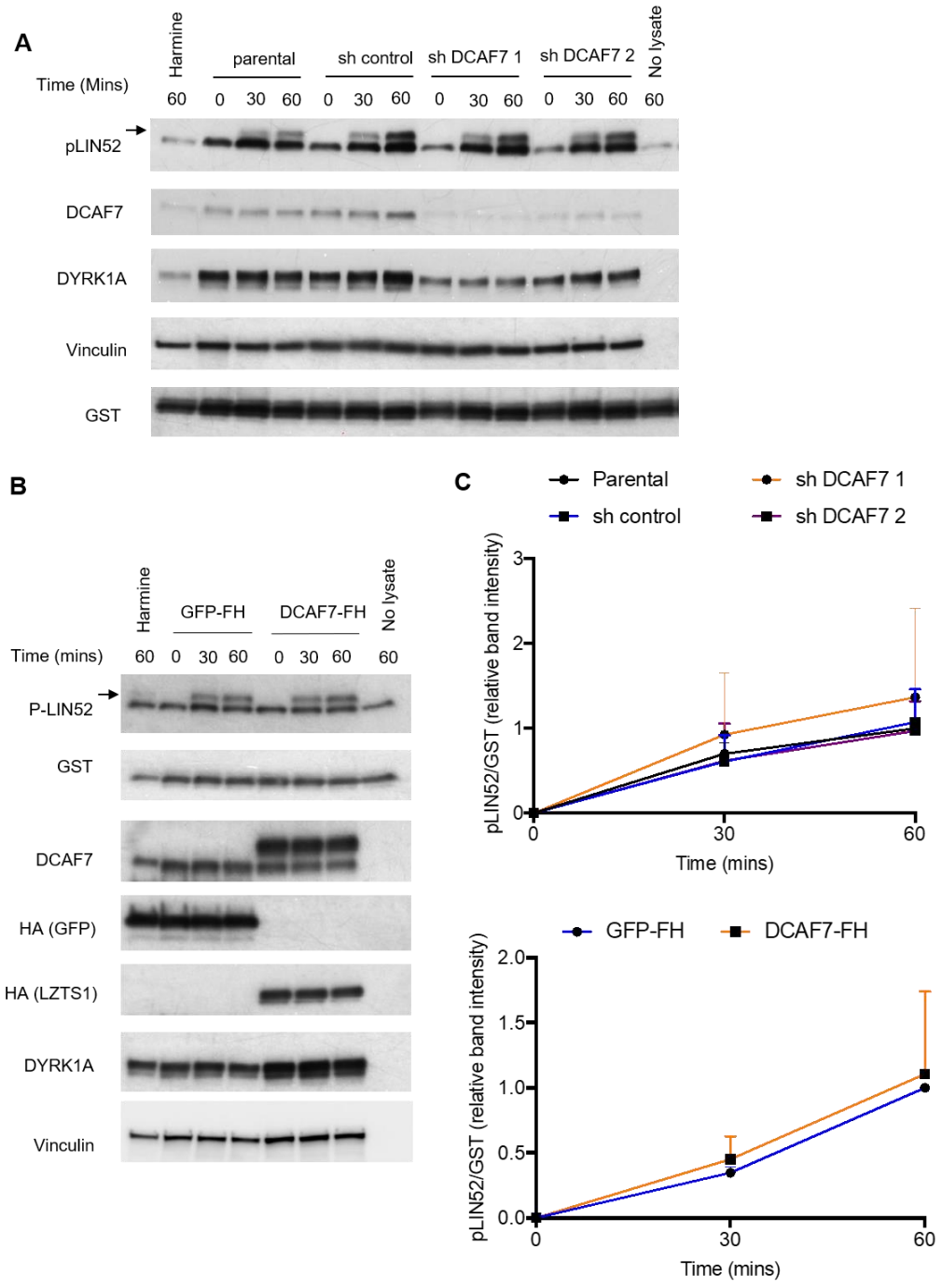

Figure 30: DCAF7 does not influence DYRK1A activity towards LIN52
(A) Cell lysates from U-2 OS control or shDCAF7 cell lines were incubated with GST-LIN52, kinase buffer and ATP for an *in-vitro* kinase assay for different time points, and analyzed by WB Representative WB from one experiment is shown. (B) U-2 OS GFP-FH or DCAF7-FH cell lysates were used for an *in-vitro* kinase assay as in (A) and analyzed by WB. Representative WB from one experiment is shown. (C) Graphs depict ImageJ densitometry analysis of p-LIN52 signal relative to GST (average from three independent experiments). Error bars show standard deviation. No statistically significant differences were found using 2-way ANOVA.

Next, we used the same approach to analyze if any of the other DYRK1A interacting proteins including RNF169, FAM117B, TROAP, LZTS1 or LZTS2 regulated the activity of DYRK1A towards LIN52. Transient depletion or overexpression of RNF169, FAM117B and TROAP did not have an effect on LIN52 phosphorylation (Figure 31 A-C). Since there was no significant effect, we only report here the quantifications of data for these assays. On the other hand, knockdown of either LZTS1 or LZTS2 led to a decrease in DYRK1A-mediated LIN52 phosphorylation (Figure 33A and 32A). We confirmed this result using an additional siRNA against LZTS1 (Figure 33B), and two different shRNA clones against LZTS2 (Figure 32B). Note that the extent of decrease in LIN52 phosphorylation correlated with the level of LZTS2 knockdown [compare shLZTS2 (1) to shLZTS2 (2) in Figure 32B].

From our biochemical experiments, we know that LZTS1 and LZTS2 bind each other. Therefore, we wanted to analyze if LZTS1 and LZTS2 have a combined effect towards LIN52 phosphorylation or if they have redundant functions. We transiently knocked down LZTS1 in U-2 OS control or the two shLZTS2 cell lines and analyzed the effect on DYRK1A mediated LIN52 phosphorylation (Figure 34). Like in Figures 32 and 33, single knockdown of LZTS1 or LZTS2 did lead to a reduction in LIN52 phosphorylation. However, combined knockdown of LZTS1 and LZTS2 failed to completely inhibit DYRK1A activity towards LIN52. Of note, knocking down LZTS1 in the cell line expressing shLZTS2 (2) gives a better inhibition of DYRK1A activity as compared to the control but it was still not a complete inhibition. Therefore, we can conclude that LZTS1 and LZTS2 regulate DYRK1A activity together and not redundantly. Of note that knock down of LZTS1 in shLZTS2 cell lines tends to further reduce LZTS2 levels suggesting that LZTS1 could be required for optimal LZTS2 levels.

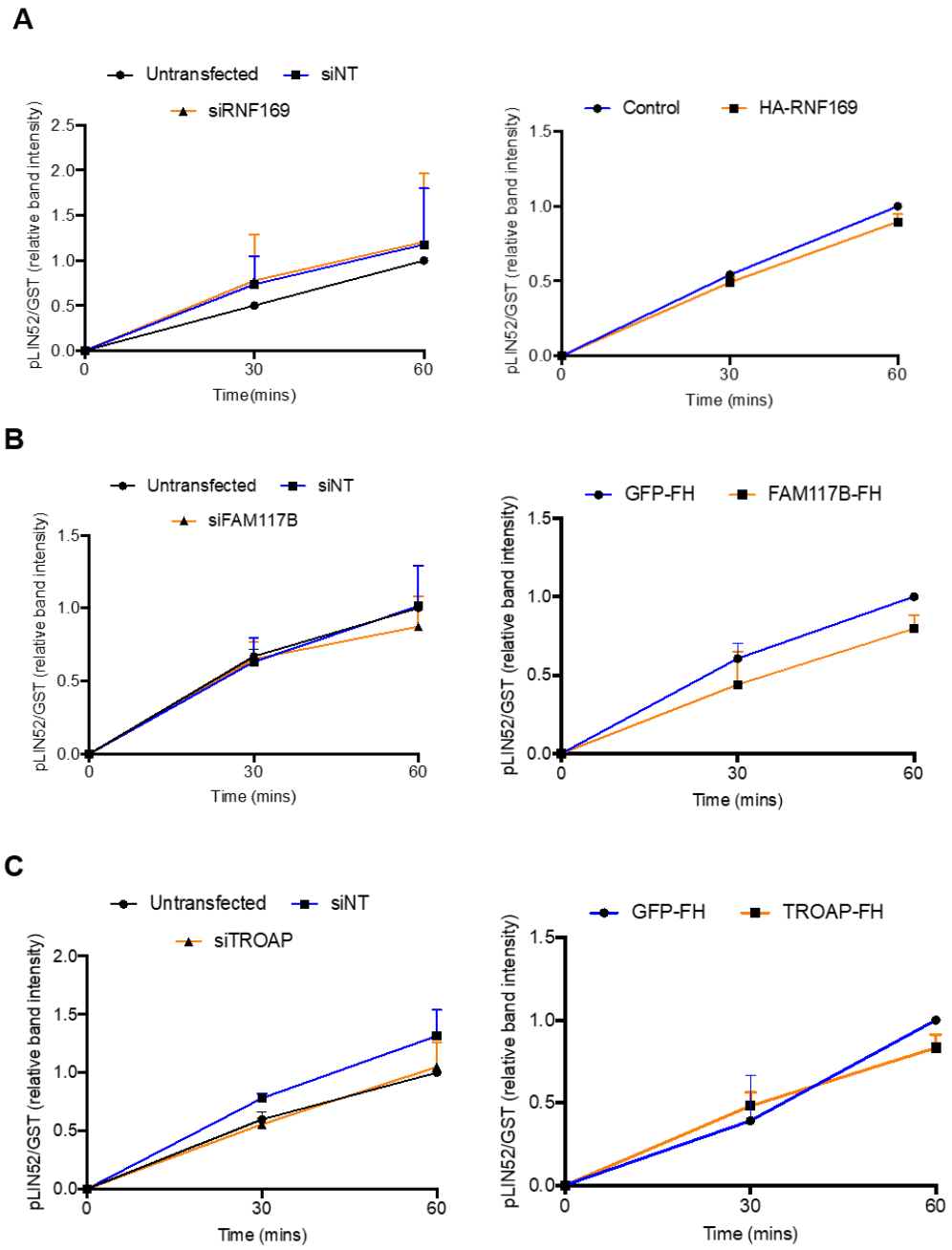

Figure 31: Depletion of RNF169, FAM117B or TROAP does not influence DYRK1A activity towards LIN52

(A-C) Cell lysates from U-2 OS control or indicated siRNA depleted proteins or overexpressed proteins were used for an *in-vitro* kinase assay as explained in Figure 30 and analyzed by WB with LIN52 S28-phospho specific antibody as described in- (Litovchick et al., 2011). GST-LIN52 signal was quantified using ImageJ analysis. Graphs show average p-LIN52 band density relative to GST band density from three independent experiments. Error bars indicate standard deviation. No statistically significant differences were found using 2-way ANOVA to compare test groups to controls.

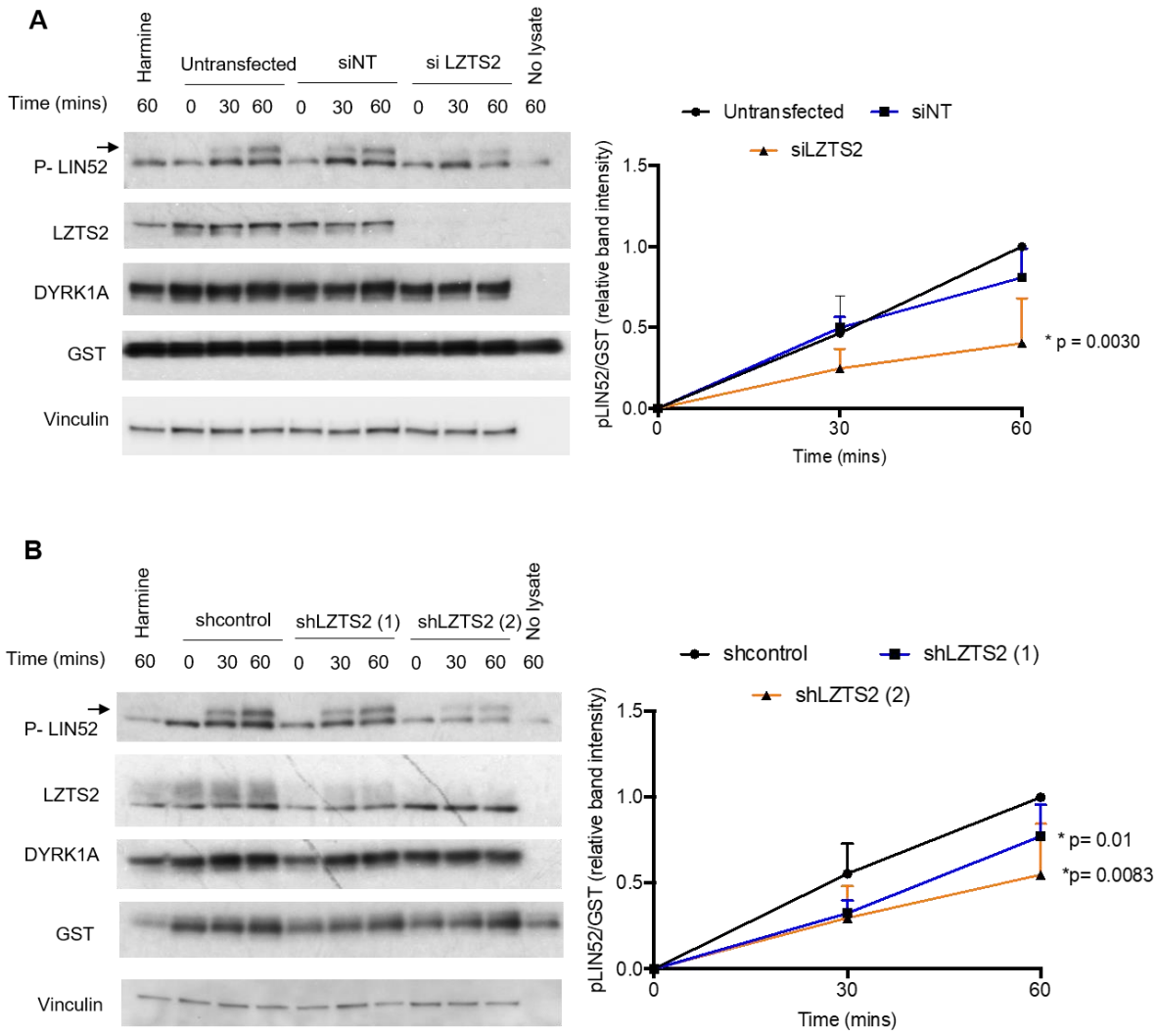

Figure 32: Depletion of LZTS2 decreases DYRK1A activity towards LIN52
(A, B) Cell lysates from U-2 OS control or siRNA/shRNA mediated LZTS2 depleted cell lines or were used for an *in-vitro* kinase assay as described in Figure 30. Representative WB's from one experiment are shown. Graphs show average p-LIN52 band density relative to GST band density from three independent experiments. Error bars indicate standard deviation. Statistical significance was calculated using 2-way ANOVA to compare test groups to untransfected (A) or shControl (B) group and significant p-values are indicated on the graphs.

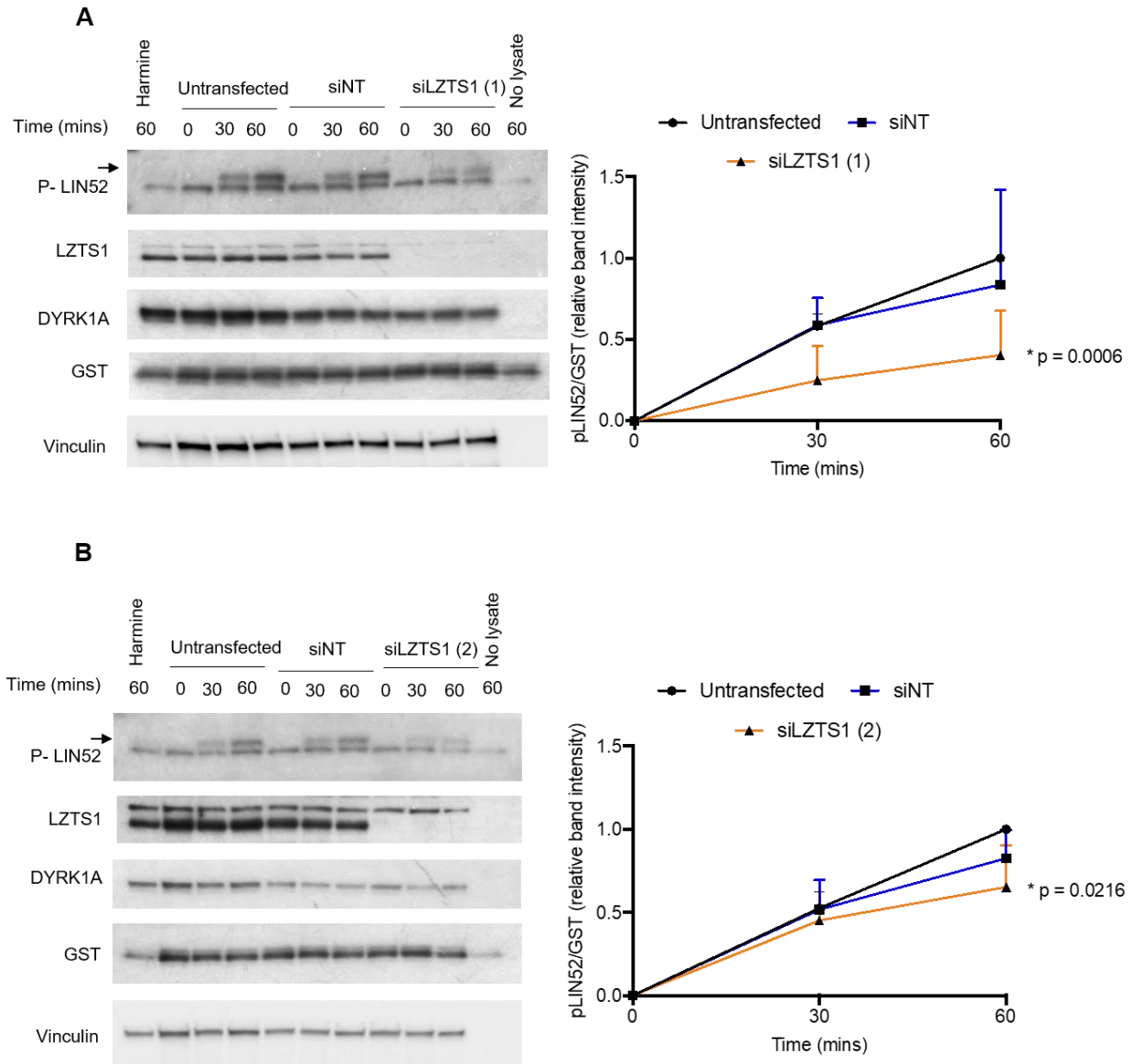

Figure 33: Depletion of LZTS1 decreases DYRK1A activity towards LIN52.
(A, B) Cell lysates from U-2 OS control or two different siRNA mediated LZTS1 depleted cell lines were used for an *in-vitro* kinase assay as described in Figure 30. Representative WB from one experiment are shown. Graphs show average p-LIN52 band density relative to GST band density from three independent experiments. Error bars indicate standard deviation. Statistical significance was calculated using 2-way ANOVA to compare test groups to untransfected controls. Significant p-values are indicated on the graphs.

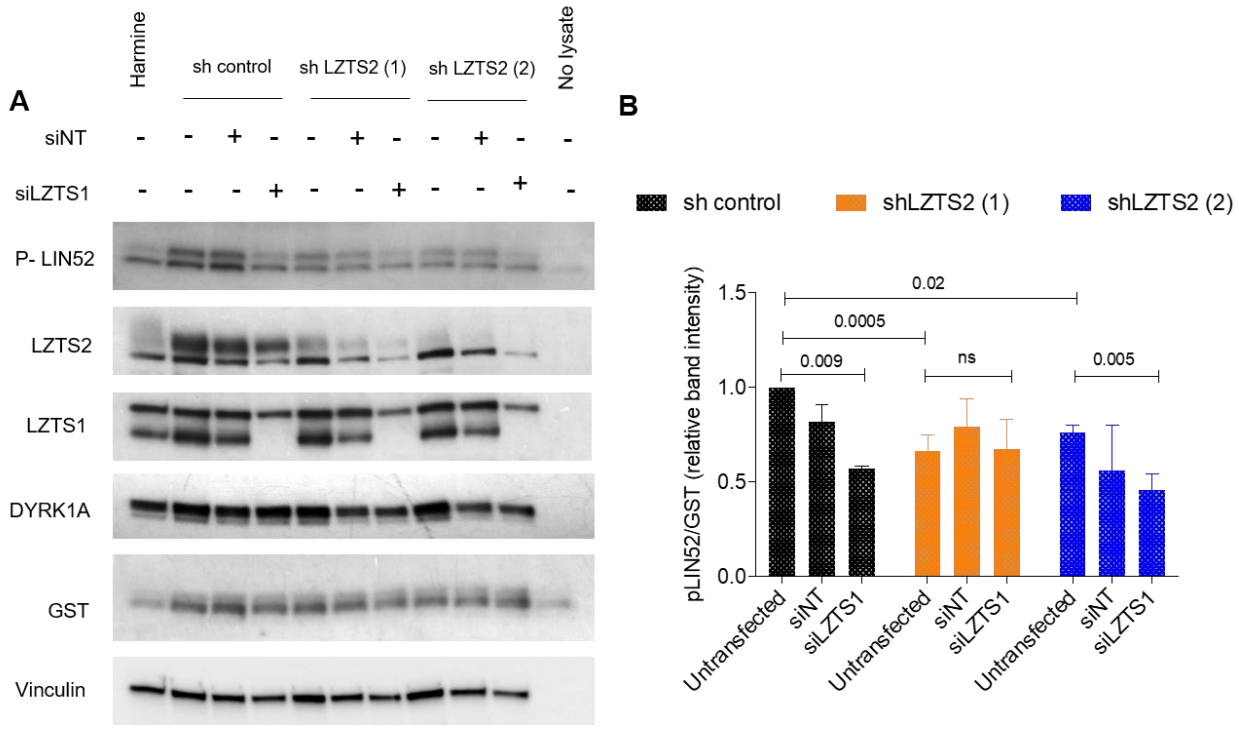

Figure 34: Depletion of both LZTS1 and LZTS2 does not completely abolish DYRK1A activity towards LIN52.
(A) Cell lysates from U-2 OS control or shLZTS2 cell lines treated with control siRNA or siRNA against LZTS1 were used for an *in-vitro* kinase assay for 60 minutes as described earlier. Graphs show average p-LIN52 band density relative to GST band density from three independent experiments. Error bars indicate standard deviation. Statistical significance was calculated using a two tailed Student's t-test and p-values are indicated on the graph.

Next, we analyzed if transient knockdown of LZTS1, LZTS2 or both had an effect on GFP-DYRK1A mediated inhibition of proliferation. We analyzed this by transiently knocking down LZTS1, LZTS2 or both in U-2 OS cells followed by GFP or GFP DYRK1A transfection (Figure 35A). The number of GFP (+)/Ki67 (+) cells were scored after immunostaining for Ki67. We observed that as compared to the GFP controls, GFP-DYRK1A was able to inhibit proliferation to a similar extent even with depletion of LZTS1 or LZTS2 or both. Therefore, LZTS1 or LZTS2 do not significantly contribute to the growth suppressive function of DYRK1A under overexpressed conditions (Figure 35 A-B). Note that the levels of LZTS1 and LZTS2 are higher

when GFP-DYRK1A is overexpressed, suggesting that DYRK1A regulates the levels of LZTS1/2.

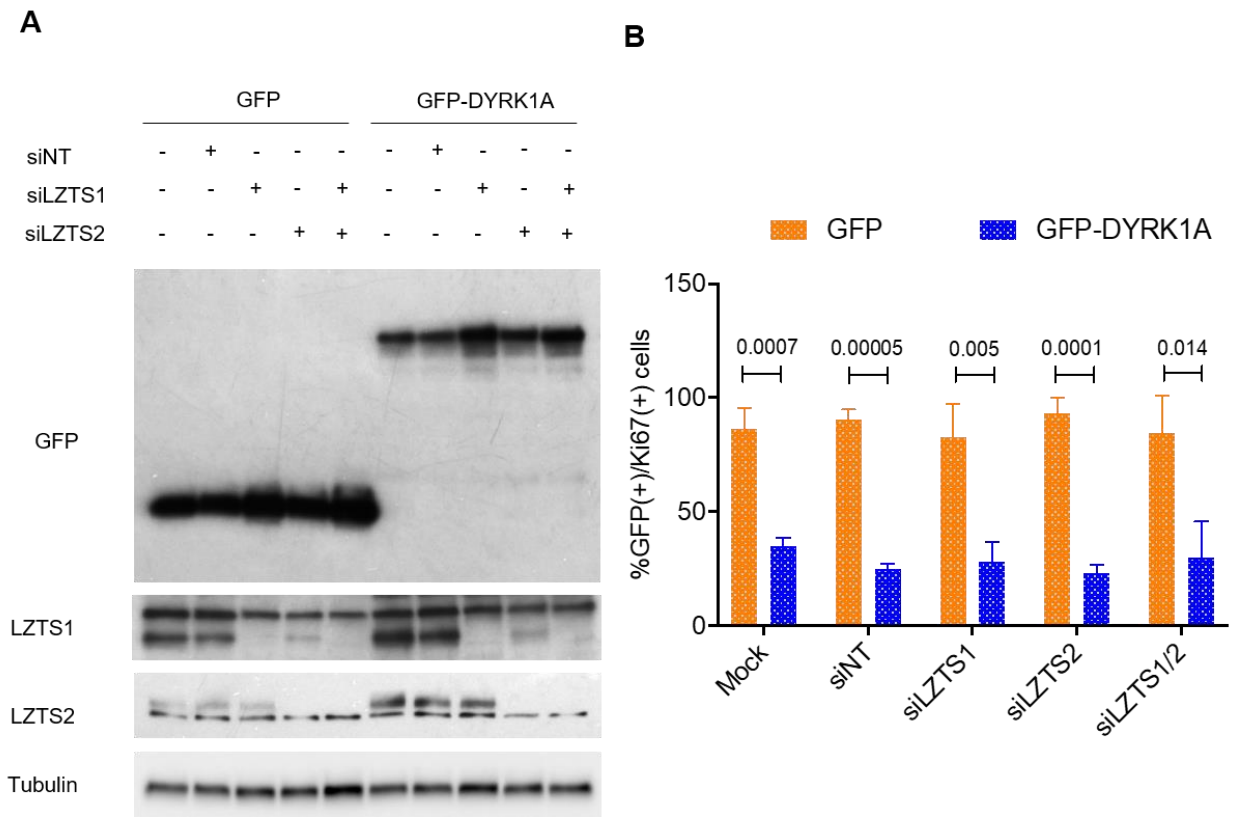

Figure 35: Effect of LZTS1 and LZTS2 on DYRK1A mediated inhibition of proliferation. (A) Representative WB indicating knockdown of LZTS1 or LZTS2 or both in U-2 OS cell lines expressing GFP or GFP-DYRK1A. These cells were fixed and immunostained with anti-Ki67 antibody. (B) Manual quantification of at least 100 GFP+/Ki67+ cells was performed for each repeat. Graphs show average values obtained from 3 biological replicates. Error bars indicate standard deviation. Statistical significance was calculated using a two tailed Student's t-test and significant p-values are shown on the graph.

Next, we investigated the effect of overexpression of LZTS1 or LZTS2 on DYRK1A activity in cell extracts, and found that neither protein affected DYRK1A activity towards LIN52 (Figure 36B). However, we noticed that the migration of both DYRK1A and LZTS2 was altered with time in LZTS2 overexpressing cells, suggesting that these proteins were post translationally

modified (Figure 36A). Interestingly, such changes were not observed in LZTS1- overexpressing cells (Figure 36B).

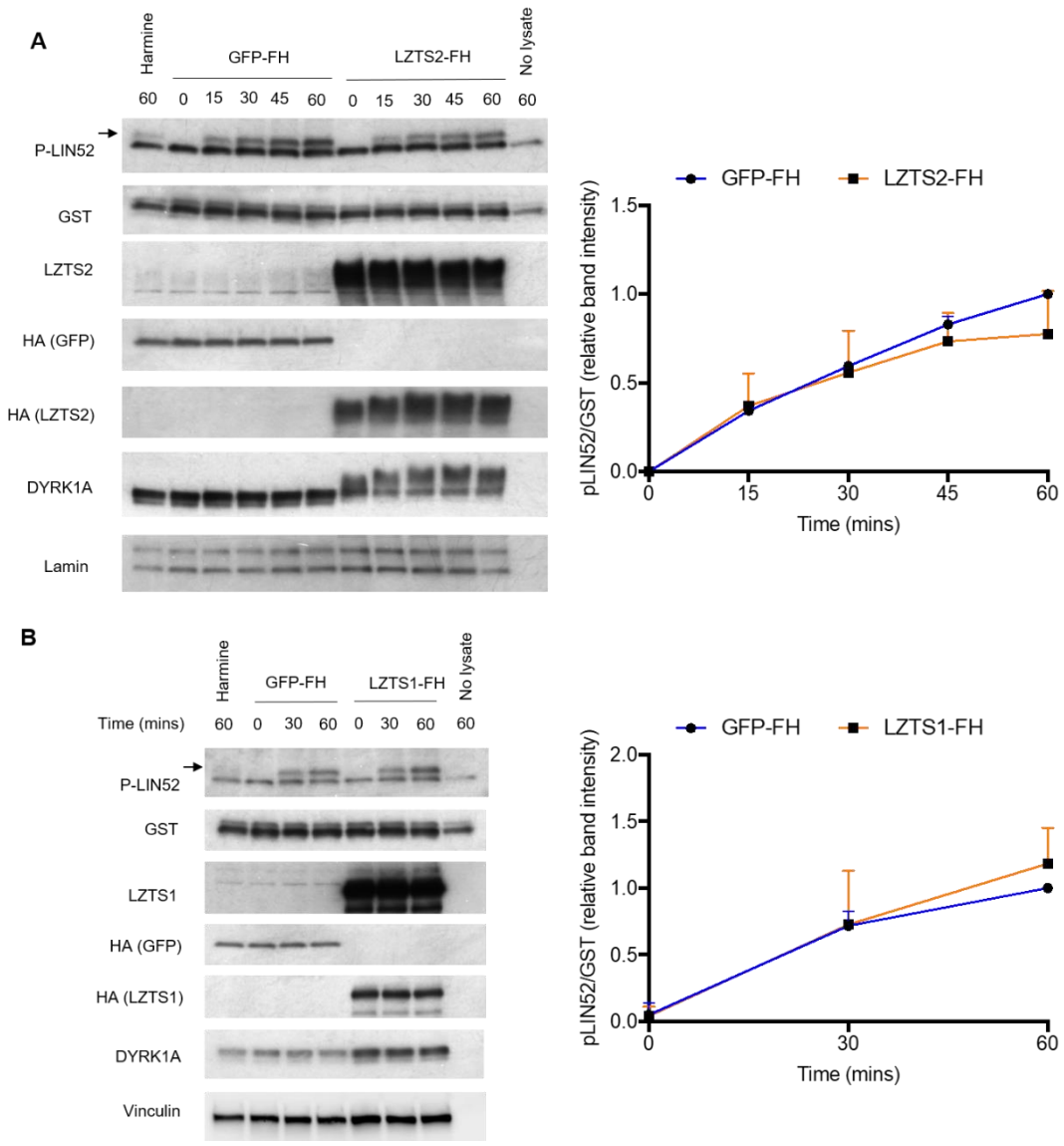

Figure 36: Effect of LZTS2 or LZTS1 overexpression on DYRK1A activity towards LIN52. (A and B) Cell lysates from control or from cells overexpressing LZTS2 (A) or LZTS1 (B) were used for an *in-vitro* kinase assay as in Figure 30 followed by WB analysis for the indicated proteins. WB shown is from one experiment (Left panels). Graphs depict average values obtained following ImageJ densitometry analysis of p-LIN52 signal relative to GST signal from three independent experiments. Error bars indicate standard deviation (Right panels). No statistically significant differences were found using 2-way ANOVA.

3.2.7. Post translational modification of DYRK1A in LZTS2 overexpressing cells is a phosphorylation

Next, we explored if the modification of DYRK1A and LZTS2 in LZTS2-overexpressing cells was due to phosphorylation. We carried out immunoprecipitation of DYRK1A from control or LZTS2 overexpressing cells followed by treatment of the beads with λ-phosphatase. WB analysis indicated that as compared to the untreated control, λ-phosphatase treatment abrogated the gel shift of DYRK1A in LZTS2 overexpressing cells, suggesting that it was indeed a phosphorylation (Figure 37A). This was also confirmed by WB analysis using a PhosTag gel (Figure 37B). This experiment also revealed that LZTS2 itself was also phosphorylated (Figure 37A).

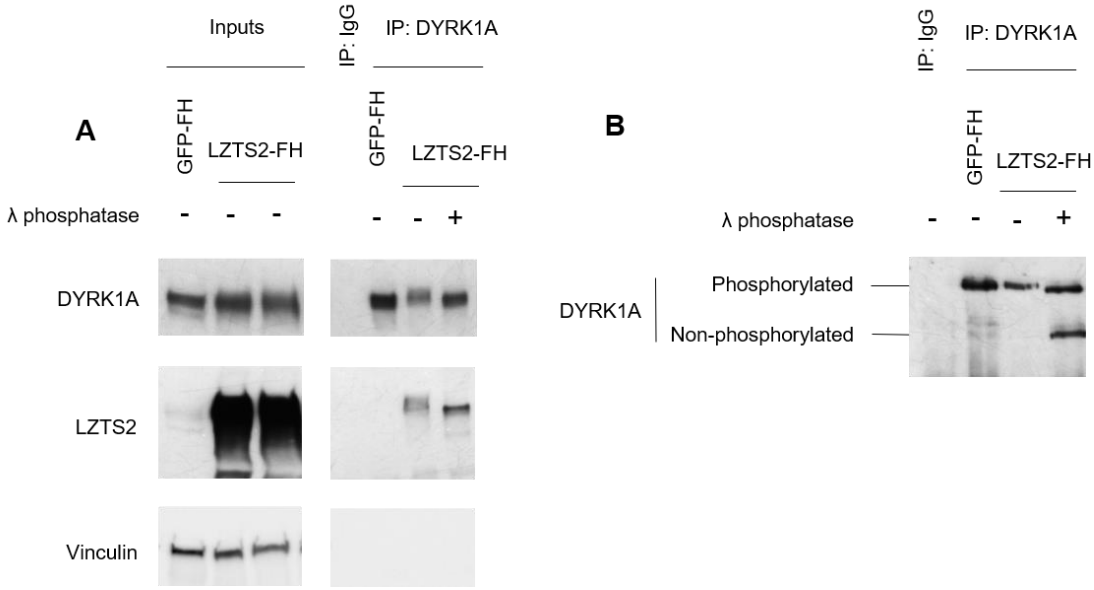

Figure 37: DYRK1A and LZTS2 in LZTS2 overexpressing cells are modified by phosphorylation.
(A) Immunoprecipitation of DYRK1A from U-2 OS GFP-FH (control) or LZTS2-FH cell lysates was performed followed by incubation of the indicated sample with λ-phosphatase and WB analysis. Inputs and 1/3rd of IP samples were loaded in (A). (B) The remaining IP samples were loaded on a PhosTag gel followed by WB detection of DYRK1A.

Next, we investigated if DYRK1A phosphorylation in LZTS2 overexpressing U-2 OS cells is caused by autophosphorylation. We treated cell lysates with Harmine or with another DYRK1A inhibitor CX4945, before performing an *in-vitro* kinase assay (Göckler et al., 2009; H. Kim et al., 2016; Walte et al., 2013). Untreated lysates or lysates treated with DMSO were used as a control. The gel shift of DYRK1A or LZTS2 was not abolished by inhibition of the kinase activity of DYRK1A, while LIN52 phosphorylation was completely blocked in the same assay (Figure 38A). Moreover, HA-tagged LZTS2 migrated in a similar way in control and DYRK1A-KO cell lines (Figure 38B). Thus, DYRK1A and LZTS2 are phosphorylated by a kinase other than DYRK1A itself in U-2 OS cells overexpressing LZTS2 (Figure 38A, B).

3.2.8. Summary

Through biochemical experiments carried out in this chapter we found that DYRK1A, along with DCAF7, exists in several hetero trimeric complexes rather than a single multi-protein complex. We also identified that DYRK1A, and not DCAF7, is required for the formation of these different complexes. We have also mapped the region of DYRK1A to which its interacting proteins bind. Through the functional characterization carried out in this chapter, we have identified LZTS1 and LZTS2 as two novel regulators of DYRK1A activity.

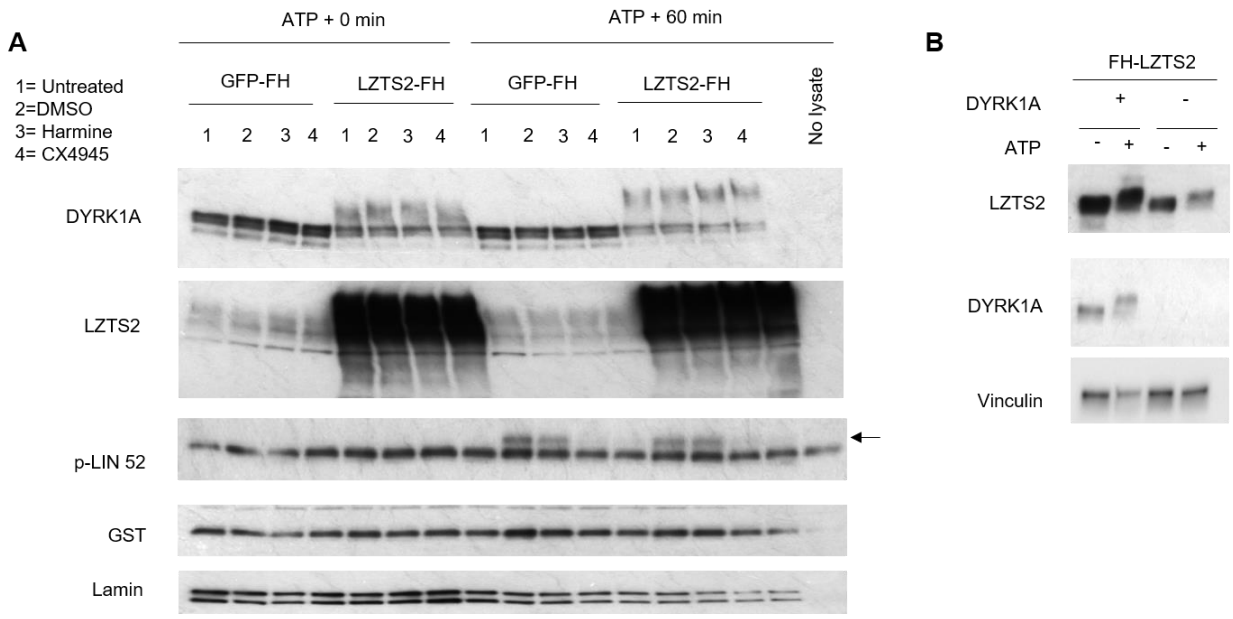

Figure 38: Effect of DYRK1A loss on DYRK1A or LZTS2 phosphorylation.
(A) Lysates from U-2 OS GFP-FH cells (control) or U-2 OS LZTS2-FH cells were treated with DMSO, Harmine or CX4945 followed by *in-vitro* kinase assay and WB analysis of indicated proteins. (B). Lysates from U-2 OS control FH-LZTS2 or U-2 OS DYRK1A KO FH-LZTS2 were incubated with ATP followed by WB analysis of indicated proteins.

3.3 DISCUSSION AND FUTURE DIRECTIONS

3.3.1 MudPIT proteomic analysis of DYRK1A interacting proteins reveals novel interactors that could help understand the regulation and substrates of DYRK1A

Except DCAF7 and RNF169, the interactome of other DYRK1A interacting proteins was not characterized in previous studies. Importantly, this study characterized the interactome of DYRK1A-interacting proteins in the T98G cell line derived from human glioblastoma, which is not transformed by viral oncoproteins that could influence protein interaction networks. Apart from DCAF7, our MudPIT proteomic analysis also provided several potential directions to elucidate and understand the function of DYRK1A in the future studies. For example, the LZTS2 interactome shows the presence of known LZTS interactors belonging to the signal-induced proliferation associated family of proteins (SIPA), including SIPAL1, 2 and 3, also known as

SPARs, which in turn regulate RAP1 signaling. It is not known if DYRK1A contributes to the function of SPARs or is regulated by RAP1. Furthermore, MudPIT proteomic analysis of FAM117B shows the presence of proteins involved in the splicing machinery like SRSF2 and SRSF3, as well as ribosomal proteins RPS15, RPL24, RPL31, RPL37A and eukaryotic translation initiation factors EIF2S1, EIF2S2 and EIF3G, suggesting that FAM117B could be involved in translation. Interestingly, five of the mitochondrial ribosomal proteins (for example: MRPS31, MRPS38) were also found in our FAM117B pull-down analysis. As we have shown that DYRK1A phosphorylates FAM117B, it will be interesting to determine if FAM117B plays a role in mitochondrial ribosomal function, translation or RNA splicing, and if DYRK1A mediated phosphorylation of FAM117B regulates these functions.

RNF169 did pull down several DNA binding proteins, which could point us towards further understanding the mechanism of DYRK1A and RNF169 mediated regulation of DNA repair. Interestingly RNF169 also pulled down some proteins that could be involved in transcription and translation. These include RPL10A, ILF2, LARP1 and ELAVL1. This suggests that DYRK1A and RNF169 could have roles in the cell apart from DNA repair.

The TROAP interactome contained the smallest number of proteins as compared to all the other DYRK1A interacting proteins, possibly because of the cell type used. Therefore, characterization of the TROAP interactome in a physiologically-relevant cell type, including breast or ovarian cancer cells, will help elucidate the function of the TROAP-DYRK1A complex.

In contrast to this, both LZTS1 and LZTS2 pulled down multiple proteins, in fact more than usually expected. This could be because of the high abundance of LZTS1 and LZTS2 in our cell lines or because of LZTS binding to a cellular compartment such as intracellular vesicles. We

also analyzed if there are any mutations in the construct used for LZTS1 and LZTS2 expression, but this was ruled out. Like DYRK1A, the interactomes of DCAF7, LZTS1, LZTS2 and FAM117B also show the presence of certain 14-3-3 proteins. Since it has been shown that DYRK1A activity can be regulated by 14-3-3 protein (Alvarez et al., 2007; D. Kim et al., 2004), it will be interesting to analyze if DCAF7, LZTS1, LZTS2 or FAM117B play a role in this function of the 14-3-3 proteins towards DYRK1A.

3.3.2 DYRK1A interacting proteins exist in different protein complexes

Through this study we have shown that although the DYRK1A interacting proteins bind DCAF7, they do not form larger multiprotein complexes. Our data so far also indicates that only a fraction of DCAF7 in the cell is bound to RNF169, LZTS1, LZTS2, FAM117B and TROAP. However, since all of these proteins bind both DYRK1A and DCAF7, it is important to study these complexes separately because they could be responsible for specific functions of DYRK1A. Moreover, unlike the RNF169-DYRK1A-DCAF7 complex that is observed in the nucleus, other proteins form a complex with DYRK1A and DCAF7 in the cytoplasm. This finding indicates that understanding the function of these different complexes of DYRK1A and DCAF7 will help in better understanding the nuclear and cytoplasmic functions of DYRK1A or the functions of DYRK1A in different sub-cellular compartments.

3.3.3 DYRK1A is required for the interaction of DCAF7 with DYRK1A binding partners

It is known that DCAF7 acts as a scaffold receptor to control HIPK2 and MEKK1 kinase functions (Ritterhoff et al., 2010). We therefore analyzed if DCAF7 is required for RNF169, FAM117B, LZTS1, LZTS2 or TROAP to bind DYRK1A. In contrast, our study demonstrated a role of DYRK1A as a scaffolding protein. In part, the requirement of DYRK1A for these proteins to bind DCAF7 could be explained by the region of DYRK1A that these proteins bind to

which is different from the DCAF7 binding region in DYRK1A. Although we have observed this role in both U-2 OS and T98G cells (T98G data not shown), it is still unknown if overexpression of DYRK1A causes more binding of these proteins to DCAF7.

An interesting result we observed was that amino acid residues 77-136 of DYRK1A were sufficient for LZTS2, FAM117B and RNF169 binding. In fact, the 77-136 fragment bound LZTS2, FAM117B and RNF169 much more tightly than the 1-176 fragment. Both of these polypeptides have an intact nuclear localization sequence. However, if the DYRK1A 1-176 is more localized in the nucleus than DYRK1A 77-136 in the cell, it is possible that DYRK1A 1-176 also binds other nuclear proteins, which interfere with binding of primarily cytoplasmic proteins LZTS2 and FAM117B to DYRK1A 1-176. In case of RNF169 which is nuclear, the nuclear proteins that bind DYRK1A 1-176 may be binding close to the RNF169 binding region in DYRK1A, causing lower binding. Another possibility is that the 1-176 fragment may fold in a different way than 77-136 fragment, leading to masking of certain epitopes required for DYRK1A interactions.

Finally, it has been shown that DYRK1A binds to DCAF7 and induces its nuclear localization (Miyata & Nishida, 2011). Interestingly, in our study DYRK1A did not dramatically influence the localization of its interactors, including DCAF7.

3.3.4 DCAF7 does not affect DYRK1A mediated growth suppression

Though DCAF7 is a major DYRK1A interacting protein, it does not appear to affect DYRK1A's activity towards LIN52 or its ability to induce growth arrest. However, we observed that when DYRK1A is induced in DCAF7 overexpressing cells for a longer time, its ability to maintain growth arrest was lower compared to that in control cells. This indicates that DCAF7 could

oppose DYRK1A in this function. TCGA analysis of DCAF7 by Dr. Mikhail Dozmorov (Appendix Figure 1) revealed that high expression of DCAF7 correlates with lower survival in breast cancer. It could be possible that DCAF7 can sequester DYRK1A, thus reducing the pool of available DYRK1A that is involved in the growth suppression function.

On screening several breast cancer cell lines for DCAF7 expression, we were able to determine that DCAF7 indeed is overexpressed in multiple breast cancer cell lines (Appendix figure 1). It would be interesting to determine if DCAF7 is required for proliferation and metastasis of these breast cancer cells and if all of DYRK1A in these cells is bound to DCAF7, thus inhibiting the tumor suppressive function of DYRK1A.

3.3.5 LZTS1 and LZTS2 are novel regulators of DYRK1A

Our study identified two novel DYRK1A interacting proteins LZTS1 and LZTS2 that could regulate DYRK1A activity. We observed that knockdown of LZTS1 or LZTS2 caused a reduction in DYRK1A kinase activity towards LIN52. However, depletion of both LZTS1 and LZTS2 did not completely abolish DYRK1A activity towards LIN52, suggesting that their functions are not redundant. Our results indicate that the LZTS proteins could be working together as a part of the same complex and influence DYRK1A activity. In support of this model, LZTS proteins form heterodimers (Schmeisser et al., 2009; Wendholt et al., 2006), and we have also confirmed that LZTS1 and LZTS2 bind to each other. Further studies will be required to analyze if disruption of the binding between LZTS1 and LZTS2 also causes the same effect on LIN52 phosphorylation. Another point to note is that we have not analyzed the effect of another DYRK1A interacting protein LZTS3 on DYRK1A activity. The residual activity of DYRK1A after LZTS1 or LZTS2 knockdown may be due to the presence of LZTS3, or some other protein which may function independent of the LZTS proteins to regulate DYRK1A activity.

Alternatively, LZTS could regulate DYRK1A in a certain subcellular compartment, for example, only in the cytoplasm.

DYRK1A mediated LIN52 phosphorylation is required for the formation of the DREAM complex, which in turn causes growth suppression (Litovchick et al., 2011). However, depletion of LZTS1/2 did not affect the ability of DYRK1A to cause growth arrest. This apparent discrepancy could be due to the specifics of the *in-vitro* kinase assay used in our study. This assay measures the ability of DYRK1A to phosphorylate a substrate, in whole cell extracts, and in this case the substrate was LIN52. This result need not necessarily match the effect of LZTS on endogenous LIN52 phosphorylation. Moreover, this result could indicate that LZTS1/2 does not affect the function of DYRK1A in the nucleus. Since LZTS1/2 bind DYRK1A in the cytoplasm, fractionating cells and carrying out *in-vitro* kinase assays will be helpful. If LZTS1/2 depletion only reduces DYRK1A kinase activity in cytoplasmic lysates but not in the nuclear lysates, this would support this model. It would also be interesting to analyze if inhibition of LZTS1/2 in the cytoplasm is able to completely inhibit DYRK1A activity as opposed to the partial inhibition observed with the whole cell lysates. The effect of LZTS proteins on DYRK1A activity can further be validated using cell lines, which have lost LZTS1 or LZTS2. We analyzed a panel of ovarian cancer cell lines for changes in LZTS2 or LZTS1 expression (Appendix Figure 2). Several cell lines had losses in LZTS1 expression (including TOV112D, SKOV3, TOV21G, OVCA420) and a few cell lines had slightly lower expression of LZTS2 (Appendix Figure 2). A DYRK1A kinase activity screen using these cell lines will be essential to validate our model.

We also observed that the overexpression of LZTS2 leads to phosphorylation of DYRK1A. It is possible that DYRK1A is required to maintain normal levels of LZTS1 and LZTS2 in the cell.

When LZTS2 is overexpressed, there may be a feed-back loop that triggers phosphorylation of DYRK1A by another kinase (our experiments have ruled out autophosphorylation). Future experiments will be needed to determine the kinase that phosphorylates DYRK1A when LZTS2 is overexpressed and to determine the functional significance of this.

CHAPTER 4: UNDERSTANDING THE ROLE OF DYRK1A and DCAF7 IN TRANSCRIPTION

A closer look at the DCAF7 interactome shown in Figure 16, Chapter 2 of the dissertation, revealed the presence of several Polycomb complex subunit proteins. These proteins were not present in our previously identified DYRK1A interactome [Chapter 1, Figure 5 and (Menon et al., 2019)]. Moreover, using an exhaustive immunoprecipitation experiment, we had identified that not all DCAF7 in the cell is bound to DYRK1A (Appendix Figure 3) suggesting that DCAF7 could have functions towards this complex independent of DYRK1A. Since we were able to detect the DYRK1A-DCAF7 complexes with other proteins both in the cytoplasm and nucleus (Chapter 2, Figure 20), we wanted to analyze if DYRK1A-DCAF7 together play a role in this complex formation or regulation. Before proceeding to the results obtained in this chapter, the following introduction to the chapter explains the Polycomb repressive complexes and gives a brief account about the known roles of DYRK1A and DCAF7 in transcription.

4.1 INTRODUCTION TO THE CHAPTER

4.1.1 Polycomb group proteins and repressive complexes

Polycomb group proteins (PcG) were first identified in Drosophila as regulators of appropriate body segmentation through Hox gene repression (Kennison, 1995; Lewis, 1978; Struhl, 1981). PcG are essential for many biological processes in mammals, including development, stem cell maintenance and differentiation, and tumor suppression (Jaenisch & Young, 2008; Margueron & Reinberg, 2011; Morey & Helin, 2010; Müller & Verrijzer, 2009; Rajasekhar & Begemann, 2007; Schuettengruber & Cavalli, 2009; Schwartz & Pirrotta, 2007; Simon & Kingston, 2013;

Sparmann & van Lohuizen, 2006; Q. Wang et al., 2018). PcG proteins assemble into multi-subunit nuclear complexes with various biochemical functions, including recognition and modification of histone posttranslational modifications (PTMs) and chromatin compaction (Simon & Kingston, 2013). The two well studied types of complexes are the Polycomb Repressive Complex 1 (PRC1) and Polycomb Repressive Complex 2 (PRC2) (Jaenisch & Young, 2008; Raphaël Margueron & Reinberg, 2011; Morey & Helin, 2010; Müller & Verrijzer, 2009; Rajasekhar & Begemann, 2007; Schuettengruber & Cavalli, 2009; Schwartz & Pirrotta, 2007; Simon & Kingston, 2013; Sparmann & van Lohuizen, 2006) As their names suggest, these complexes are required to maintain repressive chromatin through epigenetic mechanisms and/or chromatin compacting (Cao et al., 2002; de Napoles et al., 2004; Müller et al., 2002; H. Wang et al., 2004) The PRC 1 and 2 complexes exhibit distinct enzymatic activities: PRC2 is responsible for di- and tri-methylation of histone H3 at lysine 27 catalyzed by the EZH1/2 methyltransferases (Ferrari et al., 2014; Raphael Margueron et al., 2008; X. Shen et al., 2008), whereas PRC1 is responsible for monoubiquitination of histone H2A at lysine 119 (H2AK119ub1) catalyzed by the E3 ligase RING1A or RING1B (de Napoles et al., 2004; Endoh et al., 2008). For the purpose of this thesis, we concentrated on the PRC1 complex because of its relevance to DYRK1A and DCAF7 that will be discussed below.

The core PRC1 complex in Drosophila contains Polycomb (Pc) (Saurin et al., 2001; Shao et al., 1999), a chromodomain-containing protein that binds to H3K27me3 (Fischle et al., 2003; Min et al., 2003); Posterior sex combs (Psc), responsible for chromatin compaction *in-vitro* (Francis et al., 2004); Polyhomeotic (Ph) and dRing, the enzyme responsible for H2A ubiquitination (H. Wang et al., 2004). Mammalian PRC1 complexes are very heterogeneous compared to Drosophila because each subunit has several homologues in the human genome and they can

associate in a combinatorial fashion (Gao et al., 2012). In mammals, several chromodomain proteins (CBX) are homologous to Pc, RING1A and RING1B are enzymes similar to dRing, several Ph homologs (PHC1-3) exist, and six Psc homologs, collectively known as Polycomb group RING fingers (PCGFs) are present (Simon & Kingston, 2013). Different combinations of these homologues in addition to other factors give rise to several distinct mammalian PRC1 complexes.

Proteomic and functional studies have enhanced the understanding of these complexes and characterized at least six distinct groups of mammalian PRC1 complexes, PRC1.1–1.6, each comprising one of six Polycomb group RING fingers (PCGFs), and the E3 ligase RING1A/B (Gao et al., 2012; Hauri et al., 2016; Kloet et al., 2016; Sanchez-Pulido et al., 2008). These PRC1 subtypes can be grouped into canonical and non-canonical complexes. PRC1.2 and PRC1.4 containing CBX proteins with chromodomains fall under canonical PRC1 complexes based on H3K27me3 recognition deposited by PRC2 (Cao et al., 2002; Fischle et al., 2003; Gao et al., 2012; Min et al., 2003; Scelfo et al., 2015), and Figure 39. The other complexes are termed as non-canonical (Figure 39). How the non-canonical sub-complexes are recruited to chromatin is not understood, but RYBP containing-PRC1 complexes adopt a PRC2/H3K27me3-independent mechanism for targeting chromatin. There are two molecular functions attributed to PRC1, including chromatin compaction (Levine et al., 2002; Shao et al., 1999) and monoubiquitination of histone H2A at Lysine 119 (H. Wang et al., 2004).

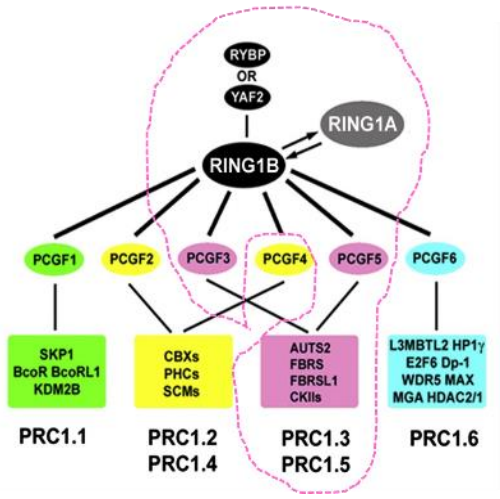

Figure 39: Schematic representation of the different PRC1 complexes.
[Adopted from (Gao et al., 2012)]. The PRC1.3/5 complex is highlighted with a pink outline.

4.1.2 PRC1.3/5

PCGF3 and PCGF5 form a distinct type of PRC1 complex which contain AUTS2 (Gao et al., 2012). From here on in the thesis, we will refer to this complex as PRC1.3/5. In contrast to the repressive functions of canonical PRC1, it has been found that PRC1.3/5 could mediate transcriptional activation (Gao et al., 2014). This conversion from repressive to activating function is mediated by AUTS2 (Gao et al., 2014).

Autism susceptibility candidate 2 (*AUTS2*) maps to chromosome 7q11.2 and encodes a nuclear protein (Bedogni et al., 2010). Studies in mice revealed that AUTS2 localizes to regions of the brain both during development and in adults (Bedogni et al., 2010). In mice, homozygous neuron-specific deletion of the full-length Auts2 isoform display abnormalities in motor skills (Gao et al., 2014). Furthermore, mice with heterozygous disruption of *Auts2* display impaired emotional control and cognitive memory (Hori et al., 2015). Loss of function studies of zebrafish *auts2* using morpholinos showed that auts2 knockdown leads to abnormalities

including microcephaly, reduction of neural cells and movement disorders, as well as craniofacial dysmorphisms (Beunders et al., 2013; Oksenberg & Ahituv, 2013). Furthermore, the gene *AUTS2* is reportedly disrupted in individuals with neurological disorders, including autism spectrum disorders (ASD) (Hori et al., 2015; Oksenberg & Ahituv, 2013; Sultana et al., 2002). Similar involvement of AUTS2 and DYRK1A in neurological diseases makes the PRC1.3/5 complex especially interesting for our study. Molecular studies have revealed that AUTS2 interacts with the promoters/enhancers of various genes that are involved in brain development and/or associated with neurological disorders (Oksenberg & Ahituv, 2013). AUTS2 is responsible for the recruitment of histone acetyl transferase p300 which turns the complex into a transcriptional activator, and CK2 protein kinase which inhibits the repressive function of PRC1 (Gao et al., 2014; Hori et al., 2015). However, the exact molecular mechanisms that mediate the function of PRC1.3/5 are not well known.

4.1.3 DCAF7 and PRC1.3/5

Proteins with WD40 repeats have been shown to associate with chromatin modifying complexes that include the polycomb repressive complex 1 and complex 2 (Gao et al., 2014; Stirnimann et al., 2010). Using proteomic studies, Gao et al., showed that both AUTS2 and PCGF5; two of the components of the PRC1.3/5 complex, pulled down DCAF7 (Gao et al., 2014). Using immunoprecipitation of the PRC1.3/5 component AUTS2 followed by glycerol gradient analysis of HEK 293T cells, it has been confirmed that DCAF7 is indeed a part of the PRC1.3/5 complex (Q. Wang et al., 2018). Furthermore, using a GAL4-luciferase reporter system, DCAF7 was found to be required for PRC1.3/5 mediated transcriptional activation (Q. Wang et al., 2018). Indeed, loss of DCAF7 led to a decreased expression of genes involved in neuronal differentiation in mouse embryonic fibroblasts (Q. Wang et al., 2018).

4.1.4 DYRK1A in transcription

DYRK1A is also thought to play a role in transcription. A chromatin-wide profiling of DYRK1A revealed that DYRK1A could act as a RNA Polymerase II CTD kinase in order to facilitate transcription of certain RNA Polymerase II target genes. DYRK1A appears to be recruited to its target genes after recognizing the motif TCTCGCGAGA however it is not known how this binding is mediated. This is followed by phosphorylation of the C-terminal domain (CTD) of RNA Pol II at Ser2 and Ser5 (Di Vona et al., 2015). DCAF7 mediates the binding between RNA Pol II and DYRK1A (D. Yu et al., 2019). DYRK1A was also found to phosphorylate histone H3 in a recent study (Jang et al., 2014). Interestingly, DYRK1A interacts with histone acetyl transferases CBP and p300 in 293T cells, and DYRK1A overexpression hyper phosphorylates CBP and p300 (S. Li et al., 2018). Analysis of published ChIP-seq datasets in T98G and HeLa cells (Di Vona et al., 2015) and validation of some genes with ChIP in HEK293 cells revealed that DYRK1A indeed localizes to regions of enhancers along with CBP and p300 (S. Li et al., 2018).

However, the roles of DCAF7 or PRC1.3/5 in DYRK1A-mediated transcriptional responses are not known.

4.2. RESULTS

In order to better understand the functional relationship between DYRK1A and DCAF7, we employed MudPIT proteomic analysis of DCAF7 in T98G cells. We observed that DCAF7 immunoprecipitated several proteins that were also detected in our DYRK1A MudPIT proteomic analysis. We also observed the presence of known DCAF7 binding proteins. Importantly, we observed that DCAF7 co-precipitated all previously published components of PRC1.3/5 including PCGF3/5, RING1/2, AUTS2, FBRS, FBRSL1, CK2α, CK2α′, CK2β, YAF2 and

RYBP (Figure 40). FBRS and FBRSL1 are homologs of AUTS2. Of note, our DYRK1A proteomic analysis did not show the presence of any of the PRC1.3/5 components (Figure 40).

4.2.1 DCAF7 is a part of PRC1.3/5 but DYRK1A does not bind components of the complex.

First, using T98G cells, we validated that DCAF7 is indeed a part of PRC1.3/5 (Figure 41). We used an antibody against FBRS, a paralog of AUTS2 (genecards.org), for IP followed by WB analysis. We were able to co-immunoprecipitate DCAF7, RING1B, RING1A and CK2α with FBRS. As expected, FBRS did not bind to DYRK1A. For a reverse pull down, we used cell lysates from T98G cells stably expressing Flag and HA tagged DCAF7 (FH-DCAF7) and we immunoprecipitated DCAF7 using an anti-HA antibody. Indeed, FH-DCAF7 did bind to RING1B, RING1A, CK2α, FBRS and DYRK1A (Figure 41). Using CRISPR-Cas9 technology, we had previously generated DYRK1A KO T98G cells in the laboratory (Iness et al., 2019). In order to analyze if DYRK1A depletion had an effect on PRC1.3/5 assembly, we carried out an FBRS pull down in DYRK1A KO cells (Figure 41). PRC1.3/5 components were pulled down at levels similar to those observed in the control cell line suggesting that loss of DYRK1A did not affect the interaction between these subunits. Similar to the depletion of DYRK1A, DYRK1A overexpression also had no effect on FBRS being able to pull down components of PRC1.3/5. We also observed that FH-tagged DYRK1A was able co-immunoprecipitate DCAF7 but not any of the PRC1.3/5 components (Figure 41).

Rank	DCAF7 # Out of 3	DYRK1A # Out of 4	GFP # Out of 4	NCBI_Gene	DCAF7[a]	DYRK1A[b]	PCGSF5[c]	AUTS2[c]
1	3	4	0	**DCAF7**				
2	3	0	0	FBRS				
3	3	0	0	PCGF5				
4	3	0	0	RING1				
5	3	0	0	DIAPH1				
6	3	0	0	FBRSL1				
7	3	0	0	AUTS2				
8	3	1	0	**DYRK1B**				
9	3	0	0	PCGF3				
10	3	4	0	**TROAP**				
11	3	3	0	**FAM53C**				
12	3	3	0	**DYRK1A**				
13	3	1	0	**CCT6A**				
14	3	0	0	CCT2				
15	3	0	0	CCT4				
16	3	0	0	CCT8				
17	3	0	0	CCT7				
18	3	0	0	CSNK2A1				
19	3	0	0	CSNK2B				
20	3	0	0	CSNK2A2				
21	3	0	0	RNF2				
22	3	0	0	ZNF703				
23	3	0	0	YAF2				
24	3	0	0	RYBP				
25	3	0	0	ZNF503				
26	2	0	0	MRPL11				
27	2	4	0	**RNF169**				
28	2	3	0	**PPP1R3F**				
29	2	2	0	**SNX18**				
30	2	0	0	CTNND1				
31	2	0	0	SNRPD2				
32	2	0	0	POLR2J3				
33	2	0	0	HINT1				
34	2	0	0	WRN				
35	2	0	0	HIPK2				
36	2	0	0	LRRC59				
37	2	0	0	CANX				

Figure 40: Summary of MudPIT proteomic analysis of DCAF7.
Proteins specifically detected in at least 2 out of 3 replicates are ranked by relative enrichment in DCAF7 IP samples. The number of times each protein was detected in DCAF7 immunoprecipitation is indicated. Proteins with a blue color in the DCAF7 column are known DCAF7 binding proteins (**a**). Comparison of DYRK1A dataset to the DCAF7 dataset resulted in overlaps indicated with peach colored boxes in the DYRK1A column [**b** indicates (Menon et al., 2019)]. DCAF7 was detected as a component of the PRC1.3/5 complex with immunoprecipitation of PCGF5 and AUTS2 in a previous study [**c** indicates (Gao et al., 2014)).

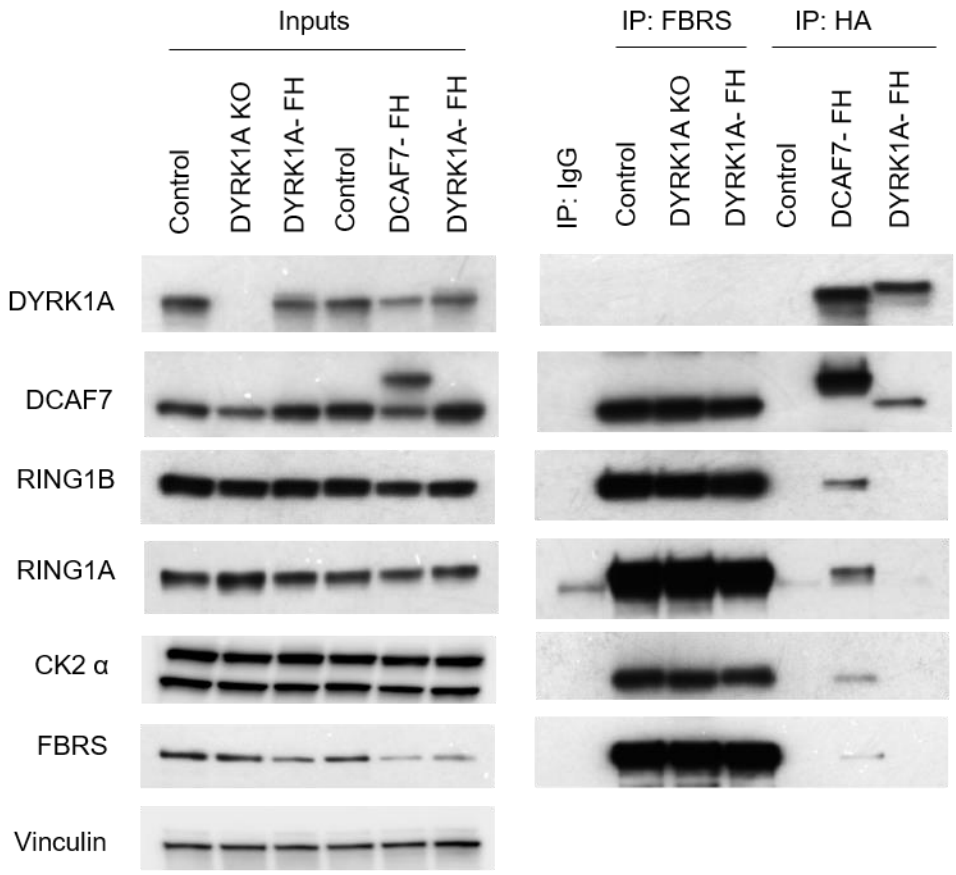

Figure 41: DCAF7 but not DYRK1A binds the components of the PRC1.3/5 complex.
IP using FBRS antibody was carried out using lysates from the indicated T98G cell lines followed by WB analysis for indicated proteins. IP analysis with an HA antibody was used as a control to show FH-DCAF7 and FH-DYRK1A pull downs followed by WB analysis for indicated proteins.

4.2.2. DYRK1A could affect the molecular composition of the PRC1.5 complex

Next, we analyzed the effect of DYRK1A on the molecular size of PRC1.3/5 using sucrose gradient ultracentrifugation. Nuclear lysates from T98G control or DYRK1A KO cell lines were loaded on top of a 10-40% sucrose gradient with 5% glycerol added for better separation, and subjected to ultracentrifugation. Following this, a total of twenty-two fractions were collected from the top of the gradient and WB analysis was performed. We observed that components of PRC1.3/5 co-fractionated together, indicating that they are present in a single complex (Figure 42). Though DYRK1A did not bind any of the PRC1.3/5 components, we observed that

DYRK1A also co-fractionated with the components of PRC1.3/5 in several fractions. Moreover, we observed that in the absence of DYRK1A, PRC1.3/5 components were present in the heavier fractions (Figure 42B compared to 42A) suggesting that DYRK1A could affect the PRC1.3/5 complex composition. Of note, we were only detecting those PRC1.3/5 components for which we were able to obtain and validate the antibodies. PRC1.3/5 also has other components that we did not detect in our WB analysis. Moreover, some of the components like RING1A/B are involved in several PRC1.3/5 complexes. Thus, it is possible that DYRK1A inhibits the formation of a more complete complex but further studies will be required to confirm this.

4.2.3. DYRK1A and DCAF7 negatively regulate the PRC1 function of monoubiquitination of H2A at K119

The only known enzymatic function of PRC1 is monoubiquitination of histone H2A at lysine 119, which is associated with a repressive chromatin state (H. Wang et al., 2004). We thus decided to analyze the effect of DYRK1A and DCAF7 on this monoubiquitination mark (H2A-K119-Ub1). Using WB analysis, we observed that overexpression of DCAF7 resulted in decreased H2A-K119-Ub1 in T98G cells (Figure 43A). This suggested that DCAF7 could be a negative regulator of PRC1 function towards H2A-K119-Ub1. Though DYRK1A does not bind PRC1.3/5 components, we evaluated the role of DYRK1A on H2A-K119-Ub1. Interestingly, we observed that DCAF7 overexpression in T98G DYRK1A-KO cells did not inhibit H2A-K119-Ub1 (Figure 43A). We further confirmed this result by transiently knocking down DYRK1A in T98G cells overexpressing DCAF7, where we observed a similar result. Indeed, siRNA-mediated DYRK1A depletion in T98G cells with DCAF7 overexpression led to an increase in H2A-K119-Ub1 signal (Figure 43A). This could be interpreted in two ways: either DCAF7

requires DYRK1A for the negative regulation of PRC1 function, or that DYRK1A and DCAF7 together inhibit H2A-K119-Ub1.

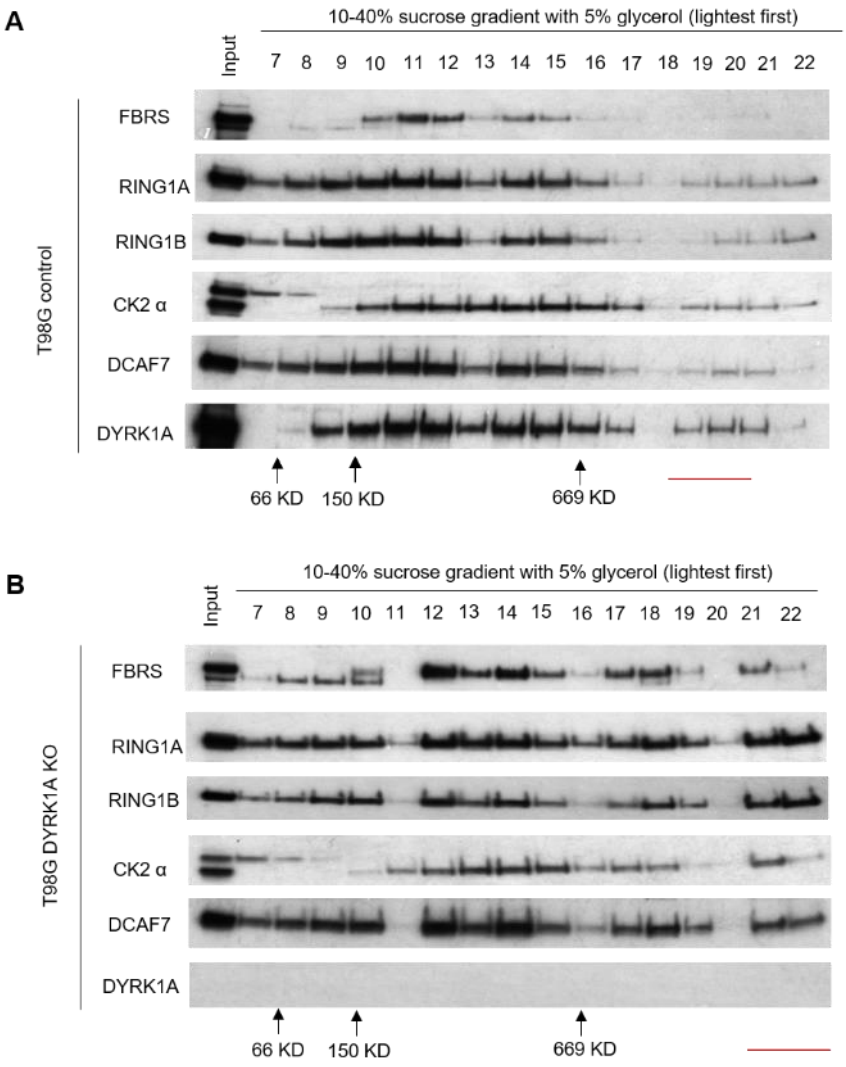

Figure 42: DYRK1A could affect the molecular size of the PRC1.3/5 complex
(A) Nuclear lysates from T98G control or (B) DYRK1A KO cells were loaded on top of a sucrose gradient followed by ultracentrifugation to separate protein complexes. Fractions were collected and analyzed using WB analysis for detection of indicated proteins. Differences in the heaviest fractions are indicated by red lines.

We further analyzed the effect of inhibition of DYRK1A kinase activity on PRC1 function using the DYRK1A inhibitor Harmine. T98G cells were serum starved for 48 hours and released in serum containing medium for 6, 12, 18 or 24 hours (Figure 43B). PRC1 is known to play a role in chromatin compaction which could be increased in quiescent cells (Levine et al., 2002; Shao et al., 1999). Our WB analysis of H2A-K119-Ub1 correlated with this function. An increased signal was observed in serum starved cells compared with a lower signal in cycling cells (Figure 43B). Interestingly, we observed that inhibition of DYRK1A with Harmine resulted in an increased H2A-K119-Ub1 signal (Figure 43B). This observation further supports that DYRK1A could play a role in regulation of PRC1 function. Of note, monoubiquitination of H2A at K119 is a collective function of all PRC1 complexes. With these experiments we could conclude that DYRK1A and DCAF7 play an inhibitory role towards global PRC1 function.

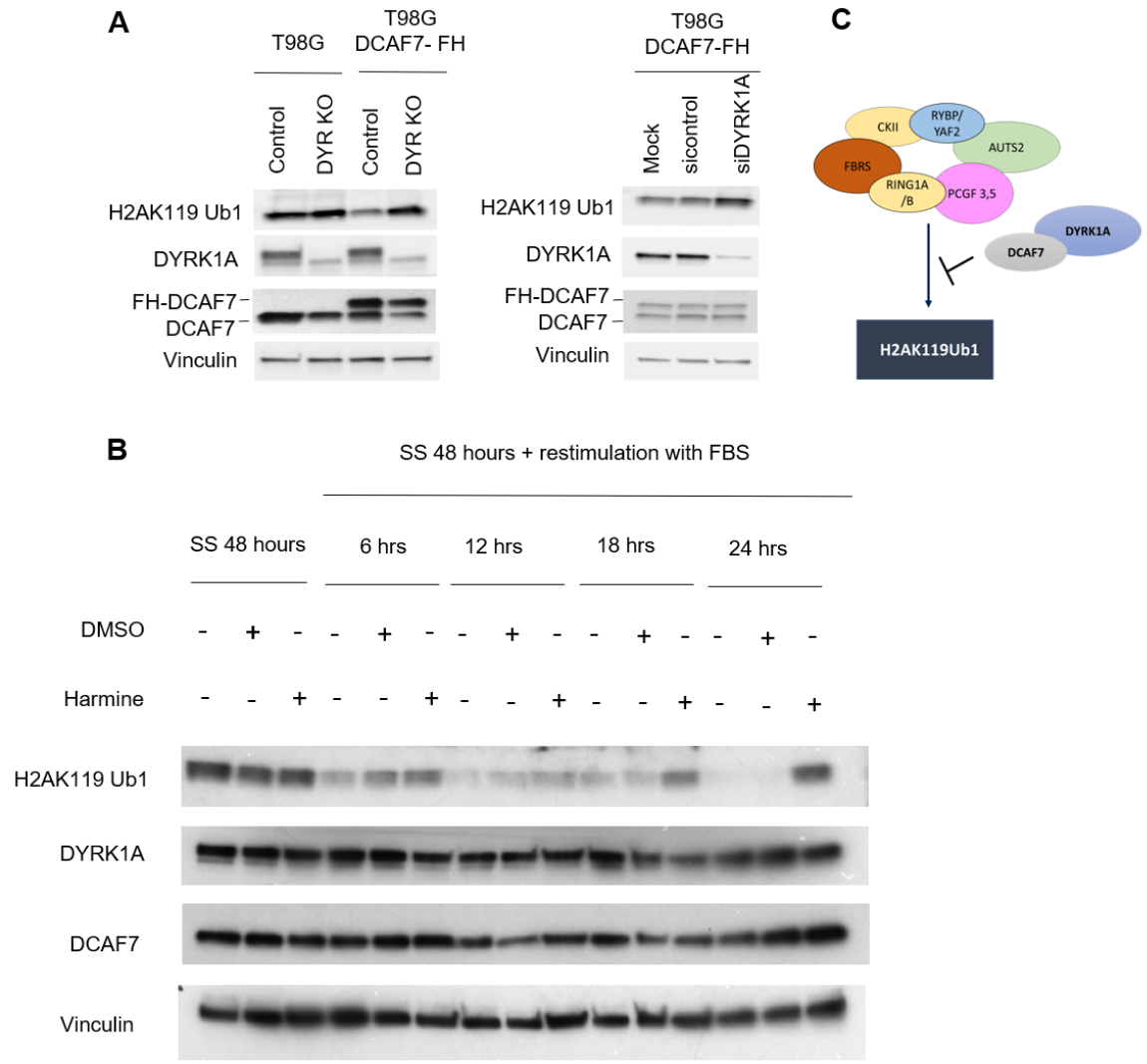

Figure 43: DYRK1A and DCAF7 regulate monoubiquitination of H2A at K119.
(A) WB analysis indicates effect of DYRK1A and DCAF7 on the known PRC1 function towards mono ubiquitination of H2A at K119 in the indicated T98G cell lines/conditions. (B) T98G cells were serum starved for 48hours followed by release with serum containing media for the indicated time points. WB analysis indicates the effect of inhibition of DYRK1A using 10μM Harmine on monoubiquitination of H2A at K119. DMSO was used as a vehicle control. (C) Schema indicating that DYRK1A and DCAF7 could inhibit the function of PRC1 towards H2AK119 monoubiquitination.

4.2.4. DYRK1A is required for the transcriptional activity of DCAF7

T98G cell lines were used for our proteomic studies of DYRK1A and DCAF7 as well as for ChIP-seq analysis by another group (Di Vona et al., 2015). The effects of DYRK1A and DCAF7 on H2A-K119 Ub1 were also observed in T98G cells. Therefore, to determine the role of DYRK1A and DCAF7 in transcription, we performed RNA-seq analysis using T98G control and DYRK1A KO cell lines with or without DCAF7 overexpression (Figure 44A, B). Cells overexpressing GFP in the presence or absence of DYRK1A were used as controls (Figure 44A, B). In order to minimize batch effects, five replicate samples were collected for each cell line at the same time. This was followed by RNA isolation and analysis of the quality of RNA. All twenty samples had an RNA integrity (RIN) value of greater than 9. We also analyzed expression of DCAF7 in each sample using RT-qPCR analysis before submission, as a quality control test (data not shown). We then submitted the samples for RNA-seq analysis. The sequencing led to the generation of approximately 30 million, 150bp single-end reads per sample. The data was analyzed for us by Dr. Mikhail Dozmorov (Department of Biostatistics and Massey Cancer Center, VCU). Principal component analysis of the RNA-seq data revealed that either loss of DYRK1A or overexpression of DCAF7 caused significant perturbations in the transcriptome (Figure 44C, D). However, overexpression of DCAF7 in the absence of DYRK1A caused relatively minor changes in global gene expression. This suggests that DYRK1A could be required for the effect of DCAF7 on transcription.

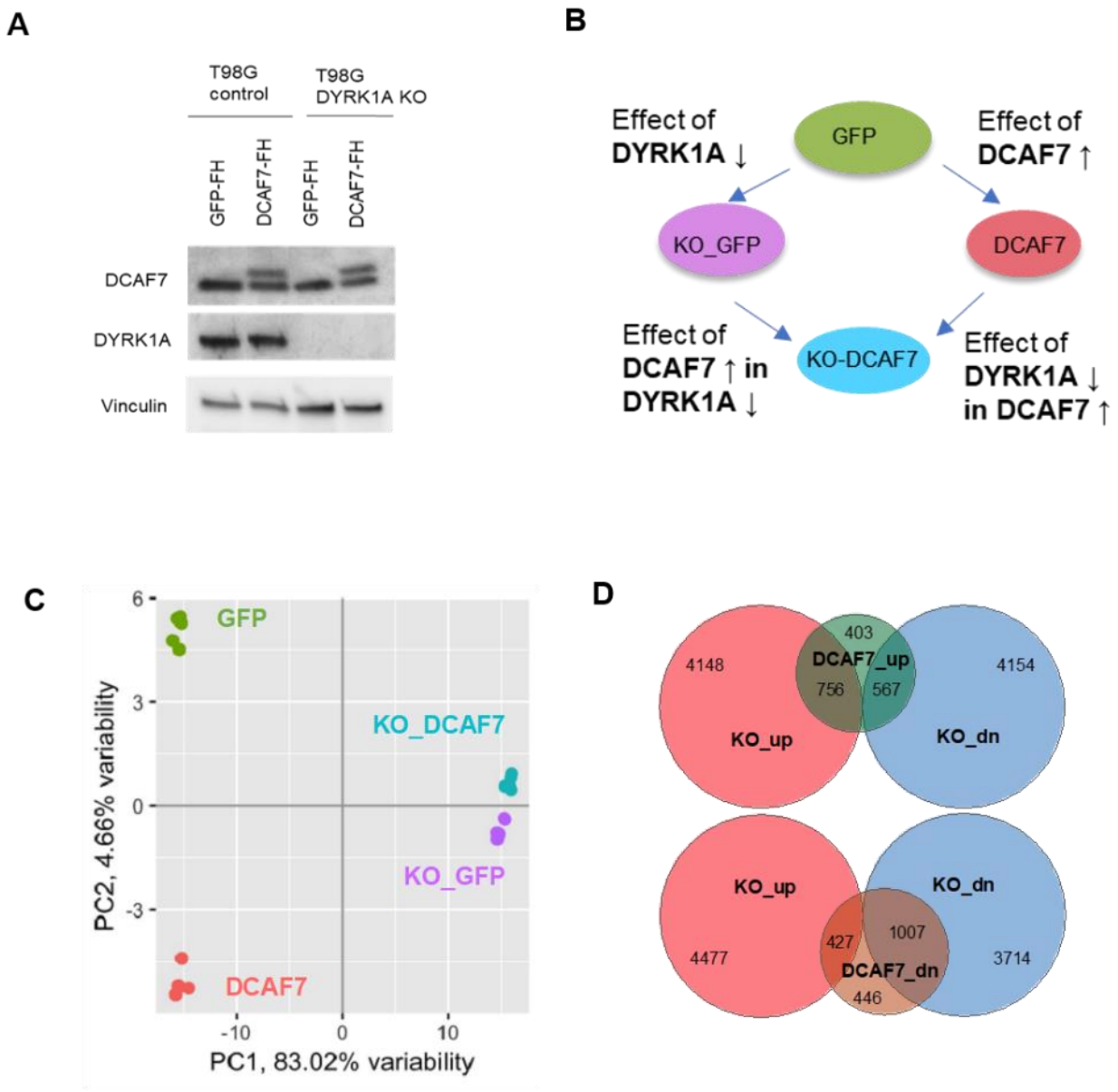

Figure 44: Summary of RNA seq analysis

(A) WB shows levels of DCAF7 and DYRK1A in the cell lines used for RNA seq analysis. Arrow indicates Flag-HA-tagged DCAF7 (B) Design of RNA-seq experiment using T98G cells to determine the effect of DYRK1A and DCAF7 on transcription. (C) Graph shows principal component analysis of the RNA-seq data. (D) Venn diagram showing overlaps of significantly up-regulated or down regulated genes

4.2.5. DYRK1A and DCAF7 regulate a common subset of genes

First, we only looked at genes that were upregulated or down regulated when DYRK1A was knocked out or when DCAF7 was overexpressed. There were multiple genes that were differentially regulated in each comparison relative to GFP control (Figure 44D). The expression of a total of 4904 genes were upregulated and 4721 were down regulated when DYRK1A was knocked out (False Discovery Rate FDR 0.05). Overexpression of DCAF7 lead to 1726 genes being upregulated and 1880 genes being downregulated as compared to the GFP control (FDR 0.05, Figure 44D). Comparison of these gene sets revealed a significant overlap (Figure 44). All overlap comparisons are highly significant (Fisher t test <0.001). This suggests that DYRK1A and DCAF7 may co-regulate a common subset of genes. Gene Set Enrichment Analysis (GSEA) was used for a biological interpretation of DEGs between conditions. This analysis revealed that both DYRK1A and/or DCAF7 regulated gene sets were significantly enriched in several functional categories (Figure 45A). Some of the categories were cell proliferation, neurological development and neurodegeneration. Furthermore, since previous studies found that DYRK1A is required for the DREAM complex assembly, it is expected that DREAM target genes should be up-regulated in DYRK1A KO cells. Indeed, ~800 target genes were up-regulated in the DYRK1A-KO cells. This result further supported the role of DYRK1A in DREAM function (Figure 45B).

In-order to confirm the RNA seq results, we used the same cell lines that we used for RNA seq analysis and performed a RT-qPCR for some of the DREAM target genes. We were able to validate the up-regulation of DREAM target genes including E2F2, ID3, ARHGAP11B, BUB1B and MYBL2 in the DYRK1A-KO samples using RT-qPCR (Figure 45C). GSEA analysis also revealed upregulation of DREAM targets with overexpression of DCAF7 (Figure 45A).

However, we were unable to find the effect of DCAF7 on the gene set upregulated by loss of DYRK1A. Since the DREAM complex represses the expression of several genes, it is possible DYRK1A KO and DCAF7 overexpression regulate the expression of the different subsets of DREAM target genes. Another possibility is that DCAF7 causes a very subtle effect on the genes validated by RT-qPCR and therefore an effect was not observed.

A

Gene Set Name	p-value	Gene Set Name	p-value
Up in DCAF7		Up in DYRK1A-KO	
CP: REACTOME_CELL_CYCLE	2.2E-26	CP: KEGG_MAPK_SIGNALING_PATHWAY	3.8E-16
CP: KEGG_FOCAL_ADHESION	1.7E-16	CP: REACTOME_AXON_GUIDANCE	2.1E-12
CP: KEGG_MAPK_SIGNALING_PATHWAY	2.8E-11	CP: REACTOME_CELL_CYCLE	7.3E-12
CP: REACTOME_AXON_GUIDANCE	1.8E-09	CP: REACTOME_DNA_REPLICATION	2.6E-09
C2: FISCHER_DREAM_TARGETS	6.2E-63	C2: GOBERT_OLIGODENDROCYTE_DIFF_UP	3.2E-49
C2: BLALOCK_ALZHEIMERS_DISEASE_DN	3.1E-48	C2: BLALOCK_ALZHEIMERS_DISEASE_UP	2.9E-42
C2: BLALOCK_ALZHEIMERS_DISEASE_UP	1.4E-46	C2: FISCHER_DREAM_TARGETS	2.1E-38
C2: GOBERT_OLIGODENDROCYTE_DIFF_UP	1.7E-43	C2: GOBERT_OLIGODENDROCYTE_DIFF_DN	1.7E-32
Down in DCAF7		Down in DYRK1A-KO	
CP: REACTOME_DEVELOPMENTAL_BIOLOGY	1.7E-17	CP: REACTOME_IMMUNE_SYSTEM	7.6E-31
CP: KEGG_WNT_SIGNALING_PATHWAY	3.8E-15	CP: REACTOME_EXTRACELL_MATRIX_ORG	2.1E-24
CP: KEGG_AXON_GUIDANCE	1.4E-13	CP: KEGG_HEMATOPOIETIC_CELL_LINEAGE	4.5E-13
CP: KEGG_MAPK_SIGNALING_PATHWAY	1.4E-11	CP: KEGG_TYPE_I_DIABETES_MELLITUS	3.4E-12
CP: REACTOME_SIGNAL_BY_RHO_GTPASES	1.6E-11	CP: KEGG_ALZHEIMERS_DISEASE	1.1E-09
CP: PID_HEDGEHOG_GLI_PATHWAY	1.0E-08	CP: REACTOME_AXON_GUIDANCE	1.2E-08
C2: BLALOCK_ALZHEIMERS_DISEASE_UP	2.3E-82	C2: NUYTTEN_EZH2_TARGETS_UP	4.6E-104
C2: GOBERT_OLIGODENDROCYTE_DIFF_DN	1.9E-58	C2: BLALOCK_ALZHEIMERS_DISEASE_DN	1.7E-44
C2: NUYTTEN_EZH2_TARGETS_UP	7.1E-56	C2: BLALOCK_ALZHEIMERS_DISEASE_UP	1.4E-42

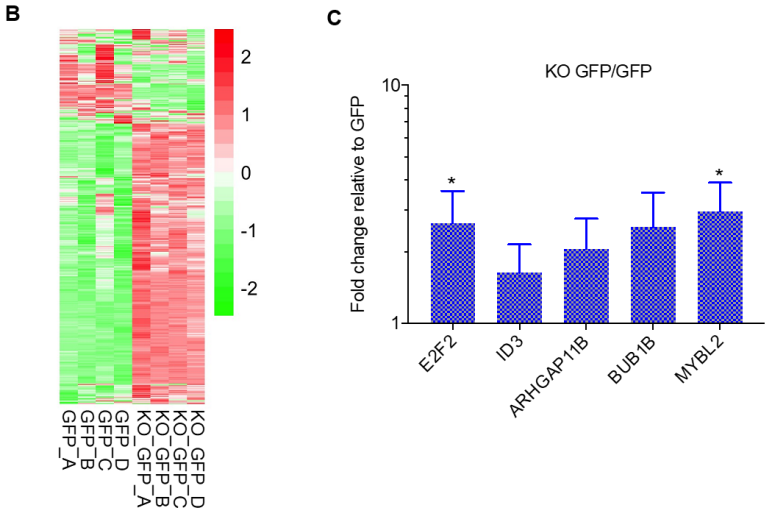

Figure 45: DYRK1A and DCAF7 affect genes in different functional categories and DREAM target genes are upregulated in DYRK1A KO samples.
(A) Table shows top functional categories identified using MSigDB Gene set enrichment (GSEA) tool for each indicated dataset (B) Heatmap showing changes in DREAM target gene set in DYRK1A KO data set as compared to control from four biological replicates. (C) RT-qPCR validation of DREAM target genes from T98G GFP-FH or T98G KO GFP-FH cell lines. Graph shows average of three biological repeats. Error bars show standard deviation. Statistical significance was calculated using two tailed Student's t- test. * - p value ≤0.05.

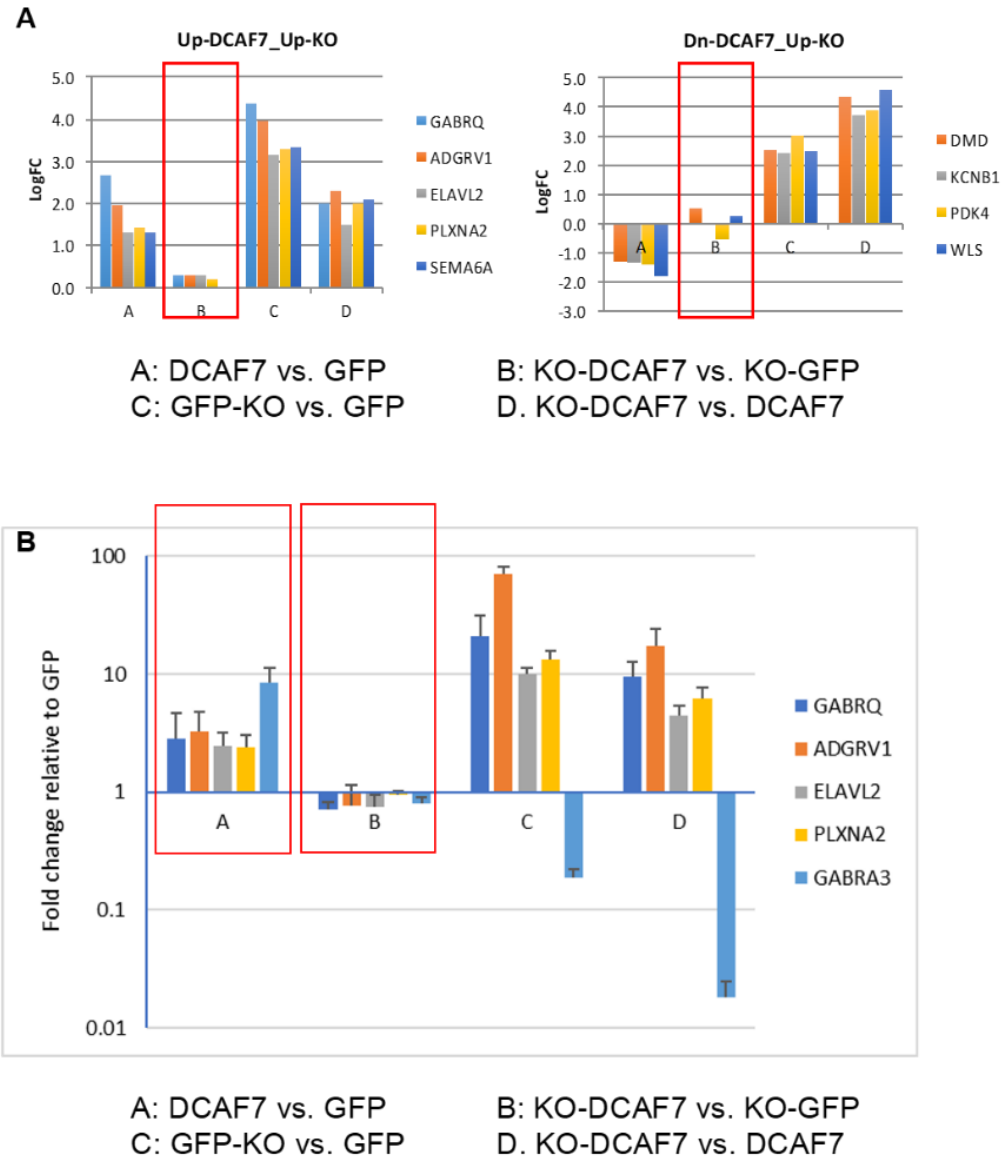

Figure 46: DCAF7 requires DYRK1A for its effect on transcription of a subset of genes. (A) Average RNA-seq Log Fold change (FC) values of DEGs regulated by both DYRK1A and DCAF7 showing lack of response to DCAF7 overexpression in the absence of DYRK1A (red boxes). (B) RT-qPCR validation of the indicated genes regulated by both DYRK1A and DCAF7 confirms the lack of response to DCAF7 overexpression in the absence of DYRK1A (compare red boxes).

Further, we identified a set of DEGs for further validation. These genes were altered in both DYRK1A and DCAF7 analyses with LogFC at least ± 1.0, and having a role in neurological

disease or cancer. These genes could be divided into 4 major categories: 1) genes that were upregulated with DYRK1A loss or DCAF7 overexpression; 2) genes that were downregulated with DYRK1A loss or DCAF7 overexpression; 3) genes that were up regulated with DYRK1A loss but downregulated with DCAF7 overexpression and 4) genes that were down regulated with DYRK1A loss but upregulated with DCAF7 overexpression (Figure 47). Looking at the average FC values obtained by RNA seq analysis for a subset of these genes, we were able to conclude that DCAF7 requires DYRK1A for its transcriptional activity (Figure 46A). We also confirmed this using RT-qPCR analysis for a subset of genes regulated by both DYRK1A and DCAF7 (Figure 46B).

We performed RT-qPCR analysis for the validation set to analyze the DYRK1A and DCAF7-regulated expression of these genes. This was carried out in the same cell lines as the RNA seq analysis. We were able to validate the expression of all selected DEGs (Figure 48). We were therefore able to conclude that DYRK1A and DCAF7 could regulate gene expression in the same as well as in the opposite direction.

Gene	Disease Link/ Function	Expression Category
GABRAQ	Seizures, Usher Syndrome	**Up in DYRK1A KO, Up in DCAF7 overexpression**
ADGRV1	Autism, Cancer	
ELAVL2	Autism, CNS development	
PLXNA2	Axon Guidance	
GABRA3	Epilepsy	**Down in DYRK1A KO, Up in DCAF7 Overexpression**
SELENOP	Alzheimer's disease	
KCNB1	Neurodevelopmental disorders	**Up in DYRK1A KO, Down in DCAF7 Overexpression**
WLS	ER stress	
TOX	Driver in T-ALL, inhibits NHEJ	
PDK4	Insulin resistance	
NETO1	Learning and memory	**Down in DYRK1A KO, Down in DCAF7 overexpression**
FOXA2	Ovarian and Uterine cancer	
DNER	Brain specific receptor	

Figure 47: DYRK1A and DCAF7 co-regulate a common subset of genes.
Differentially expressed genes are shown in both DYRK1A and DCAF7 analyses that are implicated in neurological disease or cancer. The four different expression categories are indicated along with the gene name and disease link/function.

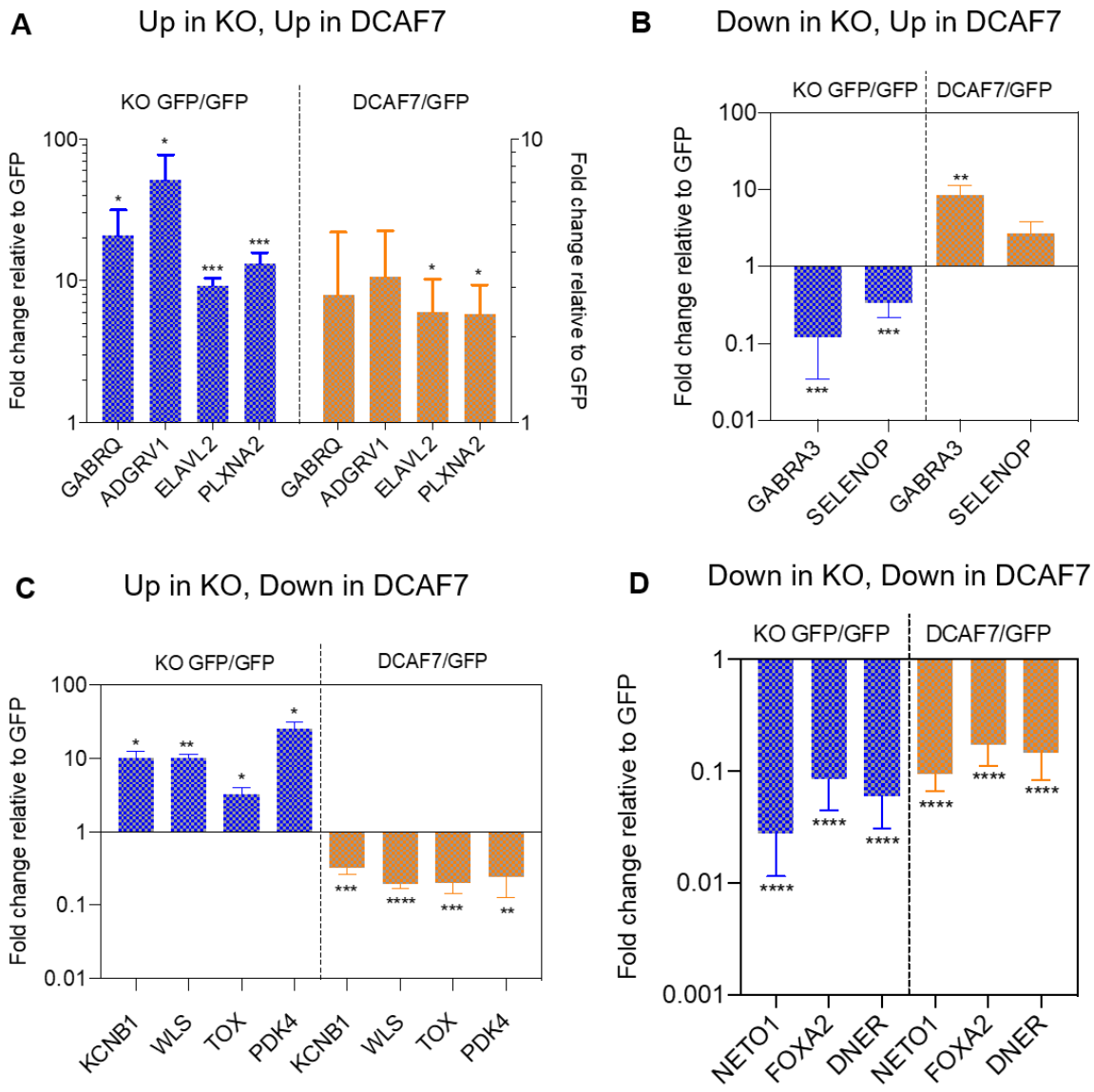

Figure 48: DYRK1A and DCAF7 regulate a common subset of genes that have relevance in disease.

RT-qPCR validations of genes indicated in Figure 47 using T98G GFP-FH, T98G DYRK1A KO GFP-FH or T98G DCAF7-FH cell lines. Graphs indicate average of three biological replicates. Error bars show standard deviation. Statistical significance was calculated using two tailed Student's t-test. P-values: *≤0.05; ** ≤ 0.01; *** ≤ 0.001; **** ≤ 0.0001 (A) Genes upregulated in both DYRK1A KO and DCAF7 overexpression conditions. (B) Genes downregulated in DYRK1A KO and upregulated in DCAF7 overexpression conditions. (C) Genes upregulated with DYRK1A KO but down regulated with DCAF7 overexpression. (D) Genes down regulated in both DYRK1A KO and DCAF7 overexpression conditions.

4.2.6. There is an overlap between DEGs and published DYRK1A ChIP-seq datasets

DYRK1A has been shown to play a role in transcription (Di Vona et al., 2015). In this study Di Vona et al., carried out ChIP-seq analysis in order to identify the genomic regions that DYRK1A binds to under cycling or serum starved conditions in T98G cells. Since our RNA-seq analysis was also carried out using T98G cells, we analyzed if there is an overlap of DYRK1A bound genes from the ChIP-seq dataset with the DEGs identified through our RNA-seq analysis. Indeed, there was an overlap of genes that were both up and down regulated with DYRK1A-KO (Figure 49 and Appendix tables 7,8). Out of the ~4905 genes that were upregulated in DYRK1A-KO cells, the genomic regions of 306 genes were bound by DYRK1A (Figure 49A, Appendix table 7). Out of the ~4722 genes downregulated when DYRK1A is knocked out, 240 genes had DYRK1A bound genomic regions (Figure 49B, Appendix table 8). This suggests that DYRK1A binds to the genomic regions of these genes and could possibly regulate expression by direct binding.

Interestingly, we also observed an overlap with genes that were up and down regulated with DCAF7 overexpression (Figure 50, Appendix table 9). Out of ~1727 genes upregulated with DCAF7 overexpression; 91 genes were directly bound by DYRK1A (Di Vona et al., 2015). Further 106 of the ~1881 genes downregulated with DCAF7 overexpression were also directly bound by DYRK1A. These results give us a starting point for the future ChIP validations in order to further understand the mechanism by which DYRK1A and DCAF7 regulate the expression of these genes.

There were also published ChIP-seq datasets available for AUTS2. However, this study was carried out in HEK293T cells (Gao et al., 2014). Even though the cell types are different, we observed a considerable overlap between genes bound by AUTS2 and genes bound by

DYRK1A, and identified a total of 65 genes bound by both AUTS2 and DYRK1A (Figure 51, Appendix table 10). Further analysis of these genes will help us understand the influence of DYRK1A on the PRC1.3/5 regulated genes.

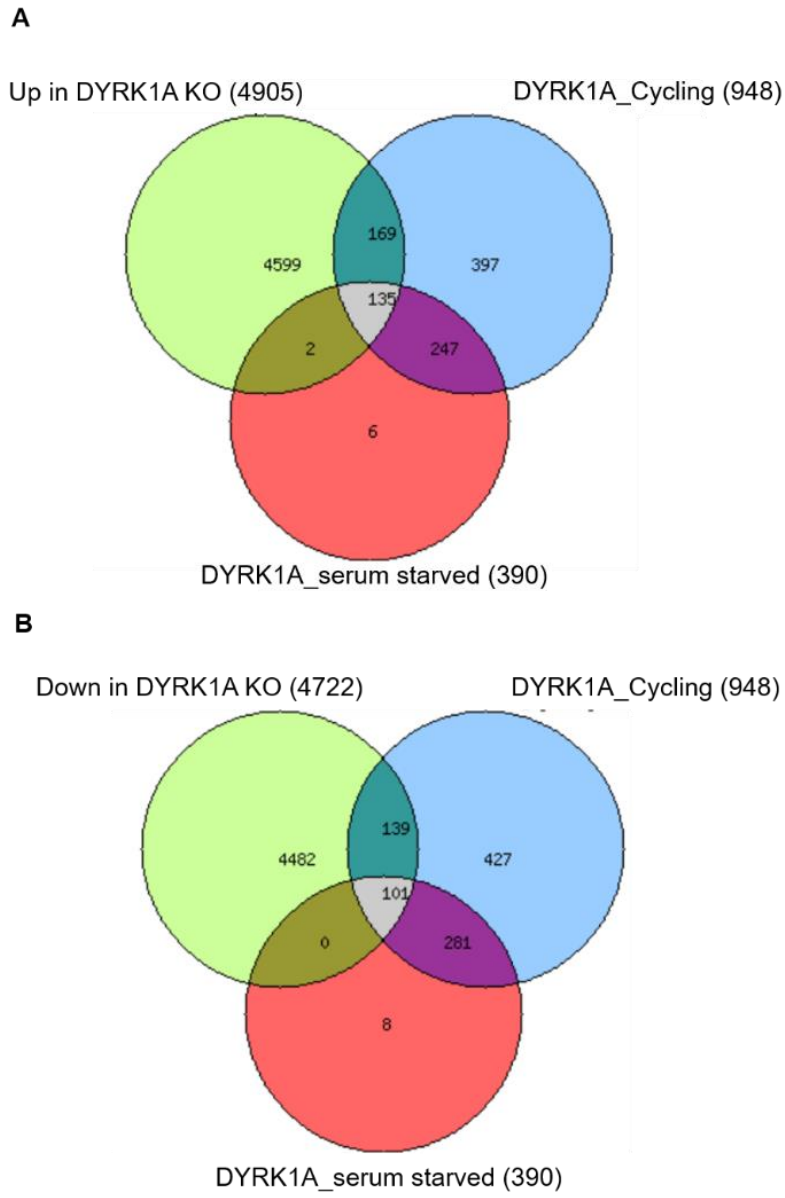

Figure 49: Overlap of DYRK1A regulated genes with DYRK1A ChIP-seq datasets
(A) Overlap of Genes Up in DYRK1A KO with DYRK1A bound genes under cycling and serum starved conditions. (B) Overlap of Genes Down in DYRK1A KO with DYRK1A bound genes under cycling and serum starved conditions [ChIP-seq dataset obtained from (Di Vona et al., 2015)]. Refer Appendix Table 7 and 8 for the list of the overlapping genes.

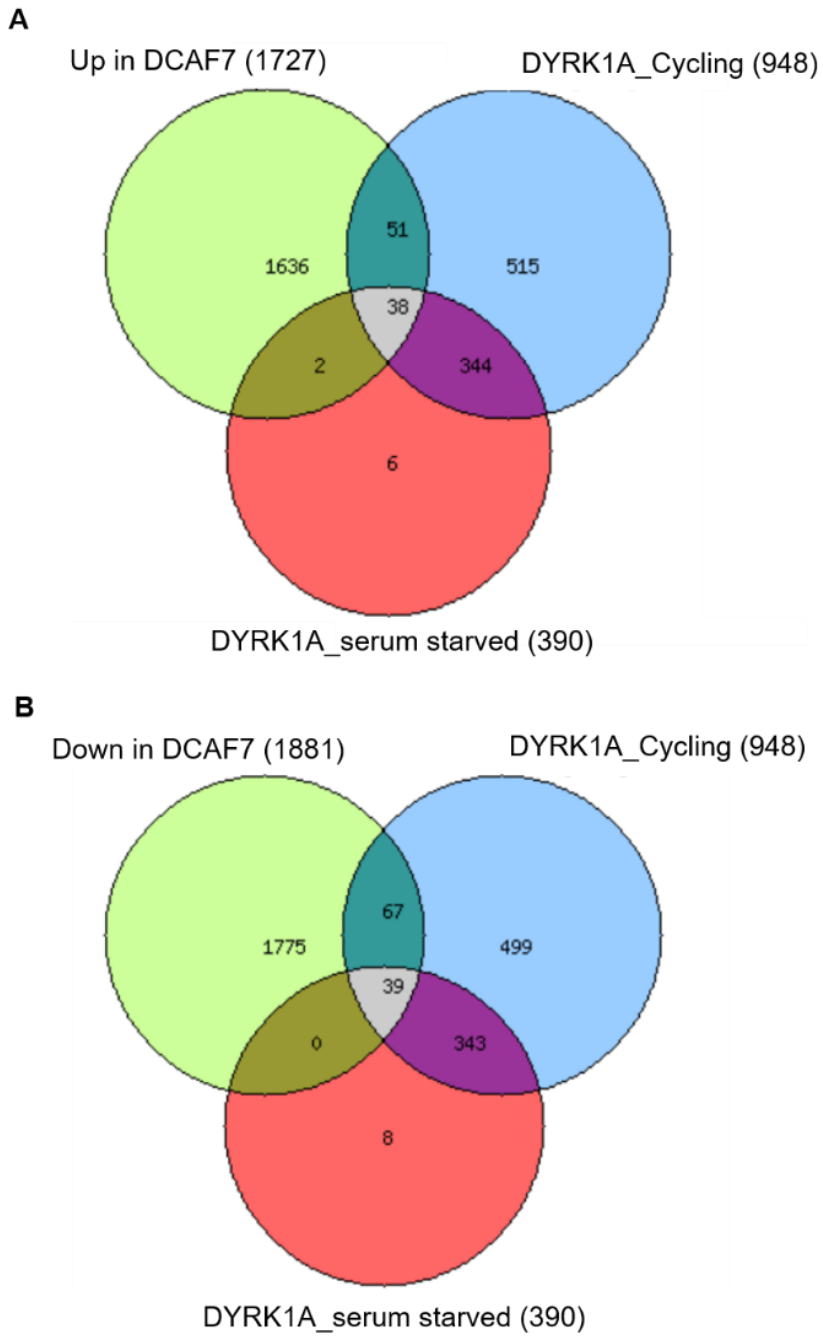

Figure 50: Overlap of DCAF7 regulated genes with DYRK1A ChIP-seq datasets
(A) Overlap of Genes Up in DCAF7 overexpression with DYRK1A bound genes under cycling and serum starved conditions (B) Overlap of Genes down in DCAF7 overexpression with DYRK1A bound genes under cycling and serum starved conditions [ChIP-seq dataset obtained from (Di Vona et al., 2015)]. Refer Appendix Table 9 for the list of the overlapping genes.

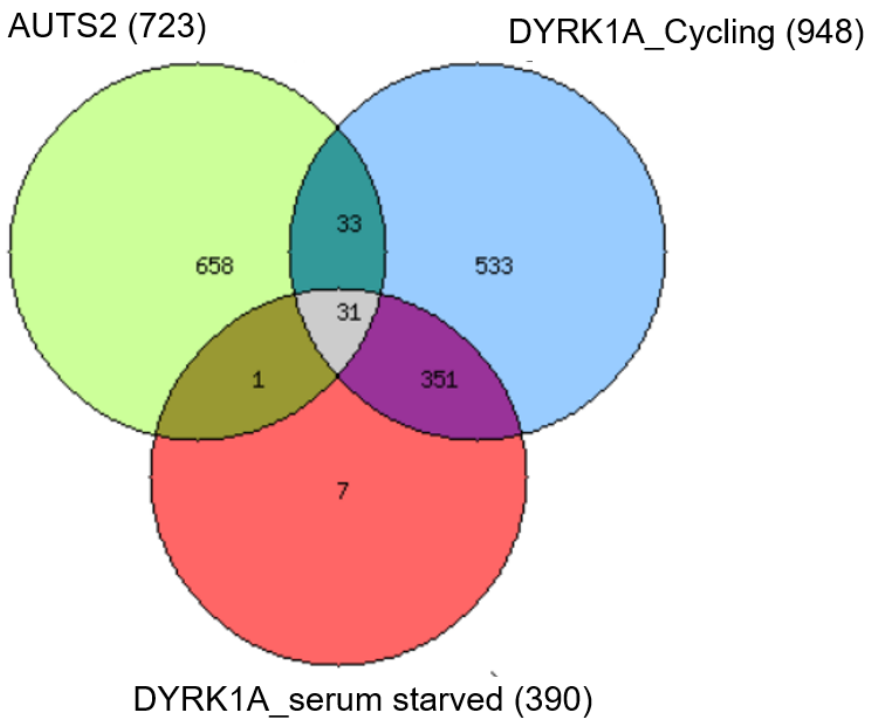

Figure 51: Overlap of genes bound by AUTS2 and genes bound by DYRK1A under cycling and serum starved conditions.
[DYRK1A ChIP-seq dataset obtained from (Di Vona et al., 2015); AUTS2 ChIP-seq dataset was obtained from (Gao et al., 2014)]. Refer Appendix Table 10 for the list of the overlapping genes.

4.3. DISCUSSION AND FUTURE DIRECTIONS

4.3.1 DCAF7 is a part of PRC1.3/5 but DYRK1A does not bind components of the complex

Proteomic studies by our lab and others revealed that DCAF7 bound several proteins belonging to the PRC1.3/5 complex (this dissertation and the BioGrid database, Figure 16). However, only our study investigated the DCAF7 interactome in T98G cells. The presence of PRC1.3/5 components in DCAF7 proteomic analysis from different cell types across different studies demonstrates that DCAF7 is indeed a part of this complex. Moreover, out of the several PRC1 complexes, DCAF7 only pulls down components of the non-canonical PRC1.3/5 complex, suggesting a possible specific function of DCAF7 in this type of PRC1 complex.

Indeed, we confirmed the interaction of DCAF7 with components of the PRC1.5-AUTS2 complex in T98G cells. Although DYRK1A and DCAF7 interact stoichiometrically, our results indicated that DYRK1A is not a part of the PRC1.3/5 complex. Using exhaustive immunoprecipitation to deplete DYRK1A from T98G cells lysates we have observed that not all of the DCAF7 in the cell is bound to DYRK1A (Appendix Figure 3). This suggests that DCAF7 could have protein interactions independent of DYRK1A.

4.3.2. DYRK1A affects the molecular size of AUTS2-PRC1

Although DYRK1A did not bind PRC1.3/5 components, its absence altered the molecular size of the complex. It is important to note that we did not detect all the components of the complex due to limited availability of antibodies. It is possible that some of the AUTS2-PRC1 components that we did not detect can be phosphorylated and regulated by DYRK1A. One angle to the future studies would be to analyze if any of the AUTS2-PRC1 components are phosphorylated by DYRK1A, leading to their degradation. This would explain the formation of a more stable and complete complex in the absence of DYRK1A.

4.3.3. DYRK1A and DCAF7 regulate PRC1 function

The only known function of the PRC1.3/5 complex is to catalyze H2A-K119 monoubiquitylation, which mediates transcriptional repression. This monoubiquitylation is inhibited by CK2 mediated phosphorylation of RING1B, leading to transcriptional activation (Gao et al., 2014). We observed that inhibition of DYRK1A by Harmine leads to an increase in H2A-K119 monoubiquitylation. Since this is a readout of global PRC1 function and not AUTS2-PRC1 alone, it is possible that DYRK1A phosphorylates and inhibits some component of PRC1. It will also be important to analyze the extent of global PRC1 function that is affected by DYRK1A. Moreover, since DYRK1A and CK2 are phylogenetically similar (Aranda et al.,

2011; Kannan & Neuwald, 2004), it will be important to analyze if they are redundant with respect to their function towards PRC1. Harmine inhibits only DYRK1A and DYRK1B while CX4945 is primarily a CK2 inhibitor that was also found to potently inhibit DYRK1A (H. Kim et al., 2016). Thus, comparing the effect of CX4945 to effect of other DYRK1A inhibitors on PRC1 function, we can determine if inhibition of both CK2 and DYRK1A causes a further increase in PRC1 function.

Our results also indicated that overexpression of DCAF7 led to a decrease in AUTS2-PRC1 function and this decrease was dependent on DYRK1A. This points to the possibility that DYRK1A and DCAF7 could regulate a common subset of genes that are also regulated by PRC1.3/5. Although the regulatory regions bound by DYRK1A are known, ChIP-seq analysis will be needed to analyze the genomic region bound by DCAF7. Further, ChIP- seq analysis to determine AUTS2 bound regions in the same cell type followed by an overlap of all of these datasets would be helpful to understand the mechanism through which DYRK1A and DCAF7 regulate PRC1.3/5 function.

4.3.4. DYRK1A and DCAF7 regulate a common subset of genes

Interestingly, our RNA-seq analysis and RT-qPCR validations indicated that DYRK1A and DCAF7 regulate a common sub-set of genes. Interestingly, several genes co-regulated by both DYRK1A and DCAF7 are implicated in neurological disorders and cancer. This is important because DYRK1A itself is implicated in both of these disease conditions. We have already shown that DYRK1A is required for the transcriptional role of DCAF7 but the mechanism of this regulation needs to be studied.

Moreover, many of the genes regulated by DYRK1A or DCAF7, or both DYRK1A and DCAF7 overlap with genes to whose genomic regions DYRK1A is known to bind. It could be possible that both DYRK1A and DCAF7 bind to the regulatory regions of these genes or it could be possible that one recruits the other. Due to its WD-40 repeats, it is also possible that DCAF7 has scaffolding functions bringing together DYRK1A and certain other transcriptional regulators. Given a large number of genes influenced by both DYRK1A and DCAF7, it is possible that these proteins may act as regulators of gene expression, for example as enhancers or activators. There is a study that analyzed published DYRK1A datasets to find that DYRK1A indeed localizes to regions of enhancers along with CBP and p300 (S. Li et al., 2018). Therefore, future studies will be required to elucidate the mechanism of DYRK1A and DCAF7 in transcription.

CHAPTER 5: PERSPECTIVES AND IMPACT

Although DYRK1A is implicated in human neurological conditions and in cancer, the functions and regulation of DYRK1A in the cell are not very well understood hence making it difficult to target DYRK1A for therapy. The findings presented in this dissertation significantly advance our understanding of DYRK1A function by characterizing the extended network of its protein-protein interactions and by detailed analysis of the functional interaction between DYRK1A and its most significant partners in the cell. Significantly, we found that DYRK1A (and its stoichiometric partner DCAF7) are involved in numerous distinct tertiary complexes that are involved in different cellular processes both in the nucleus and in the cytoplasm. Further studies will characterize the role of DYRK1A-DCAF7 in these cellular pathways.

In Chapter 2, we describe a novel role of DYRK1A in the DNA damage response pathway. Genomic instability is a major hallmark of cancer, and the ability of the genome maintenance systems to sense and repair damaged DNA is crucial for the homeostasis of the cell. Defects in these repair systems cause an increase mutation burden, driving tumorigenesis. Indeed, some familial cancer syndromes results from germline mutations in DNA repair genes, whereas most cancers have acquired alterations in DNA damage and repair pathways. Moreover, development of resistance to current chemotherapeutics is a direct function of genomic instability and is a major therapeutic challenge that requires further research before it can be overcome. Apart from cancer, several neurological disorders also result from defects in DNA repair genes. Our finding that DYRK1A levels can influence DNA repair will help us better understand the DNA damage response and DNA repair pathways and allow us to modulate these processes.

Sustained proliferative advantage remains one of the most important and fundamental features in cancer. The ability to regulate cell cycle progression in a controlled manner is lost in cancer cells and as a result, this deregulation allows them to evade cell cycle checkpoints, leading to sustained and aberrant proliferation. DYRK1A is a cell cycle regulator that prevents the uncontrolled proliferation of cells by promoting cell cycle exit and entry into quiescence. This important function must be considered when DYRK1A is targeted for therapy of conditions associated with its gain-of-function, such as Down syndrome and Alzheimer's disease. Through the work in Chapter 3 of this dissertation, we have identified several DYRK1A-interacting-proteins, and their respective protein interactomes, which could not only be utilized in future studies to better understand the regulation and substrates of DYRK1A, but also be used to characterize the function of the DYRK1A interacting proteins in different cellular pathways, including regulation of cell proliferation. Understanding of the physiological role of the DYRK1A complexes in the cell will help to design more precise inhibitors of only its desired functions. We have also identified a previously unknown scaffolding function of DYRK1A in the protein complexes identified in our study. If this scaffolding function of DYRK1A is required in different cellular pathways, it could help us better understand the phenotypic effect of DYRK1A dosage in different diseases.

We also identified LZTS1 and LZTS2 as novel regulators of DYRK1A activity. DYRK1A is a multifunctional kinase that phosphorylates numerous substrates in the cell. Therefore, targeting DYRK1A for therapy becomes difficult. However, if we are able to understand the mechanism by which LZTS1 and LZTS2 regulate DYRK1A kinase activity, we could potentially target LZTS1 and LZTS2 proteins in conditions where there is increased DYRK1A activity, like in Down syndrome.

Through Chapter 4 in the dissertation we have identified that DYRK1A and DCAF7 could inhibit the function of the PRC1 complex. By understanding the mechanism through which DYRK1A and DCAF7 affect the global PRC1 activity, we better understand the regulation of this complex which is perturbed in several developmental disorders and cancer. Further, our RNA-seq data has revealed that DYRK1A and DCAF7 could influence a common sub-set of genes implicated in neurological disorders or cancer. This was previously unknown and can be exploited further for therapy.

CHAPTER 6: MATERIALS AND METHODS

5.1. Cell lines

Human glioblastoma T98G, osteosarcoma U-2OS, HEK293T, Phoenix cells (modified HEK293T), were obtained from ATCC and used from early passage master stocks. Human ovarian cancer cell lines were obtained from ATCC or were a gift from Dr. Ronny Drapkin. Human Breast cancer cell lines were a gift from Dr. Jennifer Koblinski. All cell lines were cultured according to ATCC specifications and regularly checked for mycoplasma contamination using PCR assay and DAPI staining. T98G and U-2 OS cells stably expressing Flag-HA (FH) epitope tagged DYRK1A, GFP, DCAF7, LZTS2, LZTS1, TROAP or FAM117B were established using pMSCV retroviral vectors and puromycin selection as described in (Litovchick et al., 2011). U-2 OS cells stably expressing shRNA's against DCAF7 (Mission shRNA Millipore sigma, Catalog# SHCLNG-NM_005828; clones TRCN0000147504 and TRCN0000149770) or LZTS2 (Mission shRNA Millipore Sigma, Catalog # SHCLNG-NM_032429; clones TRCN0000419617 and TRCN0000412326) or non-targeting control (gift from Dr. Steven Grossman) were established using pLKO1 lentiviral vectors followed by puromycin selection. U-2 OS cell lines expressing DYRK1A in a doxycycline-inducible fashion were also used (Himpel et al., 2001; Litovchick et al., 2011).

DYRK1A-KO U-2 OS (Menon et al., 2019) and T98G cell lines (Iness et al., 2019) were established using GeneArt CRISPR Nuclease vector with OFP reporter (Life Technologies) harboring human or mouse DYRK1A-specific guide sequences. The control cell line was similarly established using a non-targeting construct provided with the kit. Briefly, cells were

transfected with sgRNA-CRISPR plasmids, FACS-sorted for OFP expression and grown as single-cell clones in 96-well plates that were screened for DYRK1A expression using immunoblotting. Two independent clones lacking DYRK1A expression were expanded and validated using antibodies against different epitopes in DYRK1A as well as genomic sequencing of the nested PCR-amplified fragment surrounding the sgRNA-targeted region. T98G cell lines have more than one copy of DYRK1A. Therefore, to verify that we had obtained single cell clones of DYRK1A KO cell lines, the nested amplified genomic regions were purified, cloned into Promega pGEM®-T Easy vector. Multiple DNA clones were sequenced to confirm the presence of mutations and the absence of the wild type sequences.

Table 1: Sequences of guiding RNA used to create indicated DYRK1A KO cell lines

Cell line	Top strand (5′-3′)	Bottom (5′-3′)
U-2 OS	TGTAAAGGCATATGATCGTG	CACGATCATATGCCTTTACA
T98G	TCAGCAACCTCTAACTAACC	GGTTAGTTAGAGGTTGCTGA

5.2. MudPIT proteomic analysis

MudPIT proteomic analysis was performed as described previously in (Florens & Washburn, 2006; Litovchick et al., 2007) using Finnigan LTQ linear ion trap mass spectrometer equipped with an electrospray ionization source. T98G cells stably expressing either Flag-HA tagged DYRK1A, DCAF7, LZTS2, LZTS1, FAM117B, TROAP or GFP (control) were used for immunoprecipitations with anti-HA antibody agarose beads (clone HA7, Sigma, Catalog#A2095). For RNF169, U-2 OS cells stably expressing HA-RNF169 were used for immunoprecipitation as described for the other proteins. Proteins were eluted from beads using HA peptide (Sigma, Catalog #I2149), concentrated and digested with trypsin. Tryptic peptides were resolved using Quaternary Agilent 1100 series HPLC and microcapillary multi-dimensional C_{18}-SCX-C_{18} matrix using fully automated 10-step chromatography run and electrosprayed into

mass spectrometer. Full MS spectra were recorded on the peptides over a 400 to 1,600 m/z range, followed by five tandem mass (MS/MS) events sequentially generated in a data-dependent manner on the first to fifth most intense ions selected from the full MS spectrum (at 35% collision energy). SEQUEST (Eng et al., 1994) was used to match MS/MS spectra to peptides in a database of 58622 amino acid sequences, consisting of 29147 human proteins (non-redundant entries from NCBI 2011-08-16 release). To estimate relative protein levels, spectral counts were normalized using Normalized Spectral Abundance Factors (NSAFs) (Litovchick et al., 2007; Swanson et al., 2009). Average NSAFs were calculated from four biological replicate DYRK1A pull-down experiments. Average NSAFs for all other proteins were calculated from three biological experiments. The analysis was carried out at the Proteomics Core at the Proteomics center at Stowers institute (Selene Swanson, Laurence Florens and Michael Washburn).

5.3. Immunoblotting and immunoprecipitation

For immunoblotting, cells were lysed in EBC or RIPA buffers supplemented with protease inhibitors (Millipore-Sigma catalog#539131), phosphatase inhibitors (Millipore-Sigma catalog# 524625) and β-ME for 10 min at 4°C and then centrifuged at 14,000g for 15 min at 4°C. Protein concentrations were determined by DC protein assay (BioRad). Protein samples were resolved using polyacrylamide gels (BioRad), transferred to a nitrocellulose membrane (GE Healthcare) and probed by specific antibodies, as recommended by manufacturer. For immunoprecipitation, cell extracts were incubated with appropriate antibodies (1 μg/ml) and Protein A Sepharose beads (GE Healthcare, Catalog #17078001) overnight at 4°C, washed five times with lysis buffer and re-suspended in 2X Laemmli sample buffer (BioRad, Catalog # 161-0737). Antibodies used in this study are listed in Table 2.

5.4. Cytonuclear fractionation

Cells were seeded at desired densities followed by cyto-nuclear fractionation using a commercially available kit (Active Motif, Catalog# 40010) and following manufacturer's instructions followed by IP/WB analysis.

5.5. Chemicals and treatments

To induce DNA damage, cells were exposed to gamma irradiation using MDS Nordion Gammacell 40 research irradiator with a ^{137}Cs source (ON, Canada) as described in (Menon et al., 2019). Harmine (Sigma; catalog No. H8646) and CX4945 (Selleckchem, Catalog no. # S2248) dissolved in DMSO were used for cell treatments at 10 μM final concentrations.

For phosphorylation assays, λ-phosphatase (NEB, Catalog # P0753S) was used either directly on immunoprecipitated sample or cell lysates according to manufacturer's protocol followed by WB analysis. PhosTag Acrylamide reagent (NARD institute limited, catalog # AAL-107) was added to prepare 7.5% polyacrylamide gels for resolving phosphorylated forms of proteins.

Table 2: List of antibodies used in the thesis

Antibody	Species	Source	Purpose	Catalog number
DYRK1A (clone 7D10)	Mouse	Sigma	WB	WH0001859MI
DYRK1A	Rabbit	Bethyl	IP/WB	A303-801A
RNF169	Rabbit	Abcam	WB	ab188237
RNF169	Rabbit	Bethyl	IP/WB	A304-097A
FAM117B	Rabbit	Bethyl	WB	BL19741
TROAP	Rabbit	Bethyl	IP	BL19735
TROAP	Rabbit	Proteintech	IP/WB	13634-1-AP
DCAF7	Rabbit	Abcam	WB	ab138490
LZTS2	Rabbit	Bethyl	IP/WB	BL19733
LZTS2	Rabbit	Invitrogen	IP/WB	PA5-60871
LZTS1	Rabbit	Bethyl	IP/WB	BL19723
LZTS1	Rabbit	Invitrogen	IP/WB	PA5-52274
RING1A	Rabbit	Bethyl	WB	A303-552A
RING1B/RNF2	Rabbit	Bethyl	WB	A302-869A
FBRS	Rabbit	Invitrogen	IP/WB	PA5-60615
CK2α	Rabbit	Bethyl	WB	A300-198A
Ubiquityl-Histone H2A (Lys 119)	Rabbit	Cell Signaling	WB	D27C4
Ubiquitin (P4D1)	Mouse	Santacruz	WB	sc-8017
Ubiquitin (FK2)	Mouse	R&D Biosyste	IF	A-106
USP7	Rabbit	Bethyl	WB	A300-033A
BRCA1	Rabbit	Bethyl	WB	A300-000A
p53	Mouse	DO-1	WB	sc-126
H2AX (pSer139)- 20E3	Rabbit	Cell Signaling	WB/IF	9718S
53BP1 (19/53BP1)	Mouse	BD Bioscience	IF/WB	612523
GFP (D5.1)	Rabbit	Cell Signaling	WB	3724S
GFP-Trap agarose		Chromotek	IP	gta-20
HA-Tag (HA.11)	Mouse	BioLegend	WB/IF	16B12
HA-Tag (C29F4)	Rabbit	Cell Signaling	WB/IF	3724
HA-agarose	Mouse	Sigma	IP	A2095
Ki67	Rabbit	Millipore	IF/FACS	AB9260
p-LIN52	Rabbit	Litovchick lab	WB	
GST (B14)	Mouse	Santacruz	WB	sc-138
Vinculin (hVIN-1)	Mouse	Sigma	WB	V9131
Tubulin	Mouse	Sigma	WB	SAB1411818
Lamin	Rabbit	Cell Signaling	WB	29565
β-actin (13E5)	Rabbit	Cell Signaling	WB	4970S
Normal Rabbit IgG	Rabbit	Millipore	IP	NI01-100VG
Anti-Mouse IgG	Goat	Jackson Immur	WB	115-035-003
Anti-Rabbit IgG	Goat	Jackson Immur	WB	111-035-003
Anti-Rabbit IgG Light Chain	Mouse	Jackson Immuno	Researcl	211-032-171
Anti-Rabbit Alexa Fluor 488	Rabbit	Invitrogen	IF	A-11008
Anti-Mouse Alexa Fluor 594	Goat	Jackson Immur	IF	115-585-146
Anti-Rabbit Cy-3 conjugated IgG	Donkey	Jackson Immur	IF/FACS	711-166-152

5.6. RNAi and plasmids

siRNA oligos used in this study were from Ambion/ Thermo Fisher Scientific as indicated in table 3. siRNA transfections were performed using Lipofectamine RNAiMAX (Invitrogen, catalog# 13778075) according to the manufacturer's instructions. GFP-tagged rat Dyrk1a wild-type and mutant constructs in pEGFP-C1 were a kind gift from Dr. Walter Becker (Glenewinkel et al., 2016). GFP-tagged mouse Dyrk1a wild-type and mutant constructs in pEGFP-N1 were a kind gift from Dr. Garriella D'Arcangelo (Yabut et al., 2010). HA-RNF169-pcDNA3 and GFP-RNF169 constructs were a gift from Dr. Niels Mailand (Poulsen et al., 2012). The phosphosite mutants of RNF169 were generated using the QuikChange II XL site directed mutagenesis kit (Agilent Technologies, Catalog # 200521) and verified by sequencing. Plasmid transfections were performed using either TransIT-2020 transfection reagent (Mirus Bio, Catalog# MIR5400), BioT reagent (Bioland Scientific LLC, Catalog# B01-01) or polyethylenimine reagent (Polysciences Inc., Catalog#23966) that was prepared according to manufacturer's protocol.

Table 3: List of siRNAs used in the thesis

Target	Type	Catalog	ID	Source
RNF169	Silencer select	4392420	s48512	Ambion/Thermofisher
FAM117B	Silencer select	4392420	s45493	Ambion/Thermofisher
LZTS2	Silencer select	4392420	s39013	Ambion/Thermofisher
LZTS1	Silencer select	4392420	s22063, s22062	Ambion/Thermofisher
TROAP	Silencer	AM167908	16369	Ambion/Thermofisher
DYRK1A	Silencer select	4390824	s4399	Ambion/Thermofisher
Negative control	Silencer select	4390846	No. 2	Ambion/Thermofisher
Negative control	Silencer	AM4611	No. 1	Ambion/Thermofisher

5.7. In-vitro kinase assays

Cell extracts (0.8 mg/ml) were prepared using EBC buffer, supplemented with EDTA-free protease inhibitors (Roche Diagnostics, Catalog#11836170001), phosphatase inhibitors and β-ME. Cell extract from a control cell line was treated with 10μM Harmine for 30 minutes on ice. The cell lysates and the Harmine treated control were then incubated with 1X kinase buffer (Cell Signaling Technologies, Catalog# 9802S), 10 mM $MnCl_2$, 200μM ATP (Cell signaling Technologies Catalog# 9804), and incubated at 30°C with 300 ng GST-LIN52 in a 100 μL reaction volume. The reaction was allowed to proceed for different time periods (0, 30, 45 or 60 minutes) and reaction was terminated by adding SDS-PAGE loading buffer and heating at 95°C for 10 min. Phosphorylation of GST-LIN52 was analyzed by WB analysis.

5.8. Immunofluorescence

Cells were seeded on glass coverslips in 6-well dishes and allowed to attach for 24h. After washing in PBS three times, cells were fixed in 4% formaldehyde for 20 min, blocked and permeabilized with 0.2% Triton X-100 in PBS containing 5% BSA for 30 min followed by incubation with primary and secondary antibodies. The coverslips were mounted in Fluoroshield mounting medium with DAPI (Abcam) and viewed using Zeiss Axio AX10 Imager fluorescence microscope for DNA damage-based assays. Images were acquired at 60x magnification using AxioVision software. For foci counts, the images were analyzed using ImageJ FIJI software (Schindelin et al., 2012). Briefly, images in JPEG format were processed to find the total number of foci (maxima). A noise tolerance value of 20 or 30 was used, and it was the same for all samples within each comparison group. For 53BP1, average foci per cell and number of cells with greater than 10 foci were calculated. For HA-RNF169, average foci per HA-positive cell and number of HA-positive cells with greater than 5 or 10 foci were calculated. To analyze

53BP1 in HA-RNF169 expressing cell lines, 53BP1 foci were scored only in the HA-positive cells. At least three biological repeats, defined as independently plated and treated series of cell samples, were analyzed for each quantitative analysis. For each biological repeat, more than 100 cells per experimental condition were typically scored. Some experiments were analyzed by two different observers, and all data were included in the analysis. The Zeiss Cell Observer Spinning Disc confocal microscope was used for capturing images for localization analysis; images were acquired at 63X magnification using ZEN 3.0 software (blue edition).

5.9. Gradient centrifugation

T98G cells were scraped using ice-cold PBS containing protease and phosphatase inhibitors, collected by centrifugation and extracted using buffer containing 10 mM HEPES, 2 mM $MgCl_2$, 10 mM KCl, 0.5% NP-40, 0.5 mM EDTA, 150 mM NaCl, H_2O, 1 mM DTT, protease and phosphatase inhibitors. For glycerol gradient analysis, 200 µL of clarified cell lysate containing approximately 6 mg/ml of protein was loaded on top of a pre-formed glycerol gradient (5 ml, 5–45% in lysis buffer made using a gradient maker). Another gradient was also loaded with protein weight markers (25 µg each) including bovine serum albumin (Sigma, Catalog# A8531), yeast alcohol dehydrogenase from yeast (Sigma, Catalog# A 8656), and bovine thyroglobulin (Sigma, Catalog# T9145). The samples were then centrifuged using SW55Ti rotor at 45,000 rpm at 4°C for 18h, after which 200 µL fractions were collected from the top of the gradient and analyzed by Western blotting or Coomassie staining (for markers).

For sucrose gradient analysis, solutions of 45% sucrose (solution A), 5% sucrose (solution D), 2:1 – 2 parts of solution A and 1 part of solution D (solution B) and 1:2- 1 part of solution A and 2 parts of solution D were made (solution C) in lysis buffer. A volume of 1mL of solution A was

pipetted into the centrifuge tube and frozen followed by sequential layering and freezing of solutions B, C and D. Just before the gradients were ready to be run, the gradient was thawed at room temperature for 30 minutes and cell lysates were loaded followed by centrifugation using SW55Ti rotor at 40,000 rpm 4°C for 18h, and collection of fractions. WB analysis was carried out as described for glycerol gradient analysis.

5.10. DR-GFP assay

DR-GFP reporter cell lines were established by transfecting the DR-GFP reporter construct [gift from Dr. Maria Jasin, Addgene plasmid # 26475; (Pierce et al., 1999)] into the control or DYRK1A-KO U-2 OS cells followed by puromycin selection as described (Yakovlev, 2013). The cells stably expressing the DR-GFP reporter were infected with adenovirus to express I-SceI at MOI =50. To monitor the HRR efficiency, GFP positive cells were detected 48h post-infection using flow cytometry as described (Pierce et al., 1999; Yakovlev, 2013)

5.11. FACS analysis

Cells were grown to desired densities, transfected with indicated constructs, trypsinized, collected by centrifugation and fixed overnight in 70% chilled ethanol. The next day, cells were incubated with PI (50µg/mL) and RNase A solution (100µg/ml, Sigma, Catalog #R4642) made in PBS at room temperature for 1hour. The cells (at least 10,000 per condition) were then analyzed using FACS Canto II flow cytometer (Becton Dickinson, San Jose, CA, USA).

For Ki67 staining, U-2 OS cells were plated followed by transfection with indicated constructs. 72 hours post transfection, cells were trypsinized and fixed in 1% formaldehyde solution by incubating at room temperature for 20 minutes. This was followed by blocking and

permeabilization at room temperature for 20 minutes, followed by staining with primary antibody and secondary antibodies. FACS analysis was performed using BD LSR-Fortessa flow cytometer (Becton Dickinson, San Jose, CA, USA) with at least 10,000 cells per condition.

5.12. Growth assay

U-2 OS control or DYRK1A inducible cell lines were seeded at a density of 3500 cells per well of a 12 well plate. Cells were allowed to attach overnight followed by addition of Doxycyline (Sigma, Catalog#9891-5G) containing medium such that the final concentration of Doxcycline is 1μg/mL. Cells were allowed to grow for 8 days and stained with crystal violet (Sigma, Catalog # HT 90132). The relative cell density was quantified by dissolving the dye in 10% (v/v) glacial acetic acid (ACROS, Cat# 64-19-7) and measuring the absorbance at 590 nm, after which the ratio of cell density relative to the uninduced control was calculated.

5.13. RNA-seq analysis

Five replicates from each sample were collected in Trizol LS reagent (Invitrogen) followed by isolation of RNA using Qiagen RNeasy Mini Kit (Catalog # 74104). RNA integrity was analyzed using Agilent BioAnalyzer 2100 (Dr. Vladimir Lee, Genomics core- VCU) and samples were sent for RNA-seq analysis (Genome Sequencing Facility, UT Health- San Antonio). Briefly, RNA from five replicate samples were used to prepare mRNA libraries that were analyzed using Illumina Hi-Seq 2500. Resulting files containing single end reads were assessed for quality using FastQC tools and trimmed using Trimmomatic (Bolger et al., 2014). The reads were aligned to the latest assembly of the human genome (GRCh38/hg38) using Subread, and DEGs were determined using DESeq2 (Love et al., 2014) and Edge R (Robinson et al., 2010) packages using

a False discovery rate (FDR) of 0.05. The analysis of RNA seq data was performed by Dr. Mikhail Dosmorov.

5.14. RT-qPCR assays

RNA isolation was carried out using Trizol LS reagent (Invitrogen) followed by cDNA synthesis using sensiFAST cDNA synthesis kit (Bioline; Catalog #BIO-65053). Thermoscientific maxima SYBR Green/ Rox qPCR master mix (Catalog #K0222) was used for qPCR analysis along with gene specific primers (Table 4) and the reactions were run on an Eppendorf realplex mastercycler. Fold changes in mRNA expression were calculated relative to controls using the $2^{-\Delta\Delta Ct}$ method.

5.15. Statistical analysis and bioinformatic tools

For quantitation of cell-staining based experiments including foci counts and Ki67 staining, 100 or more cells per conditions were typically scored. To calculate statistical significance, data from at least three biological replicates was analyzed using two-tailed Student's t-test. For kinase assays, ImageJ quantifications from three biological replicates were analyzed using 2-way Anova. For analysis of differential gene expression, two tailed student's t-test was used to calculate significance.

For protein networks analysis, list of proteins detected in at least three out of four DYRK1A MudPIT analyzes or two out of four times for LZTS1, LZTS2, FAM117B, RNF169 and TROAP were analyzed using MetaScape web-based software (metascape.org) that integrates data from BioGrid (Chatr-Aryamontri et al., 2015) and other protein databases with custom datasets to build protein-protein interaction networks. Protein-protein interaction networks were custom formatted using Cytoscape_3.7.1 software.

Table 4: List of qPCR primers used in the thesis

Gene (Human)	Forward (5'>3')	Reverse (5'>3')
GABRQ	TCCGCCTGAGACCGAATTTT	TCTGTTCAATGCTCGTGACA
ADGRV1	TCTCATCAGGGAAAAGGGAACC	CTGCCAGGGGGAAAGGTGATA
ELAVL2	AGAAGGTATCCAGGACCGCT	AAGCCATATTGAGCAGATTGTCC
PLXNA2	ACAGGCCTGGGAACCTAATC	ACTACCAGGCTAAGCAACCG
GABRA3	GTCAGACACTGACATGGAGTACA	GGGCCATCAAATTTCAGTCTTTCA
SELENOP	CAGCTGATACCTGTGCATACTG	TCCTTCTTTCTTCAGTTTTACTCGC
KCNB1	TACTGGAGAAGCCCAATTCCT	GCAATGGTGGAGAGGACGATG
WLS	AAAGGATATCCGGTTGGTGGG	GGTCTTCATGGCAAACCACAC
TOX	AAGATGAAGGCGATGATACCTCT	GCTCATTGGGATCCTTCTTCT
PDK4	GCAGTGGTCCAAGATGCCTT	GTTCAACTGTTGCCCGCATT
NETO1	TATCCCAGCAAGTATCCCCCT	CAATGCACTGTCTTGGAGCG
FOXA2	AGAGCCCGAGGGCTACTCC	TCATGTACGTGTTCATGCCGT
DNER	ACCTCAGTCAAGATTCGGCA	CACTGTTGGAATCCTGTGGC
E2F2	GACAGGACTGAGGACAACCT	GGCACAGGTAGACTTCGATGG
ID3	CTACAGCGCGTCATCGACTA	CTCGGCTGTCTGGATGGGAA
ARHGAP11B	ACACATTCCAAGCTTTCTTGTCG	TCCGAAAAAGCCCTTCGGTA
BUB1B	AGGGTGCAGCTGGATGTTTT	ACAATTCACCATCTTTTAGCTCAG
MYBL2	CATTGTGGATGAGGATGTGAAGC	TGGTTGAGCAAGCTGTTGTCTTC
DCAF7	CGCCCATGACAAAGAGGTCTA	TGCTGTGTTCTAGATGGCGG
18s rRNA	AACCCGTTGAACCCCATT	CCATCCAATCGGTAGTAGCG
GAPDH	GATGACATCAAGAAGGTGGTGAA	GTCTTACTCCTTGGAGGCCATGT

REFERENCES

Adayev, T., Chen-Hwang, M.-C., Murakami, N., Wegiel, J., & Hwang, Y.-W. (2006). Kinetic properties of a MNB/DYRK1A mutant suitable for the elucidation of biochemical pathways. Biochemistry, 45(39), 12011–12019. https://doi.org/10.1021/bi060632j

Ahn, K.-J., Jeong, H. K., Choi, H.-S., Ryoo, S.-R., Kim, Y. J., Goo, J.-S., Choi, S.-Y., Han, J.-S., Ha, I., & Song, W.-J. (2006). DYRK1A BAC transgenic mice show altered synaptic plasticity with learning and memory defects. Neurobiology of Disease, 22(3), 463–472. https://doi.org/10.1016/j.nbd.2005.12.006

Altafaj, X., Dierssen, M., Baamonde, C., Martí, E., Visa, J., Guimerà, J., Oset, M., González, J. R., Flórez, J., Fillat, C., & Estivill, X. (2001). Neurodevelopmental delay, motor abnormalities and cognitive deficits in transgenic mice overexpressing Dyrk1A (minibrain), a murine model of Down's syndrome. Human Molecular Genetics, 10(18), 1915–1923. https://doi.org/10.1093/hmg/10.18.1915

Alvarez, M., Altafaj, X., Aranda, S., & de la Luna, S. (2007). DYRK1A Autophosphorylation on Serine Residue 520 Modulates Its Kinase Activity via 14-3-3 Binding. Molecular Biology of the Cell, 18(4), 1167–1178. https://doi.org/10.1091/mbc.E06-08-0668

Álvarez, M., Estivill, X., & Luna, S. de la. (2003). DYRK1A accumulates in splicing speckles through a novel targeting signal and induces speckle disassembly. Journal of Cell Science, 116(15), 3099–3107. https://doi.org/10.1242/jcs.00618

An, L., Dong, C., Li, J., Chen, J., Yuan, J., Huang, J., Chan, K. M., Yu, C.-H., & Huen, M. S. Y. (2018). RNF169 limits 53BP1 deposition at DSBs to stimulate single-strand annealing repair. Proceedings of the National Academy of Sciences of the United States of America, 115(35), E8286–E8295. https://doi.org/10.1073/pnas.1804823115

Aranda, S., Laguna, A., & Luna, S. de la. (2011). DYRK family of protein kinases: Evolutionary relationships, biochemical properties, and functional roles. The FASEB Journal, 25(2), 449–462. https://doi.org/10.1096/fj.10-165837

Arnold, J. M., Choong, D. Y. H., Lai, J., Campbell, I. G., & Chenevix-Trench, G. (2006). Mutation and expression analysis of LZTS1 in ovarian cancer. Cancer Letters, 233(1), 151–157. https://doi.org/10.1016/j.canlet.2005.03.008

Azorsa, D. O., Robeson, R. H., Frost, D., Meec hoovet, B., Brautigam, G. R., Dickey, C., Beaudry, C., Basu, G. D., Holz, D. R., Hernandez, J. A., Bisanz, K. M., Gwinn, L., Grover, A., Rogers, J., Reiman, E. M., Hutton, M., Stephan, D. A., Mousses, S., & Dunckley, T. (2010). High-content siRNA screening of the kinome identifies kinases involved in Alzheimer's disease-related tau hyperphosphorylation. BMC Genomics, 11, 25. https://doi.org/10.1186/1471-2164-11-25

Bain, J., McLauchlan, H., Elliott, M., & Cohen, P. (2003). The specificities of protein kinase inhibitors: An update. The Biochemical Journal, 371(Pt 1), 199–204. https://doi.org/10.1042/BJ20021535

Becker, W., Soppa, U., & Tejedor, F. J. (2014). DYRK1A: A potential drug target for multiple Down syndrome neuropathologies. CNS & Neurological Disorders Drug Targets, 13(1), 26–33. https://doi.org/10.2174/18715273113126660186

Becker, W., Weber, Y., Wetzel, K., Eirmbter, K., Tejedor, F. J., & Joost, H.-G. (1998). Sequence Characteristics, Subcellular Localization, and Substrate Specificity of DYRK-related Kinases, a Novel Family of Dual Specificity Protein Kinases. Journal of Biological Chemistry, 273(40), 25893–25902. https://doi.org/10.1074/jbc.273.40.25893

Bedogni, F., Hodge, R. D., Nelson, B. R., Frederick, E. A., Shiba, N., Daza, R. A., & Hevner, R. F. (2010). Autism susceptibility candidate 2 (Auts2) encodes a nuclear protein expressed in developing brain regions implicated in autism neuropathology. Gene Expression Patterns: GEP, 10(1), 9–15. https://doi.org/10.1016/j.gep.2009.11.005

Bennett, C. B., Lewis, A. L., Baldwin, K. K., & Resnick, M. A. (1993). Lethality induced by a single site-specific double-strand break in a dispensable yeast plasmid. Proceedings of the National Academy of Sciences of the United States of America, 90(12), 5613–5617. https://doi.org/10.1073/pnas.90.12.5613

Beunders, G., Voorhoeve, E., Golzio, C., Pardo, L. M., Rosenfeld, J. A., Talkowski, M. E., Simonic, I., Lionel, A. C., Vergult, S., Pyatt, R. E., van de Kamp, J., Nieuwint, A., Weiss, M. M., Rizzu, P., Verwer, L. E. N. I., van Spaendonk, R. M. L., Shen, Y., Wu, B., Yu, T., … Sistermans, E. A. (2013). Exonic deletions in AUTS2 cause a syndromic form of intellectual disability and suggest a critical role for the C terminus. American Journal of Human Genetics, 92(2), 210–220. https://doi.org/10.1016/j.ajhg.2012.12.011

Bolger, A. M., Lohse, M., & Usadel, B. (2014). Trimmomatic: A flexible trimmer for Illumina sequence data. Bioinformatics (Oxford, England), 30(15), 2114–2120. https://doi.org/10.1093/bioinformatics/btu170

Branca, C., Shaw, D. M., Belfiore, R., Gokhale, V., Shaw, A. Y., Foley, C., Smith, B., Hulme, C., Dunckley, T., Meechoovet, B., Caccamo, A., & Oddo, S. (2017). Dyrk1 inhibition improves Alzheimer's disease-like pathology. Aging Cell, 16(5), 1146–1154. https://doi.org/10.1111/acel.12648

Bronicki, L. M., Redin, C., Drunat, S., Piton, A., Lyons, M., Passemard, S., Baumann, C., Faivre, L., Thevenon, J., Rivière, J.-B., Isidor, B., Gan, G., Francannet, C., Willems, M., Gunel, M., Jones, J. R., Gleeson, J. G., Mandel, J.-L., Stevenson, R. E., … Aylsworth, A. S. (2015). Ten new cases further delineate the syndromic intellectual disability phenotype caused by mutations in DYRK1A. European Journal of Human Genetics, 23(11), 1482–1487. https://doi.org/10.1038/ejhg.2015.29

Cabeza-Arvelaiz, Y., Sepulveda, J. L., Lebovitz, R. M., Thompson, T. C., & Chinault, A. C. (2001). Functional identification of LZTS1 as a candidate prostate tumor suppressor gene on human chromosome 8p22. Oncogene, 20(31), 4169–4179. https://doi.org/10.1038/sj.onc.1204539

Califano, D., Pignata, S., Pisano, C., Greggi, S., Laurelli, G., Losito, N. S., Ottaiano, A., Gallipoli, A., Pasquinelli, R., De Simone, V., Cirombella, R., Fusco, A., & Chiappetta, G.

(2010). FEZ1/LZTS1 protein expression in ovarian cancer. Journal of Cellular Physiology, 222(2), 382–386. https://doi.org/10.1002/jcp.21962

Cam, H., Balciunaite, E., Blais, A., Spektor, A., Scarpulla, R. C., Young, R., Kluger, Y., & Dynlacht, B. D. (2004). A common set of gene regulatory networks links metabolism and growth inhibition. Molecular Cell, 16(3), 399–411. https://doi.org/10.1016/j.molcel.2004.09.037

Canny, M. D., Moatti, N., Wan, L. C. K., Fradet-Turcotte, A., Krasner, D., Mateos-Gomez, P. A., Zimmermann, M., Orthwein, A., Juang, Y.-C., Zhang, W., Noordermeer, S. M., Seclen, E., Wilson, M. D., Vorobyov, A., Munro, M., Ernst, A., Ng, T. F., Cho, T., Cannon, P. M., … Durocher, D. (2018). Inhibition of 53BP1 favors homology-dependent DNA repair and increases CRISPR-Cas9 genome-editing efficiency. Nature Biotechnology, 36(1), 95–102. https://doi.org/10.1038/nbt.4021

Cao, R., Wang, L., Wang, H., Xia, L., Erdjument-Bromage, H., Tempst, P., Jones, R. S., & Zhang, Y. (2002). Role of histone H3 lysine 27 methylation in Polycomb-group silencing. Science (New York, N.Y.), 298(5595), 1039–1043. https://doi.org/10.1126/science.1076997

Chapman, J. R., Sossick, A. J., Boulton, S. J., & Jackson, S. P. (2012). BRCA1-associated exclusion of 53BP1 from DNA damage sites underlies temporal control of DNA repair. Journal of Cell Science, 125(Pt 15), 3529–3534. https://doi.org/10.1242/jcs.105353

Chatr-Aryamontri, A., Breitkreutz, B.-J., Oughtred, R., Boucher, L., Heinicke, S., Chen, D., Stark, C., Breitkreutz, A., Kolas, N., O'Donnell, L., Reguly, T., Nixon, J., Ramage, L., Winter, A., Sellam, A., Chang, C., Hirschman, J., Theesfeld, C., Rust, J., … Tyers, M. (2015). The BioGRID interaction database: 2015 update. Nucleic Acids Research, 43(Database issue), D470-478. https://doi.org/10.1093/nar/gku1204

Chen, J., Feng, W., Jiang, J., Deng, Y., & Huen, M. S. Y. (2012). Ring finger protein RNF169 antagonizes the ubiquitin-dependent signaling cascade at sites of DNA damage. The Journal of Biological Chemistry, 287(33), 27715–27722. https://doi.org/10.1074/jbc.M112.373530

Chen, J.-Y., Lin, J.-R., Tsai, F.-C., & Meyer, T. (2013). Dosage of Dyrk1a shifts cells within a p21-cyclin D1 signaling map to control the decision to enter the cell cycle. Molecular Cell, 52(1), 87–100. https://doi.org/10.1016/j.molcel.2013.09.009

Chen, L., Zhu, Z., Sun, X., Dong, X.-Y., Wei, J., Gu, F., Sun, Y.-L., Zhou, J., Dong, J.-T., & Fu, L. (2009). Down-regulation of tumor suppressor gene FEZ1/LZTS1 in breast carcinoma involves promoter methylation and associates with metastasis. Breast Cancer Research and Treatment, 116(3), 471–478. https://doi.org/10.1007/s10549-008-0147-6

Chen, W., Salto-Tellez, M., Palanisamy, N., Ganesan, K., Hou, Q., Tan, L. K., Sii, L. H., Ito, K., Tan, B., Wu, J., Tay, A., Tan, K. C., Ang, E., Tan, B. K., Tan, P. H., Ito, Y., & Tan, P. (2007). Targets of genome copy number reduction in primary breast cancers identified by integrative genomics. Genes, Chromosomes & Cancer, 46(3), 288–301. https://doi.org/10.1002/gcc.20411

Chen, Z., Zhou, Y., Luo, R., Liu, K., & Chen, Z. (2019). Trophinin-associated protein expression is an independent prognostic biomarker in lung adenocarcinoma. Journal of Thoracic Disease, 11(5), 2043–2050. https://doi.org/10.21037/jtd.2019.04.86

Chung, J., Marini, S., Pera, J., Norrving, B., Jimenez-Conde, J., Roquer, J., Fernandez-Cadenas, I., Tirschwell, D. L., Selim, M., Brown, D. L., Silliman, S. L., Worrall, B. B., Meschia, J. F., Demel, S., Greenberg, S. M., Slowik, A., Lindgren, A., Schmidt, R., Traylor, M., … Anderson, C. D. (2019). Genome-wide association study of cerebral small vessel disease reveals established and novel loci. Brain: A Journal of Neurology, 142(10), 3176–3189. https://doi.org/10.1093/brain/awz233

Cobrinik, D. (2005). Pocket proteins and cell cycle control. Oncogene, 24(17), 2796–2809. https://doi.org/10.1038/sj.onc.1208619

Couzens, A. L., Knight, J. D. R., Kean, M. J., Teo, G., Weiss, A., Dunham, W. H., Lin, Z.-Y., Bagshaw, R. D., Sicheri, F., Pawson, T., Wrana, J. L., Choi, H., & Gingras, A.-C. (2013). Protein interaction network of the mammalian Hippo pathway reveals mechanisms of kinase-phosphatase interactions. Science Signaling, 6(302), rs15. https://doi.org/10.1126/scisignal.2004712

Cui, Q.-Z., Tang, Z.-P., Zhang, X.-P., Zhao, H.-Y., Dong, Q.-Z., Xu, K., & Wang, E.-H. (2013). Leucine zipper tumor suppressor 2 inhibits cell proliferation and regulates Lef/Tcf-dependent transcription through Akt/GSK3β signaling pathway in lung cancer. The Journal of Histochemistry and Cytochemistry: Official Journal of the Histochemistry Society, 61(9), 659–670. https://doi.org/10.1369/0022155413495875

de Napoles, M., Mermoud, J. E., Wakao, R., Tang, Y. A., Endoh, M., Appanah, R., Nesterova, T. B., Silva, J., Otte, A. P., Vidal, M., Koseki, H., & Brockdorff, N. (2004). Polycomb group proteins Ring1A/B link ubiquitylation of histone H2A to heritable gene silencing and X inactivation. Developmental Cell, 7(5), 663–676. https://doi.org/10.1016/j.devcel.2004.10.005

de Vetten, N., Quattrocchio, F., Mol, J., & Koes, R. (1997). The an11 locus controlling flower pigmentation in petunia encodes a novel WD-repeat protein conserved in yeast, plants, and animals. Genes & Development, 11(11), 1422–1434. https://doi.org/10.1101/gad.11.11.1422

Degoutin, J. L., Milton, C. C., Yu, E., Tipping, M., Bosveld, F., Yang, L., Bellaiche, Y., Veraksa, A., & Harvey, K. F. (2013). Riquiqui and minibrain are regulators of the hippo pathway downstream of Dachsous. Nature Cell Biology, 15(10), 1176–1185. https://doi.org/10.1038/ncb2829

Dierssen, M., & de Lagrán, M. M. (2006). DYRK1A (Dual-Specificity Tyrosine-Phosphorylated and -Regulated Kinase 1A): A Gene with Dosage Effect During Development and Neurogenesis. The Scientific World Journal, 6, 1911–1922. https://doi.org/10.1100/tsw.2006.319

Di Vona, C., Bezdan, D., Islam, A. B. M. M. K., Salichs, E., López-Bigas, N., Ossowski, S., & de la Luna, S. (2015). Chromatin-wide Profiling of DYRK1A Reveals a Role as a Gene-Specific RNA Polymerase II CTD Kinase. Molecular Cell, 57(3), 506–520. https://doi.org/10.1016/j.molcel.2014.12.026

Dolnik, A., Kanwal, N., Mackert, S., Halbedl, S., Proepper, C., Bockmann, J., Schoen, M., Boeckers, T. M., Kühl, S. J., & Schmeisser, M. J. (2016). Sipa1l3/SPAR3 is targeted to postsynaptic specializations and interacts with the Fezzin ProSAPiP1/Lzts3. Journal of Neurochemistry, 136(1), 28–35. https://doi.org/10.1111/jnc.13353

Duchon, A., & Herault, Y. (2016). DYRK1A, a Dosage-Sensitive Gene Involved in Neurodevelopmental Disorders, Is a Target for Drug Development in Down Syndrome. Frontiers in Behavioral Neuroscience, 10. https://doi.org/10.3389/fnbeh.2016.00104

Durocher, D., & Pelletier, L. (2016). 53BP1 Goes Back to Its p53 Roots. Molecular Cell, 64(1), 3–4. https://doi.org/10.1016/j.molcel.2016.09.024

Endoh, M., Endo, T. A., Endoh, T., Fujimura, Y., Ohara, O., Toyoda, T., Otte, A. P., Okano, M., Brockdorff, N., Vidal, M., & Koseki, H. (2008). Polycomb group proteins Ring1A/B are functionally linked to the core transcriptional regulatory circuitry to maintain ES cell identity. Development, 135(8), 1513–1524. https://doi.org/10.1242/dev.014340

Eng, J. K., McCormack, A. L., & Yates, J. R. (1994). An approach to correlate tandem mass spectral data of peptides with amino acid sequences in a protein database. Journal of the American Society for Mass Spectrometry, 5(11), 976–989. https://doi.org/10.1016/1044-0305(94)80016-2

Escribano-Díaz, C., Orthwein, A., Fradet-Turcotte, A., Xing, M., Young, J. T. F., Tkáč, J., Cook, M. A., Rosebrock, A. P., Munro, M., Canny, M. D., Xu, D., & Durocher, D. (2013). A cell cycle-dependent regulatory circuit composed of 53BP1-RIF1 and BRCA1-CtIP controls DNA repair pathway choice. Molecular Cell, 49(5), 872–883. https://doi.org/10.1016/j.molcel.2013.01.001

Fernández-Martínez, P., Zahonero, C., & Sánchez-Gómez, P. (2015). DYRK1A: The double-edged kinase as a protagonist in cell growth and tumorigenesis. Molecular & Cellular Oncology, 2(1). https://doi.org/10.4161/23723548.2014.970048

Ferrari, K. J., Scelfo, A., Jammula, S., Cuomo, A., Barozzi, I., Stützer, A., Fischle, W., Bonaldi, T., & Pasini, D. (2014). Polycomb-dependent H3K27me1 and H3K27me2 regulate active transcription and enhancer fidelity. Molecular Cell, 53(1), 49–62. https://doi.org/10.1016/j.molcel.2013.10.030

Ferrer, I., Barrachina, M., Puig, B., Martínez de Lagrán, M., Martí, E., Avila, J., & Dierssen, M. (2005). Constitutive Dyrk1A is abnormally expressed in Alzheimer disease, Down syndrome, Pick disease, and related transgenic models. Neurobiology of Disease, 20(2), 392–400. https://doi.org/10.1016/j.nbd.2005.03.020

Fischle, W., Wang, Y., & Allis, C. D. (2003). Histone and chromatin cross-talk. Current Opinion in Cell Biology, 15(2), 172–183. https://doi.org/10.1016/s0955-0674(03)00013-9

Florens, L., & Washburn, M. P. (2006). Proteomic Analysis by Multidimensional Protein Identification Technology. In D. Nedelkov & R. W. Nelson (Eds.), New and Emerging Proteomic Techniques (pp. 159–175). Humana Press. https://doi.org/10.1385/1-59745-026-X:159

Fotaki, V., Dierssen, M., Alcántara, S., Martínez, S., Martí, E., Casas, C., Visa, J., Soriano, E., Estivill, X., & Arbonés, M. L. (2002). Dyrk1A Haploinsufficiency Affects Viability and Causes Developmental Delay and Abnormal Brain Morphology in Mice. Molecular and Cellular Biology, 22(18), 6636–6647. https://doi.org/10.1128/MCB.22.18.6636-6647.2002

Francis, N. J., Kingston, R. E., & Woodcock, C. L. (2004). Chromatin compaction by a polycomb group protein complex. Science (New York, N.Y.), 306(5701), 1574–1577. https://doi.org/10.1126/science.1100576

Friedman, E. (2007). Mirk/Dyrk1B in cancer. Journal of Cellular Biochemistry, 102(2), 274–279. https://doi.org/10.1002/jcb.21451

Fukuda, M. N., & Nozawa, S. (1999). Trophinin, tastin, and bystin: A complex mediating unique attachment between trophoblastic and endometrial epithelial cells at their respective apical cell membranes. Seminars in Reproductive Endocrinology, 17(3), 229–234. https://doi.org/10.1055/s-2007-1016230

Gao, Z., Lee, P., Stafford, J. M., von Schimmelmann, M., Schaefer, A., & Reinberg, D. (2014). An AUTS2-Polycomb complex activates gene expression in the CNS. Nature, 516(7531), 349–354. https://doi.org/10.1038/nature13921

Gao, Z., Zhang, J., Bonasio, R., Strino, F., Sawai, A., Parisi, F., Kluger, Y., & Reinberg, D. (2012). PCGF homologs, CBX proteins, and RYBP define functionally distinct PRC1 family complexes. Molecular Cell, 45(3), 344–356. https://doi.org/10.1016/j.molcel.2012.01.002

García-Cerro, S., Rueda, N., Vidal, V., Lantigua, S., & Martínez-Cué, C. (2017). Normalizing the gene dosage of Dyrk1A in a mouse model of Down syndrome rescues several Alzheimer's disease phenotypes. Neurobiology of Disease, 106, 76–88. https://doi.org/10.1016/j.nbd.2017.06.010

Glenewinkel, F., Cohen, M. J., King, C. R., Kaspar, S., Bamberg-Lemper, S., Mymryk, J. S., & Becker, W. (2016). The adaptor protein DCAF7 mediates the interaction of the adenovirus E1A oncoprotein with the protein kinases DYRK1A and HIPK2. Scientific Reports, 6. https://doi.org/10.1038/srep28241

Göckler, N., Jofre, G., Papadopoulos, C., Soppa, U., Tejedor, F. J., & Becker, W. (2009). Harmine specifically inhibits protein kinase DYRK1A and interferes with neurite formation. The FEBS Journal, 276(21), 6324–6337. https://doi.org/10.1111/j.1742-4658.2009.07346.x

Godoy, H., Mhawech-Fauceglia, P., Beck, A., Miliotto, A., Miller, A., Lele, S., & Odunsi, K. (2013). Developmentally restricted differentiation antigens are targets for immunotherapy in epithelial ovarian carcinoma. International Journal of Gynecological Pathology: Official Journal of the International Society of Gynecological Pathologists, 32(6), 536–540. https://doi.org/10.1097/PGP.0b013e318275a550

Granno, S., Nixon-Abell, J., Berwick, D. C., Tosh, J., Heaton, G., Almudimeegh, S., Nagda, Z., Rain, J.-C., Zanda, M., Plagnol, V., Tybulewicz, V. L. J., Cleverley, K., Wiseman, F. K., Fisher, E. M. C., & Harvey, K. (2019). Downregulated Wnt/β-catenin signalling in the Down syndrome hippocampus. Scientific Reports, 9(1), 7322. https://doi.org/10.1038/s41598-019-43820-4

Guard, S. E., Poss, Z. C., Ebmeier, C. C., Pagratis, M., Simpson, H., Taatjes, D. J., & Old, W. M. (2019). The nuclear interactome of DYRK1A reveals a functional role in DNA damage repair. Scientific Reports, 9(1), 6539. https://doi.org/10.1038/s41598-019-42990-5

Guimera, J., Casas, C., Estivill, X., & Pritchard, M. (1999). HumanMinibrainHomologue (MNBH/DYRK1): Characterization, Alternative Splicing, Differential Tissue Expression, and Overexpression in Down Syndrome. Genomics, 57(3), 407–418. https://doi.org/10.1006/geno.1999.5775

Hämmerle, B., Carnicero, A., Elizalde, C., Ceron, J., Martínez, S., & Tejedor, F. J. (2003). Expression patterns and subcellular localization of the Down syndrome candidate protein MNB/DYRK1A suggest a role in late neuronal differentiation. The European Journal of Neuroscience, 17(11), 2277–2286. https://doi.org/10.1046/j.1460-9568.2003.02665.x

Hanks, S. K., & Hunter, T. (1995). The eukaryotic protein kinase superfamily: Kinase (catalytic) domain structure and classification1. The FASEB Journal, 9(8), 576–596. https://doi.org/10.1096/fasebj.9.8.7768349

Hasle, H., Clemmensen, I. H., & Mikkelsen, M. (2000). Risks of leukaemia and solid tumours in individuals with Down's syndrome. Lancet (London, England), 355(9199), 165–169. https://doi.org/10.1016/S0140-6736(99)05264-2

Hauri, S., Comoglio, F., Seimiya, M., Gerstung, M., Glatter, T., Hansen, K., Aebersold, R., Paro, R., Gstaiger, M., & Beisel, C. (2016). A High-Density Map for Navigating the Human Polycomb Complexome. Cell Reports, 17(2), 583–595. https://doi.org/10.1016/j.celrep.2016.08.096

He, J., Yu, L., Wang, C.-M., & Zhou, X.-F. (2018). MiR-1275 promotes non-small cell lung cancer cell proliferation and metastasis by regulating LZTS3 expression. European Review for Medical and Pharmacological Sciences, 22(9), 2680–2687. https://doi.org/10.26355/eurrev_201805_14964

He, Y., & Liu, X. (2015). The tumor-suppressor gene LZTS1 suppresses hepatocellular carcinoma proliferation by impairing PI3K/Akt pathway. Biomedicine & Pharmacotherapy = Biomedecine & Pharmacotherapie, 76, 141–146. https://doi.org/10.1016/j.biopha.2015.10.006

Himpel, S, Panzer, P., Eirmbter, K., Czajkowska, H., Sayed, M., Packman, L. C., Blundell, T., Kentrup, H., Grötzinger, J., Joost, H. G., & Becker, W. (2001). Identification of the autophosphorylation sites and characterization of their effects in the protein kinase DYRK1A. Biochemical Journal, 359(Pt 3), 497–505.

Himpel, Sunke, Tegge, W., Frank, R., Leder, S., Joost, H.-G., & Becker, W. (2000). Specificity Determinants of Substrate Recognition by the Protein Kinase DYRK1A. Journal of Biological Chemistry, 275(4), 2431–2438. https://doi.org/10.1074/jbc.275.4.2431

Hori, K., Nagai, T., Shan, W., Sakamoto, A., Abe, M., Yamazaki, M., Sakimura, K., Yamada, K., & Hoshino, M. (2015). Heterozygous Disruption of Autism susceptibility candidate 2 Causes Impaired Emotional Control and Cognitive Memory. PLoS ONE, 10(12). https://doi.org/10.1371/journal.pone.0145979

Hornbeck, P. V., Kornhauser, J. M., Tkachev, S., Zhang, B., Skrzypek, E., Murray, B., Latham, V., & Sullivan, M. (2012). PhosphoSitePlus: A comprehensive resource for investigating the structure and function of experimentally determined post-translational modifications in man and

mouse. Nucleic Acids Research, 40(Database issue), D261–D270. https://doi.org/10.1093/nar/gkr1122

Hu, H., Xu, L., Chen, Y., Luo, S.-J., Wu, Y.-Z., Xu, S.-H., Liu, M.-T., Lin, F., Mei, Y., Yang, Q., Qiang, Y.-Y., Lin, Y.-W., Deng, Y.-J., Lin, T., Sha, Y.-Q., Huang, B.-J., & Zhang, S.-J. (2019). The Upregulation of Trophinin-Associated Protein (TROAP) Predicts a Poor Prognosis in Hepatocellular Carcinoma. Journal of Cancer, 10(4), 957–967. https://doi.org/10.7150/jca.26666

Hu, Q., Botuyan, M. V., Cui, G., Zhao, D., & Mer, G. (2017). Mechanisms of Ubiquitin-Nucleosome Recognition and Regulation of 53BP1 Chromatin Recruitment by RNF168/169 and RAD18. Molecular Cell, 66(4), 473-487.e9. https://doi.org/10.1016/j.molcel.2017.04.009

Huang, J., Li, Y., Lu, Z., Che, Y., Sun, S., Mao, S., Lei, Y., Zang, R., Li, N., Zheng, S., Liu, C., Wang, X., Sun, N., & He, J. (2019). Analysis of functional hub genes identifies CDC45 as an oncogene in non-small cell lung cancer—A short report. Cellular Oncology (Dordrecht), 42(4), 571–578. https://doi.org/10.1007/s13402-019-00438-y

Iness, A. N., Felthousen, J., Ananthapadmanabhan, V., Sesay, F., Saini, S., Guiley, K. Z., Rubin, S. M., Dozmorov, M., & Litovchick, L. (2019). The cell cycle regulatory DREAM complex is disrupted by high expression of oncogenic B-Myb. Oncogene, 38(7), 1080–1092. https://doi.org/10.1038/s41388-018-0490-y

Ishii, H., Baffa, R., Numata, S. I., Murakumo, Y., Rattan, S., Inoue, H., Mori, M., Fidanza, V., Alder, H., & Croce, C. M. (1999). The FEZ1 gene at chromosome 8p22 encodes a leucine-zipper protein, and its expression is altered in multiple human tumors. Proceedings of the National Academy of Sciences of the United States of America, 96(7), 3928–3933. https://doi.org/10.1073/pnas.96.7.3928

Isono, M., Niimi, A., Oike, T., Hagiwara, Y., Sato, H., Sekine, R., Yoshida, Y., Isobe, S.-Y., Obuse, C., Nishi, R., Petricci, E., Nakada, S., Nakano, T., & Shibata, A. (2017). BRCA1 Directs the Repair Pathway to Homologous Recombination by Promoting 53BP1 Dephosphorylation. Cell Reports, 18(2), 520–532. https://doi.org/10.1016/j.celrep.2016.12.042

Jaenisch, R., & Young, R. (2008). Stem cells, the molecular circuitry of pluripotency and nuclear reprogramming. Cell, 132(4), 567–582. https://doi.org/10.1016/j.cell.2008.01.015

Jang, S. M., Azebi, S., Soubigou, G., & Muchardt, C. (2014). DYRK1A phoshorylates histone H3 to differentially regulate the binding of HP1 isoforms and antagonize HP1-mediated transcriptional repression. EMBO Reports, 15(6), 686–694. https://doi.org/10.15252/embr.201338356

Jaspers, J. E., Kersbergen, A., Boon, U., Sol, W., van Deemter, L., Zander, S. A., Drost, R., Wientjens, E., Ji, J., Aly, A., Doroshow, J. H., Cranston, A., Martin, N. M. B., Lau, A., O'Connor, M. J., Ganesan, S., Borst, P., Jonkers, J., & Rottenberg, S. (2013). Loss of 53BP1 causes PARP inhibitor resistance in Brca1-mutated mouse mammary tumors. Cancer Discovery, 3(1), 68–81. https://doi.org/10.1158/2159-8290.CD-12-0049

Ji, J., Lee, H., Argiropoulos, B., Dorrani, N., Mann, J., Martinez-Agosto, J. A., Gomez-Ospina, N., Gallant, N., Bernstein, J. A., Hudgins, L., Slattery, L., Isidor, B., Le Caignec, C., David, A., Obersztyn, E., Wiśniowiecka-Kowalnik, B., Fox, M., Deignan, J. L., Vilain, E., … Quintero-Rivera, F. (2015). DYRK1A haploinsufficiency causes a new recognizable syndrome with microcephaly, intellectual disability, speech impairment, and distinct facies. European Journal of Human Genetics: EJHG, 23(11), 1473–1481. https://doi.org/10.1038/ejhg.2015.71

Jiao, Y., Li, Y., Lu, Z., & Liu, Y. (2019). High Trophinin-Associated Protein Expression Is an Independent Predictor of Poor Survival in Liver Cancer. Digestive Diseases and Sciences, 64(1), 137–143. https://doi.org/10.1007/s10620-018-5315-x

Jin, J., Arias, E. E., Chen, J., Harper, J. W., & Walter, J. C. (2006). A family of diverse Cul4-Ddb1-interacting proteins includes Cdt2, which is required for S phase destruction of the replication factor Cdt1. Molecular Cell, 23(5), 709–721. https://doi.org/10.1016/j.molcel.2006.08.010

Jing, K., Mao, Q., & Ma, P. (2018). Decreased expression of TROAP suppresses cellular proliferation, migration and invasion in gastric cancer. Molecular Medicine Reports, 18(3), 3020–3026. https://doi.org/10.3892/mmr.2018.9230

Johnson, D. T., Luong, R., Lee, S. H., Peng, Y., Shaltouki, A., Lee, J. T., Lin, D., Wang, Y., & Sun, Z. (2013). Deletion of leucine zipper tumor suppressor 2 (Lzts2) increases susceptibility to tumor development. The Journal of Biological Chemistry, 288(6), 3727–3738. https://doi.org/10.1074/jbc.M112.417568

Kaczmarski, W., Barua, M., Mazur-Kolecka, B., Frackowiak, J., Dowjat, W., Mehta, P., Bolton, D., Hwang, Y.-W., Rabe, A., Albertini, G., & Wegiel, J. (2014). Intracellular distribution of differentially phosphorylated dual-specificity tyrosine phosphorylation-regulated kinase 1A (DYRK1A). Journal of Neuroscience Research, 92(2), 162–173. https://doi.org/10.1002/jnr.23279

Kannan, N., & Neuwald, A. F. (2004). Evolutionary constraints associated with functional specificity of the CMGC protein kinases MAPK, CDK, GSK, SRPK, DYRK, and CK2α. Protein Science : A Publication of the Protein Society, 13(8), 2059–2077. https://doi.org/10.1110/ps.04637904

Kawara, H., Akahori, R., Wakasugi, M., Sancar, A., & Matsunaga, T. (2019). DCAF7 is required for maintaining the cellular levels of ERCC1-XPF and nucleotide excision repair. Biochemical and Biophysical Research Communications, 519(1), 204–210. https://doi.org/10.1016/j.bbrc.2019.08.147

Kawaue, T., Shitamukai, A., Nagasaka, A., Tsunekawa, Y., Shinoda, T., Saito, K., Terada, R., Bilgic, M., Miyata, T., Matsuzaki, F., & Kawaguchi, A. (2019). Lzts1 controls both neuronal delamination and outer radial glial-like cell generation during mammalian cerebral development. Nature Communications, 10(1), 2780. https://doi.org/10.1038/s41467-019-10730-y

Kennison, J. A. (1995). The Polycomb and trithorax group proteins of Drosophila: Trans-regulators of homeotic gene function. Annual Review of Genetics, 29, 289–303. https://doi.org/10.1146/annurev.ge.29.120195.001445

Kim, D., Won, J., Shin, D. W., Kang, J., Kim, Y. J., Choi, S. Y., Hwang, M.-K., Jeong, B.-W., Kim, G. S., Joe, C. O., Chung, S.-H., & Song, W.-J. (2004). Regulation of Dyrk1A kinase activity by 14-3-3. Biochemical and Biophysical Research Communications, 323(2), 499–504. https://doi.org/10.1016/j.bbrc.2004.08.102

Kim, E. J., Sung, J. Y., Lee, H. J., Rhim, H., Hasegawa, M., Iwatsubo, T., Min, D. S., Kim, J., Paik, S. R., & Chung, K. C. (2006). Dyrk1A Phosphorylates α-Synuclein and Enhances Intracellular Inclusion Formation. Journal of Biological Chemistry, 281(44), 33250–33257. https://doi.org/10.1074/jbc.M606147200

Kim, H., Lee, K.-S., Kim, A.-K., Choi, M., Choi, K., Kang, M., Chi, S.-W., Lee, M.-S., Lee, J.-S., Lee, S.-Y., Song, W.-J., Yu, K., & Cho, S. (2016). A chemical with proven clinical safety rescues Down-syndrome-related phenotypes in through DYRK1A inhibition. Disease Models & Mechanisms, 9(8), 839–848. https://doi.org/10.1242/dmm.025668

Kloet, S. L., Makowski, M. M., Baymaz, H. I., van Voorthuijsen, L., Karemaker, I. D., Santanach, A., Jansen, P. W. T. C., Di Croce, L., & Vermeulen, M. (2016). The dynamic interactome and genomic targets of Polycomb complexes during stem cell differentiation. Nature Structural & Molecular Biology, 23(7), 682–690. https://doi.org/10.1038/nsmb.3248

Komorek, J., Kuppuswamy, M., Subramanian, T., Vijayalingam, S., Lomonosova, E., Zhao, L.-J., Mymryk, J. S., Schmitt, K., & Chinnadurai, G. (2010). Adenovirus type 5 E1A and E6 proteins of low-risk cutaneous beta-human papillomaviruses suppress cell transformation through interaction with FOXK1/K2 transcription factors. Journal of Virology, 84(6), 2719–2731. https://doi.org/10.1128/JVI.02119-09

Korbel, J. O., Tirosh-Wagner, T., Urban, A. E., Chen, X.-N., Kasowski, M., Dai, L., Grubert, F., Erdman, C., Gao, M. C., Lange, K., Sobel, E. M., Barlow, G. M., Aylsworth, A. S., Carpenter, N. J., Clark, R. D., Cohen, M. Y., Doran, E., Falik-Zaccai, T., Lewin, S. O., … Korenberg, J. R. (2009). The genetic architecture of Down syndrome phenotypes revealed by high-resolution analysis of human segmental trisomies. Proceedings of the National Academy of Sciences of the United States of America, 106(29), 12031–12036. https://doi.org/10.1073/pnas.0813248106

Kropp, M., & Wilson, S. I. (2012). The expression profile of the tumor suppressor gene Lzts1 suggests a role in neuronal development. Developmental Dynamics: An Official Publication of the American Association of Anatomists, 241(5), 984–994. https://doi.org/10.1002/dvdy.23777

Lee, J., & Zhou, P. (2007). DCAFs, the missing link of the CUL4-DDB1 ubiquitin ligase. Molecular Cell, 26(6), 775–780. https://doi.org/10.1016/j.molcel.2007.06.001

Levine, S. S., Weiss, A., Erdjument-Bromage, H., Shao, Z., Tempst, P., & Kingston, R. E. (2002). The core of the polycomb repressive complex is compositionally and functionally conserved in flies and humans. Molecular and Cellular Biology, 22(17), 6070–6078. https://doi.org/10.1128/mcb.22.17.6070-6078.2002

Lewis, E. B. (1978). A gene complex controlling segmentation in Drosophila. Nature, 276(5688), 565–570. https://doi.org/10.1038/276565a0

Li, Kai, Zhang, R., Wei, M., Zhao, L., Wang, Y., Feng, X., Yang, Y., Yang, S., & Zhang, L. (2019). TROAP Promotes Breast Cancer Proliferation and Metastasis. BioMed Research International, 2019, 6140951. https://doi.org/10.1155/2019/6140951

Li, Ke, Zhao, S., Karur, V., & Wojchowski, D. M. (2002). DYRK3 Activation, Engagement of Protein Kinase A/cAMP Response Element-binding Protein, and Modulation of Progenitor Cell Survival. Journal of Biological Chemistry, 277(49), 47052–47060. https://doi.org/10.1074/jbc.M205374200

Li, S., Xu, C., Fu, Y., Lei, P.-J., Yao, Y., Yang, W., Zhang, Y., Washburn, M. P., Florens, L., Jaiswal, M., Wu, M., & Mohan, M. (2018). DYRK1A interacts with histone acetyl transferase p300 and CBP and localizes to enhancers. Nucleic Acids Research, 46(21), 11202–11213. https://doi.org/10.1093/nar/gky754

Lian, Y., Fan, W., Huang, Y., Wang, H., Wang, J., Zhou, L., Wu, X., Deng, M., & Huang, Y. (2018). Downregulated Trophinin-Associated Protein Plays a Critical Role in Human Hepatocellular Carcinoma Through Upregulation of Tumor Cell Growth and Migration. Oncology Research, 26(5), 691–701. https://doi.org/10.3727/096504017X15101398724809

Lin, C.-W., Chang, Y.-L., Chang, Y.-C., Lin, J.-C., Chen, C.-C., Pan, S.-H., Wu, C.-T., Chen, H.-Y., Yang, S.-C., Hong, T.-M., & Yang, P.-C. (2013). MicroRNA-135b promotes lung cancer metastasis by regulating multiple targets in the Hippo pathway and LZTS1. Nature Communications, 4, 1877. https://doi.org/10.1038/ncomms2876

Litovchick, L., Florens, L. A., Swanson, S. K., Washburn, M. P., & DeCaprio, J. A. (2011). DYRK1A protein kinase promotes quiescence and senescence through DREAM complex assembly. Genes & Development, 25(8), 801–813. https://doi.org/10.1101/gad.2034211

Litovchick, L., Sadasivam, S., Florens, L., Zhu, X., Swanson, S. K., Velmurugan, S., Chen, R., Washburn, M. P., Liu, X. S., & DeCaprio, J. A. (2007). Evolutionarily Conserved Multisubunit RBL2/p130 and E2F4 Protein Complex Represses Human Cell Cycle-Dependent Genes in Quiescence. Molecular Cell, 26(4), 539–551. https://doi.org/10.1016/j.molcel.2007.04.015

Liu, F., Liang, Z., Wegiel, J., Hwang, Y.-W., Iqbal, K., Grundke-Iqbal, I., Ramakrishna, N., & Gong, C.-X. (2008). Overexpression of Dyrk1A contributes to neurofibrillary degeneration in Down syndrome. FASEB Journal: Official Publication of the Federation of American Societies for Experimental Biology, 22(9), 3224–3233. https://doi.org/10.1096/fj.07-104539

Liu, X., Yang, X., Li, Y., Zhao, S., Li, C., Ma, P., & Mao, B. (2016). Trip12 is an E3 ubiquitin ligase for USP7/HAUSP involved in the DNA damage response. FEBS Letters, 590(23), 4213–4222. https://doi.org/10.1002/1873-3468.12471

Lochhead, P. A., Sibbet, G., Kinstrie, R., Cleghon, T., Rylatt, M., Morrison, D. K., & Cleghon, V. (2003). dDYRK2: A novel dual-specificity tyrosine-phosphorylation-regulated kinase in Drosophila. Biochemical Journal, 374(Pt 2), 381–391. https://doi.org/10.1042/BJ20030500

Lovat, F., Ishii, H., Schiappacassi, M., Fassan, M., Barbareschi, M., Galligioni, E., Gasparini, P., Baldassarre, G., Croce, C. M., & Vecchione, A. (2014). LZTS1 downregulation confers

paclitaxel resistance and is associated with worse prognosis in breast cancer. Oncotarget, 5(4), 970–977. https://doi.org/10.18632/oncotarget.1630

Love, M. I., Huber, W., & Anders, S. (2014). Moderated estimation of fold change and dispersion for RNA-seq data with DESeq2. Genome Biology, 15(12), 550. https://doi.org/10.1186/s13059-014-0550-8

Malumbres, M., & Barbacid, M. (2009). Cell cycle, CDKs and cancer: A changing paradigm. Nature Reviews. Cancer, 9(3), 153–166. https://doi.org/10.1038/nrc2602

Margueron, Raphael, Li, G., Sarma, K., Blais, A., Zavadil, J., Woodcock, C. L., Dynlacht, B. D., & Reinberg, D. (2008). Ezh1 and Ezh2 maintain repressive chromatin through different mechanisms. Molecular Cell, 32(4), 503–518. https://doi.org/10.1016/j.molcel.2008.11.004

Margueron, Raphaël, & Reinberg, D. (2011). The Polycomb complex PRC2 and its mark in life. Nature, 469(7330), 343–349. https://doi.org/10.1038/nature09784

Martí, E., Altafaj, X., Dierssen, M., de la Luna, S., Fotaki, V., Alvarez, M., Pérez-Riba, M., Ferrer, I., & Estivill, X. (2003). Dyrk1A expression pattern supports specific roles of this kinase in the adult central nervous system. Brain Research, 964(2), 250–263. https://doi.org/10.1016/S0006-8993(02)04069-6

Mayanagi, T., Yasuda, H., & Sobue, K. (2015). PSD-Zip70 Deficiency Causes Prefrontal Hypofunction Associated with Glutamatergic Synapse Maturation Defects by Dysregulation of Rap2 Activity. The Journal of Neuroscience: The Official Journal of the Society for Neuroscience, 35(42), 14327–14340. https://doi.org/10.1523/JNEUROSCI.2349-15.2015

Medina, M., Hernández, F., & Avila, J. (2016). New Features about Tau Function and Dysfunction. Biomolecules, 6(2). https://doi.org/10.3390/biom6020021

Melchior, B., Mittapalli, G. K., Lai, C., Duong-Polk, K., Stewart, J., Güner, B., Hofilena, B., Tjitro, A., Anderson, S. D., Herman, D. S., Dellamary, L., Swearingen, C. J., Sunil, K. C., & Yazici, Y. (2019). Tau pathology reduction with SM07883, a novel, potent, and selective oral DYRK1A inhibitor: A potential therapeutic for Alzheimer's disease. Aging Cell, 18(5). https://doi.org/10.1111/acel.13000

Menon, V. R., Ananthapadmanabhan, V., Swanson, S., Saini, S., Sesay, F., Yakovlev, V., Florens, L., DeCaprio, J. A., P. Washburn, M., Dozmorov, M., & Litovchick, L. (2019). DYRK1A regulates the recruitment of 53BP1 to the sites of DNA damage in part through interaction with RNF169. Cell Cycle, 18(5), 531–551. https://doi.org/10.1080/15384101.2019.1577525

Min, J., Zhang, Y., & Xu, R.-M. (2003). Structural basis for specific binding of Polycomb chromodomain to histone H3 methylated at Lys 27. Genes & Development, 17(15), 1823–1828. https://doi.org/10.1101/gad.269603

MiR-1275 promotes non-small cell lung cancer cell proliferation and metastasis by regulating LZTS3 expression. (2018, May 11). European Review. https://www.europeanreview.org/article/14964

Miyata, Y., & Nishida, E. (2011). DYRK1A binds to an evolutionarily conserved WD40-repeat protein WDR68 and induces its nuclear translocation. Biochimica et Biophysica Acta (BBA) - Molecular Cell Research, 1813(10), 1728–1739. https://doi.org/10.1016/j.bbamcr.2011.06.023

Miyata, Y., Shibata, T., Aoshima, M., Tsubata, T., & Nishida, E. (2014). The molecular chaperone TRiC/CCT binds to the Trp-Asp 40 (WD40) repeat protein WDR68 and promotes its folding, protein kinase DYRK1A binding, and nuclear accumulation. The Journal of Biological Chemistry, 289(48), 33320–33332. https://doi.org/10.1074/jbc.M114.586115

Morey, L., & Helin, K. (2010). Polycomb group protein-mediated repression of transcription. Trends in Biochemical Sciences, 35(6), 323–332. https://doi.org/10.1016/j.tibs.2010.02.009

Morita, K., Lo Celso, C., Spencer-Dene, B., Zouboulis, C. C., & Watt, F. M. (2006). HAN11 binds mDia1 and controls GLI1 transcriptional activity. Journal of Dermatological Science, 44(1), 11–20. https://doi.org/10.1016/j.jdermsci.2006.06.001

Morriss, G. R., Jaramillo, C. T., Mikolajczak, C. M., Duong, S., Jaramillo, M. S., & Cripps, R. M. (2013). The Drosophila wings apart gene anchors a novel, evolutionarily conserved pathway of neuromuscular development. Genetics, 195(3), 927–940. https://doi.org/10.1534/genetics.113.154211

Müller, J., Hart, C. M., Francis, N. J., Vargas, M. L., Sengupta, A., Wild, B., Miller, E. L., O'Connor, M. B., Kingston, R. E., & Simon, J. A. (2002). Histone methyltransferase activity of a Drosophila Polycomb group repressor complex. Cell, 111(2), 197–208. https://doi.org/10.1016/s0092-8674(02)00976-5

Müller, J., & Verrijzer, P. (2009). Biochemical mechanisms of gene regulation by polycomb group protein complexes. Current Opinion in Genetics & Development, 19(2), 150–158. https://doi.org/10.1016/j.gde.2009.03.001

Murakami, N., Bolton, D. C., Kida, E., Xie, W., & Hwang, Y.-W. (2012). Phosphorylation by Dyrk1A of clathrin coated vesicle-associated proteins: Identification of the substrate proteins and the effects of phosphorylation. PloS One, 7(4), e34845. https://doi.org/10.1371/journal.pone.0034845

Murakami, N., Bolton, D., & Hwang, Y.-W. (2009). Dyrk1A binds to multiple endocytic proteins required for formation of clathrin-coated vesicles. Biochemistry, 48(39), 9297–9305. https://doi.org/10.1021/bi9010557

Nadano, D., Nakayama, J., Matsuzawa, S.-I., Sato, T.-A., Matsuda, T., & Fukuda, M. N. (2002). Human tastin, a proline-rich cytoplasmic protein, associates with the microtubular cytoskeleton. The Biochemical Journal, 364(Pt 3), 669–677. https://doi.org/10.1042/BJ20011836

Najas, S., Arranz, J., Lochhead, P. A., Ashford, A. L., Oxley, D., Delabar, J. M., Cook, S. J., Barallobre, M. J., & Arbonés, M. L. (2015). DYRK1A-mediated Cyclin D1 Degradation in Neural Stem Cells Contributes to the Neurogenic Cortical Defects in Down Syndrome. EBioMedicine, 2(2), 120–134. https://doi.org/10.1016/j.ebiom.2015.01.010

Neurodevelopmental delay, motor abnormalities and cognitive deficits in transgenic mice overexpressing Dyrk1A (minibrain), a murine model of Down's syndrome | Human Molecular Genetics | Oxford Academic. (n.d.). Retrieved March 28, 2020, from https://academic.oup.com/hmg/article/10/18/1915/2901502

Nissen, R. M., Amsterdam, A., & Hopkins, N. (2006). A zebrafish screen for craniofacial mutants identifies wdr68 as a highly conserved gene required for endothelin-1 expression. BMC Developmental Biology, 6, 28. https://doi.org/10.1186/1471-213X-6-28

Nonaka, D., Fabbri, A., Roz, L., Mariani, L., Vecchione, A., Moore, G. W., Tavecchio, L., Croce, C. M., & Sozzi, G. (2005). Reduced FEZ1/LZTS1 expression and outcome prediction in lung cancer. Cancer Research, 65(4), 1207–1212. https://doi.org/10.1158/0008-5472.CAN-04-3461

Ohira, M., Seki, N., Nagase, T., Suzuki, E., Nomura, N., Ohara, O., Hattori, M., Sakaki, Y., Eki, T., Murakami, Y., Saito, T., Ichikawa, H., & Ohki, M. (1997). Gene identification in 1.6-Mb region of the Down syndrome region on chromosome 21. Genome Research, 7(1), 47–58. https://doi.org/10.1101/gr.7.1.47

Oksenberg, N., & Ahituv, N. (2013). The role of AUTS2 in neurodevelopment and human evolution. Trends in Genetics: TIG, 29(10), 600–608. https://doi.org/10.1016/j.tig.2013.08.001

Okui, M., Ide, T., Morita, K., Funakoshi, E., Ito, F., Ogita, K., Yoneda, Y., Kudoh, J., & Shimizu, N. (1999). High-Level Expression of the Mnb/Dyrk1A Gene in Brain and Heart during Rat Early Development. Genomics, 62(2), 165–171. https://doi.org/10.1006/geno.1999.5998

Olasz, E. B., Seline, L. N., Schock, A. M., Duncan, N. E., Lopez, A., Lazar, J., Flister, M. J., Lu, Y., Liu, P., Sokumbi, O., Harwood, C. A., Proby, C. M., Neuburg, M., & Lazarova, Z. (2015). MicroRNA-135b Regulates Leucine Zipper Tumor Suppressor 1 in Cutaneous Squamous Cell Carcinoma. PloS One, 10(5), e0125412. https://doi.org/10.1371/journal.pone.0125412

Onken, M. D., Worley, L. A., & Harbour, J. W. (2008). A metastasis modifier locus on human chromosome 8p in uveal melanoma identified by integrative genomic analysis. Clinical Cancer Research: An Official Journal of the American Association for Cancer Research, 14(12), 3737–3745. https://doi.org/10.1158/1078-0432.CCR-07-5144

Panier, S., & Boulton, S. J. (2014). Double-strand break repair: 53BP1 comes into focus. Nature Reviews. Molecular Cell Biology, 15(1), 7–18. https://doi.org/10.1038/nrm3719

Park, J., Oh, Y., Yoo, L., Jung, M.-S., Song, W.-J., Lee, S.-H., Seo, H., & Chung, K. C. (2010). Dyrk1A phosphorylates p53 and inhibits proliferation of embryonic neuronal cells. The Journal of Biological Chemistry, 285(41), 31895–31906. https://doi.org/10.1074/jbc.M110.147520

Park, J., Song, W.-J., & Chung, K. C. (2009). Function and regulation of Dyrk1A: Towards understanding Down syndrome. Cellular and Molecular Life Sciences: CMLS, 66(20), 3235–3240. https://doi.org/10.1007/s00018-009-0123-2

Park, J., Sung, J. Y., Park, J., Song, W.-J., Chang, S., & Chung, K. C. (2012). Dyrk1A negatively regulates the actin cytoskeleton through threonine phosphorylation of N-WASP. Journal of Cell Science, 125(1), 67–80. https://doi.org/10.1242/jcs.086124

Paull, T. T. (2015). Mechanisms of ATM Activation. Annual Review of Biochemistry, 84, 711–738. https://doi.org/10.1146/annurev-biochem-060614-034335

Peng, Y., Clark, C., Luong, R., Tu, W. H., Lee, J., Johnson, D. T., Das, A., Carroll, T. J., & Sun, Z. (2011). The leucine zipper putative tumor suppressor 2 protein LZTS2 regulates kidney development. The Journal of Biological Chemistry, 286(46), 40331–40342. https://doi.org/10.1074/jbc.M111.302059

Peng, Z., Liao, Z., Matsumoto, Y., Yang, A., & Tomkinson, A. E. (2016). Human DNA Ligase I Interacts with and Is Targeted for Degradation by the DCAF7 Specificity Factor of the Cul4-DDB1 Ubiquitin Ligase Complex. The Journal of Biological Chemistry, 291(42), 21893–21902. https://doi.org/10.1074/jbc.M116.746198

Pierce, A. J., Johnson, R. D., Thompson, L. H., & Jasin, M. (1999). XRCC3 promotes homology-directed repair of DNA damage in mammalian cells. Genes & Development, 13(20), 2633–2638. https://doi.org/10.1101/gad.13.20.2633

Poulsen, M., Lukas, C., Lukas, J., Bekker-Jensen, S., & Mailand, N. (2012). Human RNF169 is a negative regulator of the ubiquitin-dependent response to DNA double-strand breaks. The Journal of Cell Biology, 197(2), 189–199. https://doi.org/10.1083/jcb.201109100

Proteomic Analysis by Multidimensional Protein Identification Technology | Springer Nature Experiments. (n.d.). Retrieved March 29, 2020, from https://experiments.springernature.com/articles/10.1385/1-59745-026-X:159

Querfurth, H. W., & LaFerla, F. M. (2010). Alzheimer's Disease. New England Journal of Medicine, 362(4), 329–344. https://doi.org/10.1056/NEJMra0909142

Rajasekhar, V. K., & Begemann, M. (2007). Concise Review: Roles of Polycomb Group Proteins in Development and Disease: A Stem Cell Perspective. STEM CELLS, 25(10), 2498–2510. https://doi.org/10.1634/stemcells.2006-0608

Raveau, M., Shimohata, A., Amano, K., Miyamoto, H., & Yamakawa, K. (2018). DYRK1A-haploinsufficiency in mice causes autistic-like features and febrile seizures. Neurobiology of Disease, 110, 180–191. https://doi.org/10.1016/j.nbd.2017.12.003

Reim, D., Weis, T. M., Halbedl, S., Delling, J. P., Grabrucker, A. M., Boeckers, T. M., & Schmeisser, M. J. (2016). The Shank3 Interaction Partner ProSAPiP1 Regulates Postsynaptic SPAR Levels and the Maturation of Dendritic Spines in Hippocampal Neurons. Frontiers in Synaptic Neuroscience, 8, 13. https://doi.org/10.3389/fnsyn.2016.00013

Ritterhoff, S., Farah, C. M., Grabitzki, J., Lochnit, G., Skurat, A. V., & Schmitz, M. L. (2010). The WD40-repeat protein Han11 functions as a scaffold protein to control HIPK2 and MEKK1 kinase functions. The EMBO Journal, 29(22), 3750–3761. https://doi.org/10.1038/emboj.2010.251

Roberts, J. L., Hovanes, K., Dasouki, M., Manzardo, A. M., & Butler, M. G. (2014). Chromosomal microarray analysis of consecutive individuals with autism spectrum disorders or learning disability presenting for genetic services. Gene, 535(1), 70–78. https://doi.org/10.1016/j.gene.2013.10.020

Robinson, M. D., McCarthy, D. J., & Smyth, G. K. (2010). edgeR: A Bioconductor package for differential expression analysis of digital gene expression data. Bioinformatics (Oxford, England), 26(1), 139–140. https://doi.org/10.1093/bioinformatics/btp616

Roewenstrunk, J., Di Vona, C., Chen, J., Borras, E., Dong, C., Arató, K., Sabidó, E., Huen, M. S. Y., & de la Luna, S. (2019). A comprehensive proteomics-based interaction screen that links DYRK1A to RNF169 and to the DNA damage response. Scientific Reports, 9(1), 6014. https://doi.org/10.1038/s41598-019-42445-x

Rogakou, E. P., Pilch, D. R., Orr, A. H., Ivanova, V. S., & Bonner, W. M. (1998). DNA double-stranded breaks induce histone H2AX phosphorylation on serine 139. The Journal of Biological Chemistry, 273(10), 5858–5868. https://doi.org/10.1074/jbc.273.10.5858

Ryoo, S.-R., Cho, H.-J., Lee, H.-W., Jeong, H. K., Radnaabazar, C., Kim, Y.-S., Kim, M.-J., Son, M.-Y., Seo, H., Chung, S.-H., & Song, W.-J. (2008). Dual-specificity tyrosine(Y)-phosphorylation regulated kinase 1A-mediated phosphorylation of amyloid precursor protein: Evidence for a functional link between Down syndrome and Alzheimer's disease. Journal of Neurochemistry, 104(5), 1333–1344. https://doi.org/10.1111/j.1471-4159.2007.05075.x

Sacher, F., Möller, C., Bone, W., Gottwald, U., & Fritsch, M. (2007). The expression of the testis-specific Dyrk4 kinase is highly restricted to step 8 spermatids but is not required for male fertility in mice. Molecular and Cellular Endocrinology, 267(1), 80–88. https://doi.org/10.1016/j.mce.2006.12.041

Sanchez-Pulido, L., Devos, D., Sung, Z. R., & Calonje, M. (2008). RAWUL: A new ubiquitin-like domain in PRC1 Ring finger proteins that unveils putative plant and worm PRC1 orthologs. BMC Genomics, 9, 308. https://doi.org/10.1186/1471-2164-9-308

Sandell, L. L., & Zakian, V. A. (1993). Loss of a yeast telomere: Arrest, recovery, and chromosome loss. Cell, 75(4), 729–739. https://doi.org/10.1016/0092-8674(93)90493-a

Sardiu, M. E., Cai, Y., Jin, J., Swanson, S. K., Conaway, R. C., Conaway, J. W., Florens, L., & Washburn, M. P. (2008). Probabilistic assembly of human protein interaction networks from label-free quantitative proteomics. Proceedings of the National Academy of Sciences of the United States of America, 105(5), 1454–1459. https://doi.org/10.1073/pnas.0706983105

Saurin, A. J., Shao, Z., Erdjument-Bromage, H., Tempst, P., & Kingston, R. E. (2001). A Drosophila Polycomb group complex includes Zeste and dTAFII proteins. Nature, 412(6847), 655–660. https://doi.org/10.1038/35088096

Scelfo, A., Piunti, A., & Pasini, D. (2015). The controversial role of the Polycomb group proteins in transcription and cancer: How much do we not understand Polycomb proteins? The FEBS Journal, 282(9), 1703–1722. https://doi.org/10.1111/febs.13112

Schindelin, J., Arganda-Carreras, I., Frise, E., Kaynig, V., Longair, M., Pietzsch, T., Preibisch, S., Rueden, C., Saalfeld, S., Schmid, B., Tinevez, J.-Y., White, D. J., Hartenstein, V., Eliceiri, K., Tomancak, P., & Cardona, A. (2012). Fiji: An open-source platform for biological-image analysis. Nature Methods, 9(7), 676–682. https://doi.org/10.1038/nmeth.2019

Schmeisser, M. J., Grabrucker, A. M., Bockmann, J., & Boeckers, T. M. (2009). Synaptic cross-talk between N-methyl-D-aspartate receptors and LAPSER1-beta-catenin at excitatory synapses. The Journal of Biological Chemistry, 284(42), 29146–29157. https://doi.org/10.1074/jbc.M109.020628

Schmit, F., Korenjak, M., Mannefeld, M., Schmitt, K., Franke, C., von Eyss, B., Gagrica, S., Hänel, F., Brehm, A., & Gaubatz, S. (2007). LINC, a human complex that is related to pRB-containing complexes in invertebrates regulates the expression of G2/M genes. Cell Cycle (Georgetown, Tex.), 6(15), 1903–1913. https://doi.org/10.4161/cc.6.15.4512

Schneider, C. A., Rasband, W. S., & Eliceiri, K. W. (2012). NIH Image to ImageJ: 25 years of image analysis. Nature Methods, 9(7), 671–675. https://doi.org/10.1038/nmeth.2089

Scholzen, T., & Gerdes, J. (2000). The Ki-67 protein: From the known and the unknown. Journal of Cellular Physiology, 182(3), 311–322. https://doi.org/10.1002/(SICI)1097-4652(200003)182:3<311::AID-JCP1>3.0.CO;2-9

Schuettengruber, B., & Cavalli, G. (2009). Recruitment of Polycomb group complexes and their role in the dynamic regulation of cell fate choice. Development, 136(21), 3531–3542. https://doi.org/10.1242/dev.033902

Schwartz, Y. B., & Pirrotta, V. (2007). Polycomb silencing mechanisms and the management of genomic programmes. Nature Reviews. Genetics, 8(1), 9–22. https://doi.org/10.1038/nrg1981

Shao, Z., Raible, F., Mollaaghababa, R., Guyon, J. R., Wu, C. T., Bender, W., & Kingston, R. E. (1999). Stabilization of chromatin structure by PRC1, a Polycomb complex. Cell, 98(1), 37–46. https://doi.org/10.1016/S0092-8674(00)80604-2

Shen, X., Liu, Y., Hsu, Y.-J., Fujiwara, Y., Kim, J., Mao, X., Yuan, G.-C., & Orkin, S. H. (2008). EZH1 mediates methylation on histone H3 lysine 27 and complements EZH2 in maintaining stem cell identity and executing pluripotency. Molecular Cell, 32(4), 491–502. https://doi.org/10.1016/j.molcel.2008.10.016

Shen, Z., Lin, L., Cao, B., Zhou, C., Hao, W., & Ye, D. (2018). LZTS2 promoter hypermethylation: A potential biomarker for the diagnosis and prognosis of laryngeal squamous cell carcinoma. World Journal of Surgical Oncology, 16(1), 42. https://doi.org/10.1186/s12957-018-1349-y

Siddiqui-Jain, A., Drygin, D., Streiner, N., Chua, P., Pierre, F., O'Brien, S. E., Bliesath, J., Omori, M., Huser, N., Ho, C., Proffitt, C., Schwaebe, M. K., Ryckman, D. M., Rice, W. G., & Anderes, K. (2010). CX-4945, an orally bioavailable selective inhibitor of protein kinase CK2, inhibits prosurvival and angiogenic signaling and exhibits antitumor efficacy. Cancer Research, 70(24), 10288–10298. https://doi.org/10.1158/0008-5472.CAN-10-1893

Simon, J. A., & Kingston, R. E. (2013). Occupying chromatin: Polycomb mechanisms for getting to genomic targets, stopping transcriptional traffic, and staying put. Molecular Cell, 49(5), 808–824. https://doi.org/10.1016/j.molcel.2013.02.013

Skurat, A. V., & Dietrich, A. D. (2004). Phosphorylation of Ser640 in muscle glycogen synthase by DYRK family protein kinases. The Journal of Biological Chemistry, 279(4), 2490–2498. https://doi.org/10.1074/jbc.M301769200

Smith, B., Medda, F., Gokhale, V., Dunckley, T., & Hulme, C. (2012). Recent advances in the design, synthesis, and biological evaluation of selective DYRK1A inhibitors: A new avenue for a disease modifying treatment of Alzheimer's? ACS Chemical Neuroscience, 3(11), 857–872. https://doi.org/10.1021/cn300094k

Smith, E. J., Leone, G., DeGregori, J., Jakoi, L., & Nevins, J. R. (1996). The accumulation of an E2F-p130 transcriptional repressor distinguishes a G0 cell state from a G1 cell state. Molecular and Cellular Biology, 16(12), 6965–6976. https://doi.org/10.1128/mcb.16.12.6965

Soppa, U., Schumacher, J., Florencio Ortiz, V., Pasqualon, T., Tejedor, F. J., & Becker, W. (2014). The Down syndrome-related protein kinase DYRK1A phosphorylates p27(Kip1) and Cyclin D1 and induces cell cycle exit and neuronal differentiation. Cell Cycle (Georgetown, Tex.), 13(13), 2084–2100. https://doi.org/10.4161/cc.29104

Sparmann, A., & van Lohuizen, M. (2006). Polycomb silencers control cell fate, development and cancer. Nature Reviews. Cancer, 6(11), 846–856. https://doi.org/10.1038/nrc1991

Spillantini, M. G., Schmidt, M. L., Lee, V. M.-Y., Trojanowski, J. Q., Jakes, R., & Goedert, M. (1997). α-Synuclein in Lewy bodies. Nature, 388(6645), 839–840. https://doi.org/10.1038/42166

Stiff, T., O'Driscoll, M., Rief, N., Iwabuchi, K., Löbrich, M., & Jeggo, P. A. (2004). ATM and DNA-PK function redundantly to phosphorylate H2AX after exposure to ionizing radiation. Cancer Research, 64(7), 2390–2396. https://doi.org/10.1158/0008-5472.can-03-3207

Stirnimann, C. U., Petsalaki, E., Russell, R. B., & Müller, C. W. (2010). WD40 proteins propel cellular networks. Trends in Biochemical Sciences, 35(10), 565–574. https://doi.org/10.1016/j.tibs.2010.04.003

Struhl, G. (1981). A gene product required for correct initiation of segmental determination in Drosophila. Nature, 293(5827), 36–41. https://doi.org/10.1038/293036a0

Sultana, R., Yu, C.-E., Yu, J., Munson, J., Chen, D., Hua, W., Estes, A., Cortes, F., de la Barra, F., Yu, D., Haider, S. T., Trask, B. J., Green, E. D., Raskind, W. H., Disteche, C. M., Wijsman, E., Dawson, G., Storm, D. R., Schellenberg, G. D., & Villacres, E. C. (2002). Identification of a novel gene on chromosome 7q11.2 interrupted by a translocation breakpoint in a pair of autistic twins. Genomics, 80(2), 129–134. https://doi.org/10.1006/geno.2002.6810

Swanson, S. K., Florens, L., & Washburn, M. P. (2009). Generation and Analysis of Multidimensional Protein Identification Technology Datasets. In M. S. Lipton & L. Paša-Tolic (Eds.), Mass Spectrometry of Proteins and Peptides: Methods and Protocols (pp. 1–20). Humana Press. https://doi.org/10.1007/978-1-59745-493-3_1

Tejedor, F. J., & Hämmerle, B. (2011). MNB/DYRK1A as a multiple regulator of neuronal development. The FEBS Journal, 278(2), 223–235. https://doi.org/10.1111/j.1742-4658.2010.07954.x

Tejedor, F., Zhu, X. R., Kaltenbach, E., Ackermann, A., Baumann, A., Canal, I., Heisenberg, M., Fischbach, K. F., & Pongs, O. (1995). minibrain: A new protein kinase family involved in postembryonic neurogenesis in Drosophila. Neuron, 14(2), 287–301. https://doi.org/10.1016/0896-6273(95)90286-4

Teufel, A., Weinmann, A., Galle, P. R., & Lohse, A. W. (2005). In silico characterization of LZTS3, a potential tumor suppressor. Oncology Reports, 14(2), 547–551.

Thyssen, G., Li, T.-H., Lehmann, L., Zhuo, M., Sharma, M., & Sun, Z. (2006). LZTS2 is a novel beta-catenin-interacting protein and regulates the nuclear export of beta-catenin. Molecular and Cellular Biology, 26(23), 8857–8867. https://doi.org/10.1128/MCB.01031-06

Toyooka, S., Fukuyama, Y., Wistuba, I. I., Tockman, M. S., Minna, J. D., & Gazdar, A. F. (2002). Differential expression of FEZ1/LZTS1 gene in lung cancers and their cell cultures. Clinical Cancer Research: An Official Journal of the American Association for Cancer Research, 8(7), 2292–2297.

Varjosalo, M., Keskitalo, S., Van Drogen, A., Nurkkala, H., Vichalkovski, A., Aebersold, R., & Gstaiger, M. (2013). The protein interaction landscape of the human CMGC kinase group. Cell Reports, 3(4), 1306–1320. https://doi.org/10.1016/j.celrep.2013.03.027

Vecchione, A., Baldassarre, G., Ishii, H., Nicoloso, M. S., Belletti, B., Petrocca, F., Zanesi, N., Fong, L. Y. Y., Battista, S., Guarnieri, D., Baffa, R., Alder, H., Farber, J. L., Donovan, P. J., & Croce, C. M. (2007). Fez1/Lzts1 absence impairs Cdk1/Cdc25C interaction during mitosis and predisposes mice to cancer development. Cancer Cell, 11(3), 275–289. https://doi.org/10.1016/j.ccr.2007.01.014

Velazquez, R., Meechoovet, B., Ow, A., Foley, C., Shaw, A., Smith, B., Oddo, S., Hulme, C., & Dunckley, T. (2019). Chronic Dyrk1 Inhibition Delays the Onset of AD-Like Pathology in 3xTg-AD Mice. Molecular Neurobiology, 56(12), 8364–8375. https://doi.org/10.1007/s12035-019-01684-9

Walte, A., Rüben, K., Birner-Gruenberger, R., Preisinger, C., Bamberg-Lemper, S., Hilz, N., Bracher, F., & Becker, W. (2013). Mechanism of dual specificity kinase activity of DYRK1A. The FEBS Journal, 280(18), 4495–4511. https://doi.org/10.1111/febs.12411

Wang, B., Doan, D., Roman Petersen, Y., Alvarado, E., Alvarado, G., Bhandari, A., Mohanty, A., Mohanty, S., & Nissen, R. M. (2013). Wdr68 requires nuclear access for craniofacial development. PloS One, 8(1), e54363. https://doi.org/10.1371/journal.pone.0054363

Wang, H., Wang, L., Erdjument-Bromage, H., Vidal, M., Tempst, P., Jones, R. S., & Zhang, Y. (2004). Role of histone H2A ubiquitination in Polycomb silencing. Nature, 431(7010), 873–878. https://doi.org/10.1038/nature02985

Wang, Q., Geng, Z., Gong, Y., Warren, K., Zheng, H., Imamura, Y., & Gao, Z. (2018). WDR68 is essential for the transcriptional activation of the PRC1-AUTS2 complex and neuronal differentiation of mouse embryonic stem cells. Stem Cell Research, 33, 206–214. https://doi.org/10.1016/j.scr.2018.10.023

Wang, X.-X., Liu, B.-B., Wu, X., Su, D., Zhu, Z., & Fu, L. (2015). Loss of Leucine Zipper Putative Tumor Suppressor 1 (LZTS1) Expression Contributes to Lymph Node Metastasis of Breast Invasive Micropapillary Carcinoma. Pathology Oncology Research: POR, 21(4), 1021–1026. https://doi.org/10.1007/s12253-015-9923-x

Wang, X.-X., Zhu, Z., Su, D., Lei, T., Wu, X., Fan, Y., Li, X., Zhao, J., Fu, L., Dong, J.-T., & Fu, L. (2011). Down-regulation of leucine zipper putative tumor suppressor 1 is associated with poor prognosis, increased cell motility and invasion, and epithelial-to-mesenchymal transition characteristics in human breast carcinoma. Human Pathology, 42(10), 1410–1419. https://doi.org/10.1016/j.humpath.2010.12.007

Wegiel, J., Gong, C.-X., & Hwang, Y.-W. (2011). The role of DYRK1A in neurodegenerative diseases. The FEBS Journal, 278(2), 236–245. https://doi.org/10.1111/j.1742-4658.2010.07955.x

Wegiel, J., Kuchna, I., Nowicki, K., Frackowiak, J., Dowjat, K., Silverman, W. P., Reisberg, B., deLeon, M., Wisniewski, T., Adayev, T., Chen-Hwang, M.-C., & Hwang, Y.-W. (2004). Cell type- and brain structure-specific patterns of distribution of minibrain kinase in human brain. Brain Research, 1010(1), 69–80. https://doi.org/10.1016/j.brainres.2004.03.008

Wendholt, D., Spilker, C., Schmitt, A., Dolnik, A., Smalla, K.-H., Proepper, C., Bockmann, J., Sobue, K., Gundelfinger, E. D., Kreutz, M. R., & Boeckers, T. M. (2006). ProSAP-interacting protein 1 (ProSAPiP1), a novel protein of the postsynaptic density that links the spine-associated Rap-Gap (SPAR) to the scaffolding protein ProSAP2/Shank3. The Journal of Biological Chemistry, 281(19), 13805–13816. https://doi.org/10.1074/jbc.M601101200

Wu, X.-H., Wang, Y., Zhuo, Z., Jiang, F., & Wu, Y.-D. (2012). Identifying the hotspots on the top faces of WD40-repeat proteins from their primary sequences by β-bulges and DHSW tetrads. PloS One, 7(8), e43005. https://doi.org/10.1371/journal.pone.0043005

Xu, S., Li, Y., Lu, Y., Huang, J., Ren, J., Zhang, S., Yin, Z., Huang, K., Wu, G., & Yang, K. (2018). LZTS2 inhibits PI3K/AKT activation and radioresistance in nasopharyngeal carcinoma by interacting with p85. Cancer Letters, 420, 38–48. https://doi.org/10.1016/j.canlet.2018.01.067

Yabut, O., Domogauer, J., & D'Arcangelo, G. (2010). Dyrk1A Overexpression Inhibits Proliferation and Induces Premature Neuronal Differentiation of Neural Progenitor Cells. Journal of Neuroscience, 30(11), 4004–4014. https://doi.org/10.1523/JNEUROSCI.4711-09.2010

Yakovlev, V. A. (2013). Nitric oxide-dependent downregulation of BRCA1 expression promotes genetic instability. Cancer Research, 73(2), 706–715. https://doi.org/10.1158/0008-5472.CAN-12-3270

Yang, S., Liu, X., Yin, Y., Fukuda, M. N., & Zhou, J. (2008). Tastin is required for bipolar spindle assembly and centrosome integrity during mitosis. FASEB Journal: Official Publication

of the Federation of American Societies for Experimental Biology, 22(6), 1960–1972. https://doi.org/10.1096/fj.07-081463

Ye, J., Chu, C., Chen, M., Shi, Z., Gan, S., Qu, F., Pan, X., Yang, Q., Tian, Y., Wang, L., Yang, W., & Cui, X. (2019). TROAP regulates prostate cancer progression via the WNT3/survivin signalling pathways. Oncology Reports, 41(2), 1169–1179. https://doi.org/10.3892/or.2018.6854

Ye, X., & Lv, H. (2018). MicroRNA-519d-3p inhibits cell proliferation and migration by targeting TROAP in colorectal cancer. Biomedicine & Pharmacotherapy = Biomedecine & Pharmacotherapie, 105, 879–886. https://doi.org/10.1016/j.biopha.2018.04.114

Yousefelahiyeh, M., Xu, J., Alvarado, E., Yu, Y., Salven, D., & Nissen, R. M. (2018). DCAF7/WDR68 is required for normal levels of DYRK1A and DYRK1B. PloS One, 13(11), e0207779. https://doi.org/10.1371/journal.pone.0207779

Yu, D., Cattoglio, C., Xue, Y., & Zhou, Q. (2019). A complex between DYRK1A and DCAF7 phosphorylates the C-terminal domain of RNA polymerase II to promote myogenesis. Nucleic Acids Research, 47(9), 4462–4475. https://doi.org/10.1093/nar/gkz162

Yu, E.-J., Hooker, E., Johnson, D. T., Kwak, M. K., Zou, K., Luong, R., He, Y., & Sun, Z. (2017). LZTS2 and PTEN collaboratively regulate ß-catenin in prostatic tumorigenesis. PloS One, 12(3), e0174357. https://doi.org/10.1371/journal.pone.0174357

Zemke, N. R., & Berk, A. J. (2017). The Adenovirus E1A C Terminus Suppresses a Delayed Antiviral Response and Modulates RAS Signaling. Cell Host & Microbe, 22(6), 789-800.e5. https://doi.org/10.1016/j.chom.2017.11.008

Zhang, Y., Wang, Y., Guo, Y., Liao, Z., Xu, R., & Ruan, Z. (2015). [MiR-135b promotes the invasion and metastasis of hepatocellular carcinoma cells]. Xi Bao Yu Fen Zi Mian Yi Xue Za Zhi = Chinese Journal of Cellular and Molecular Immunology, 31(10), 1316–1321.

Zhu, Q., Sharma, N., He, J., Wani, G., & Wani, A. A. (2015). USP7 deubiquitinase promotes ubiquitin-dependent DNA damage signaling by stabilizing RNF168. Cell Cycle (Georgetown, Tex.), 14(9), 1413–1425. https://doi.org/10.1080/15384101.2015.1007785

APPENDIX

APPENDIX CONTENTS

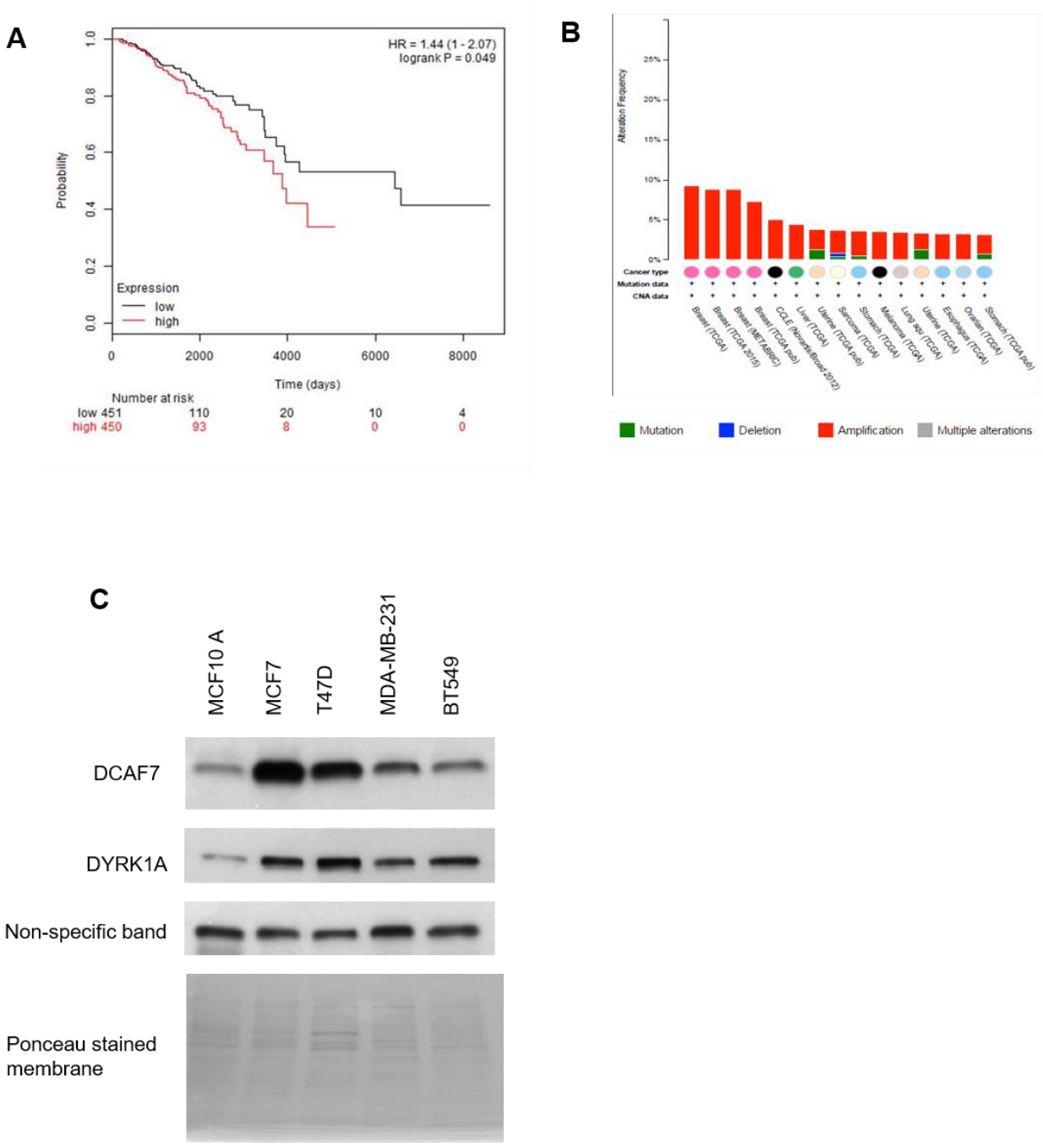

Appendix Figure 1: DCAF7 gene in human cancers
(A) High expression of DCAF7 in breast cancer (red lines) negatively affects survival (TCGA data- Dr. Mikhail Dozmorov) (B) DCAF7 undergoes frequent amplifications in breast cancer (cBioPortal). (C) Expression of DCAF7 and DYRK1A in human breast epithelial (MCF10A) and human breast cancer cell lines (MCF7, T47D, MDAMB-231, BT549).

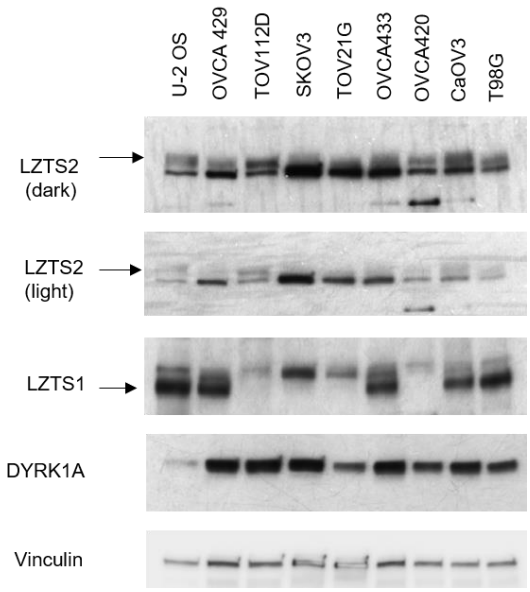

Appendix Figure 2: WB indicating levels of LZTS1 and LZTS2 in indicated ovarian cancer cell lines. T98G glioblastoma and U-2 OS osteosarcoma cell lines were used as controls.

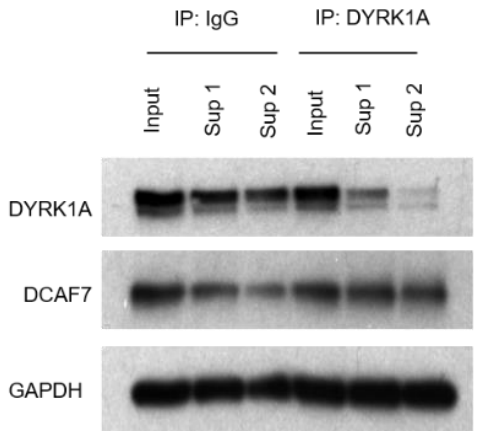

Appendix Figure 3: All DCAF7 in the cell is not bound to DYRK1A.
T98G cell lysates were subjected to sequential immunoprecipitation with a non-specific control antibody (IgG) or with an antibody specific to DYRK1A. The supernatant (indicated as Sup1, Sup2) was collected after each round of immunoprecipitation and levels of DYRK1A and DCAF7 were analyzed by WB analysis. GAPDH was used as a loading control.

DCAF7 dNSAF AVG	DCAF7 Detected # Out of 3	GFP-CTAP Detected # Out of 3	DCAF7:GFP-CTAP	Locus	Description	NCBI_Gene	Length	MW	pI
0.030677	3	0	∞	gi|108936958|ref|NP_005819.3|	**DDB1- and CUL4-associated factor 7**	**DCAF7**	342	38926	5.5
0.004271	3	0	∞	gi|578836477|ref|XP_006724042.1|	**dual specificity tyrosine-phosphorylation-regulated kinase 1A**	**DYRK1A**	754	84557	8.8
0.003544	3	0	∞	gi|768013459|ref|XP_011527477.1|	casein kinase II subunit alpha	CSNK2A2	391	45144	7.7
0.002912	3	0	∞	gi|4502643|ref|NP_001753.1|	T-complex protein 1 subunit zeta	CCT6A	531	58024	6.7
0.002016	3	0	∞	gi|23503295|ref|NP_001311.3|	casein kinase II subunit beta	CSNK2B	215	24942	5.6
0.001581	3	0	∞	gi|51479192|ref|NP_002922.2|	E3 ubiquitin-protein ligase RING1	RING1	406	42429	5.6
0.001502	3	0	∞	gi|208431810|ref|NP_001129119.1|	protein FAM53C	FAM53C	392	43091	8.6
0.001216	3	0	∞	gi|119395758|ref|NP_005210.3|	protein diaphanous homolog 1	DIAPH1	1272	141347	5.4
0.001199	3	0	∞	gi|767988718|ref|XP_011544217.1|	probable fibrosin-1	FBRS	980	103769	9.5
0.001158	3	0	∞	gi|4503097|ref|NP_001887.1|	casein kinase II subunit alpha	CSNK2A2	350	41213	8.6
0.001124	3	0	∞	gi|530401926|ref|XP_005266228.1|	fibrosin-1-like protein isoform X3	FBRSL1	1085	115367	9.4
0.001065	3	0	∞	gi|530427297|ref|XP_005272307.1|	polycomb group RING finger protein 3	PCGF3	242	28115	8.2
0.000992	3	0	∞	gi|13376611|ref|NP_079345.1|	zinc finger protein 703	ZNF703	590	58222	8.8
0.000946	3	0	∞	gi|767947342|ref|XP_011514312.1|	autism susceptibility gene 2 protein	AUTS2	1266	139763	9.4
0.000914	3	0	∞	gi|38455427|ref|NP_006421.2|	T-complex protein 1 subunit delta	CCT4	539	57924	7.8
0.000889	3	0	∞	gi|767910102|ref|XP_011508154.1|	E3 ubiquitin-protein ligase RING2	RNF2	336	37655	6.8
0.000804	3	0	∞	gi|767964062|ref|XP_011538574.1|	polycomb group RING finger protein 5	PCGF5	236	27512	6.5
0.000776	3	0	∞	gi|5453607|ref|NP_006420.1|	T-complex protein 1 subunit eta	CCT7	543	59367	7.6
0.000674	3	0	∞	gi|300244514|ref|NP_001177906.1|	YY1-associated factor 2	YAF2	138	15115	9.9
0.000652	3	0	∞	gi|578823153|ref|XP_006719244.1|	PREDICTED: tastin	TROAP	868	93449	7.2
0.000476	3	0	∞	gi|21464101|ref|NP_036611.2|	14-3-3 protein gamma	YWHAG	247	28303	4.9
0.000454	3	0	∞	gi|768057171|ref|XP_011547115.1|	dual specificity tyrosine-phosphorylation-regulated kinase 1B	DYRK1B	689	75127	9.4
0.000323	3	0	∞	gi|112363092|ref|NP_036366.3|	RING1 and YY1-binding protein	RYBP	228	24822	9.6
0.000268	3	0	∞	gi|24432032|ref|NP_116161.2|	zinc finger protein 503	ZNF503	646	62555	8.7
0.000219	3	0	∞	gi|530421618|ref|XP_005272744.1|	protein phosphatase 1 regulatory subunit 3F	PPP1R3F	798	82726	4.6
0.000143	3	0	∞	gi|148839382|ref|NP_001092108.1|	E3 ubiquitin-protein ligase RNF169	RNF169	708	77194	9.1
0.000062	3	0	∞	gi|374092020|ref|NP_006448.4|	PDZ and LIM domain protein 5	PDLIM5	596	63975	8.2
0.001179	3	1	19.01612903	gi|48762932|ref|NP_006576.2|	T-complex protein 1 subunit theta	CCT8	548	59621	5.6
0.001003	3	2	11.39772727	gi|5453603|ref|NP_006422.1|	T-complex protein 1 subunit beta	CCT2	535	57488	6.4
0.002089	3	3	11.17112299	gi|57863257|ref|NP_110379.2|	T-complex protein 1 subunit alpha	TCP1	556	60344	6.1
0.000878	3	1	7.080645161	gi|63162572|ref|NP_005989.3|	T-complex protein 1 subunit gamma	CCT3	545	60534	6.5
0.000198	3	2	7.071428571	gi|301171345|ref|NP_001180343.1|	tubulin alpha-8 chain	TUBA8	383	42954	5.1
0.000807	2	0	∞	gi|7705618|ref|NP_057134.1|	39S ribosomal protein L11, mitochondrial	MRPL11	192	20683	9.9
0.000796	2	0	∞	gi|393715117|ref|NP_004891.4|	DNA dC-_dU-editing enzyme APOBEC-3B	APOBEC3B	382	45951	6.3
0.000303	2	0	∞	gi|13654278|ref|NP_112487.1|	SRA stem-loop-interacting RNA-binding protein	SLIRP	109	12349	10.2
0.000262	2	0	∞	gi|4885413|ref|NP_005331.1|	histidine triad nucleotide-binding protein 1	HINT1	126	13802	7
0.000254	2	0	∞	gi|71772415|ref|NP_001025180.1|	40S ribosomal protein S15a	RPS15A	130	14839	10.1
0.000252	2	0	∞	gi|332634984|ref|NP_001091084.2|	DNA-directed RNA polymerase II subunit RPB11-b2	POLR2J3	115	13074	6.3
0.000203	2	0	∞	gi|5730023|ref|NP_006657.1|	ruvB-like 2	RUVBL2	463	51157	5.6
0.0002	2	0	∞	gi|68160937|ref|NP_005073.2|	E3 ubiquitin/ISG15 ligase TRIM25	TRIM25	630	70974	8.1
0.000178	2	0	∞	gi|110735439|ref|NP_000544.2|	Werner syndrome ATP-dependent helicase	WRN	1432	162460	6.3
0.000158	2	0	∞	gi|4506753|ref|NP_003698.1|	ruvB-like 1	RUVBL1	456	50228	6.4
0.000155	2	0	∞	gi|530370210|ref|XP_005246543.1|	mannose-1-phosphate guanyltransferase alpha	GMPPA	420	46291	7.2
0.000143	2	0	∞	gi|325301072|ref|NP_001191455.1|	translocon-associated protein subunit delta	SSR4	184	20213	5.8
0.000139	2	0	∞	gi|289629265|ref|NP_001166216.1|	protein transport protein Sec23B	SEC23B	767	86479	6.9
0.000129	2	0	∞	gi|164420685|ref|NP_073577.3|	homeodomain-interacting protein kinase 2	HIPK2	1198	130965	8.4
0.000108	2	0	∞	gi|157057543|ref|NP_443102.2|	sorting nexin-18	SNX18	628	68895	5.7
0.000079	2	0	∞	gi|767952979|ref|XP_011515331.1|	RNA-binding protein 12B	RBM12B	1001	118103	6.8
0.000051	2	0	∞	gi|767938662|ref|XP_011532966.1|	calnexin isoform X2	CANX	646	73410	4.6
0.000026	2	0	∞	gi|304555583|ref|NP_001123525.2|	elongation factor 1-delta	EEF1D	647	71422	6.4
0.000474	2	1	12.15384615	gi|13124875|ref|NP_074035.1|	myosin-11 isoform SM2A	MYH11	1938	223575	5.5
0.000432	2	1	9.818181818	gi|431822377|ref|NP_001258929.1|	dedicator of cytokinesis protein 7	DOCK7	2100	238532	6.8
0.001578	2	2	7.205479452	gi|530383156|ref|XP_005248783.1|	unconventional myosin-VI	MYO6	1253	145015	8.6
0.000143	2	3	6.80952381	gi|116805348|ref|NP_055309.2|	trinucleotide repeat-containing gene 6A protein	TNRC6A	1962	210296	7
0.004469	2	3	6.486211901	gi|10863945|ref|NP_066964.1|	X-ray repair cross-complementing protein 5	XRCC5	732	82705	5.8

Appendix Table 1: List of proteins detected by MudPIT proteomic analysis of DCAF7

FAM117B-FL dNSAF AVG	FAM117B-FL Detected # Out of 3	GFP-CTAP Detected # Out of 4	FAM117B-FL:GFP-CTAP	Locus	Description	NCBI_Gene	Length	MW	pI
0.237479	3	1	969.302	gi|83267868|ref|NP_001032584.1|	dynein light chain 1, cytoplasmic	DYNLL1	89	10366	7.4
0.071217	**3**	**0**	**∞**	**gi|254910983|ref|NP_775782.2|**	**protein FAM117B**	**FAM117B**	**589**	**61968**	**9.8**
0.057198	3	0	∞	gi|767953588|ref|XP_011515591.1|	14-3-3 protein zeta/delta	YWHAZ	245	27745	4.8
0.03839	3	1	238.4472	gi|21328448|ref|NP_647539.1|	14-3-3 protein beta/alpha	YWHAB	246	28082	4.8
0.031779	3	2	46.6652	gi|5803227|ref|NP_006817.1|	14-3-3 protein theta	YWHAQ	245	27764	4.8
0.014981	**3**	**0**	**∞**	**gi|108936958|ref|NP_005819.3|**	**DDB1- and CUL4-associated factor 7**	**DCAF7**	**342**	**38926**	**5.5**
0.010188	3	1	80.85714	gi|5803225|ref|NP_006752.1|	14-3-3 protein epsilon	YWHAE	255	29174	4.7
0.009108	3	1	37.17551	gi|18087855|ref|NP_542408.1|	dynein light chain 2, cytoplasmic	DYNLL2	89	10350	7.4
0.008456	3	0	∞	gi|4507951|ref|NP_003396.1|	14-3-3 protein eta	YWHAH	246	28219	4.8
0.004821	3	0	∞	gi|4506619|ref|NP_000977.1|	60S ribosomal protein L24	RPL24	157	17779	11.3
0.003545	3	0	∞	gi|4506633|ref|NP_000984.1|	60S ribosomal protein L31	RPL31	125	14463	10.5
0.002811	**3**	**0**	**∞**	**gi|578836477|ref|XP_006724042.1|**	**dual specificity tyrosine-phosphorylation-regulated kinase 1A**	**DYRK1A**	**754**	**84557**	**8.8**
0.002315	2	0	∞	gi|4506643|ref|NP_000989.1|	60S ribosomal protein L37a	RPL37A	92	10275	10.4
0.00123	3	0	∞	gi|4506901|ref|NP_003008.1|	serine/arginine-rich splicing factor 3	SRSF3	164	19330	11.6
0.000857	2	0	∞	gi|4506687|ref|NP_001009.1|	40S ribosomal protein S15	RPS15	145	17040	10.4
0.000771	3	0	∞	gi|767950480|ref|XP_011542667.1|	paraneoplastic antigen Ma2	PNMA2	364	41509	4.8
0.000695	3	0	∞	gi|148727341|ref|NP_009109.3|	serine-threonine kinase receptor-associated protein	STRAP	350	38438	5.1
0.00069	3	0	∞	gi|66346679|ref|NP_001018077.1|	plasminogen activator inhibitor 1 RNA-binding	SERBP1	408	44965	8.6
0.000576	3	0	∞	gi|77812674|ref|NP_001030005.1|	H/ACA ribonucleoprotein complex subunit 2	NHP2	90	10071	10
0.000536	2	0	∞	gi|7705618|ref|NP_057134.1|	39S ribosomal protein L11, mitochondrial	MRPL11	192	20683	9.9
0.000531	3	0	∞	gi|23503259|ref|NP_699170.1|	tRNA pseudouridine synthase-like 1	PUSL1	303	33233	9.9
0.000481	2	0	∞	gi|345197222|ref|NP_001230807.1|	four and a half LIM domains protein 3	FHL3	172	18918	7.6
0.000427	3	0	∞	gi|22907039|ref|NP_055323.2|	DNA dC-_dU-editing enzyme APOBEC-3C	APOBEC3C	190	22826	7.6
0.000383	3	0	∞	gi|767904731|ref|XP_011539919.1|	filamin-binding LIM protein	FBLIM1	373	40670	6
0.000358	2	0	∞	gi|4758256|ref|NP_004085.1|	eukaryotic translation initiation factor 2 subunit 1	EIF2S1	315	36112	5.1
0.000355	2	0	∞	gi|5922001|ref|NP_006475.1|	dual specificity tyrosine-phosphorylation-regulated kinase 1B	DYRK1B	601	66336	9.1
0.000327	2	0	∞	gi|8922549|ref|NP_060624.1|	histone chaperone ASF1B	ASF1B	202	22434	4.6
0.000283	2	0	∞	gi|51317376|ref|NP_001003796.1|	NHP2-like protein 1	SNU13	128	14174	8.5
0.000274	2	0	∞	gi|16554616|ref|NP_115865.1|	28S ribosomal protein S6, mitochondrial	MRPS6	125	14227	9.3
0.000263	2	0	∞	gi|521258690|ref|NP_001265585.1|	small nuclear ribonucleoprotein Sm D3	SNRPD3	126	13916	10.3
0.000251	3	0	∞	gi|68160937|ref|NP_005073.2|	E3 ubiquitin/ISG15 ligase TRIM25	TRIM25	630	70974	8.1
0.000246	2	0	∞	gi|767951904|ref|XP_011515883.1|	transcription elongation factor B polypeptide 1	TCEB1	112	12473	4.8
0.000244	3	0	∞	gi|768004861|ref|XP_011526754.1|	kelch-like ECH-associated protein 1	KEAP1	624	69666	6.4
0.000237	3	0	∞	gi|56118219|ref|NP_001007226.1|	insulin-like growth factor 2 mRNA-binding protein 2	IGF2BP2	556	61843	8.3
0.000236	2	0	∞	gi|7661730|ref|NP_054737.1|	28S ribosomal protein S28, mitochondrial	MRPS28	187	20843	9.1
0.000219	3	0	∞	gi|15147219|ref|NP_150093.1|	transcriptional activator protein Pur-beta	PURB	312	33241	5.4
0.000206	3	0	∞	gi|87239981|ref|NP_003738.2|	tankyrase-1	TNKS	1327	142039	7
0.000193	2	0	∞	gi|306482646|ref|NP_001182356.1|	serine/arginine-rich splicing factor 2	SRSF2	221	25476	11.9
0.000184	2	0	∞	gi|18139549|ref|NP_085151.1|	histone-lysine N-methyltransferase SETD7	SETD7	366	40721	4.6
0.000183	3	0	∞	gi|49472822|ref|NP_003746.2|	eukaryotic translation initiation factor 3 subunit G	EIF3G	320	35611	6.1
0.000171	2	0	∞	gi|169636418|ref|NP_115867.2|	39S ribosomal protein L38, mitochondrial	MRPL38	380	44597	7.5
0.000169	3	0	∞	gi|544346109|ref|NP_001269672.1|	SPATS2-like protein	SPATS2L	498	54945	9.7
0.000169	2	0	∞	gi|530371187|ref|XP_005247022.1|	general transcription factor 3C polypeptide 3	GTF3C3	494	56384	6.6
0.000164	3	0	∞	gi|13994259|ref|NP_114108.1|	28S ribosomal protein S5, mitochondrial	MRPS5	430	48006	9.9
0.000164	3	0	∞	gi|767985150|ref|XP_011520272.1|	thrombospondin-1	THBS1	1170	129383	4.9
0.000162	3	0	∞	gi|767974361|ref|XP_011536692.1|	nucleosome assembly protein 1-like 1	NAP1L1	403	46832	4.5
0.000161	2	0	∞	gi|29826335|ref|NP_003899.2|	eukaryotic translation initiation factor 2 subunit 2	EIF2S2	333	38388	5.8
0.000156	3	0	∞	gi|186928854|ref|NP_005821.2|	28S ribosomal protein S31, mitochondrial	MRPS31	395	45319	9.3
0.000133	3	0	∞	gi|17402904|ref|NP_478126.1|	exosome complex component MTR3	EXOSC6	272	28235	6.3
0.000132	3	0	∞	gi|768010611|ref|XP_011525532.1|	zinc finger protein 574	ZNF574	896	98900	8.1

Appendix Table 2: List of top 50 proteins detected by MudPIT proteomic analysis of FAM117B

LZTS2 dNSAF AVG	LZTS2 Detected # Out of 3	GFP-CTAP Detected # Out of 3	LZTS2:GFP-CTAP	Locus	Description	NCBI_Gene	Length	MW	pI
0.010264	**3**	**0**	**∞**	**gi|108936958|ref|NP_005819.3|**	**DDB1- and CUL4-associated factor 7**	**DCAF7**	**342**	**38926**	**5.5**
0.005095	3	0	∞	gi|578836477|ref|XP_006724042.1|	**dual specificity tyrosine-phosphorylation-regulated kinase 1A**	**DYRK1A**	754	84557	8.8
0.003806	3	0	∞	gi|767912565|ref|XP_011542546.1|	signal-induced proliferation-associated 1-like protein 2	SIPA1L2	1722	190436	6.8
0.002753	**3**	**0**	**∞**	**gi|767950531|ref|XP_011542689.1|**	**leucine zipper putative tumor suppressor 1**	**LZTS1**	**596**	**66613**	**7.1**
0.002222	3	0	∞	gi|768007560|ref|XP_011524959.1|	signal-induced proliferation-associated 1-like protein 3	SIPA1L3	1781	194608	8.3
0.001475	3	0	∞	gi|545746375|ref|NP_001271175.1|	signal-induced proliferation-associated 1-like protein 1	SIPA1L1	1782	197407	8.3
0.001429	3	0	∞	gi|122937500|ref|NP_001074002.1|	protein unc-119 homolog B	UNC119B	251	28137	5.7
0.001064	3	0	∞	gi|768057171|ref|XP_011547115.1|	dual specificity tyrosine-phosphorylation-regulated kinase 1B	DYRK1B	689	75127	9.4
0.000723	3	0	∞	gi|21464101|ref|NP_036611.2|	14-3-3 protein gamma	YWHAG	247	28303	4.9
0.000697	3	0	∞	gi|767935349|ref|XP_011541469.1|	protein Shroom1	SHROOM1	852	90786	6.1
0.000598	3	0	∞	gi|115511046|ref|NP_009098.3|	zinc finger MYM-type protein 6	ZMYM6	1325	148088	8.2
0.000582	3	0	∞	gi|44890068|ref|NP_005086.2|	zinc finger MYM-type protein 4	ZMYM4	1548	172787	6.8
0.000417	3	0	∞	gi|530426085|ref|XP_005260950.1|	leucine zipper putative tumor suppressor 3	**LZTS3**	673	71791	7.6
0.000189	3	0	∞	gi|11321601|ref|NP_002618.1|	ATP-dependent 6-phosphofructokinase, platelet type	PFKP	784	85596	7.6
0.000109	3	0	∞	gi|4507729|ref|NP_001060.1|	tubulin beta-2A chain	TUBB2A	445	49907	4.9
0.038582	**3**	**1**	**964.55**	**gi|530394499|ref|XP_005270281.1|**	**leucine zipper putative tumor suppressor 2**	**LZTS2**	**669**	**72759**	**6.5**
0.012743	3	2	81.6859	gi|283436222|ref|NP_001164006.1|	ATPase family AAA domain-containing protein 3A	ATAD3A	586	66218	9.2
0.003093	3	3	20.21569	gi|14389309|ref|NP_116093.1|	tubulin alpha-1C chain isoform c	TUBA1C	449	49895	5.1
0.000641	3	2	19.42424	gi|237649019|ref|NP_001153682.1|	calcium-binding mitochondrial carrier protein Aralar2	SLC25A13	676	74304	8.6
0.002162	3	2	19.13274	gi|217272849|ref|NP_001136067.1|	prolyl 4-hydroxylase subunit alpha-1	P4HA1	534	61049	6
0.000742	3	3	14.26923	gi|18105007|ref|NP_004332.2|	CAD protein	CAD	2225	242981	6.5
0.019113	3	3	6.379506	gi|29788785|ref|NP_821133.1|	tubulin beta chain	TUBB	444	49671	4.9
0.000594	3	1	5.881188	gi|426214088|ref|NP_001258766.1|	reticulocalbin-2	RCN2	335	39139	4.5
0.042142	3	3	5.084087	gi|55956899|ref|NP_000217.2|	keratin, type I cytoskeletal 9	KRT9	623	62064	5.2
0.001352	2	0	∞	gi|75677353|ref|NP_114127.3|	ATPase family AAA domain-containing protein 3B	ATAD3B	648	72573	9.2
0.001095	2	0	∞	gi|4827048|ref|NP_005139.1|	protein unc-119 homolog A	UNC119	240	26962	6.4
0.000964	2	0	∞	gi|768037835|ref|XP_011529275.1|	PDZ domain-containing protein 11	PDZD11	140	16131	7.2
0.000958	2	0	∞	gi|187830777|ref|NP_001119584.1|	cellular tumor antigen p53	TP53	393	43653	6.8
0.00079	2	0	∞	gi|578810654|ref|XP_006714791.1|	prolyl 4-hydroxylase subunit alpha-2	P4HA2	535	60902	5.7
0.000686	2	0	∞	gi|7657257|ref|NP_055580.1|	mitochondrial import receptor subunit TOM20 homolog	TOMM20	145	16298	8.6
0.000651	2	0	∞	gi|5802968|ref|NP_006809.1|	protein AF1q	MLLT11	90	10061	4.5
0.000633	2	0	∞	gi|332634984|ref|NP_001091084.2|	DNA-directed RNA polymerase II subunit RPB11-b2	POLR2J3	115	13074	6.3
0.00059	2	0	∞	gi|23308693|ref|NP_689948.1|	zinc finger and BTB domain-containing protein 9	ZBTB9	473	50602	6.8
0.000562	2	0	∞	gi|530339647|ref|NP_001268861.1|	condensin-2 complex subunit G2	NCAPG2	1143	130960	6.9
0.000528	2	0	∞	gi|66529294|ref|NP_000296.2|	serum paraoxonase/arylesterase 2	PON2	354	39381	5.6
0.000516	2	0	∞	gi|530426780|ref|XP_005266156.1|	TNF receptor-associated factor 2	TRAF2	533	59135	7.5
0.000514	2	0	∞	gi|578823153|ref|XP_006719244.1|	tastin	TROAP	868	93449	7.2
0.000513	2	0	∞	gi|109689718|ref|NP_001035937.1|	monoacylglycerol lipase ABHD12	ABHD12	398	45097	8.6
0.000478	2	0	∞	gi|148368978|ref|NP_689512.2|	condensin-2 complex subunit H2	NCAPH2	605	68227	4.7
0.000433	2	0	∞	gi|157057543|ref|NP_443102.2|	sorting nexin-18	SNX18	628	68895	5.7
0.000421	2	0	∞	gi|31543831|ref|NP_001061.2|	tubulin gamma-1 chain	TUBG1	451	51170	6.1
0.000383	2	0	∞	gi|767969890|ref|XP_011541020.1|	condensin-2 complex subunit D3	NCAPD3	1498	168890	7.5
0.000377	2	0	∞	gi|5730009|ref|NP_006501.1|	zinc finger protein RFP	TRIM27	513	58490	6.2
0.000367	2	0	∞	gi|11386135|ref|NP_000700.1|	2-oxoisovalerate dehydrogenase subunit alpha, mitochondrial	BCKDHA	445	50471	8.3
0.000349	2	0	∞	gi|153085461|ref|NP_001093138.1|	HIG1 domain family member 1A, mitochondrial isoform	HIGD1A	107	11770	9.4
0.000344	2	0	∞	gi|767953588|ref|XP_011515591.1|	PREDICTED: 14-3-3 protein zeta/delta	YWHAZ	245	27745	4.8
0.000329	2	0	∞	gi|4506189|ref|NP_002783.1|	proteasome subunit alpha type-7	PSMA7	248	27887	8.5
0.000323	2	0	∞	gi|4506753|ref|NP_003698.1|	ruvB-like 1	RUVBL1	456	50228	6.4
0.000322	2	0	∞	gi|187960098|ref|NP_001120800.1|	medium-chain specific acyl-CoA dehydrogenase, mitochondrial isoform	ACADM	425	47020	8.3
0.000308	2	0	∞	gi|194018488|ref|NP_000278.3|	peroxisome biogenesis factor 6	PEX6	980	104061	6.3

Appendix Table 3: List of top 50 proteins detected by MudPIT proteomic analysis of LZTS2

LZTS1 dNSAF AVG	LZTS1 Detected # Out of 3	GFP-CTAP Detected # Out of 3	LZTS1:GFP-CTAP	Locus	Description	NCBI_Gene	Length	MW	pI
0.079012	**3**	**0**	**∞**	**gi|767950531|ref|XP_011542689.1|**	**leucine zipper putative tumor suppressor 1**	**LZTS1**	**596**	**66613**	**7.1**
0.012714	3	0	∞	gi|122937500|ref|NP_001074002.1|	protein unc-119 homolog B	UNC119B	251	28137	5.7
0.003781	3	0	∞	gi|4827048|ref|NP_005139.1|	protein unc-119 homolog A	UNC119	240	26962	6.4
0.003154	3	0	∞	gi|21361647|ref|NP_006612.2|	putative adenosylhomocysteinase 2	AHCYL1	530	58951	6.9
0.003012	3	0	∞	gi|314122177|ref|NP_001186600.1|	calumenin isoform c precursor	CALU	323	38051	4.6
0.002244	3	0	∞	gi|21464101|ref|NP_036611.2|	14-3-3 protein gamma	YWHAG	247	28303	4.9
0.00222	3	0	∞	gi|5730023|ref|NP_006657.1|	ruvB-like 2	RUVBL2	463	51157	5.6
0.002135	3	0	∞	gi|767924420|ref|XP_011532466.1|	protein O-linked-mannose beta-1,4-N-acetylglucosaminyltransferase 2	POMGNT2	580	66615	8.6
0.002091	3	0	∞	gi|4506753|ref|NP_003698.1|	ruvB-like 1	RUVBL1	456	50228	6.4
0.0019	3	0	∞	gi|153085461|ref|NP_001093138.1|	HIG1 domain family member 1A, mitochondrial	HIGD1A	107	11770	9.4
0.001899	3	0	∞	gi|530392883|ref|XP_005269499.1|	PREDICTED: erlin-1	ERLIN1	348	39171	7.9
0.001663	**3**	**0**	**∞**	**gi|108936958|ref|NP_005819.3|**	**DDB1- and CUL4-associated factor 7**	**DCAF7**	**342**	**38926**	**5.5**
0.001579	3	0	∞	gi|66529294|ref|NP_000296.2|	serum paraoxonase/arylesterase 2	PON2	354	39381	5.6
0.001391	3	0	∞	gi|17388799|ref|NP_490647.1|	dnaJ homolog subfamily B member 6	DNAJB6	326	36087	9.1
0.001244	3	0	∞	gi|530387549|ref|XP_005273449.1|	erlin-2	ERLIN2	339	37840	5.6
0.001171	3	0	∞	gi|11321601|ref|NP_002618.1|	ATP-dependent 6-phosphofructokinase, platelet type	PFKP	784	85596	7.6
0.001041	3	0	∞	gi|768044351|ref|XP_011544912.1|	ribonuclease inhibitor	RNH1	461	49974	4.8
0.00103	3	0	∞	gi|767948171|ref|XP_011514665.1|	MICOS complex subunit MIC19	MIC19	232	26753	7.8
0.000998	3	0	∞	gi|767935349|ref|XP_011541469.1|	protein Shroom1	SHROOM1	852	90786	6.1
0.000972	3	0	∞	gi|19923483|ref|NP_057406.2|	ras-related protein Rab-14	RAB14	215	23897	6.2
0.000934	3	0	∞	gi|5453559|ref|NP_006347.1|	ATP synthase subunit d, mitochondrial	ATP5H	161	18491	5.3
0.000907	3	0	∞	gi|33239451|ref|NP_872590.1|	proliferating cell nuclear antigen	PCNA	261	28769	4.7
0.000864	3	0	∞	gi|6912430|ref|NP_036537.1|	protein-S-isoprenylcysteine O-methyltransferase	ICMT	284	31938	8
0.000858	3	0	∞	gi|578821561|ref|XP_006718676.1|	protein phosphatase 6 regulatory subunit 3	PPP6R3	873	97669	4.6
0.000823	3	0	∞	gi|11559927|ref|NP_071383.1|	28S ribosomal protein S14, mitochondrial	MRPS14	128	15139	11.4
0.000817	3	0	∞	gi|13654278|ref|NP_112487.1|	SRA stem-loop-interacting RNA-binding protein, mitochondrial isoform	SLIRP	109	12349	10.2
0.000782	**3**	**0**	**∞**	**gi|578836477|ref|XP_006724042.1|**	**dual specificity tyrosine-phosphorylation-regulated kinase 1A**	**DYRK1A**	**754**	**84557**	**8.8**
0.000776	3	0	∞	gi|225543166|ref|NP_056195.3|	sorting and assembly machinery component 50 homolog	SAMM50	469	51976	6.9
0.000757	3	0	∞	gi|21359867|ref|NP_001907.2|	cytochrome c1, heme protein, mitochondrial precursor	CYC1	325	35390	9
0.00075	3	0	∞	gi|13435356|ref|NP_006109.2|	HCLS1-associated protein X-1	HAX1	279	31621	4.9
0.000727	3	0	∞	gi|767953588|ref|XP_011515591.1|	14-3-3 protein zeta/delta	YWHAZ	245	27745	4.8
0.0007	3	0	∞	gi|31543831|ref|NP_001061.2|	tubulin gamma-1 chain	TUBG1	451	51170	6.1
0.00069	3	0	∞	gi|89903012|ref|NP_001034891.1|	cell division control protein 42 homolog	CDC42	191	21259	6.5
0.000688	3	0	∞	gi|530407434|ref|XP_005255087.1|	cytosolic Fe-S cluster assembly factor NUBP2	NUBP2	130	13793	5.1
0.000679	3	0	∞	gi|109689718|ref|NP_001035937.1|	monoacylglycerol lipase ABHD12	ABHD12	398	45097	8.6
0.000676	3	0	∞	gi|92110027|ref|NP_060129.2|	glutaminyl-peptide cyclotransferase-like protein	QPCTL	382	42924	9.8
0.000652	3	0	∞	gi|169404009|ref|NP_003135.2|	translocon-associated protein subunit alpha	SSR1	286	32235	4.5
0.000633	3	0	∞	gi|530395344|ref|XP_005252973.1|	rho-related GTP-binding protein RhoG	RHOG	191	21308	8.1
0.000605	3	0	∞	gi|187830777|ref|NP_001119584.1|	cellular tumor antigen p53	TP53	393	43653	6.8
0.000605	3	0	∞	gi|21361565|ref|NP_001679.2|	ATP synthase F(0) complex subunit B1, mitochondrial precursor	ATP5F1	256	28909	9.4
0.000556	3	0	∞	gi|4502227|ref|NP_001168.1|	ADP-ribosylation factor-like protein 1	ARL1	181	20418	5.7
0.000534	3	0	∞	gi|521258690|ref|NP_001265585.1|	small nuclear ribonucleoprotein Sm D3	SNRPD3	126	13916	10.3
0.000527	3	0	∞	gi|4506613|ref|NP_000974.1|	60S ribosomal protein L22 proprotein	RPL22	128	14787	9.2
0.000522	3	0	∞	gi|46852178|ref|NP_064507.3|	E3 ubiquitin-protein ligase KCMF1	KCMF1	381	41945	5.7
0.000497	3	0	∞	gi|205830453|ref|NP_001128634.1|	catechol O-methyltransferase isoform MB-COMT	COMT	271	30037	5.5
0.000488	3	0	∞	gi|530376692|ref|XP_005248174.1|	transmembrane protein 33	TMEM33	247	27978	9.7
0.000483	3	0	∞	gi|15721937|ref|NP_114403.1|	28S ribosomal protein S24, mitochondrial precursor	MRPS24	167	19015	9.4
0.000482	3	0	∞	gi|20270303|ref|NP_620124.1|	mitochondrial Rho GTPase 2	RHOT2	618	68118	5.9
0.000482	3	0	∞	gi|530419305|ref|XP_005261210.1|	putative ribonuclease	YBEY	168	19436	8.1
0.000481	3	0	∞	gi|5453998|ref|NP_006382.1|	importin-7	IPO7	1038	119516	4.8

Appendix Table 4: List of top 50 proteins detected by MudPIT proteomic analysis of LZTS1

RNF169 dNSAF AVG	RNF169 Detected # Out of 3	Control Detected # Out of 3	RNF169:Control	NCBI_Gene	Locus	Description	Length	MW	pI
0.004144	**3**	**0**	**∞**	**RNF169**	**gi|767967816|ref|XP_011543191.1|**	**E3 ubiquitin-protein ligase RNF169**	**729**	**79394**	**9.1**
0.002413	3	0	∞	USP7	gi|150378533|ref|NP_003461.2|	ubiquitin carboxyl-terminal hydrolase 7 isoform 1	1102	128302	5.6
0.000644	**3**	**0**	**∞**	**DCAF7**	**gi|108936958|ref|NP_005819.3|**	**DDB1- and CUL4-associated factor 7**	**342**	**38926**	**5.5**
0.000607	**3**	**0**	**∞**	**DYRK1A**	**gi|768020356|ref|XP_011527785.1|**	**dual specificity tyrosine-phosphorylation-regulated kinase 1A**	**763**	**85584**	**8.7**
0.000344	3	0	∞	ACTR1A	gi|5031569|ref|NP_005727.1|	alpha-centractin	376	42614	6.6
0.000693	3	0	∞	SLC25A5	gi|156071459|ref|NP_001143.2|	ADP/ATP translocase 2	298	32852	9.7
0.000267	3	0	∞	ILF2	gi|24234747|ref|NP_004506.2|	ILF2:interleukin enhancer-binding factor 2	390	43062	5.3
0.000951	3	0	∞	RPL10A	gi|15431288|ref|NP_009035.3|	60S ribosomal protein L10a	217	24831	9.9
0.000239	2	0	∞	WDR6	gi|197927448|ref|NP_060501.3|	WD repeat-containing protein 6	1151	125001	6.9
0.000028	2	0	∞	SIPA1L1	gi|545746375|ref|NP_001271175.1|	signal-induced proliferation-associated 1-like protein 1	1782	197407	8.3
0.000279	2	0	∞	DYNLL2	gi|18087855|ref|NP_542408.1|	dynein light chain 2, cytoplasmic	89	10350	7.4
0.000515	2	0	∞	KPNB1	gi|19923142|ref|NP_002256.2|	importin subunit beta-1	876	97170	4.8
0.000333	2	0	∞	PSMC2	gi|4506209|ref|NP_002794.1|	26S protease regulatory subunit 7	433	48634	5.9
0.000099	2	0	∞	MCM7	gi|33469968|ref|NP_005907.3|	DNA replication licensing factor MCM7	719	81308	6.5
0.000106	2	0	∞	LRCH3	gi|578807822|ref|XP_006713854.1|	leucine-rich repeat and calponin homology domain-containing protein 3	777	86083	6.7
0.002086	2	0	∞	SRSF9	gi|4506903|ref|NP_003760.1|	serine/arginine-rich splicing factor 9	221	25542	8.6
0.000051	2	0	∞	TARDBP	gi|6678271|ref|NP_031401.1|	TAR DNA-binding protein 43	414	44740	6.2
0.00016	2	0	∞	ATP1A1	gi|21361181|ref|NP_000692.2|	ATP1A1:sodium/potassium-transporting ATPase subunit alpha-1	1023	112896	5.5
0.000862	2	0	∞	ELAVL1	gi|38201714|ref|NP_001410.2|	ELAVL1:ELAV-like protein 1	326	36092	9.2
0.001085	2	0	∞	RPS17	gi|4506693|ref|NP_001012.1|	40S ribosomal protein S17	135	15550	9.8
0.000869	2	0	∞	TMOD1	gi|260763922|ref|NP_001159588.1|	tropomodulin-1	359	40569	5.1
0.000021	2	0	∞	DOCK7	gi|431822375|ref|NP_001258928.1|	dedicator of cytokinesis protein 7	2129	241410	6.8
0.000634	2	0	∞	FLG2	gi|62122917|ref|NP_001014364.1|	FLG2:filaggrin-2	2391	248072	8.3
0.000062	2	0	∞	LARP1	gi|39725634|ref|NP_056130.2|	LARP1:la-related protein 1	1019	116465	9.1
0.000397	2	0	∞	SMARCE1	gi|21264355|ref|NP_003070.3|	SWI/SNF-related matrix-associated actin-dependent regulator of chromatin subfamily E member 1	411	46649	4.9
0.000155	2	0	∞	ZNF185	gi|530422917|ref|XP_005274794.1|	zinc finger protein 185	690	73613	7
0.000057	2	0	∞	PPP1R12C	gi|14149716|ref|NP_060077.1|	protein phosphatase 1 regulatory subunit 12C	782	84881	5.6

Appendix Table 5: List of proteins detected by MudPIT proteomic analysis of RNF169

NTAP-TROA dNSAF AVG	NTAP-TROA Detected # Out of 3	GFP-CTAP Detected # Out of 3	NTAP-TROA:GFP-CTAP	Locus	Description	NCBI_Gene	Length	MW	pI
0.003868	**3**	**0**	**∞**	**gi|578823153|ref|XP_006719244.1|**	**tastin**	**TROAP**	**868**	**93449**	**7.2**
0.001995	3	3	13.03922	gi|14389309|ref|NP_116093.1|	tubulin alpha-1C chain	TUBA1C	449	49895	5.1
0.001886	**3**	**0**	**∞**	**gi|578836477|ref|XP_006724042.1|**	**dual specificity tyrosine-phosphorylation-regulated kinase 1A**	**DYRK1A**	**754**	**84557**	**8.8**
0.001525	**3**	**0**	**∞**	**gi|108936958|ref|NP_005819.3|**	**DDB1- and CUL4-associated factor 7**	**DCAF7**	**342**	**38926**	**5.5**
0.000997	3	3	6.828767	gi|32698730|ref|NP_065823.1|	nuclear fragile X mental retardation-interacting protein 2	NUFIP2	695	76121	8.7
0.014143	2	3	5.849049	gi|124494247|ref|NP_001074419.1|	unconventional myosin-Ic	MYO1C	1044	119628	9.5
0.003002	2	3	7.014019	gi|5453599|ref|NP_006127.1|	F-actin-capping protein subunit alpha-2	CAPZA2	286	32949	5.8
0.001921	2	3	5.910769	gi|45359846|ref|NP_987100.1|	ras GTPase-activating protein-binding protein 2	G3BP2	449	50817	5.4
0.001204	2	0	∞	gi|4506633|ref|NP_000984.1|	60S ribosomal protein L31	RPL31	125	14463	10.5
0.001062	2	1	27.23077	gi|13124875|ref|NP_074035.1|	myosin-11 isoform SM2A	MYH11	1938	223575	5.5
0.000761	2	3	11.19118	gi|383792189|ref|NP_059867.3|	ataxin-2-like protein	ATXN2L	1062	112091	8.7
0.000693	2	2	10.04348	gi|227430301|ref|NP_001153059.1|	CD109 antigen isoform 2 preproprotein	CD109	1428	159695	5.8
0.000574	2	0	∞	gi|16905517|ref|NP_473357.1|	serine/arginine-rich splicing factor 10	SRSF10	262	31301	11.3
0.000292	2	0	∞	gi|40807443|ref|NP_955445.1|	protein regulator of cytokinesis 1	PRC1	606	70249	6.7
0.000141	2	0	∞	gi|18379349|ref|NP_006364.2|	synaptic vesicle membrane protein VAT-1 homolog	VAT1	393	41920	6.3
0.000095	2	0	∞	gi|574584803|ref|NP_001276052.1|	tubulin beta-4A chain	TUBB4A	495	54467	5

Appendix Table 6: List of proteins detected by MudPIT proteomic analysis of TROAP

Up in DYRK1A KO and overlap with DYRK1A ChIP-seq dataset							
Serum starved + Cycling (135 genes)			Cycling only (169 genes)				Serum starved only (2 genes)
ADAT1	EXOC8	PUF60	ABCC10	HDAC6	PLEKHA6	SRP14	CNN2
AHCTF1	FAM76A	PXMP2	ABHD18	HGH1	PLEKHG2	SRRT	TMEM259
ALDH16A1	FBXL5	QRICH1	ABTB2	HMBOX1	PMF1	SUSD2	
ASH2L	FBXO31	R3HDM1	ACBD4	HOMER2	PNKP	TAF6	
ASXL1	FLNA	RAB33B	ADNP	HOXC6	POLR1C	TBL3	
ATAD3A	FOXC2	RBM15	ALKBH2	ICMT	POLR3E	TCF3	
ATF2	FUBP1	RCC1	AP4E1	ID1	PPM1G	THAP7	
ATF4	GAS8	RFC5	ARHGAP32	IFRD1	PPOX	TIA1	
ATXN7L2	GGA3	RING1	ARHGEF18	IGFBP3	PPP1R10	TMEM183A	
BANP	GPATCH3	SCAMP5	ASF1B	IL17RD	PPP1R12A	TMEM262	
BAZ2B	GRWD1	SEC22C	BAK1	INTS9	PRDM11	TRIP6	
BCAR3	HERC1	SENP7	BRF1	KANK1	PRKDC	TROAP	
BRI3BP	HERPUD2	SETD5	CARMIL1	KIF24	PRMT5	TUBGCP6	
C1orf74	HNRNPH3	SLC12A2	CDKN1B	KIN	PROSER3	UBALD1	
C2orf68	HSD17B8	SLC25A4	CENPC	KLC2	PRPF4	UBXN11	
C6orf89	HUWE1	SMARCA5	CFAP45	LOXL2	PRPF40B	UMAD1	
CAND1	ILF2	SMG5	CFDP1	LRFN3	PRR14	UNG	
CD2AP	KIAA1191	SPDL1	CHMP1A	LTA4H	PRTG	USP21	
CDC20	LIN7C	SPRTN	CLASP1	LY6G5B	PTGER4	USP54	
CDC25B	LUC7L2	SRCAP	CLTB	MAD2L1	R3HDM4	VAMP2	
CDC5L	MAD1L1	SRSF10	COL1A1	MCM4	RAB17	VPS37C	
CENPB	MAPK14	STRIP1	CYTH1	MDM4	RAD18	VPS51	
CENPT	MAU2	SUV39H1	DDX19A	MED16	RGL2	WDR46	
CEP350	MBTPS1	THAP11	DFFA	MGRN1	RIC8B	WDR59	
CHAF1A	MED22	TIPIN	DIDO1	MPZL1	RPS15	WDR90	
CIAPIN1	MGME1	TMEM209	DLX1	MRE11	SELENON	YIPF3	
COPB2	MRM2	TMEM79	DYRK1A	MRI1	SEMA3B	ZBTB25	
COQ9	MTHFSD	TMPO	E2F2	MYBL2	SF1	ZDHHC5	
CORO7	MYO19	TRAPPC2	EFHD1	NANS	SIPA1L1	ZFP30	
CSDE1	NANP	TRIM7	EID2	NCL	SIRT5	ZFPM1	
CYGB	NCAPG2	TTC23	EIF1AD	NCOA7	SLC12A9	ZKSCAN2	
DBNDD1	NDUFS7	TUBGCP5	EPOP	NFATC2IP	SLC4A3	ZNF136	
DBR1	NFYC	UBE2D3	FBRS	NFIB	SLC6A9	ZNF184	
DCAF16	NKTR	UHRF2	FDPS	NMRAL1	SMARCAD1	ZNF790	
DDHD2	NOL9	USP39	FKBPL	NOA1	SMARCC2		
DDX20	NOP14	WDR6	FMNL1	NPTN	SMC1A		
DENR	NUDT1	WDR77	FUS	NUDT5	SMC5		
DHX37	OFD1	XPC	GCAT	NUP37	SMG7		
DNAJA3	PFKFB2	YOD1	GDF7	PACS2	SNAP29		
DNAJC27	PHF12	ZCCHC14	GDI2	PARP2	SNRNP70		
DPP9	PIH1D1	ZFP91	GGT5	PDE12	SNRPC		
EFHC1	POLDIP3	ZNF48	GID8	PEX14	SPATA33		
EHD1	POLE	ZNF500	GOLGA8B	PFDN6	SPC25		
EMD	POLG	ZNF839	GSN	PHC2	SPTY2D1		
ETFA	POP7	ZNF850	HASPIN	PI4KA	SREK1		

Appendix table 7: Overlap of DYRK1A regulated genes (obtained by RNA-seq) with DYRK1A ChIP-seq dataset [under Serum starved or Cycling conditions (Di Vona et al., 2015)]**.** Related to Figure 49A.

Down in DYRK1A KO and overlap with DYRK1A ChIP-seq dataset						
Serum starved + Cycling (101 genes)			Cycling only (139 genes)			
AKAP11	MKKS	SSR1	ACADSB	FTCD	PPP1R2	UPF3A
ASPH	MMS22L	SURF2	ACO2	GPN3	PRDX4	ZNF286A
C5orf24	MRPL57	TMCO1	ADGRF1	GRB2	PSENEN	ZNF697
C6orf120	MRPS7	TMEM245	ADGRG1	HARS2	PSMD10	ZNF792
CCDC77	MTFR1L	TOPORS	AHCY	HES7	PTPN1	
CCNC	NAA35	UBC	AIDA	HIGD2A	RAB27A	
CCNG1	NAA38	VDAC3	AKT1S1	HINT1	RACK1	
CCT8	NCOA4	VMP1	ANKRD49	HMGN5	RBM26	
CDK12	NOL11	WDR27	ARCN1	ICAM1	RICTOR	
CHST7	NPR3	ZBTB2	ATG4A	IFT74	RIN1	
CNP	NRBF2	ZBTB6	B4GAT1	IKBKG	RPS15A	
COASY	NSUN3		BCLAF1	IKZF5	RPS7	
COX11	PAXBP1		BZW1	ITGA10	RPS9	
CUL5	PBLD		C11orf54	KCTD2	SACM1L	
DCTN2	PGK1		C12orf57	LAMTOR4	SAP18	
DHFR2	PIGN		C20orf27	LIN37	SBDS	
DNAJB4	PLOD2		CASTOR1	LSM14A	SEC63	
DNTTIP2	PPP4R3B		CCNJ	LYRM7	SEMA7A	
ECHS1	PRDX1		CCR7	MAGT1	SH3BGRL	
ERGIC2	PSMB3		CD320	MAP3K7	SLC39A9	
ETF1	PSMD5		CDC26	MDH1B	SMNDC1	
FAM135A	PTPRN2		CETN2	MLF2	SNRPG	
FGFR1OP2	PTRH2		CETN3	MOB1A	SP9	
FMC1	PTTG1		CHUK	MRPL19	SPTBN4	
GGNBP2	RBPJ		CHURC1	MRPL58	SSR4	
GLCE	RNF167		CLPX	MRPS18B	SUCLG1	
GP1BA	RPL10A		CNPY2	MTHFD2L	TAF1D	
GPR19	RPL12		COL1A2	MTRF1L	TAPBPL	
HSD17B1	RPL13A		COPS3	MYNN	TBC1D17	
HSPA4	RPL17		COQ3	NKAP	TFPT	
HSPH1	RPL23		COX7B	NOP16	TFRC	
IFT80	RPL26		DIS3	NPM1	TIMM17A	
IMP3	RPL27A		DRG1	NSDHL	TMEM107	
INTS13	RPL7A		DSE	NTMT1	TMEM11	
IREB2	RPS6		DZIP3	NUDT19	TMEM127	
KAZALD1	RRAGA		EDRF1	NUDT2	TMEM132B	
LAMP1	SEC62		EIF3L	OST4	TRIM41	
LPXN	SFXN3		ENDOV	PCMTD1	TSEN34	
LRSAM1	SKA3		EXT2	PCYOX1	TSPYL1	
LTV1	SLC39A7		F8	PHB	TSPYL4	
MAGOHB	SLU7		FAM136A	PIBF1	TTC14	
MAP1LC3B	SMIM10L1		FAM216A	PLAA	TTC30B	
MAP3K7CL	SMIM27		FASTKD2	PLCD3	TTC32	
MATR3	SPAG16		FGF1	POFUT2	TXNDC9	
MICU2	SRP19		FOXG1	POLR2H	UBAC1	

Appendix table 8: Overlap of DYRK1A regulated genes (obtained by RNA-seq) with DYRK1A ChIP-seq dataset [under Serum starved or Cycling conditions (Di Vona et al., 2015)]. Related to Figure 49B**.**

Up in DCAF7 overexpression and overlap with DYRK1A ChIP-seq dataset						Dn in DCAF7 overexpression and overlap with DYRK1A ChIP-seq dataset				
Serum starved + Cycling (38 genes)		Cycling only (51 genes)			Serum starved only (2 genes)	Serum starved + Cycling (39 genes)		Cycling only (67 genes)		
ADAT1	MAK16	ABCC10	KPNA2	SIRT5	CNN2	AGBL5	PTPRN2	ACADSB	EIF3L	RIN1
ASH2L	MAPK14	CARMIL1	LOXL2	SLC44A1	GGH	ALDH16A1	RC3H2	ADGRF1	EPHB3	RPS7
ASPH	MICU2	CETN2	MAD2L1	SNRPC		ATF4	RIMS3	AIDA	FOXG1	SLC12A9
C1orf74	MRPL57	COL1A2	MRPS18B	SPTY2D1		BANP	RPL13A	ATF7	GSN	SLC39A9
C6orf89	MYO19	DHX8	MYBL2	TADA3		C2orf68	RPL27A	B4GAT1	HDAC10	SMARCC2
CHAF1A	NCAPG2	DIS3	NCOA7	TFRC		CDC25B	RPL4	C11orf54	HDAC6	SMARCD2
COPB2	NOP14	DZIP3	NOP16	TP53		CENPB	RPL7A	C12orf57	IKZF5	SMNDC1
DBR1	NPR3	FAM216A	NUDT5	TRIM27		CHST7	RPS11	CAMK2D	ITGA10	SNAI1
DCAF16	PGK1	FGF1	PDE12	UBXN11		CYGB	RPS16	CCNJ	LRFN3	TFPT
DHX37	PIGW	FKBPL	PFDN6	WDR46		ECHS1	SFXN3	CHUK	LSM14A	TIA1
EFHC1	PLOD2	FUS	PHB	WDR90		FAM135A	SLC12A2	CLASP1	LY6G5C	TMEM127
FLNA	PTRH2	GDI2	POFUT2	ZNF697		FBXO31	SLC25A11	CNIH2	MBLAC1	TROAP
GMPPA	SEC22C	GOLGA8B	POLR1C	ZNF790		FOXC2	SNX33	CNPY2	NFIB	TSPYL1
GORASP2	SETD5	HMGN5	PSMB2			GLCE	SURF1	COL1A1	NUDT19	TSPYL4
HSD17B8	SKA3	IGFBP3	RAD18			HERC1	SURF2	CREBZF	P2RX6	TTC32
HSPH1	SLC39A7	INTS9	RBM26			KAZALD1	YPEL4	CTNNBIP1	PCYOX1	TUBGCP6
LAMP1	SS18L2	KANK1	RFC3			LPXN		DLX1	PHC2	U2AF1L4
LSM3	SSR1	KBTBD6	SAP18			LRRC28		DUSP4	PLCD3	UBAC1
MAGOHB	TMEM79	KIF24	SEMA3B			MIF4GD		EBF1	PLEKHG2	VAMP1
						PAOX		EDRF1	PROSER3	ZFP36
						PAXBP1		EFNA5	PSENEN	ZNF792
						PCGF2		EID2	PTCH2	
						POLDIP3		EID2B	RAB27A	

Appendix table 9: Overlap of DCAF7 regulated genes (obtained by RNA-seq) with DYRK1A ChIP-seq dataset [under Serum starved or Cycling conditions (Di Vona et al., 2015)]. Related to Figure 50A and 50B.

Overlap of DYRK1A Chip-Seq dataset with AUTS2 ChIP-seq dataset						
Serum starved + Cycling (31 genes)			Cycling only (33 genes)			Serum starved only (1 gene)
ALDH16A1	MED1	RPL17	ACTRT3	MTRNR2L1	RPS15	TRAPPC6B
ARF3	MED22	RPL17-C18orf32	BCLAF1	MYNN	SMC5	
ATF4	METTL16	RPL7A	C19orf53	NDUFA11	SNRPG	
C18orf32	MYO19	RPS16	CNPY2	NUDT19	TIMM17A	
C5orf24	NCAPG2	RPS28	DRG1	PICK1	U2AF1L4	
CCNG1	NDUFA7	SUPT5H	DSE	PKLR	VMAC	
CCT8	NOL9	TAS1R1	FDPS	PLEKHG2	VPS8	
DNTTIP2	PIGW	TMEM245	GTF3C5	POLR1C	YIPF3	
IREB2	PIH1D1	UBC	GUK1	PPM1G	ZFP36	
LRSAM1	PPCDC		HOXC5	PSENEN	ZNF345	
MAP3K7CL	RPL12		LIN37	PSMB2	ZNF790	

Appendix table 10: Overlap of genes bound by AUTS2 and genes bound by DYRK1A [under Cycling or Serum starved conditions (Di Vona et al., 2015)]. Related to Figure 51.